CHARACTERIZATION OF TIME-DEPENDENT CHANGES IN STRENGTH AND STIFFNESS OF FLORIDA BASE MATERIALS

FINAL REPORT

Sponsored by the Florida Department of Transportation Research Center
Contract Number BD545-44

Dr. Dennis R. Hiltunen, P.E.
Principal Faculty Investigator

Dr. Reynaldo Roque, P.E., Dr. Bjorn Birgisson, P.E., and Dr. Micheal McVay, P.E.
Faculty Co-Investigators

Ulas Toros
Luis A. Campos
Graduate Student Investigators

DEPARTMENT OF CIVIL & COASTAL ENGINEERING
UNIVERSITY OF FLORIDA

October 2008

The opinions, findings, and conclusions expressed in this publication are those of the authors and not necessarily those of the State of Florida Department of Transportation.

METRIC CONVERSION TABLE

SYMBOL (US)		MULTIPLY BY	TO FIND	SYMBOL (SI)
		LENGTH		
in	inches	25.4	millimeters	**mm**
ft	feet	0.305	meters	**m**
yd	yards	0.914	meters	**m**
mi	miles	1.61	kilometers	**km**
		AREA		
in^2	squareinches	645.2	square millimeters	**mm^2**
ft^2	squarefeet	0.093	square meters	**m^2**
yd^2	square yard	0.836	square meters	**m^2**
ac	acres	0.405	hectares	**ha**
mi^2	square miles	2.59	square kilometers	**km^2**
		VOLUME		
fl oz	fluid ounces	29.57	milliliters	**mL**
gal	gallons	3.785	liters	**L**
ft^3	cubic feet	0.028	cubic meters	**m^3**
yd^3	cubic yards	0.765	cubic meters	**m^3**
		MASS		
oz	ounces	28.35	grams	**g**
lb	pounds	0.454	kilograms	**kg**
T	short tons (2000 lb)	0.907	megagrams (or "metric ton")	**Mg (or "t")**
		TEMPERATURE (exact degrees)		
°F	Fahrenheit	5 (F-32)/9 or (F-32)/1.8	Celsius	**°C**
		FORCE and PRESSURE or STRESS		
lbf	poundforce	4.45	newtons	**N**
lbf/in^2	poundforce per square inch	6.89	kilopascals	**kPa**

SYMBOL (SI)		MULTIPLY BY	TO FIND	SYMBOL (US)
		LENGTH		
mm	millimeters	0.039	inches	**in**
m	meters	3.28	feet	**ft**
m	meters	1.09	yards	**yd**
km	kilometers	0.621	miles	**mi**
		AREA		
mm^2	square millimeters	0.0016	square inches	**in^2**
m^2	square meters	10.764	square feet	**ft^2**
m^2	square meters	1.195	square yards	**yd^2**
ha	hectares	2.47	acres	**ac**
km^2	square kilometers	0.386	square miles	**mi^2**
		VOLUME		
mL	milliliters	0.034	fluid ounces	**fl oz**
L	liters	0.264	gallons	**gal**
m^3	cubic meters	35.314	cubic feet	**ft^3**
m^3	cubic meters	1.307	cubic yards	**yd^3**
		MASS		
g	grams	0.035	ounces	**oz**
kg	kilograms	2.202	pounds	**lb**
Mg (or "t")	megagrams (or "metric ton")	1.103	short tons (2000 lb)	**T**
		TEMPERATURE (exact degrees)		
°C	Celsius	1.8C+32	Fahrenheit	**°F**
		FORCE and PRESSURE or STRESS		
N	newtons	0.225	poundforce	**lbf**
kPa	kilopascals	0.145	poundforce per square inch	**lbf/in^2**

1. Report No.	2. Government Accession No.	3. Recipient's Catalog No.
4. Title and Subtitle Characterization of Time-Dependent Changes in Strength and Stiffness of Florida Base Materials		5. Report Date October 2008 6. Performing Organization Code
7. Author(s) Ulas Toros, Dennis R. Hiltunen, Luis A. Campos, Reynaldo Roque, Micheal C. McVay, and Bjorn Birgisson		8. Performing Organization Report No.
9. Performing Organization Name and Address Department of Civil and Coastal Engineering University of Florida 365 Weil Hall, P.O. Box 116580 Gainesville, FL 32611-6580		10. Work Unit No. (TRAIS) 11. Contract or Grant No. BD545-44
12. Sponsoring Agency Name and Address Florida Department of Transportation 605 Suwannee Street, MS 30 Tallahassee, FL 32399		13. Type of Report and Period Covered Final Report 14. Sponsoring Agency Code

15. Supplementary Notes

16. Abstract

Resilient modulus and Young's modulus are parameters increasingly used to fundamentally characterize the behavior of pavement materials both in the laboratory and in the field. This study documents the small-strain Young's modulus and larger-strain resilient modulus response of unbound aggregate base coarse materials to various environmental conditions. The small-strain Young's modulus experiments were conducted on laboratory compacted materials and field core materials by the authors. The State Material Office conducted the resilient modulus experiments on laboratory compacted materials. The results of both tests are presented in this study. It is shown that the small-strain Young's modulus is not constant, even when held at constant moisture, and that significant changes in modulus will occur with drying and wetting of the material. The response to drying and wetting cycles appears to be repeatable, and suggests that the underlying mechanism that controls the response is reversible. It is also shown that the larger-strain resilient modulus demonstrated similar trends with small-strain Young's modulus, but the rate of change and magnitude of the effect are different between materials. The material response to drying and wetting cycles appears to be reasonably repeatable. Comparison of both experiments revealed that the change in Young's modulus with drying is much more dramatic than the resilient modulus, indicating that the drying effect is significantly reduced with higher strain. Lastly, the evidence suggests that these changes can be explained by the science of unsaturated soil mechanics: changes in moisture or moisture distribution results in changes in internal pore pressure, which affect the effective confining pressure constraining the material. The influence of this phenomenon is observed but is not as dramatic at higher strain. Based upon these results it appears that a pavement design process based on resilient modulus for the base material should account for changes in moisture content anticipated in the base during the life of the pavement structure. The authors are aware that a procedure for the effects of moisture changes and other seasonal effects on the resilient modulus of the base material has been implemented in the new Mechanistic-Empirical (M-E) Pavement Design Guide. It is thus recommended that this procedure be utilized in conjunction with the findings reported herein to design pavements in Florida.

17. Key Word	18. Distribution Statement
Free-free Resonant Column, Resilient Modulus, Unbound Aggregate, Florida Lime-rock, Florida Base Coarse, Cementation, Matric Suction, Negative Pore Water Pressure, Unsaturated Soil	No Restrictions

19. Security Classif. (of this report)	20. Security Classif. (of this page)	21. No. of Pages	22. Price
Unclassified	Unclassified	224 Pages	

EXECUTIVE SUMMARY

Resilient modulus and Young's modulus are parameters increasingly used to fundamentally characterize the behavior of pavement materials both in the laboratory and in the field. This study documents the small-strain Young's modulus and larger-strain resilient modulus response of unbound aggregate base materials to various environmental conditions.

The small-strain Young's modulus experiments were conducted on laboratory compacted materials and field core materials by the author. The State Materials Office (SMO) conducted the resilient modulus experiments on laboratory compacted materials. The results of both tests are presented in this study.

It is shown that the small-strain Young's modulus is not constant, even when held at constant moisture, and that significant changes in modulus will occur with drying and wetting of the material. The response to drying and wetting cycles appears to be repeatable, and suggests that the underlying mechanism that controls the response is reversible. It is also shown that the larger-strain resilient modulus demonstrates similar trends with small-strain Young's modulus, but the rate of change and magnitude of the effect are different between materials. The material response to drying and wetting cycles appears to be reasonably repeatable.

Comparison of both experiments revealed that the change in Young's modulus with drying is much more dramatic than the resilient modulus, indicating that the drying effect is significantly reduced with higher strain.

Lastly, the evidence suggests that these changes can be explained by the science of unsaturated soil mechanics: changes in moisture or moisture distribution results in changes in internal pore pressure, which affect the effective confining pressure constraining the material. The influence of this phenomenon is observed but is not as dramatic at higher strain.

Based upon these results it appears that a pavement design process based on resilient modulus for the base material should account for changes in moisture content anticipated in the base during the life of the pavement structure. The authors are aware that a procedure for the effects of moisture changes and other seasonal effects on the resilient modulus of base material has been implemented in the new Mechanistic-Empirical (M-E) Pavement Design Guide. It is thus recommended that this procedure be utilized in conjunction with the findings reported herein to design pavements in Florida.

TABLE OF CONTENTS

LIST OF TABLES

LIST OF FIGURES

CHAPTER 1
INTRODUCTION

1.1 Problem Statement

Roadway field studies in Florida have documented beneficial improvements with time in stiffness and strength properties of Florida limerock base materials (Zimpfer [1988], Gartland and Eades [1979], Smith and Lofroos [1981], McClellan et al. [2000]).

Investigation of strength, time, and environmental condition relationships were initiated following the 1962 Interim Design Guide based on the American Association of State Highway Officials (AASHO)* Road Test. This interim guide required from each state department of transportation (DOT) to establish layer coefficients applicable to its own practices and based on its own experience due to widely varying environment, traffic, and construction practices.

In the late 1960's, the Office of Materials and Research (OMR)** began a field evaluation program of existing pavements, which included trenching, laboratory tests, and field tests to rate and determine the strength and performance of Florida limestone base materials. From 1968 to 1971, test mine studies were conducted on various base materials to characterize their resistance to repeated loads at optimum moisture, soaked moisture, and drained conditions. In the mid 1970's, a minimum Limerock Bearing Ratio (LBR) strength requirement was added to the limerock base specification. In the early 1980's, Dynaflect and field plate load tests were used in pavement evaluation to determine soil support and modulus of base and subgrade materials.

In several of these studies, it has been documented that the mechanical properties of limerock base change with time. Strength gain investigation of base materials of Florida, conducted by Zimpfer, from 1977 to 1978 on high carbonate limerock, from 1978 to 1979 on

---

*AASHO was changed to American Association of State Highway and Transportation Officials (AASHTO) on November 13, 1973

**Former name of State Materials Office

low carbonate limerock, and from 1979 to 1980 on low carbonate shell-rock were based on LBR tests, test-pit plate tests, and laboratory unconfined compression tests. In all cases investigated, the plate test modulus and the unconfined compression strength increased with both aging and drying. It was suggested that one or some of the following factors caused these changes: internal friction (for low carbonate limerock), reduction in field moisture, reconsolidation of the carbonate base, and cementation.

With regard to layer coefficients used in design, Zimpfer et al. (1973) compared Florida limestone and AASHO crushed limestone (i.e., layer coefficient (a_2) = 0.14 and LBR = 140) and established a layer coefficient of 0.15 for limerock materials and a minimum LBR strength requirement of 100 to be used in the state of Florida based on these comparisons.

Smith and Lofroos (1981) recommended an increase of layer coefficient from 0.15 to 0.18 based on studies of strength and stiffness gains in limerock base materials over a period of five, six, and nine years. A layer coefficient of 0.18 for limerock base is current Florida Department of Transportation (FDOT) design practice.

The current pavement design process is transitioning from layer coefficient to resilient modulus based procedures. While previous studies have documented changes in limerock bases with time, the effect on resilient modulus has not been documented, and thus the influence of these beneficial improvements on pavement performance cannot be quantified. Further, the mechanisms for changes have not been clearly established, and this prevents introduction of expected stiffness and strength gains into future design procedures. Therefore, there is a need to more fully understand and verify the mechanisms, and quantify their influence on material properties and pavement performance.

1.2 Hypothesis

It is hypothesized by the authors that the time-dependent and moisture-dependent changes in mechanical properties of Florida limerock base course materials, compacted at typical field moisture contents, are due to the suction effects described by the science of unsaturated soil mechanics. A redistribution of moisture or a reduction in amount of moisture will increase the level of suction, which effectively increases the confining stress on the particulate material. It has been firmly established that an increase in confinement level produces an increase in mechanical properties such as stiffness and strength. This is a reversible process; an increase in moisture will lower the suction and remove the increase in effective confinement, which leads to a reduction in previously obtained mechanical properties.

1.3 Objectives of Research

The overall objective of the research is to identify, document, and recommend practical methodologies to supplement existing and future pavement design procedures with a protocol that incorporates expected stiffness and strength gains in Florida base materials. Further, there are three specific goals for this study. The first goal is to use a relatively new small-strain testing method (free-free resonant column) to study the mechanical properties of Florida limerock base course materials. The second goal is to observe and document the stiffness gains in Florida base materials with time and under varying environmental conditions. The third goal is to identify a potential mechanism causing observed stiffness gains with time and under varying environmental conditions. It is expected that the suction mechanism mentioned above can explain the changes in material response to time and environmental condition.

1.4 Scope of Research

Five aggregate sources that are used as base materials in Florida were selected to study the variation of stiffness with time and moisture condition of Florida base materials. Obviously there

are more than five sources that are utilized by the profession. However, due to project life cycle time restraints, the most commonly used base materials with high, moderate, low, and no carbonate contents were selected. The base materials include a granite-based graded aggregate from Georgia, a limestone based shell-rock from Loxahatchee, FL. Limerock from mines in Newberry, Ocala, and Miami were chosen to represent northern, central, and southern limerock sources of Florida, respectively. The standard FDOT procedures were followed to develop material testing models.

There are various means to measure the stiffness of Florida base materials with time and moisture, such as resilient modulus (M_R) test, unconfined compression (q_u) test, etc. In this study, free-free resonant column (FFRC) and M_R testing were used to determine stiffness behavior with time and moisture level of each material under different environmental conditions.

The FFRC test measures small-strain elastic modulus. One benefit of measuring small-strain modulus is to observe calcification (cementation) if it exists in the base course material. The M_R and q_u tests are high-strain tests that would break any existing calcification (cementation) bonds within the material particles, which would prevent the observation of calcification (cementation) phenomenon. Other major reasons to decide using the FFRC test include: 1) it is a non-destructive test method that provides the option to test the same compacted material sample as many times as deemed necessary, and 2) it is a quick way of testing. The materials are exposed to one of four uniform types of environmental conditions. These environment conditions are: laboratory ambient, outdoors, constant moisture, drying and wetting cycles.

The State Materials Office (SMO) carried out the M_R testing on the exact same materials, and the specimens that were used for M_R testing will be subjected to the same environmental

conditioning. The M_R test, as mentioned above, is high-strain modulus based test. The main reason to use M_R test is to observe the material response to the higher strains thought to be more indicative to field loading conditions.

1.5 Organization of Report

A discussion of the remainder of the report organization is as follows. Chapter Two presents a literature review in the form of a brief historical perspective of Florida lime-rock base design. In addition, suggested potential mechanisms causing changes in mechanical properties, including capillary effects on soil stiffness, secondary time effect on soil stiffness, and effects of cementation are reviewed.

Information regarding the five different material sources, mineralogy, and characterization of unbound aggregate base coarse materials used to reconstitute the specimens tested in this work are summarized in Chapter Three. All testing was conducted at the FDOT-State Materials Office (SMO) Research Park, Gainesville, FL.

In Chapter Four, the FF-RC and M_R tests experiments used in this research are presented. Detailed background associated with measurements of constrained compression wave velocity, constrained compression modulus, unconstrained compression wave velocity, and Young's modulus is presented. In addition, detailed description of environmental conditioning and specimen preparation for both tests and also details of core materials collected for FF-RC testing are presented.

In Chapter Five small-strain dynamic properties of unbound aggregate base course materials used in Florida measured with FF-RC test setup are presented. Response of fresh unbounded aggregate base course and core materials to FF-RC testing, under selected environmental conditioning, is also presented. Discussions of variation of material responses to

time and moisture content are included in Chapter Five. In addition, suggested potential mechanisms influencing the mechanical property responses of the materials are discussed.

Experiments on Loxahatchee, Ocala, and Miami were exposed to constant humidity and tested via FF-RC testing method. Visual analysis was also performed via environmental scanning electron microscope on materials cured for 30 days and exposed to low relative humidity levels. In Chapter Six the results of these experiments are presented.

High-strain dynamic properties of unbound aggregate base course materials used in Florida measured with resilient modulus test setup are presented in Chapter Seven. Response of fresh unbound aggregate base coarse to high-strain modulus testing, under selected environmental conditioning, is also presented. Discussions of variation of material responses to time and moisture content are included to Chapter Seven. In addition, comparisons of responses to small-strain modulus testing are discussed to further investigate the validity of hypothesized mechanism that influence the time-dependent and moisture-dependent changes in mechanical properties of Florida lime-rock base course materials.

Based upon the information presented in Chapters Two through Seven, recommendations for pavement design in Florida are presented in Chapter Eight, and a summary of the study, and a listing of the findings and conclusions are presented in Chapter Eight. Further test result details are presented in the appendices. Grain size distribution graphs and material parameters of the 2nd and 3rd replicates of each material collected are given in Appendix A. Individual small-strain modulus test results of Newberry, Ocala, Loxahatchee, Miami, Georgia and Miami, and field cores are presented in Appendix B, C, D, E, F, and G, respectively. Comparisons of small-strain modulus of five materials are presented in Appendix H, and individual large-strain modulus test results are presented in Appendix I.

CHAPTER 2
LITERATURE REVIEW: LIMEROCK BASE DESIGN IN FLORIDA

According to the FDOT Materials Manual, records indicate that from the 1950's to the early 1960's FDOT used a pavement design procedure with no direct consideration given to the strength of the base course materials. However, base course material characteristics were included following implementation of the AASHO Interim Design Guide of 1962.

Due to varying environmental conditions, traffic loads, and construction practices, the 1962 Guide required every state DOT agencies to institute layer coefficients that are appropriate to local practices and experiences. To implement the 1962 Guide, FDOT initiated the construction of experimental projects. The main principal of this program was to evaluate the design criteria, and to institute layer coefficients for Florida materials and eventually implement the layer coefficients into the design criteria. The experimental projects were built on US 90 in Marianna, Florida, on US 19 in Levy County between Suwannee River and Chiefland, and on US 90 in Okaloosa County near Crestview, Florida, respectively. Base materials, subgrade materials, and the thickness of the pavement layers were studied in these regions of the State to evaluate the environmental variables. In addition to the above, two more experimental projects were built at Lake Wales and West Palm Beach mainly to determine base material equivalencies from which data were collected to verify structural layer coefficients for base material (McClellan et al. [2001]).

In mid 1970's, Limerock Bearing Ratio (LBR) strength limitations were supplemented to the base material specifications. The Florida LBR values were related to the soil support values that are required for pavement design assessment. After intensive research and modifications, the

limerock base coefficients were set to 0.18 where LBR value is at least 100, based on Smith and Lafroos (1981).

Limerock has been specified as the "standard" base material used in Florida. In addition to limerock base materials, shell materials and cemented coquina shell materials were also considered as base materials to be used in Florida in the late 1960's, and shell-rock in the late 1980's. The basic specifications of these base materials required LBR value of at least 100 along with other requirements.

Intensive studies were conducted from early 1960's to late 1980's on observed strength gains in Florida base materials. Laboratory, FDOT test pit, and field studies were conducted on high and low carbonate limerock, bank and pit run shell, and cemented coquina shell base materials. The base materials were tested under various environmental conditions.

First, Gartland and Eades (1979) treated two Florida limestones in the laboratory to investigate the possible formation of carbonate cements. Samples were compacted in standard Florida LBR molds and subjected to one of the following methods of treatment: 1) saturated with CO_2 enriched water; 2) soil was mixed with 1% NaCl, by dry weight of the sample, prior to compaction; and 3) samples were saturated with plain distilled water.

These treatments were conducted to simulate natural cementation processes, as previous cementation experiments described in the literature produced only minor cementation. The samples were cured either by cycles of wetting and drying or through a period of continual soak.

The LBR test was used to evaluate strength of the compacted material after treatment and curing. Comparison of strength values indicated that all methods of treatment and curing resulted in increased strength. Those samples cured by continual soaking showed the largest and most consistent strength gains.

Surface area analysis was used to measure changes in particle size and pore volume resulting from the formation of carbonate cement. When samples subjected to similar treatment and curing methods were compared, there was a trend of decreasing surface area with increasing sample strength.

Visual analysis of the carbonate cements was performed on the scanning electron microscope (SEM). Grain contact cementing was evident at all particle sizes. Most treatment and curing methods showed evidence of precipitated sparry calcite crystals. The void-filling sparry calcite was most abundant in those samples cured by continual soak.

Second, Keyser et al. (1984) summarize experiments conducted by the FDOT on test pavement sections. Results of rigid plate tests indicated significant increases after about 5 years of service. Field data also indicated that drying of the materials occurred over this same time, and the authors indicate that the moisture content reduction contributed significantly to the increase in strength. The authors also suggest that other factors such as reconsolidation of the carbonate base and cementation would also contribute to the increased strength after aging.

Third, Keyser et al. (1984) also summarize experiments of strength gain under controlled environmental conditions. These investigations included laboratory unconfined compression tests and plate tests on test pit sections. LBR tests were also performed. The laboratory specimens and test pit sections were constructed at optimum moisture content and subjected to various forms of aging, including constant moisture, slow drying, cycles of heating and cooling, and oven-drying following aging. Unconfined compression strength and plate load modulus were both observed to increase with increased aging and drying, and even showed slight increases with aging while at constant moisture. The authors indicate that the largest changes during aging resulted when a loss of moisture occurred during and after aging.

Thus, it is evident that previous experimental studies have documented increases in both stiffness and strength of limerock base materials as a result of changes in time and environmental conditioning.

Gartland and Eades (1979) clearly documented that a possible mechanism for these increases is calcite-based cementation. However, it must be noted that cementation was observed for fully saturated specimens. Further, the cementation was observed only after laboratory techniques were specifically designed to induce cementation. They note that several previous cementation experiments documented in the literature were hindered by lack of precipitation of significant amounts of cement in reasonable periods of time. It should also be noted that McClellan et al. (2000) were not successful in creating cementation in laboratory specimens compacted and cured at optimum moisture content. Here, the significant increases in LBR values due to cementation observed by Gartland and Eades (1979) were not observed, despite significant efforts at mimicking the conditions necessary for cementation. The difference seems to be that the specimens were not cured while in a saturated state.

On the other hand, Keyser et al. (1984) documented both stiffness and strength increases of materials prepared at field moisture contents, and in less than a saturated condition. The authors note that these increases were typically observed in conjunction with drying or loss of moisture from the material.

The literature provides substantial evidence that so-called capillarity or suction effects significantly explain these observations. It has been well documented in the science of unsaturated soil mechanics (Lu and Likos [2005]) that increases in suction or negative pore pressure will occur as water is removed from the material, and Singh et al. (2006) document that high suction stresses are possible in aggregate base course materials. As documented by Wu,

Gray and Richart (1984), Qian et al. (1991), and Qian et al. (1993) for sand and silt soils, this increased suction stress will effectively increase confinement and hence modulus.

It has long been established that the modulus of a particulate material is directly proportional to level of confining pressure (Richart, Hall, and Woods [1970]). Among the first studies for soil, Hardin and Richart (1963) reported results of resonant column tests on sands that indicated shear modulus to be a function of isotropic confining pressure raised to power of 0.5. Many subsequent studies have affirmed these basic findings, including Fernandez (2000) and Menq (2003), both of which contain extensive discussion of the literature on this subject. Menq (2003) also demonstrates these fundamentals apply to larger particle sizes, e.g., gravels.

Cho and Santamarina (2001) conducted detailed particle level studies on the behavior of unsaturated particulate materials, including: glass beads, a mixture of kaolinite and glass beads to increase the surface area, granite powder, and natural sand. Among their significant conclusions include:

- The contribution of capillarity to interparticle forces involves not only matric suction (i.e., negative pore-water pressure), but the surface tension force along the edge of menisci as well.

- The "equivalent effective stress" due to capillary forces increases with decreasing water content, decreasing particle size, and increasing coordination. Specific surface is a meaningful parameter in the characterization of unsaturated soils.

- There are other factors in real soils that increase stiffness and strength at low saturation. As water dries, fines migrate to contacts, and form buttresses between larger particles. These buttresses increase the stiffness of the granular skeleton formed by the courser grains. At the same time, the ionic concentration in the pendular water increases and eventually reaches saturation causing the precipitation of salt crystals between the two contacting particles. Salt precipitation also increases the stiffness of the particulate skeleton. However, when specimen is re-saturated by flooding, the shear wave velocity drops to its initial value.

- Shear waves permit studying the evolution of effective interparticle forces. This is particularly valuable in the pendular regime where direct measurement of the negative pore-water pressure is not feasible. Figure 2-1 shows the results of small-strain stiffness studies of slowly drying freshly remolded unsaturated soils. It should be noted from the

Figure 2-1 C that when the specimen is re-saturated by soaking, the shear wave velocity drops to its initial values (square points). This result suggests that the light cementation that develops during drying disappears upon wetting. It should also be noted that significant stiffness changes occur with drying, even for mixture of uniform glass beads and water (Figure 2-1 A).

- The strain at menisci failure decreases with the decrease in water content. Unless the water content is extremely small, menisci will fail at strains greater than the threshold strain of the soil; therefore, partial saturation is a stabilizing force for the soil skeleton. On the other hand, small menisci may fail before the strain at peak strength of soils (depending on the degree of saturation). Thus, capillary forces at low water contents cause an increase in the small-strain stiffness of soils, but may not contribute to the peak strength.

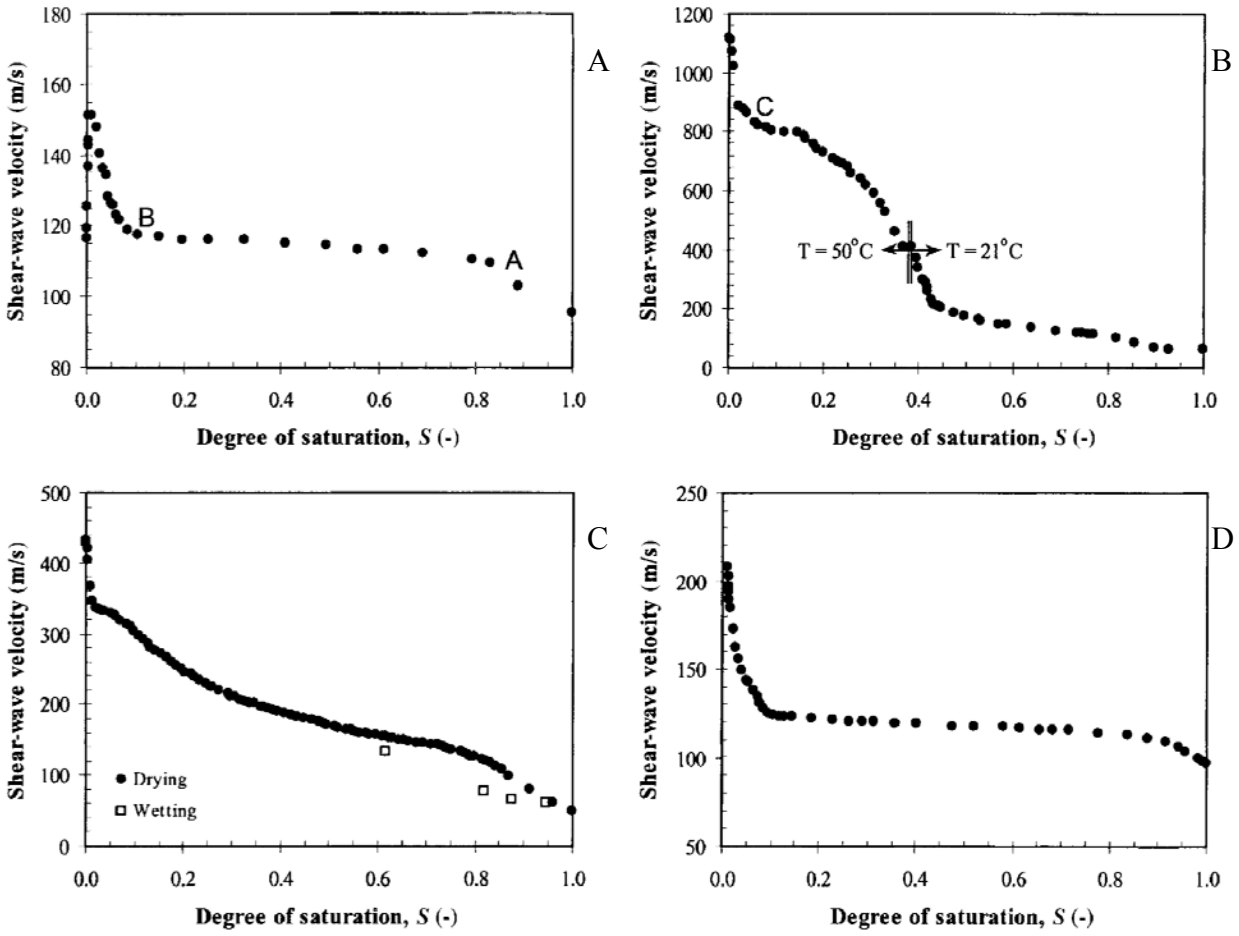

Figure 2-1. Variation of Shear-Wave Velocity with Degree of Saturation for Different Materials. A) Clean Glass Beads (De-ionized Water). B) Mixture of Kaolinite and Glass Beads. C) Granite Powder. D) Sandboil Sand (Cho and Santamarina [2001]).

CHAPTER 3
MATERIALS

3.1 Source and Mineralogy

For this study, base course aggregates from five (5) aggregate sources (mines) were selected from those commonly used in Florida to study the effects of moisture and time on stiffness properties. Mines from Newbery (Mine # 26-002), Ocala (Mine # 36-246), and Miami (Mine # 89-090) were chosen to represent limerocks from northern, central, and southern Florida, respectively. In addition, a limestone-based shell rock from Loxahatchee, FL (Mine # 93-406), and a granite-based graded aggregate from Georgia (Mine # GA 178) were included in the study. Approximate source locations are depicted in Figure 3-1.

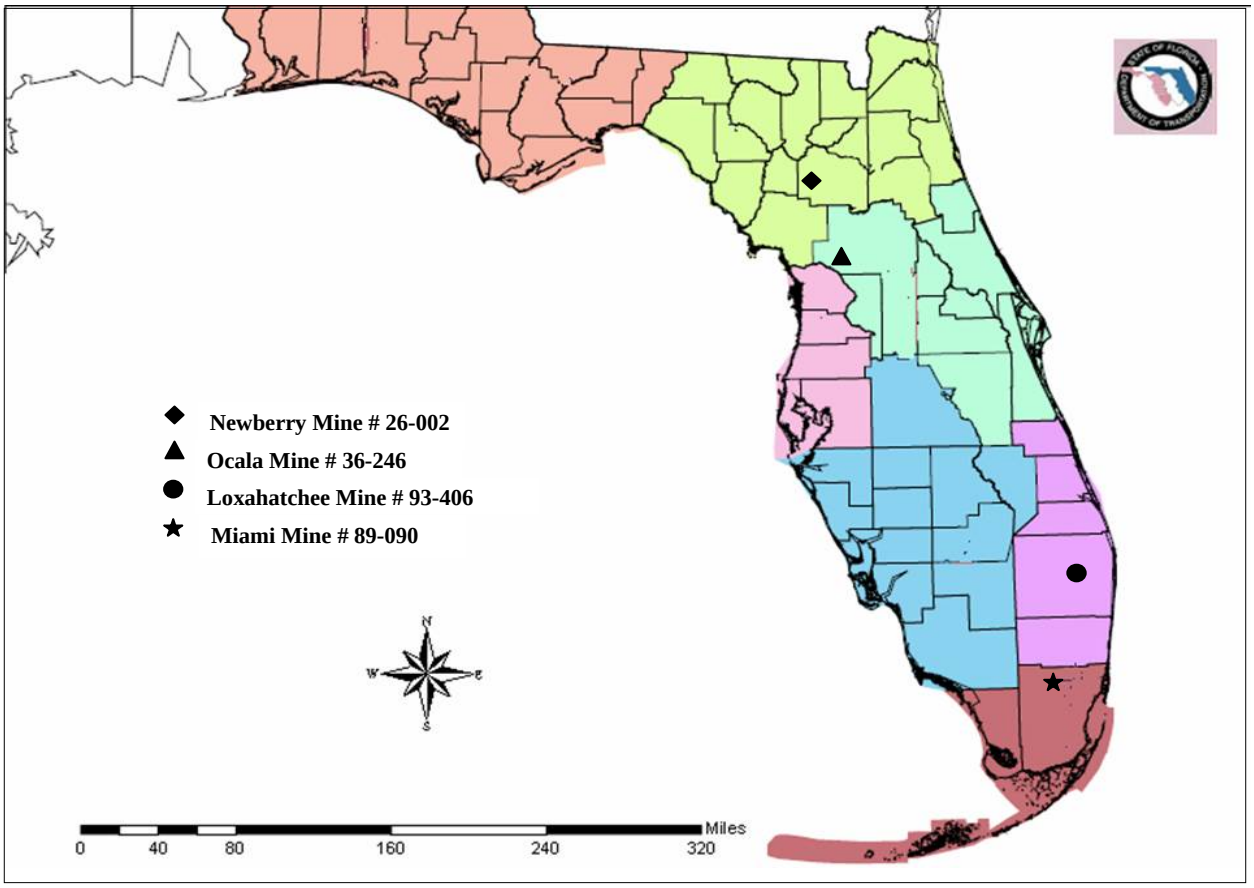

Figure 3-1. Approximate locations of Florida aggregate sources (FDOT homepage, SMO, geotechnical materials system, aggregate acceptance source maps)

The Florida base course materials referred to in this study as Ocala, Loxahatchee, Miami, and Newbery, are the from Ocala formation, Anastasia formation Coquina, Miami Oolite (Ft. Thompson formation), and Ocala formation, respectively. The appropriate mineralogy of these materials is depicted in Table 3-1.

Table 3-1. Mineralogy of base course materials (McClellan et al. [2001]).

Material	Mine No	Material Type	Formation (%)	Calcite (%)	Quartz (%)	Aragonite (%)
Ocala	36-246	Limerock	Ocala	100	---	---
Loxahatchee	93-406	Shell-Rock	Shelly sediments	38.5	37.4	24.6
Miami	87-090	Limerock	Ft. Thompson	76	18.5	---
Newberry	26-002	Limerock	Ocala	100	---	---

According to Florida Department of Environmental Protection:

The Ocala Limestone consists of white to cream, Upper Eocene marine limestones and occasional dolostones. Generally, the Ocala limestone is soft and porous, but in places, it is hard and dense because of cementation of the particles by crystalline calcite. The deposit is remarkable in that it is composed of almost pure calcium carbonate: shells of sea creatures and very tiny chalky particles. Ocala Limestone underlies almost all of Florida, but it is found at the surface of the land only in a small portion of the state. Fossils present in the Ocala Limestone include abundant large and smaller foraminifers, echinoids, bryozoans, mollusks, and rare vertebrates (Florida Department of Environmental Protection Homepage, Florida Geological Survey, Geology Topics; Ocala Limestone). The picture depicted in Figure 3-2 A is a representation of the Ocala Limestone.

The Miami Limestone (formerly the Miami Oolite) is a Pleistocene marine limestone. It occurs at or near the surface in southeastern peninsular Florida from Palm Beach County to Dade and Monroe Counties, and in the keys from Big Pine Key to the Marquesas Keys. The Miami limestone consists of two facies: an oolitic facies and a bryozoan facies. The oolitic facies

consists of white to orangish gray, oolitic limestone with scattered concentrations of fossils. Ooliths are small rounded grains so named because they look like fish eggs. Ooliths are formed by the deposition of layers of calcite around tiny particles, such as sand grains or shell fragments. The bryozoan facies consists of white to orangish gray, sandy, fossiliferous limestone. Beds of quartz sand and limey sandstones may also be present. Fossils present include mollusks, bryozoans, and corals. An excellent exposure is observable at Alice Wainright Park, in Coral Gables, Dade County (Florida Department of Environmental Protection Homepage, Florida Geological Survey, Geology Topics; Miami Limestone). The picture depicted in Figure 3-2 B is a representation of the Miami Limestone.

The Loxahatchee shell-rock is shelly sediments of Plio-Pleistocene age from the Tertiary/Quaternary period.

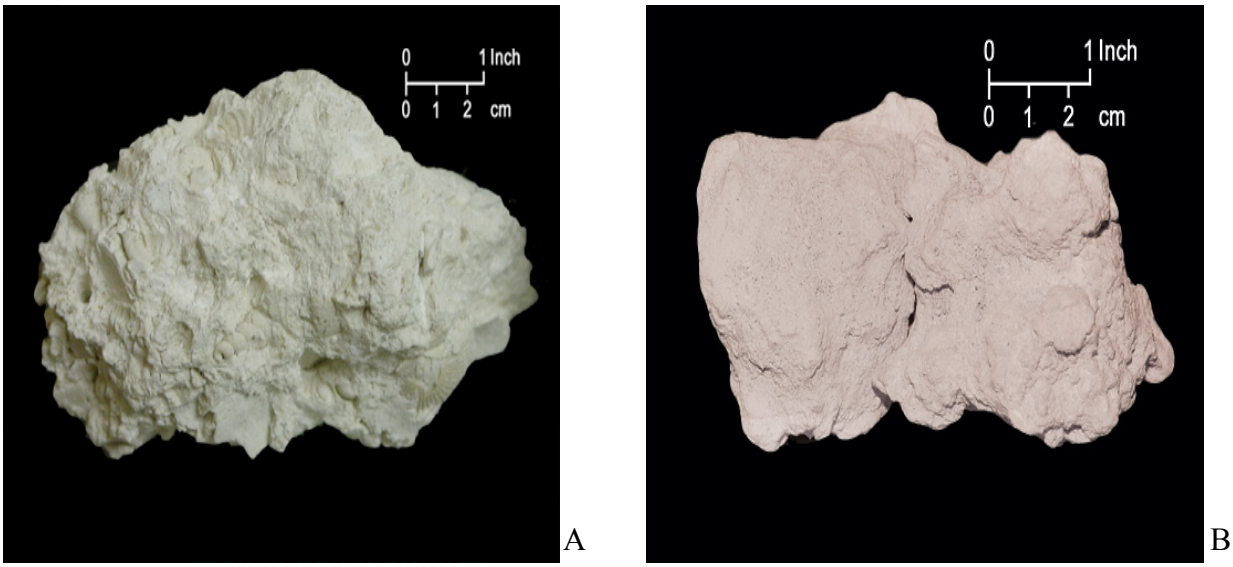

Figure 3-2. Representation of soil samples. A) The Ocala limestone. B) The Miami limestone. (Florida department of environmental protection homepage, Florida geological survey; geology topics)

3.2 Materials Collection and Characterization

To initiate the laboratory study, samples of the materials selected were provided by the FDOT-SMO. The SMO determined and provided typical index parameters, including proctor

density, grain size analysis via sieve and hydrometer, specific gravity, and Atterberg limits. Sampling of aggregates was done following the Florida Methods 1 (FM 1) T-002 that is similar to AASHTO T2. The samples were collected from aggregate stockpiles utilizing a rubber wheeled front-end loader. A sampling location on the stockpile was chosen to represent the area being sampled so that the composite sample is representative of overall stockpile. The loader removed material from the bottom of the pile perpendicular to the direction of the stockpile that was created by dumping. Materials are removed from the face of the stockpile in order to obtain a representative sample. Three buckets of material were scooped from the middle, left and right of the stockpile, respectively. The material was scooped with the front-end loader bucket from approximately 1½ feet above the ground and the material was scooped with a bucket parallel with the face of the stockpile. The bucket full of material was gently lowered from 3 to 4 feet to produce the mini sample-pile. Three mini sample-piles were created and laid side by side. The upper 1/2 to 1/3 of the mini stockpiles was back bladed with the bucket's edge to expose the center mass to be sampled. With a square-tipped shovel the material from the center of the mini stockpiles was scooped and filled into bags.

Following transport to the laboratory, the collected bags of samples were placed into a thermostatically controlled drying oven at a temperature of 110 ºF until the samples were friable. The air-dried materials were removed from the oven and put on benches in laboratory to cool down, followed by laboratory determination of index parameters.

Sieve analysis of fine and course aggregates was performed following the procedures in AASHTO T27. Gradation of materials finer than 2 mm (No. 10) sieve was performed via hydrometer test following the procedures in AASHTO T88. The grain size distribution graph of material collected from the 1st mini-stockpile of each source is depicted in Figure 3-3. Refer to

Appendix A for the grain size distribution graphs of materials collected from the 2nd and 3rd mini-stockpiles of each source.

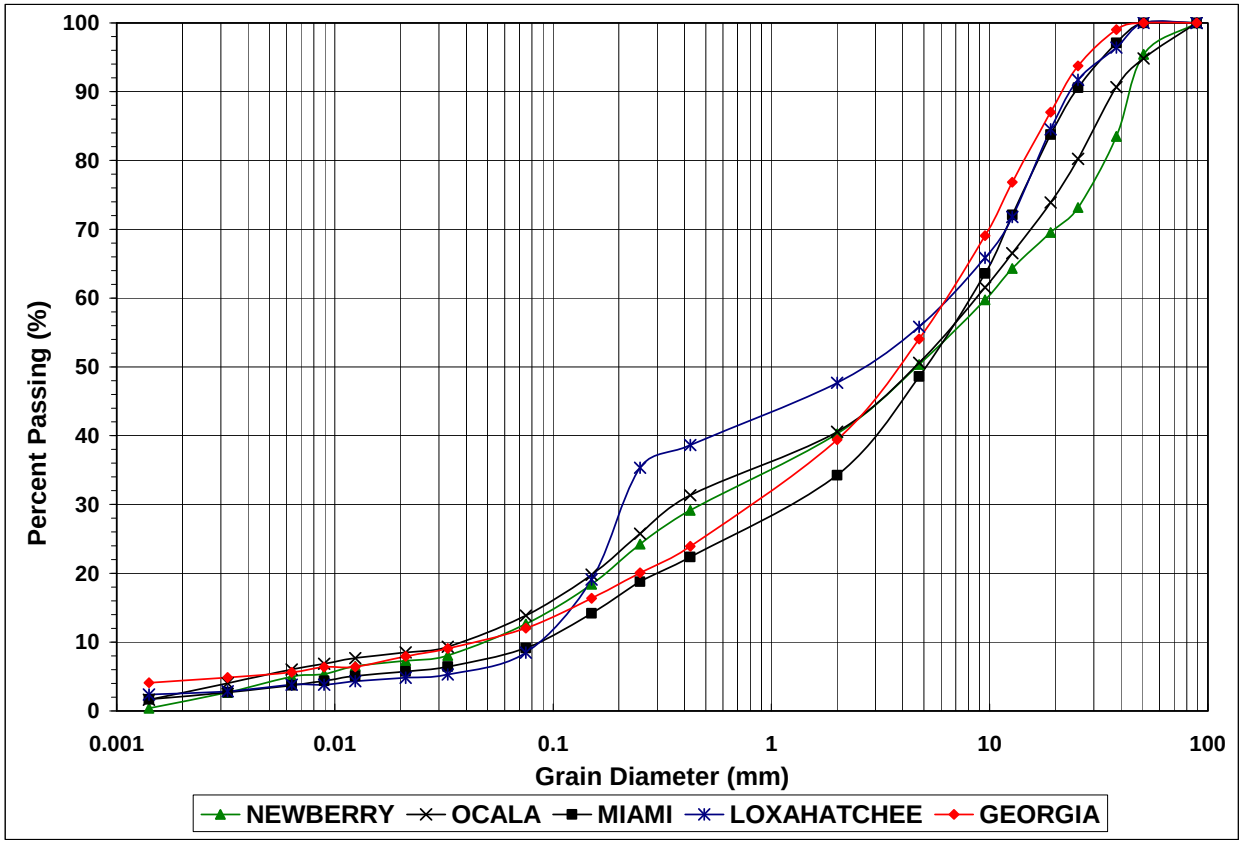

Figure 3-3. Grain size distribution of materials collected from the 1st mini-stockpiles of each source.

Determination of specific gravity of fine aggregates and course aggregate were performed following the FM 1 T-084 and T-085, which is similar to AASHTO T084 and T085 procedures, respectively.

Determination of the plastic limit and plasticity index of the soils was performed following the AASHTO T90, and the liquid limit of the soils was determined following the AASHTO T89.

Table 3-2 summarizes results for several of the index parameters for material collected from the 1st mini-stockpile of each source. Refer to Appendix A for the summarized material parameters collected from the 2nd and 3rd mini-stockpiles of each source.

Table 3-2. Material parameters of 1st mini-stockpile (replicate)

Parameter	Material				
	Georgia Granite	Loxahatchee Shell Rock	Miami Limerock	Newberry Limerock	Ocala Limerock
Unified Classification	GW-GM	GP-GM	GW-GM	GM	GM
D_{50} (mm) Mean Grain Size	3.90	2.70	5.10	4.80	4.80
D_{10} (mm) Effective Grain Size	0.045	0.088	0.088	0.05	0.05
Cu-The Uniformity* Coefficient	144.4	73.9	93.2	192	176
Cz-The Coefficient of Curvature**	2.30	0.08	2.34	0.48	0.29
Specific Gravity	2.700	2.709	2.707	2.720	2.720
Void Ratio at Optimum***	0.186	0.400	0.282	0.457	0.397
Plastic Limit	NP	NP	NP	NP	NP
Plasticity Index	NP	NP	NP	NP	NP
Liquid Limit	NP	NP	NP	NP	NP

* $Cu=D_{60}/D_{10}$

** $Cz=(D_{30})^2/D_{60}D_{10}$

*** Void ratio $(e)=((V-(W_s/G_s*\gamma_w))/(W_s/G_s*\gamma_w))$

where: V = the volume of the sample

G_s = specific gravity

W_s=weight of the soil

γ_w = unit weight of water

CHAPTER 4
EXPERIMENTS

4.1 Free-Free Resonant Column Testing

4.1.1 Introduction

Poisson's ratio, thickness, and modulus of pavement materials in layered systems are fundamental parameters affecting pavement performance; hence, these parameters are utilized to characterize the behavior of the pavement materials. These fundamental parameters are essential for a mechanistic-based design procedure and for realistic performance-based specifications, therefore these fundamental parameters should be measured accurately, and the effect of environmental conditions on the parameters should be quantified (Nazarian et al. [2002]).

In this research, the FFRC testing method (Kalinski and Thummaluru [2005]; Kim, Kweon, and Lee [1997]; Kim and Stokoe [1992]; Menq [2003]; Nazarian, Yuan, and Aellano [2002]) was used to determine the stiffness properties of Florida limerock base materials with time and under various environmental conditions. This test measures the small strain elastic modulus of the material, and the test can be conducted very quickly on specimens of material commonly compacted in a laboratory. Further, the FFRC test is nondestructive, and thus can be conducted many times on the same specimen after various types of conditioning, e.g., aging, drying, and wetting.

Two different types of stress wave measurements can be conducted on a solid rod with FFRC testing: resonance measurements and direct-arrival measurement. Since the dimensions of the specimen are known, if the resonant frequencies can be determined, the unconstrained modulus of the material can readily be determined using principles of wave propagation in a solid rod (Richart et al. [1970]). Figure 4-1 A shows a typical frequency response spectrum of the FFRC test on a cylindrical specimen of Florida limerock. In addition, if the direct arrivals can

be measured, the constrained modulus can be determined. Figure 4-1 B shows a typical instant time (direct-arrival) measurement of the FFRC test on a cylindrical specimen of Florida limerock.

4.1.2 Constrained Compression Wave Velocity and Constrained Compression Modulus

Once the cylindrical specimen is excited along the center axis, the travel time of the constrained compression wave is determined via the direct-arrival measurement. The constrained compression wave velocity, v_p, is calculated as

$$v_p = \frac{\ell}{\Delta t} \tag{4-1}$$

where: ℓ = the length of the specimen,

Δt = the measured travel time of constrained compression wave (see Figure 4-1 B).

With known constrained compression wave velocity, v_p, and the unit mass of the specimen, ρ, the small-strain constrained modulus, M, can be calculated as

$$M = \rho v_p^{\,2} = \rho\left(\frac{\ell}{\Delta t}\right)^2 \tag{4-2}$$

4.1.3 Unconstrained Compression Wave Velocity and Young's Modulus

There are three primary types of resonant vibrations that can occur in a solid cylindrical rod: longitudinal, torsional, and flexural. Resonant measurements using longitudinal waves represent a good way of measuring dynamic properties of soils, and this type of resonant measurement was used in this study. If an impulse load is applied to one end of a cylindrical specimen, seismic energy over a large range of frequencies will propagate within the specimen. The seismic energy depends on the dimensions, and the stiffness of the soil is associated with one or more frequencies. These ensnared frequencies resonate and propagate within the soil specimen.

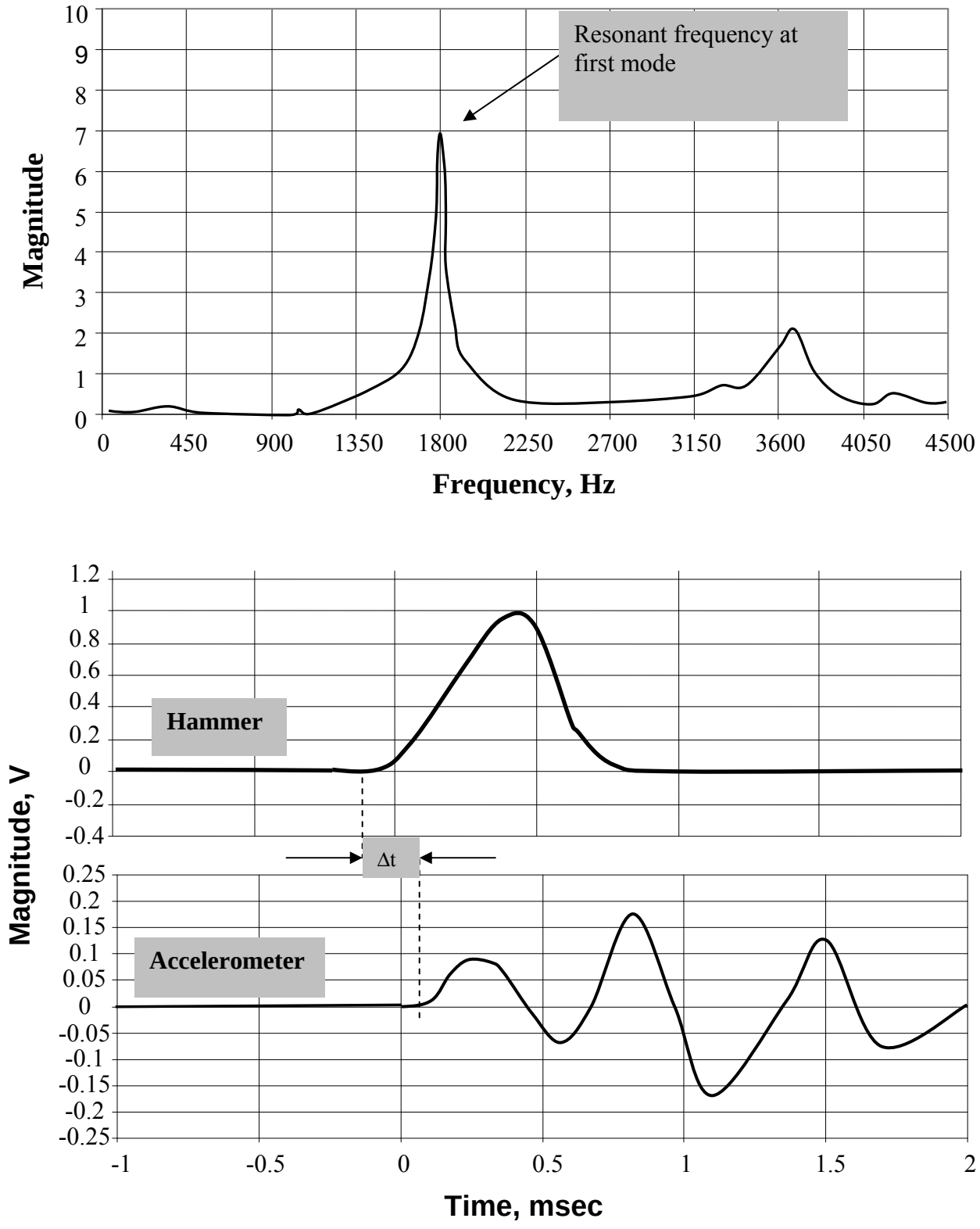

Figure 4-1. Typical Florida limerock frequency response, and instant time (direct-arrival) measurements.

The equation of motion of longitudinal waves can be expressed with the following partial-differential equation:

$$\frac{\partial^2 u}{\partial t^2} = \nu_c{}^2 \frac{\partial^2 u}{\partial x^2} \tag{4-3}$$

where: u = displacement of the element in along the axis direction,

ν_c = unconstrained compression wave velocity,

x = coordinate,

t = time.

For various boundary conditions, other solutions to the wave equations can be written as a trigonometric series, which describes the shape of a solid rod vibrating in a natural mode (Richart et al. [1970]):

$$u = U(\xi_1 \cos \omega_n t + \xi_2 \sin \omega_n t) \tag{4-4}$$

where: U = the displacement amplitude along the axis direction

ξ_1, ξ_2 = constants

Substituting Eq. 4.4 into Eq. 4.3 and evaluating the new equation gives:

$$U = \xi_3 \cos \frac{\omega_n x}{\nu_c} + \xi_4 \sin \frac{\omega_n x}{\nu_c} \tag{4-5}$$

In the FFRC test, the cylindrical specimen is suspended in the air using flexible straps and the boundary conditions are free at both ends as depicted in Figure 4-2 A. Therefore, for the cylindrical specimen of length l, the stress and the strain on the end planes are zero. The first three longitudinal resonant modes are depicted in Figure 4-2 B. Considering that $dU/dx = 0$ at x = 0 and at x = l:

$$\frac{dU}{dx} = \frac{\omega_n}{\nu_c}\left(-\xi_3 \sin \frac{\omega_n x}{\nu_c} + \xi_4 \cos \frac{\omega_n x}{\nu_c} \right) = 0 \tag{4-6}$$

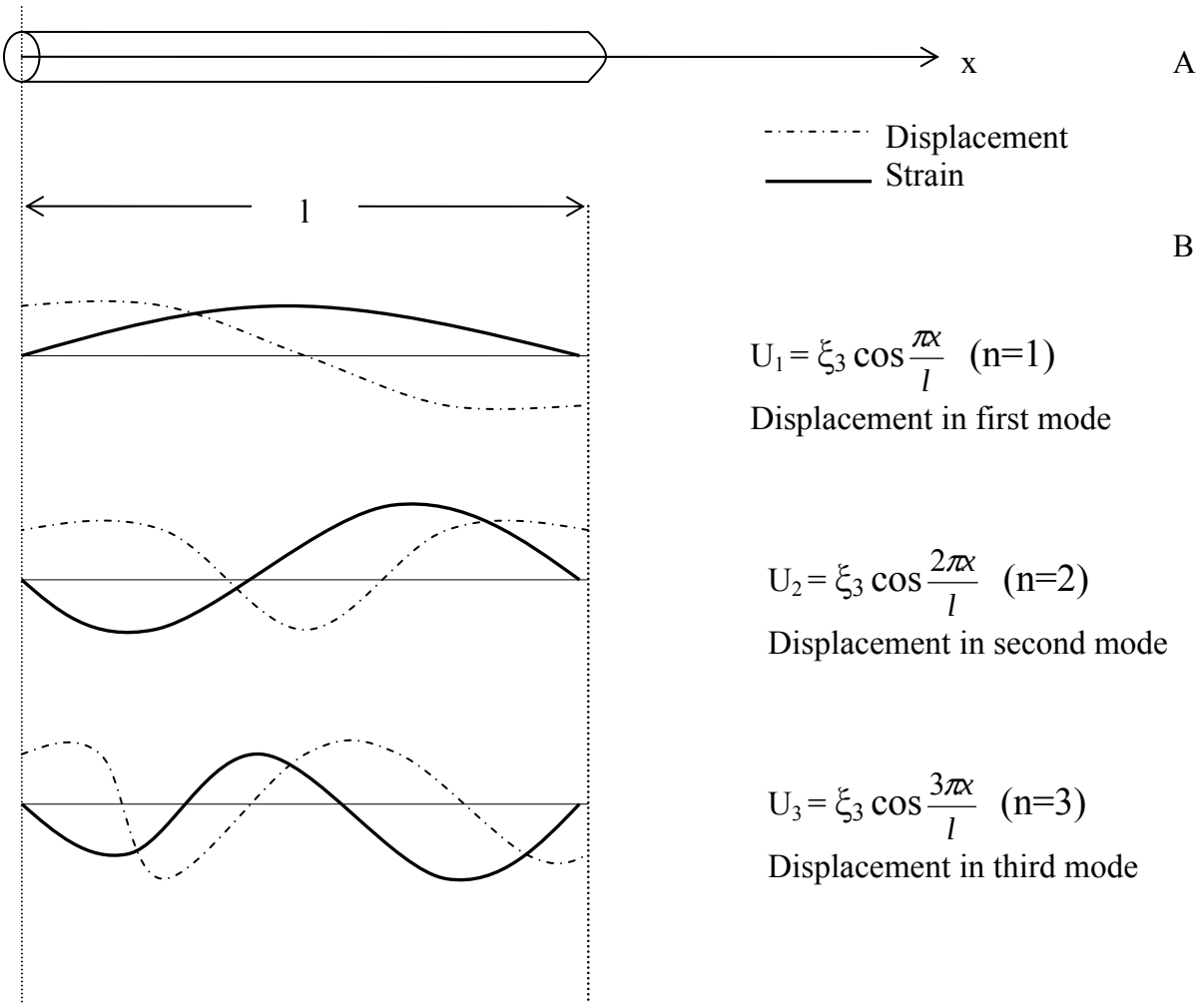

Figure 4-2. Displacement and strain amplitudes of a cylindrical specimen with free boundary conditions at both ends at the first three longitudinal resonant modes (Richart et al. [1970], Menq [2003]).

If Eq. 4-6 is evaluated at x = 0, we get $\xi_4 = 0$, and at x = l, and assuming a non trivial solution ($\xi_3 \neq 0$), we get (Richart et al. [1970]):

$$\omega_n = \frac{n\pi v_c}{\ell}, \quad \text{n = 1, 2, 3 …} \qquad 4\text{-}7$$

If a longitudinal impulse load is applied to a free-free cylindrical specimen in the first mode of vibration and the frequency f_n is measured, the unconstrained compression wave velocity can be calculated from Eq. 4-7 as follows:

$$\omega_n = 2\pi f_n = \frac{n\pi v_c}{\ell}, \text{ for n = 1 (first mode)} \quad 4\text{-}8$$

Evaluating Eq. 4-8, we get the unconstrained compression wave velocity:

$$v_c = 2 f_n \ell \quad 4\text{-}9$$

With known unconstrained compression wave velocity, v_c, and the unit mass of the specimen, ρ, the small-strain Young's modulus, E, can be calculated using the following equation:

$$E = \rho(2 f_n \ell)^2 \quad 4\text{-}10$$

Once the constrained and unconstrained wave velocities are determined, Poisson's ratio can be calculated from the combination of both as (Richart et al. [1970], Menq [2003]):

$$\upsilon_{ME} = \frac{1-\left(\frac{v_p}{v_c}\right)^2 + \sqrt{\left(\left(\frac{v_p}{v_c}\right)^2 - 1\right)^2 + 8\times\left(\frac{v_p}{v_c}\right)^2\left(\left(\frac{v_p}{v_c}\right)^2 - 1\right)}}{4\times\left(\frac{v_p}{v_c}\right)^2} \quad 4\text{-}11$$

where: υ is Poisson's ratio

With Poisson's ratio known, if deemed necessary the shear modulus of the specimen can be calculated from the Young's modulus or constrained modulus as (Richart et al. [1970]):

$$G = \frac{E}{2(1+\upsilon)} \quad 4\text{-}12$$

$$G = \frac{2M\upsilon - M}{2(\upsilon - 1)} \quad 4\text{-}13$$

4.1.4 Free-Free Resonant Column Equipment Setup

The FFRC testing system consists of several components (Figure 4-3), a dynamic signal analyzer (DSA) or (oscilloscope), an instrumented impact hammer (Figure 4-3 B), and an

accelerometer (transducer) (Figure 4-3 C). The specimens are oriented horizontally and suspended with flexible straps to achieve free-free boundary conditions (Figure 4-3 A). The basic operational principal is to generate a compression wave with an instrumented hammer at one end of the specimen, and monitor the response from the other end of the specimen with the piezoelectric accelerometer (Figure 4-3 D). The output signals from the accelerometer and hammer are recorded with a signal analyzer, which performs data acquisition and signal processing.

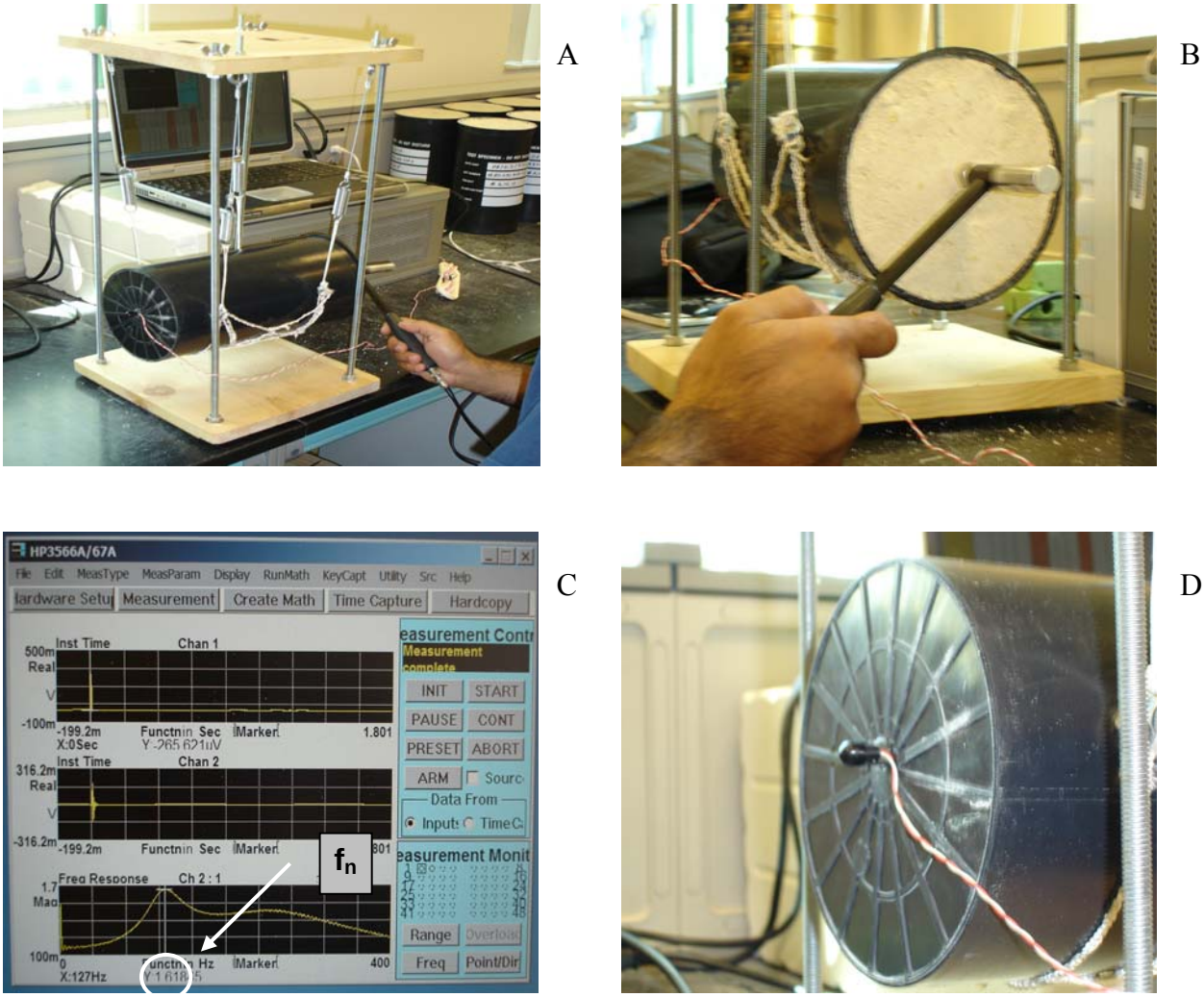

Figure 4-3. Free-free resonant column test equipment and setup. A) Overall setup. B) Instrumented impact hammer. C) Data acquisition. D) Piezoelectric accelerometer.

In the seismic tests, the locations of the accelerometer and impact on the specimen ends have negligible or no effect on the resonant frequencies, but the amplitude associated with each resonance varies with these parameters. Even though the amplitudes are not as important as the frequency at the peak amplitude, the appropriate locations should be chosen for a more strong result (Nazarian et al. [2002]). After a series of tests conducted, the best test setup observed was when the excitation is applied near the center of the specimen, and the location of the accelerometer works best when it is placed on the same half of the specimen as the source, but not beyond two third-radius out from the center (Nazarian et al. [2002]). Following these recommendations and studies, the accelerometer used in this study was glued to the center of one end of the specimen. For higher repeatability and better results, a gentle impact of the instrumented hammer was applied as close to the center as possible.

Following initial equipment setup, the FFRC system was subjected to verification tests using synthetic samples. Three cylindrical synthetic specimens were used ranging approximating from very soft sub-grade soil to that of a sub-base material (Durometer: A60, A95, D75, soft to stiff, respectively).

These synthetic specimens were composed of polypropylene and polyurethane components, and were selected to provide a range of stiffness typical of soil and base materials. These materials are known to be durable, tough, and have a high resistance to abrasion, ozone, radiation, weather, and oxygen. S. Nazarian agreed to independently test the same samples at University of Texas at El Paso facilities to corroborate the results determined with the Florida system. Table 4-1 shows the negligible differences between the University of Florida and University of Texas at El Paso FFRC testing system.

Table 4-1. The FFRC test results of synthetic specimens.

	A60	A95	D75
University of Florida, 1st mode Resonant Frequency (Hz)	128	670	1544
University of Texas–El Paso, 1st mode Resonant Frequency (Hz)	125	680.5	1546

4.1.5 Free-Free Resonant Column Environmental Conditioning

In order to observe, quantify, and document the influence of time and environmental conditions on the stiffness behavior of Florida base materials, the base materials were subjected to the following environmental conditions:

Ambient Condition: There were two ambient conditions: laboratory ambient condition and outdoor ambient condition. In laboratory ambient, the specimens were stationed on benches inside the laboratory (Figure 4-4 A), and were exposed to the laboratory ambient air. In outdoor ambient, the specimens were stationed on benches outside the laboratory (Figure 4-4 B), and were exposed to the natural environmental conditions. In both cases, the specimens remained in plastic cylinder molds. Immediately prior to resonant column testing, the specimen weight was monitored to determine the concurrent moisture content and unit mass of the specimen (ρ). The resonant column testing was monitored periodically as appropriate.

Constant Moisture: In constant moisture environmental conditioning, the specimens were exposed to a moist, nearly 100% humidity condition in a curing room to maintain the optimum moisture content level of each specimen (Figure 4-4 C). The specimens remained in cylindrical molds, and the open end of the specimen was sealed to avoid the penetration of water vapors into the specimen, which could significantly alter the moisture content of the specimen (Figure 4-4 D). Immediately prior to each resonant column testing of the specimen, weight was monitored to determine the concurrent moisture content and unit mass of the specimen (ρ). The resonant column testing was monitored periodically as appropriate.

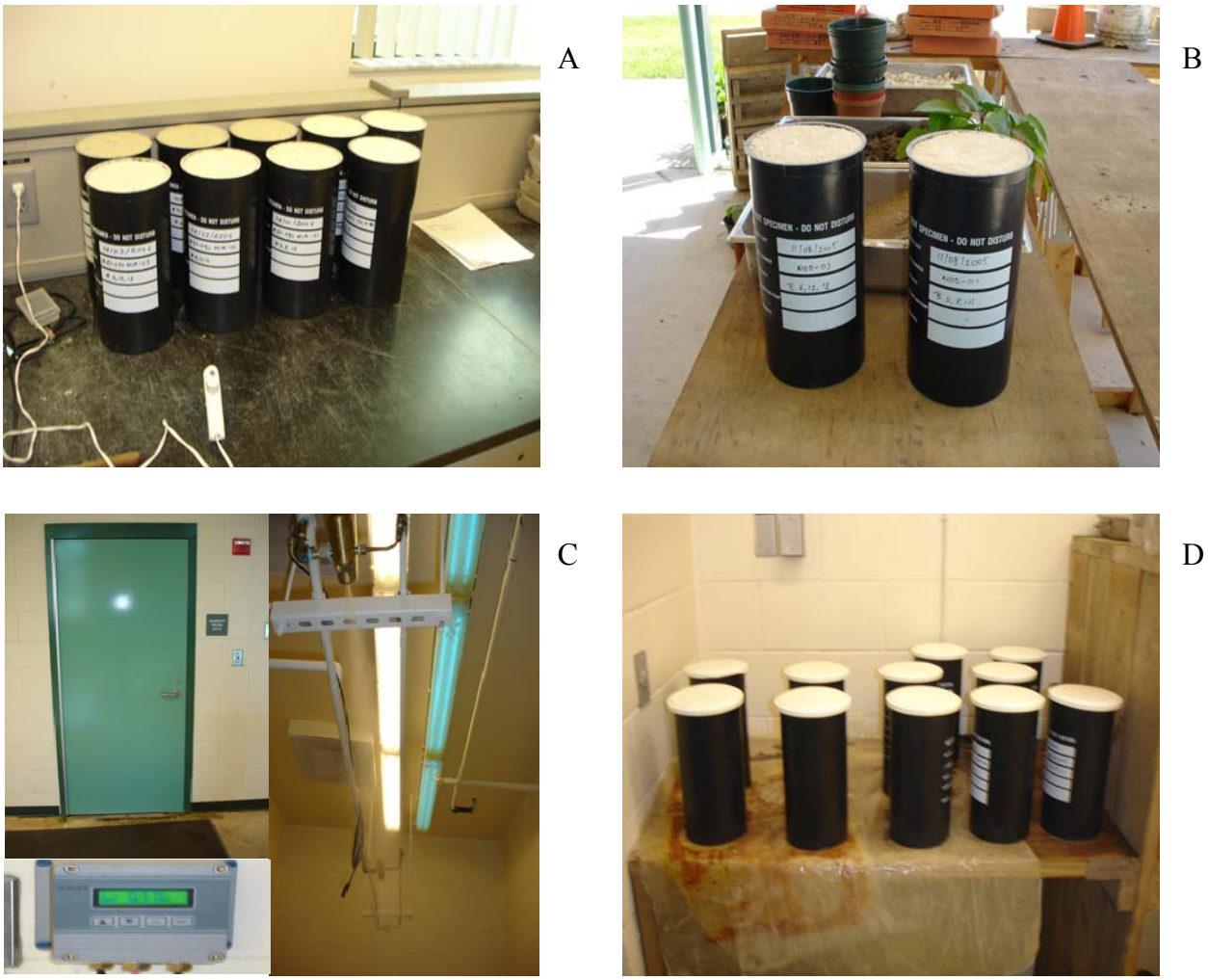

Figure 4-4. Ambient conditions. A) Laboratory ambient. B) Outdoor ambient. C) Constant moisture curing room. D) Sealed specimens.

Oven Drying: In oven drying, the specimens remained in cylindrical molds and were placed in a thermostatically controlled industrial oven (Figure 4-5 A) at 110 ºF (Figure 4-5 B) and subjected to air-drying. Immediately prior to each resonant column testing of the specimen, weight was monitored to determine the concurrent moisture content and unit mass of the specimen (ρ). The resonant column testing was monitored periodically as appropriate.

Wetting: The cylindrical plastic molds that were used for wetting were prepared by drilling holes with a diameter of 1/16-inch in a uniform manner around the base of the mold in 0.5-inch interval, and the holes were placed 0.25-inch above the base of the mold (Figure 4-6 A). The

specimens remained in plastic cylindrical molds and were placed in soaking tank, a rectangular tank approximately 26 inches in width x 60 inches in length x 10 inches in diameter (Figure 4-6 B). The water depth was maintained at 5 inches with the samples in place to allow water access through the perforated molds. Immediately prior to each resonant column testing of the specimen, weight was monitored to determine the concurrent moisture content and unit mass of the specimen (ρ). The resonant column testing was monitored periodically as appropriate.

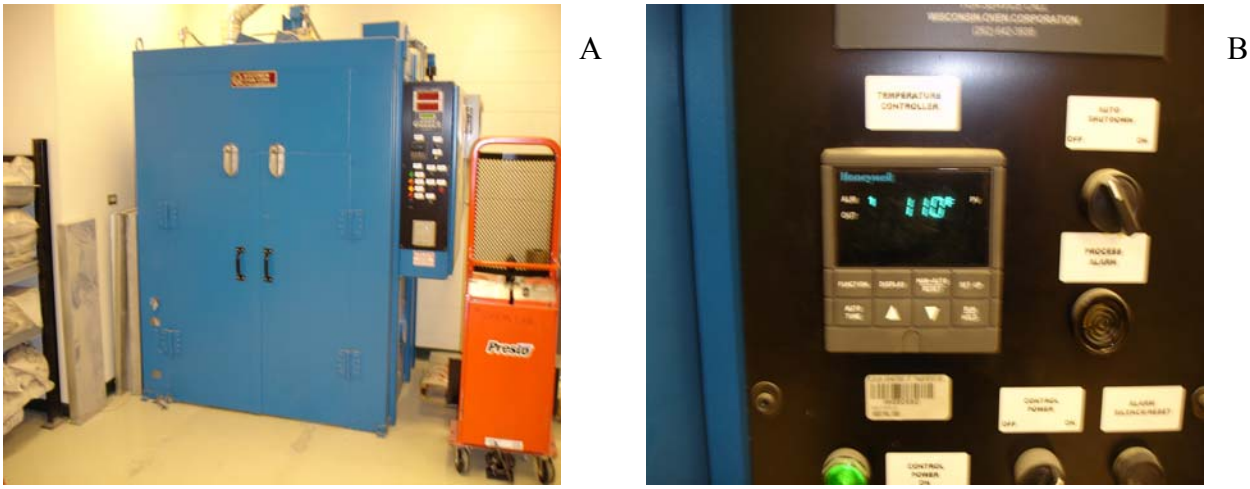

Figure 4-5. Oven drying. A) Industrial air-drying oven. B) Thermostat.

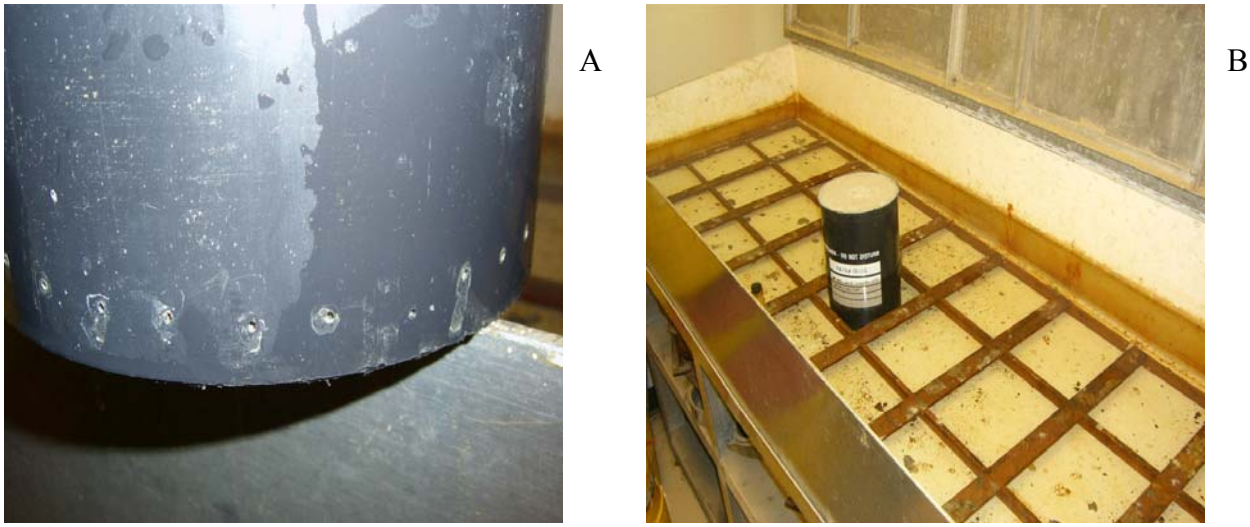

Figure 4-6. Wetting. A) Perforated mold. B) Soak tank.

4.1.6 Specimen Preparation

The material that came from the quarry was placed into oven to be air dried until it became friable. Material with particle sizes greater than ¾ - inch was crushed so that the entire sample passed the ¾ - inch sieve by use of a mechanical jaw crusher. The pieces that have not been reduced to the desired size by the mechanical crushing were broken down manually until they passed the ¾ - inch sieve.

The materials were separated into portions matching the mini stockpiles from which they were collected. Each of the separate portions was thoroughly mixed with amounts of water to reach the optimum moisture content. The samples of soil-water mixtures were placed in nylon-covered containers. Immediately prior to the compaction of the materials, representative samples weighing at least a pound were taken for moisture content determination.

Three replicates of each material were compacted within 6 inch x 12 inch plastic cylinder molds placed and clamped within a split steel mold (Figure 4-7 A). Material was placed in twelve lifts in 1-inch layers; the material was scarified after every other compacted 1-inch layer, allowing the compacted layer to bond with fresh poured material. Each layer was compacted with 56 uniformly distributed blows from a10-lb rammer, dropping free from a height of 18 inch above the approximate elevation of each finally compacted layer (Figure 4-7 B). Following compaction, the outer split mold was removed, leaving the compacted specimen within the plastic mold. Table 4-2 shows the number of compacted samples per material. Comparisons of specimen unit weights with those from Proctor tests indicated that this procedure produced specimens of maximum dry density. Table 4-3 shows the measured and targeted specimen preparation parameters for FFRC testing. Following construction, specimens of each material were exposed to one of four environmental conditions.

A

B

Figure 4-7. Specimen preparation and equipment. A) 6 inch x 12 inch plastic cylindrical mold and split steel mold. B) Compactor.

Table 4-2. Number of compacted samples per material.

Environmental Conditioning	Material Georgia Granite	Loxahatchee Shell-rock	Miami Limerock	Newberry Limerock	Ocala Limerock
Outdoor Ambient *	NA	NA	NA	3	NA
Laboratory Ambient	3	3	3	3	1**
Constant Moisture	3	3	3	3	3
Wetting-Drying Cycle	3	3	3	3	3

*Following the initial FFRC testing on Newberry materials, comparison results of outdoor ambient and laboratory ambient environmental conditioning showed negligible differences, therefore construction of specimens for outdoor ambient environmental conditioning of other sources was deemed unnecessary.

** Due to insufficient material, only one (1) replicate of Ocala limerock for laboratory ambient environmental conditioning was prepared.

Table 4-3. The FFRC testing target and measured specimen preparation parameters.

Source	Conditioning	Sample	Moisture Content		Dry Density	
			Target %	Measured %	Target pcf	Measured pcf
LOXAHATCHEE	Constant Moisture	Replicate 1	9.8	10.95	122.0	120.30
		Replicate 2	10.3	9.88	121.3	119.39
		Replicate 3	9.9	9.98	122.5	122.03
	Laboratory Ambient	Replicate 1	9.8	10.30	122.0	121.80
		Replicate 2	10.3	9.80	121.3	121.30
		Replicate 3	9.9	9.98	122.5	120.78
	Wetting & Drying	Replicate 1	9.8	11.09	122.0	120.25
		Replicate 2	10.3	10.24	121.3	120.69
		Replicate 3	9.9	10.49	122.5	121.03
MIAMI	Constant Moisture	Replicate 1	8.0	8.42	129.6	130.99
		Replicate 2	7.2	7.89	130.4	132.08
		Replicate 3	8.0	8.11	130.6	131.38
	Laboratory Ambient	Replicate 1	8.0	8.13	129.6	131.19
		Replicate 2	7.2	8.01	130.4	131.67
		Replicate 3	8.0	7.86	130.6	132.36
	Wetting & Drying	Replicate 1	8.0	7.97	129.6	131.39
		Replicate 2	7.2	8.21	130.4	130.63
		Replicate 3	8.0	8.17	130.6	131.95
GEORGIA	Constant Moisture	Replicate 1	4.8	5.51	142.3	144.08
		Replicate 2	4.8	5.56	142.8	143.85
		Replicate 3	5.0	5.14	142.5	143.59
	Laboratory Ambient	Replicate 1	4.8	5.40	142.3	143.92
		Replicate 2	4.8	5.25	142.8	143.55
		Replicate 3	5.0	5.12	142.5	144.11
	Wetting & Drying	Replicate 1	4.8	5.41	142.3	143.92
		Replicate 2	4.8	5.36	142.8	144.69
		Replicate 3	5.0	5.46	142.5	144.31

Table 4-3. Continued.

Source	Conditioning	Sample	Moisture Content		Dry Density	
			Target %	Measured %	Target pcf	Measured pcf
NEWBERRY	Constant Moisture	Replicate 1	13.0	12.51	116.5	115.78
		Replicate 2	12.5	12.70	116.1	116.31
		Replicate 3	13.0	12.61	115.9	116.25
	Outdoor Ambient	Replicate 1	13.0	12.70	116.5	116.21
		Replicate 2	12.5	12.49	116.1	115.80
		Replicate 3	13.0	12.48	115.9	115.98
	Laboratory Ambient	Replicate 1	13.0	12.68	116.5	117.03
		Replicate 2	12.5	12.60	116.1	116.08
		Replicate 3	13.0	12.57	115.9	116.11
	Wetting & Drying	Replicate 1	13.0	12.68	116.5	117.07
		Replicate 2	12.5	12.41	116.1	116.55
		Replicate 3	13.0	12.63	115.9	115.84
OCALA	Constant Moisture	Replicate 1	10.9	10.99	120.1	120.67
		Replicate 2	11.1	11.08	120.2	120.77
		Replicate 3	11.3	11.22	120.4	120.93
	Laboratory Ambient	Replicate 1	11.1	11.06	120.2	121.25
		NA	NA	NA	NA	NA
		NA	NA	NA	NA	NA
	Wetting & Drying	Replicate 1	10.9	11.15	120.1	121.56
		Replicate 2	11.1	11.20	120.2	121.57
		Replicate 3	11.3	11.26	120.4	121.51

4.1.7 Core Materials

FDOT SMO provided two intact field cores (Figure 4-8 A) drilled out from actual road sections constructed in March 1996. Both field cores were Miami (Oolite) limerock and should have similar mechanical parameters and mineralogy of Miami limerock (Mine# 87-090) used in this study. Both cores were cut to same dimensions (5.94 inch x 7 inch), named as Miami Core 01 and Miami Core 02, and identified as MC01 and MC02. The initial moisture contents of MC01 and MC02 were 0.17% and 0.15%, respectively. PVC pipes were cut to serve as molds for these field cores and were secured with two metal hose clamps. To allow absorption, 1/16-inch

diameter holes were drilled 0.25 inch above the base of the mold and in a uniform manner across the base in 0.5-inch intervals. In order to avoid excessive water absorption, one of the open ends was covered with latex. A nut was secured to the center of the field cores to attach the accelerometer as deemed necessary. Following the construction of molds (Figure 4-8 B), the field cores were subjected to wetting and drying environmental conditioning.

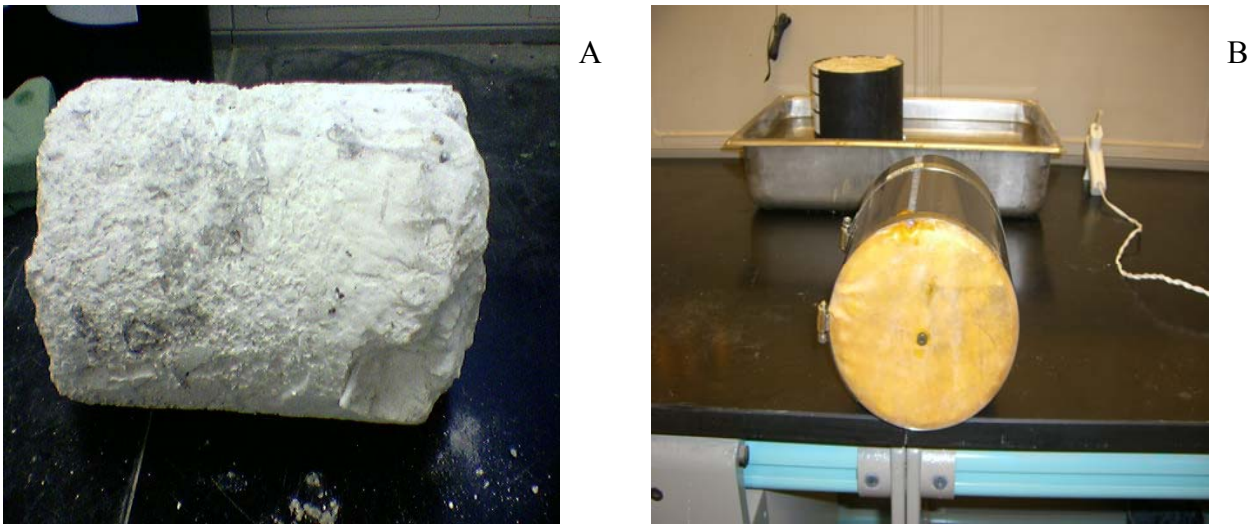

Figure 4-8. Field cores. A) Intact field core. B) Field cores after preparation.

For wetting, specimens were placed in a pan where the water depth was maintained at 1/3 of the specimen height with the samples in place to allow water access through the perforated molds. In oven drying, specimens were placed in a thermostatically controlled industrial oven at 110 ºF and subjected to air drying. In both cases, the specimens remained in the mold. Immediately prior to each resonant column testing, the specimen weight was monitored to determine the concurrent moisture content and unit mass of the specimen (ρ). The resonant column testing was monitored periodically as appropriate.

4.2 Resilient Modulus (M_R) Testing

4.2.1 Introduction

The M_R test is another way of characterizing pavement construction materials (Florida limerock base materials, in this study) under a variety of material parameters and stress conditions, and which simulates the conditions in a pavement subjected to moving wheel load. The purpose of performing M_R testing in this study is to document and quantify the effect(s) of the changes in resilient modulus for Florida limerock base materials and find answers to the following:

- Does stiffness increase also occur at working stresses and strains?
- Do the mechanisms causing stiffness and strength gains with time and under varying environmental conditions also lead to a stiffer material under a design truckload?

In addition, comparing results of both FFRC and M_R testing conducted on identical material would lead to assessing the influence of test methods on material properties.

The M_R testing in this study was performed by the FDOT SMO laboratory technicians following Section 9 of AASHTO T307-99: Resilient Modulus Test for Base/Subbase Materials. Figure 4-9 shows the M_R testing equipment and setup and a typical material sample.

4.2.2 Resilient Modulus Environmental Conditioning

In order to compare results of both FFRC and M_R testing to assess the influence of testing methods on the material properties, the specimens used for M_R testing were exposed to the following similar environmental conditioning as for the FFRC tests:

Optimum Moisture: Specimens remained in latex cover and were tested at optimum moisture immediately after compaction.

Ambient Condition: For M_R testing only outdoor ambient environmental conditioning was used and specimens remained in latex cover. In outdoor ambient, the specimens were stationed on benches outside the laboratory and were exposed to the natural environmental conditions.

Immediately prior to each M_R testing, the specimen weight was monitored to determine the concurrent necessary material parameters. M_R testing was conducted and monitored on Newberry, Ocala, Miami, and Loxahatchee materials after the specimens were exposed to outdoor ambient air for 7, 14, and 21 days. Specimens of Georgia material were tested after the specimens were exposed to outdoor ambient air for 2, 7, and 14 days.

Oven Drying: In oven drying, specimens were removed from the latex cover and placed in a thermostatically controlled industrial oven (Figure 4-5 A) at 110 ºF (Figure 4-5 B) and subjected to air drying. Immediately prior to each M_R testing, the specimen weight was monitored to determine the concurrent necessary material parameters. M_R testing was conducted and monitored on each material after the specimens were exposed to oven drying for 2 days.

Wetting: In wetting environmental conditioning, specimens remained in latex cover and were placed in soaking tank. Immediately prior to each M_R testing the specimen weight was monitored to determine the concurrent necessary material parameters. M_R testing was conducted and monitored on each material after the specimens were allowed to absorb water for 4 days.

4.2.3 Sample Preparation

Sample preparation for the M_R test was conducted by the FDOTSMO laboratory technicians following AASHTO designations T2 for “Sampling of Aggregates”, T248 for “Reducing Samples of Aggregates to Testing Size”, and Section 7 of T307-99 for “Preparation of Test Specimens.” Three replicates of 4 inch x 8 inch cylindrical specimens of each material except Georgia were prepared for each environmental condition. For Georgia material, two replicates of same dimensions were prepared for M_R testing at optimum moisture, and the same replicates were used for M_R testing under outdoor ambient conditions. One of the two replicates was used for M_R testing under drying condition following the outdoor ambient condition. Table

4-4 shows the target and measured specimen preparation parameters for M_R testing. Following construction, specimens of each material were exposed to one of four environmental conditions.

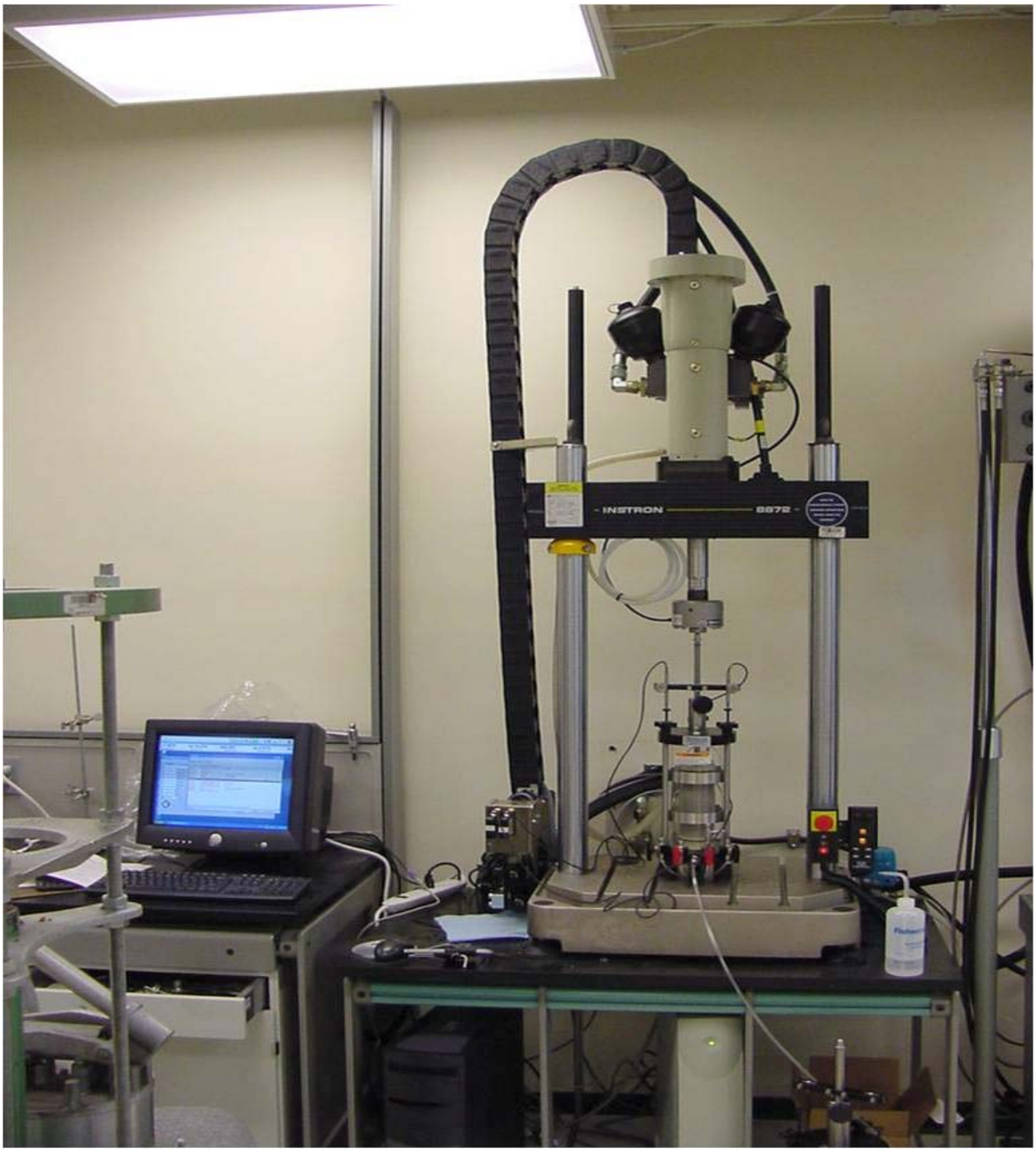

Figure 4-9. The M_R testing equipment and setup with a typical sample.

Table 4-4. The M_R testing target and measured specimen preparation parameters.

Source	Conditioning	Sample	Moisture Content		Dry Density	
			Target %	Measured %	Target pcf	Measured pcf
LOXAHATCHEE	Optimum Moisture	Replicate 1	9.8	10.0	122.0	121.8
		Replicate 2	10.3	10.1	121.3	120.7
		Replicate 3	9.9	10.0	122.5	121.7
	Outdoor Ambient	Replicate 1	9.8	9.8	122.0	121.1
		Replicate 2	10.3	10.1	121.3	119.5
		Replicate 3	9.9	9.8	122.5	121.1
	Wetting & Drying	Replicate 1	9.8	10.0	122.0	120.3
		Replicate 2	10.3	10.2	121.3	119.3
		Replicate 3	9.9	9.5	122.5	121.1
MIAMI	Optimum Moisture	Replicate 1	8.0	7.8	129.6	132.1
		Replicate 2	7.2	7.3	130.4	131.3
		Replicate 3	8.0	7.8	130.6	133.4
	Outdoor Ambient	Replicate 1	8.0	7.6	129.6	129.3
		Replicate 2	7.2	7.0	130.4	129.7
		Replicate 3	8.0	7.9	130.6	130.1
	Wetting & Drying	Replicate 1	8.0	7.9	129.6	131.5
		Replicate 2	7.2	7.3	130.4	132.4
		Replicate 3	8.0	7.7	130.6	131.4
GEORGIA	Optimum Moisture	Replicate 1	5.0	4.1	142.5	140.9
		Replicate 2	5.0	4.8	142.5	139.4
		NA	NA	NA	NA	NA
	Outdoor Ambient	NA	NA	NA	NA	NA
		NA	NA	NA	NA	NA
		NA	NA	NA	NA	NA
	Wetting & Drying	NA	NA	NA	NA	NA
		NA	NA	NA	NA	NA
		NA	NA	NA	NA	NA

Table 4-4. Continued.

Source	Conditioning	Sample	Moisture Content		Dry Density	
			Target %	Measured %	Target pcf	Measured pcf
NEWBERRY	Optimum Moisture	Replicate 1	13.0	12.9	116.5	116.5
		Replicate 2	12.5	12.4	116.1	114.3
		Replicate 3	13.0	12.9	115.9	115.4
	Outdoor Ambient	Replicate 1	13.0	12.7	116.5	116.1
		Replicate 2	12.5	13.0	116.1	114.1
		Replicate 3	13.0	12.9	115.9	116.0
	Wetting & Drying	Replicate 1	13.0	12.9	116.5	115.6
		Replicate 2	12.5	12.4	116.1	115.5
		Replicate 3	13.0	12.8	115.9	115.3
OCALA	Optimum Moisture	Replicate 1	10.9	10.9	120.1	121.7
		Replicate 2	11.1	11.2	120.2	119.9
		Replicate 3	11.3	11.4	120.4	120.6
	Outdoor Ambient	Replicate 1	10.9	10.9	120.1	120.4
		Replicate 2	11.1	11.1	120.2	118.1
		Replicate 3	11.3	12.1	120.4	119.9
	Wetting & Drying	Replicate 1	10.9	10.7	120.1	120.3
		Replicate 2	11.1	10.9	120.2	119.6
		Replicate 3	11.3	11.2	120.4	120.1

CHAPTER 5
FREE-FREE RESONANT COLUMN TEST RESULTS

5.1 Free-Free Resonant Column Test Results of Laboratory Compacted Specimens

5.1.1 Introduction

This section is designated to document and discuss the response of laboratory-compacted specimens of unbound aggregate that were exposed to environmental conditioning as discussed in the previous chapter. The figures used in this chapter demonstrate the results of the first replicate of each material. Appendices B through F present the individual results for each material in all environmental conditions and for all replicates. Appendix H compares replicates 2 and 3 of each material to all environmental conditions.

5.1.2 Constant Moisture

Figure 5-1 presents resonant column test results for each of the five materials while being held at constant moisture content. Young's modulus (E) versus time in days, both on arithmetic scale, is presented in Figure 5-1 A. The data from Figure 5-1 A is re-plotted in Figure 5-1 B on alternative scales to further illustrate the differences in behavior between the five materials. Here, modulus ratio is plotted on the vertical axis, or the Young's modulus at any time (E) divided by the Young's modulus at maximum dry density and optimum moisture content immediately following compaction (E_{opt}). The logarithm of time in minutes is plotted on the horizontal axis.

It should be noted from the figures that the small-strain modulus of all materials tested while being held at constant moisture is not constant; on the contrary, the small-strain modulus of all materials increases with increasing time. This behavior occurs under constant confinement, volume, and moisture, therefore this behavior is not due to consolidation. It should be noted from

the moisture content versus time figures, there are consistent but negligible decreases in moisture, which is believed to have very slight effect on stiffness increase.

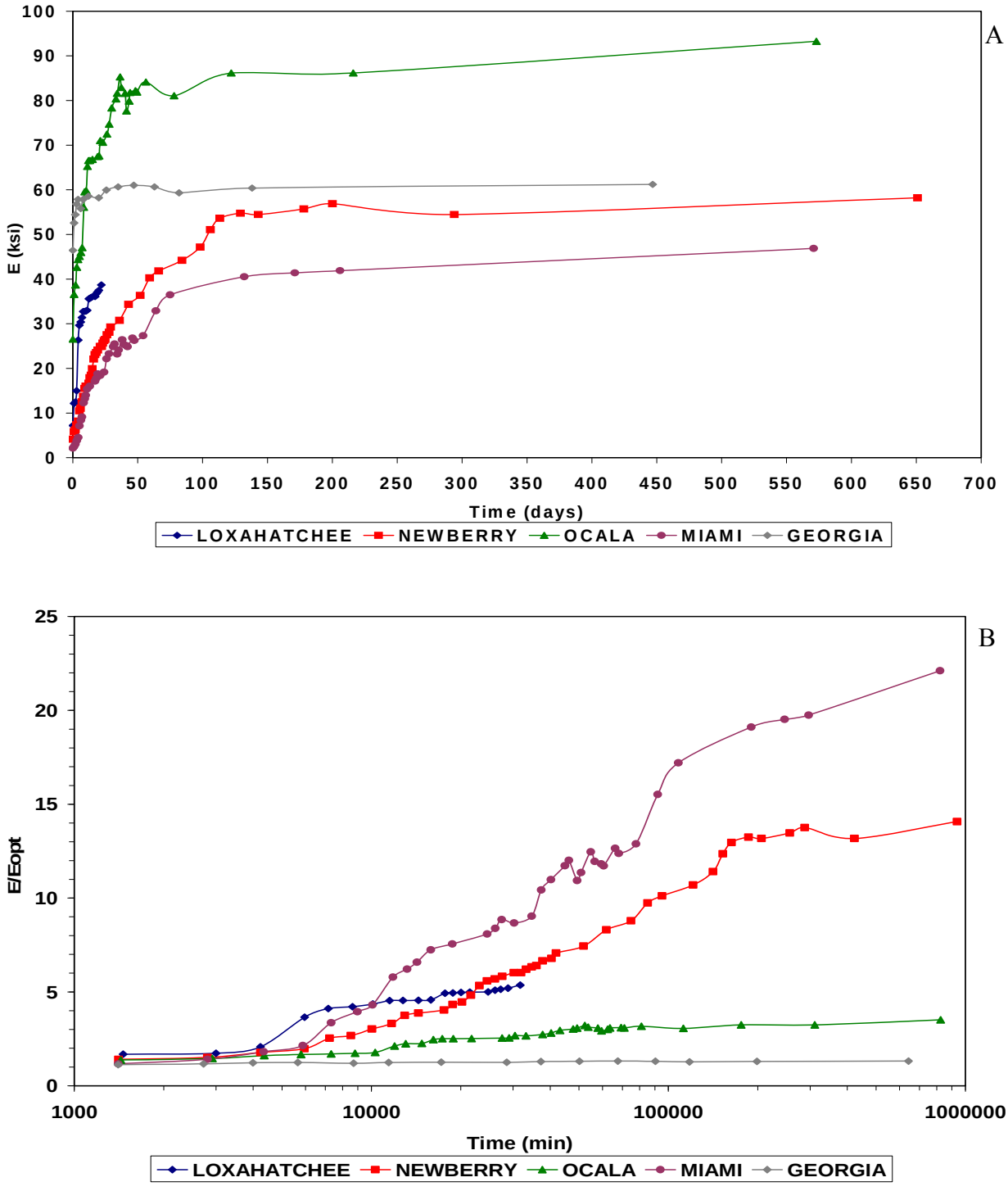

Figure 5-1. FFRC test results of first replicate exposed to constant moisture.

It should also be noted that the rate of modulus increase with time decreases with time, that is, the largest change occurs early, and then gradually diminishes.

Further, while the general trend of increasing modulus with time is common to all materials tested, the rate of increase is considerably different. The Miami limerock displays a very significant increase with time, while the increase for the Georgia granite is relatively small.

The behavior noted above is consistent with research results reported for other unbound particulate materials, most notably soils (Afifi and Woods [1971]; Wu and Woods [1987]). Described as the secondary or long-term time effect, these studies clearly demonstrated that the modulus of sand, silt, and clay soils all increase with time while at constant moisture, volume, and confining conditions. While a definitive mechanism for this behavior has not been proven, Afifi and Woods (1971) suggest that it may be due to thixotropy, and Schmertmann (1992) might attribute the behavior to so-called mechanical aging, or an increase in friction with time. Mitchell and Soga (2005) indicate that chemical processes (cementation) are a possible cause of aging.

In this study, it is hypothesized that the behavior observed could also be due to increased suction or negative pore water pressure that occurs as the water in the material redistributes following compaction into more preferential positions within the inter-particle void spaces. This increased suction effectively adds confining stress to the particulate material and thereby increases the resistance to deformation (stiffness). This phenomenon has been well documented via resonant column tests on sand and silt soils by Wu, Gray, and Richart (1984). Also, it has long been established that the modulus of a particulate material is directly proportional to level of confining pressure (Richart, Hall, and Woods [1970]). Among the first studies for soil, Hardin and Richart (1963) reported results of resonant column tests on sands that indicated shear modulus to be a function of isotropic confining pressure raised to a power of 0.5. Many

subsequent studies have affirmed these basic findings, including Fernandez (2000) and Menq (2003), both of which contain extensive discussion of the literature on this subject. Menq (2003) also demonstrates these fundamentals apply to larger particle sizes, e.g., gravels.

5.1.3 Drying

In this section, the influence of removal of water (drying) on the materials is discussed. The results produced by placement of the specimens in ambient conditions either on laboratory bench or in outdoor shade environments are very similar. Low-heat oven, laboratory bench, and outdoor shade all produced a slow drying behavior as will be depicted in the figures.

5.1.3.1 Laboratory Ambient

Figure 5-2 presents resonant column test results for each of the five materials while being exposed to laboratory ambient air. As expected, Figure 5-2 A demonstrates that placement of specimens initially at optimum moisture content (time = 0) on laboratory bench slowly drives water out from materials. Young's modulus (E) versus moisture content, both on arithmetic scale, is presented in Figure 5-2 C. Young's modulus (E) versus time in days as the material dries from optimum water content, both on arithmetic scale, is presented in Figure 5-2 B.

It should be noted from Figure 5-2 C that the materials underwent a dramatic increase in small-strain modulus as water is lost. The moisture content and modulus change occurs most significantly at the early stages of drying exposure, after which the rates decrease with increasing time (Figure 5-2 B).

As with the tests at constant moisture content, all five materials demonstrate similar trends, but the rate of change and the magnitude of the effect are different between materials. It should be noted that once again the Miami limerock changes the most, while change in Georgia granite is smallest.

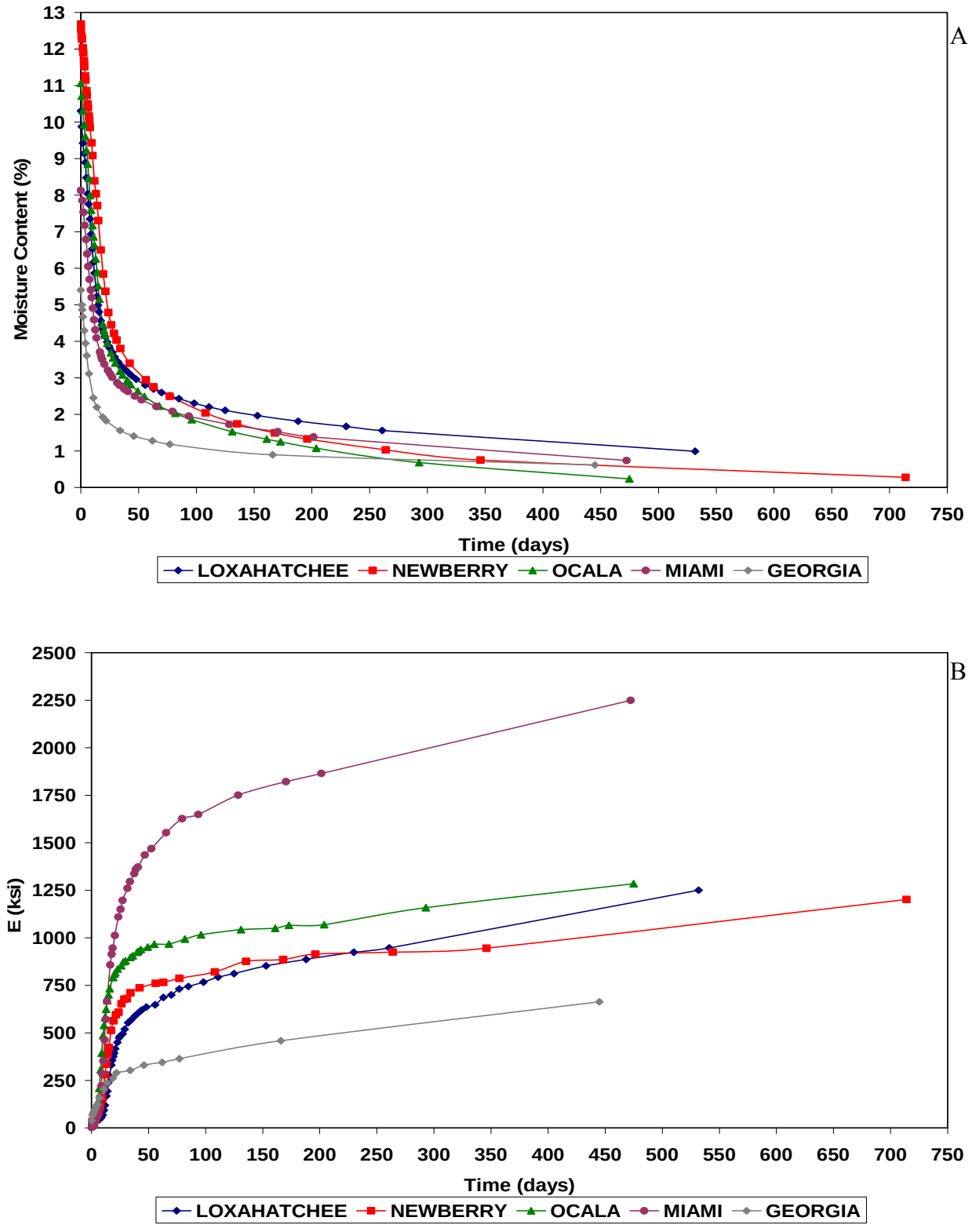

Figure 5-2. The FFRC test results of first replicate exposed to laboratory ambient.

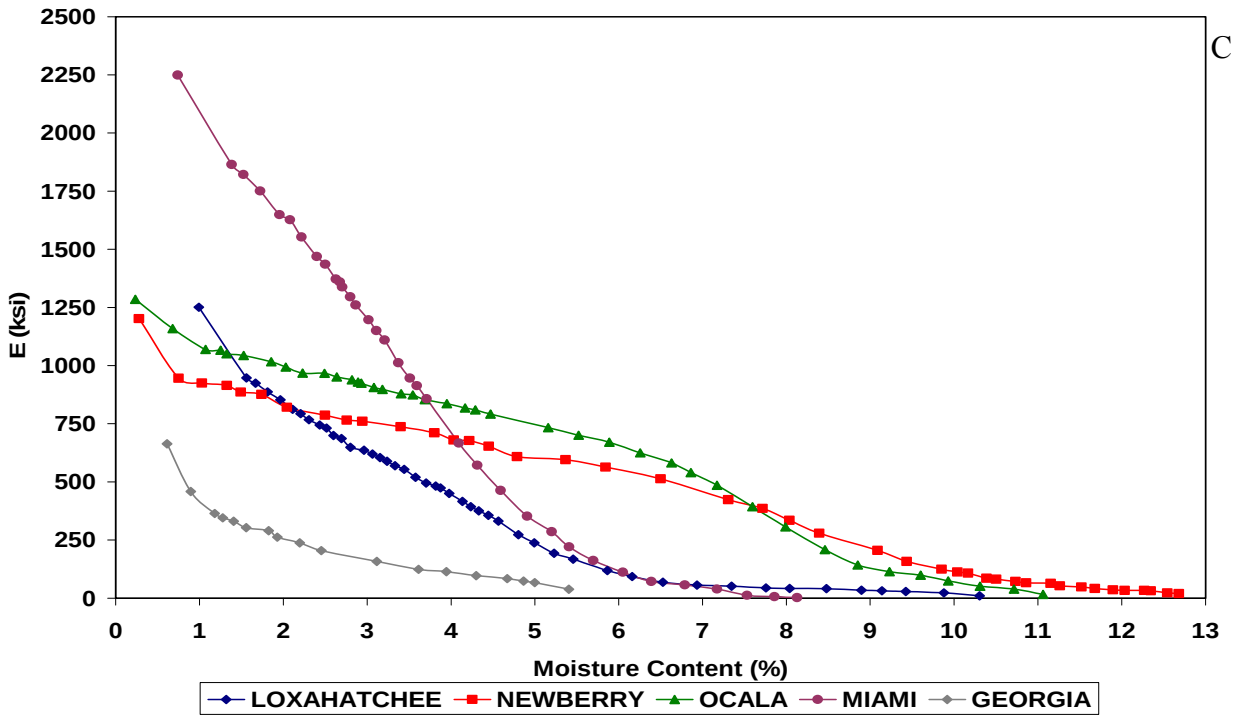

Figure 5-2. Continued.

5.1.3.2 Outdoor Ambient

Figure 5-3 presents the comparison of the resonant column test results for the first replicate of Newberry material while being exposed to outdoor shade and laboratory ambient air. Young's modulus (E) versus time in days as the material dries from optimum water content, both on arithmetic scale, is presented in Figure 5-3 A. Young's modulus (E) versus moisture content, both on arithmetic scale, is presented in Figure 5-3 B. It is noted from the figures that the results produced by placement of the specimens in ambient conditions are almost identical. Therefore, preparation of specimens for outdoor environment of other materials (Ocala, Loxahatchee, Miami, and Georgia) was deemed unnecessary.

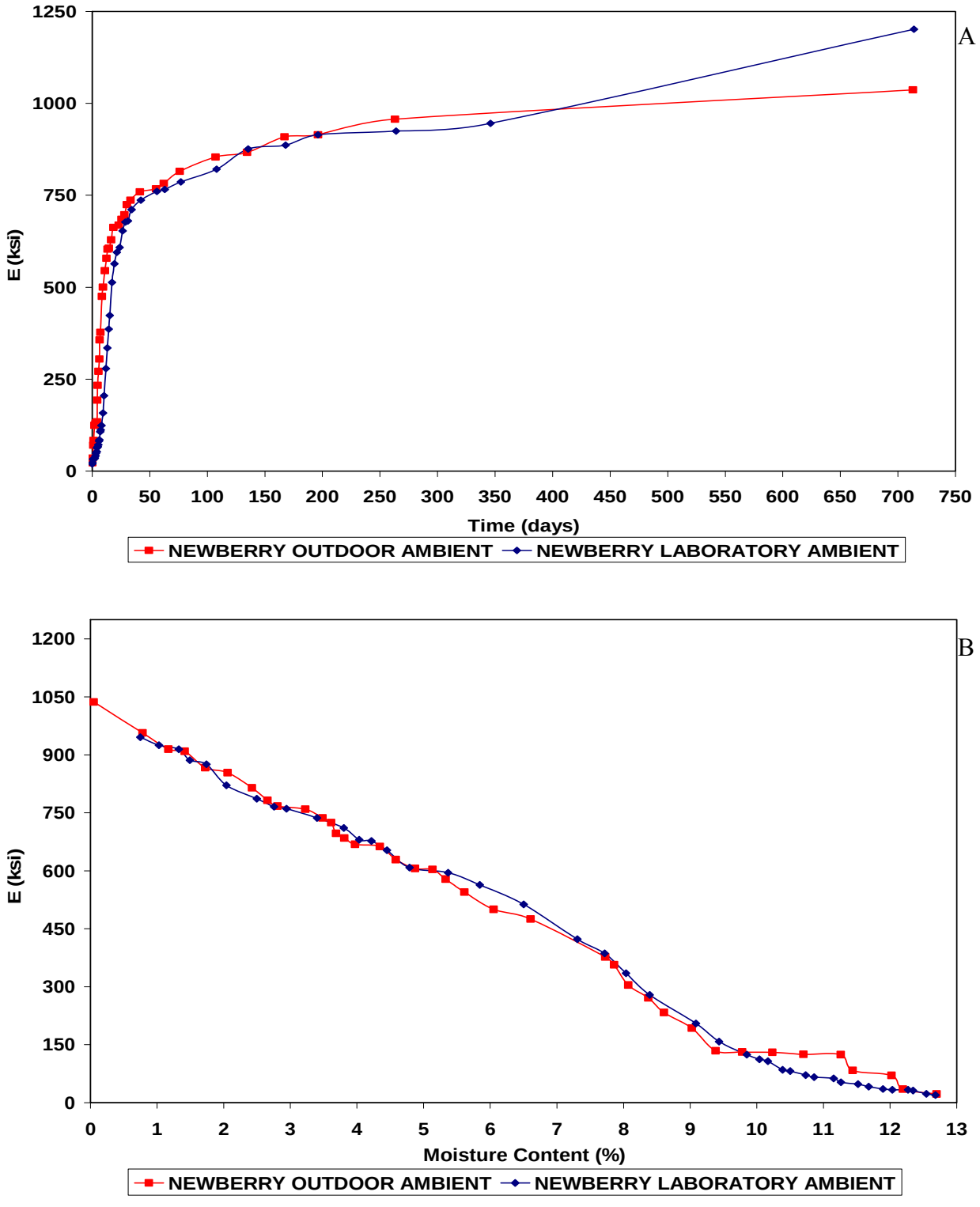

Figure 5-3. Comparisons of the FFRC test results of Newberry exposed to ambient conditions.

5.1.3.3 Oven Drying

As described in detail in the previous chapter, the specimens were put in an oven at low heat (110 ºF) for relatively slow drying. The specimens underwent several oven-drying processes during wetting and drying cycles. The influence of oven drying on the material response is shown in Figures 5-4 and 5-6. The legends D1, D2, D3, and D4 in Figure 5-6 represents the first, second, third, and fourth oven drying cycle, respectively, on same specimen of the first replicate of Loxahatchee shell-rock.

If figures regarding laboratory ambient, outdoor ambient, and oven drying are compared (Figures 5-2 C, 5-3 B, 5-4), it can be noted clearly that at any type of drying of the material produces a dramatic increase in small-strain modulus as water is lost. The moisture content and modulus change occurs most significantly at the early stages of drying exposure, after which the rates decrease with increasing time.

Regardless of the drying method, the Miami limerock changes the most, while the change in Georgia granite is smallest. It should also be noted that after a certain period and moisture level the stiffness of Loxahatchee shell-rock and Miami limerock becomes larger than Newberry and Ocala limerock.

While the mechanism cannot be proven herein via the direct measurement of pore water pressure or suction, the stiffening that occurs while materials underwent any type of drying can again be explained by increase in suction. It has been well documented in the science of unsaturated soil mechanics (Lu and Likos [2005]) that increases in suction or negative pore water pressure will occur as water is removed from the material. As documented by Wu, Gray, and Richart (1984) for sand and silt soils, this increased suction will effectively increase confinement and hence modulus. The results in Figure 5-4 are very similar in behavior to those presented by

Cho and Santamarina (2001) in which they clearly demonstrate the effects of suction mechanism on stiffness behavior while drying.

As previously discussed, Gartland and Eades (1979) have clearly demonstrated that cementation is possible in Florida limerock base materials. While Gartland and Eades (1979) measured material strength and not stiffness, it is very likely that cementation will increase material stiffness, and thus cementation is another possible mechanism to produce the results presented herein. However, in an experiment recently completed by Campos (2007), FFRC tests were conducted on laboratory samples of the same Loxahatchee, Miami, and Ocala materials compacted at 1% wet of optimum moisture content and held at constant levels of relative humidity (low = 11%, medium = 53%, high = 97%) for 30 days. In all cases (both materials and relative humidity), the moisture levels reduced with time, and the stiffness values increased significantly with time, which are consistent with the drying experiments presented herein. In addition, Environmental Scanning Electron Microscope (ESEM) image analysis of the specimen at low humidity and after 30 days of aging did not reveal any calcite cement growth. Finally, it should be noted that while the rate of change with respect to moisture content was smallest, significant stiffness increases did occur upon drying the granite-based Georgia graded aggregate presented earlier. It is expected that carbonate-based cementation cannot occur in this material.

The behavior of the Miami limerock relative to others is partially explained by the fact that this material is coarsest, well graded, and at low void ratio. This trend in parameters will all produce large small-strain modulus as demonstrated by Menq (2003). It is also hypothesized that differences between these materials could also be created by differences in the relationship between suction and moisture content, the so-called soil water characteristic curve. In fact, mercury porosemetry tests on the Loxahatchee, Miami, and Ocala materials presented by

Campos (2007) indicate that the distribution of pore size is different between these three materials, which should create different soil water characteristic curves.

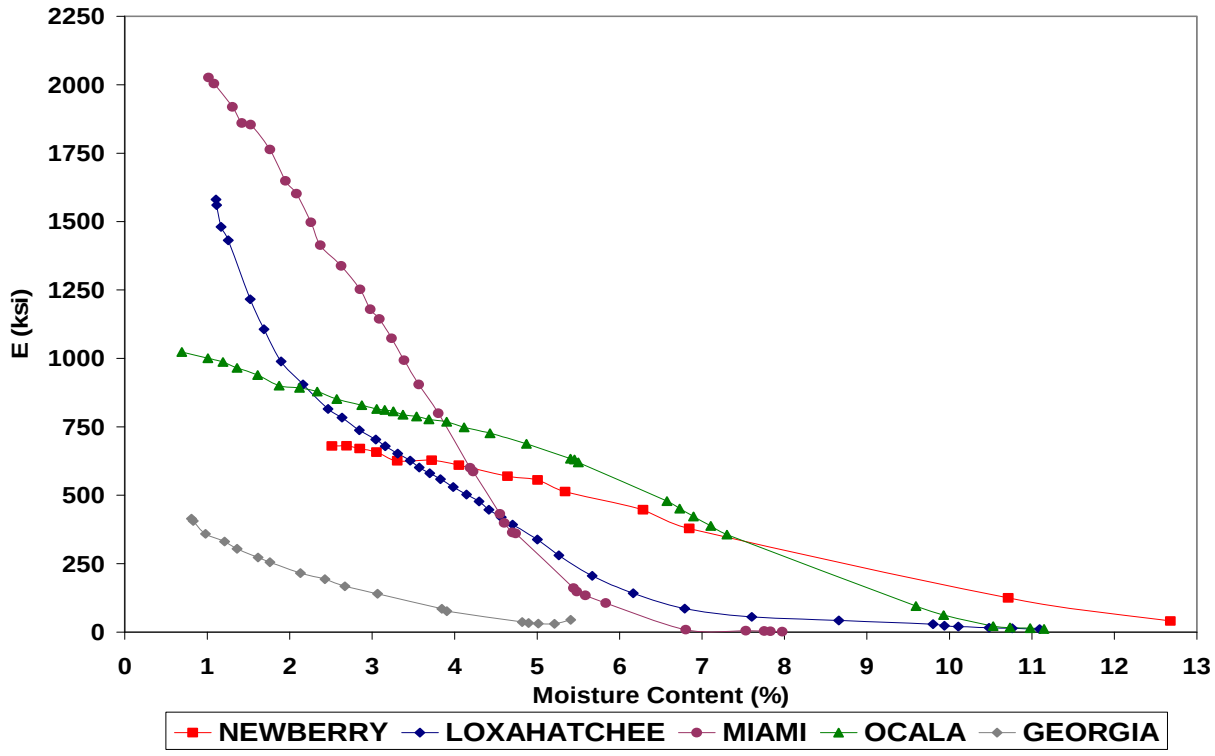

Figure 5-4. The FFRC test results of each material during first cycle of oven drying.

5.1.4 Wetting

Influence of the addition of water (wetting) on the material response is shown in both Figures 5-5 and 5-6. The legends W1, W2, and W3 in Figure 5-6 represent the first, second, and third wetting cycle, respectively, on the same specimen of the first replicate of Loxahatchee shell-rock. As expected, Figures 5-6 A demonstrates by way of example for the Loxahatchee shell-rock that placement of a nearly dry specimen in a soaking tank allows the material to slowly absorb water. Figure 5-6 B indicates that the material undergoes a dramatic decrease in small-strain modulus as water is absorbed. The moisture content and modulus change occurs most significantly at the beginning of exposure, after which the rates decrease with increasing time. This behavior is further demonstrated in Figure 5-5 for all five materials. In this figure is

plotted the Young's modulus (E) versus moisture content as the materials are wetted from a nearly dry condition. As with the tests during drying, all five materials demonstrate similar trends, but the rate of change and the magnitude of the effect are different between materials. In addition, the trends are consistent with a loss in suction and effective confinement as the moisture content of the material increases, and are similar to the behavior shown in Figure 2-1 C from Cho and Santamarina (2001).

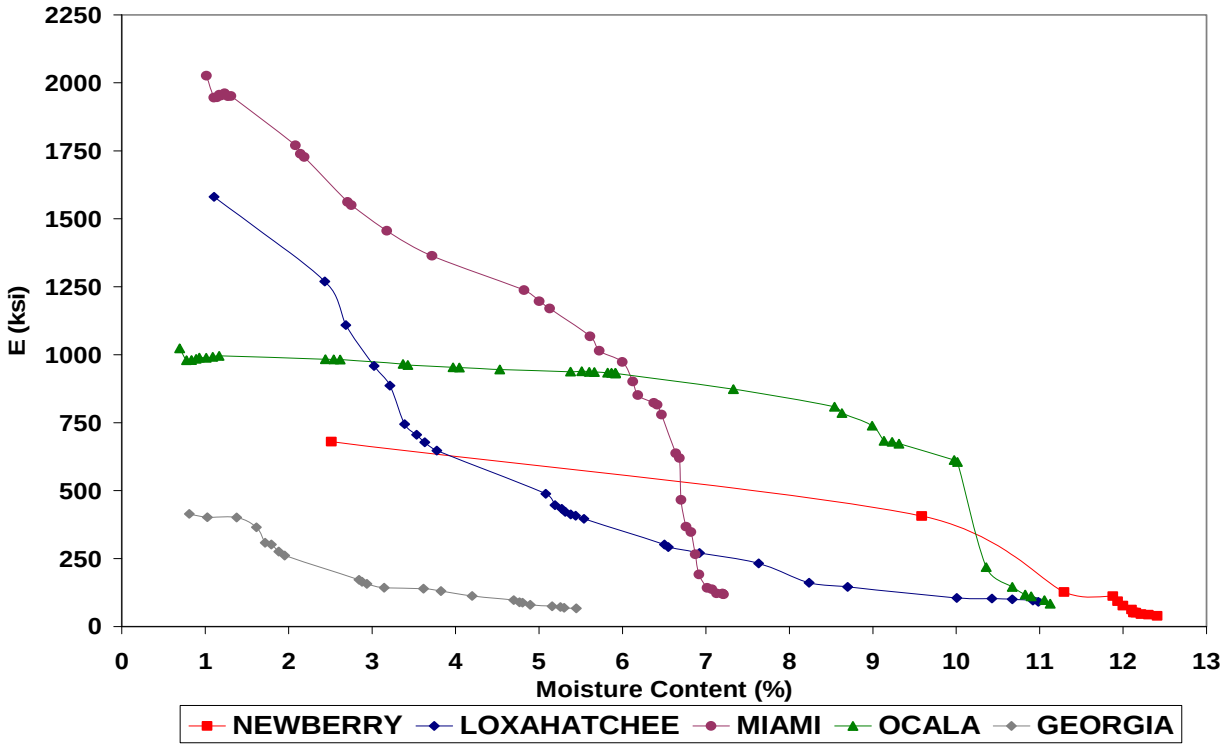

Figure 5-5. The FFRC test results of each material during first cycle of wetting.

It is also interesting to note that a close comparison of Figure 5-4 and Figure 5-5 reveals that the drying and wetting responses of a given material do not follow the same relationship. There is a hysteretic phenomenon whereby a different modulus is measured while drying to certain moisture content than while wetting to the same moisture content. This hysteretic phenomenon is well known in unsaturated soil mechanics where the suction values reached at common moisture content are different between drying and wetting (Lu and Likos [2005]).

5.1.5 Wetting and Drying Cycles

Figure 5-6 illustrates by way of example using the first replicate of Loxahatchee shell-rock that each of the materials was subjected to several cycles of drying and wetting. The previous sections described the material response to an individual drying or wetting exposure. The following will describe the observed response due to repeated application of drying and then wetting. It should be noted that while Figure 5-6 graphically depicts the response of only the Loxahatchee material, the remaining four materials exhibited very similar trends in behavior.

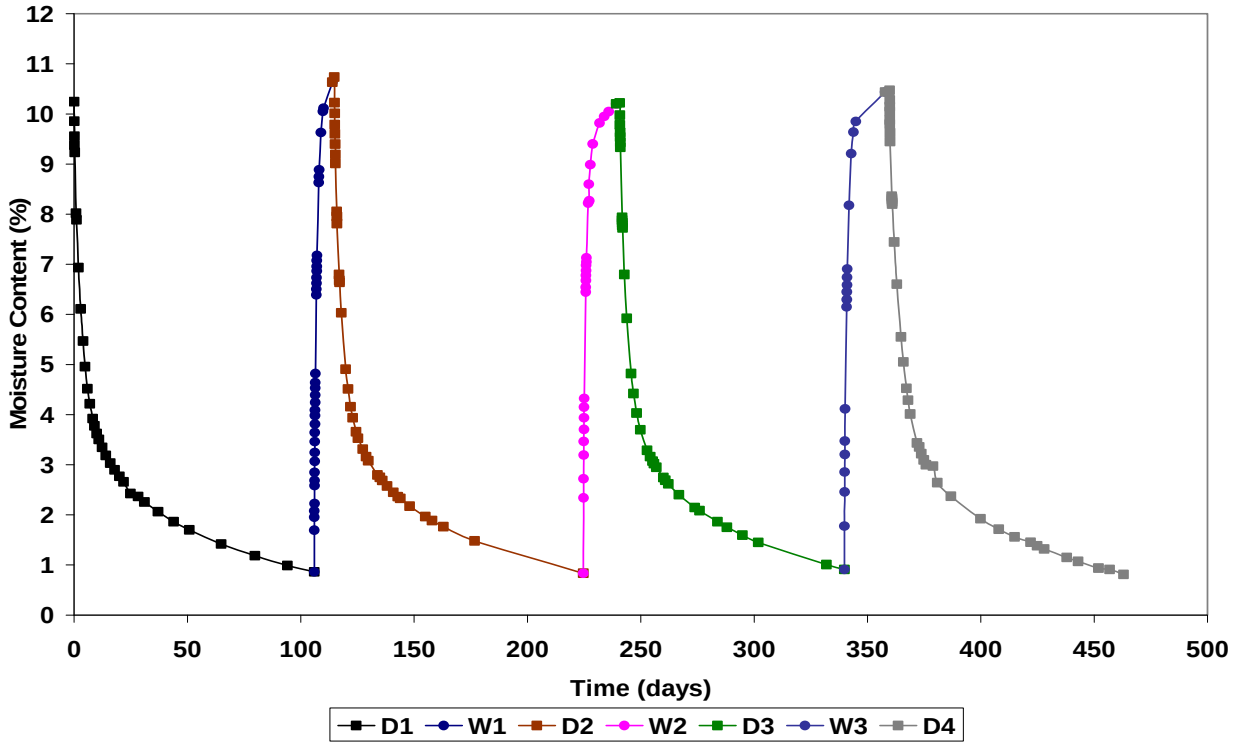

Figure 5-6. The FFRC test results for drying and wetting cycles on Loxahatchee shell-rock.

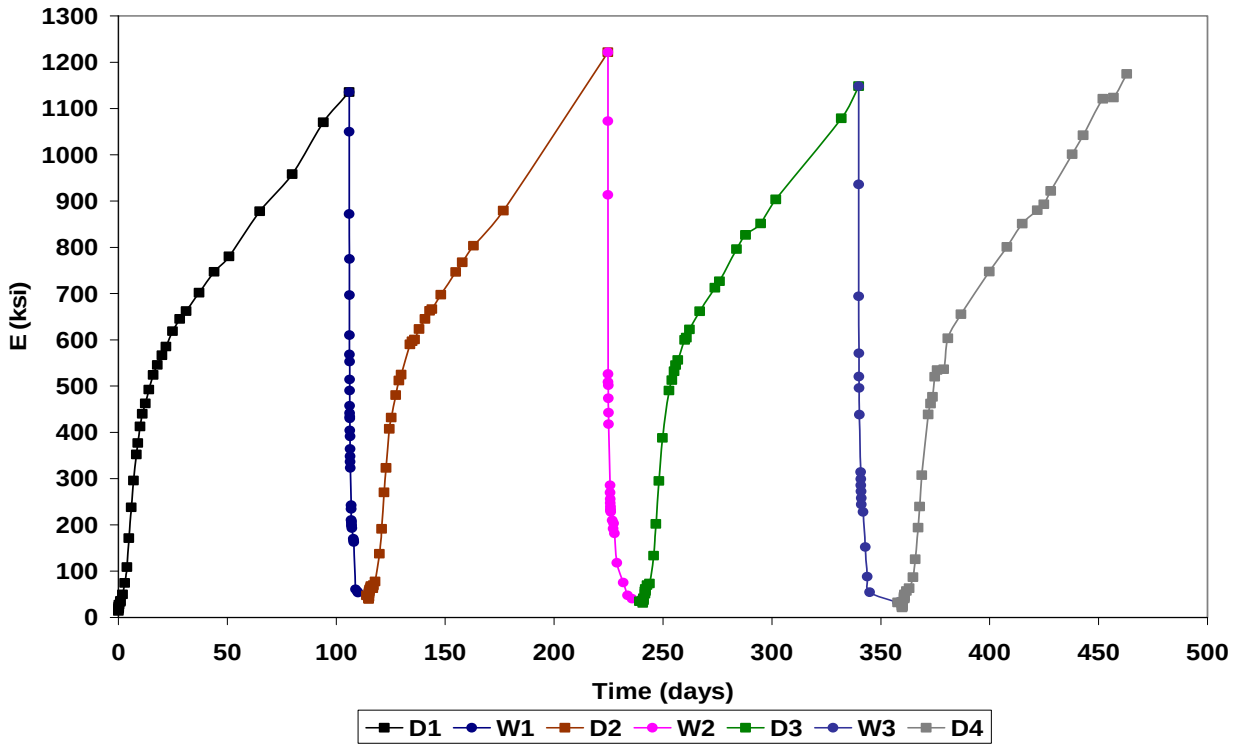

Figure 5-6. Continued.

The most important and attention grabbing phenomenon is that the material response appears to be highly repeatable. Subsequent responses to drying and wetting are very similar to the initial response. This suggests that the underlying mechanism for the response is largely reversible, and is a significant additional indication that the suction/confining stress mechanism hypothesized is plausible.

5.2 Free-Free Resonant Column Test Results for Field Cores

5.2.1 Introduction

The previous sections have documented the response of laboratory-compacted specimens of unbound aggregate to exposure of several moisture environments. It has been hypothesized that a plausible underlying mechanism for this response is suction or negative pore pressure. A significant question that arises from these results is whether this behavior occurs in the field in

unbound aggregate base course materials. This section will document test results to address this question.

5.2.2 Wetting and Drying Cycles of Field Cores

Two intact field cores were exposed to cycles of wetting and drying similar to the laboratory-compacted specimens and were subjected to the same testing routine. Figures 5-7 and 5-8 present results from laboratory resonant column tests on one of the two intact field cores that were exposed to cycles of wetting and drying. Results of the both cores are presented in Appendix G. It is indeed remarkable that it is possible to retrieve a field core intact, but this occurs frequently with some of the Florida materials. Given the results presented in the previous sections, it may not be surprising that two intact field cores were obtained from pavement sections with base course material from a Miami limerock source. Indeed, the Miami limerock can be very hard if the moisture content is below optimum.

The details about the field cores were described in the previous chapter. Each of the base course pavement sections was approximately 10 years old at time of coring. When brought to the laboratory, the cores were determined to be nearly dry. The specimens were prepared for resonant column testing by mimicking the plastic mold environment that was used for laboratory-compacted materials. Here, a split PVC sleeve was wrapped and then clamped around the core circumference. Latex and wax were then used to seal one end of the core and the other end remained exposed. Small holes were drilled around the perimeter of the covered end of the sleeve to allow water entry when placed in a shallow water bath. In this state, the cores were subjected to frequent resonant column tests while being exposed to cycles of wetting and drying.

Figure 5-7 presents moisture content and Young's modulus (E) versus time results for one of the field cores. The response of the second core was very similar.

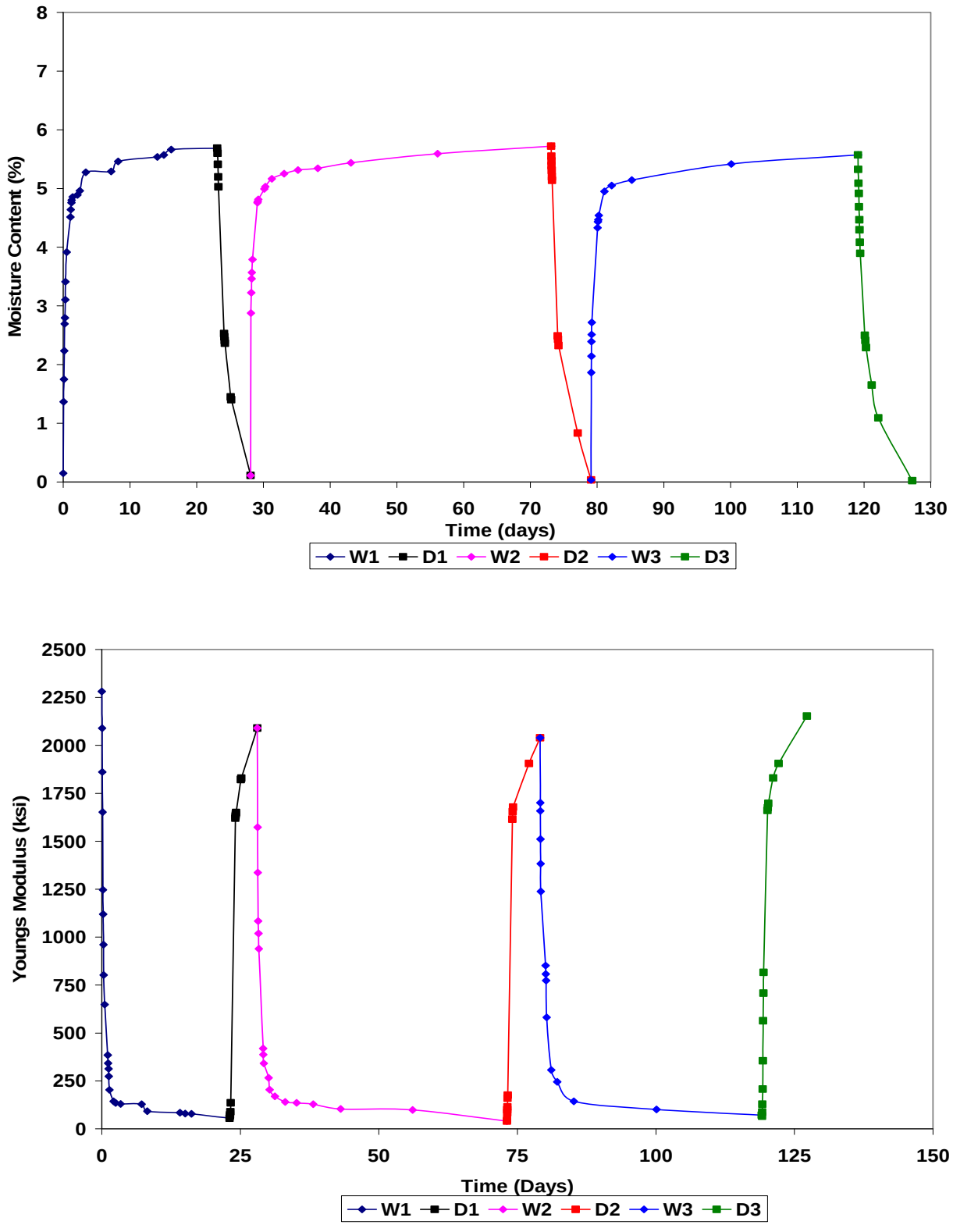

Figure 5-7. The FFRC test results for wetting and drying cycles on field core 1

Figure 5-8 presents Young's modulus (E) versus moisture content results for the first wetting and first drying cycles for each field core as well as for the Miami limerock laboratory-compacted specimen. Most notably, it should be observed that the response of the field cores appears very similar to that of the fresh, laboratory-compacted specimens. Even after 10 years of service, the softening while wetting followed by a return to high stiffness when nearly dry, appears to be very repeatable and reversible. Indeed, Figure 5-8 demonstrates that the response is similar to that of a laboratory-compacted specimen of material from the same general source in south Florida, and that aging has not significantly altered the material response. These results appear to provide further justification for an underlying mechanism of changes in pore pressure, a largely reversible and repeatable phenomenon.

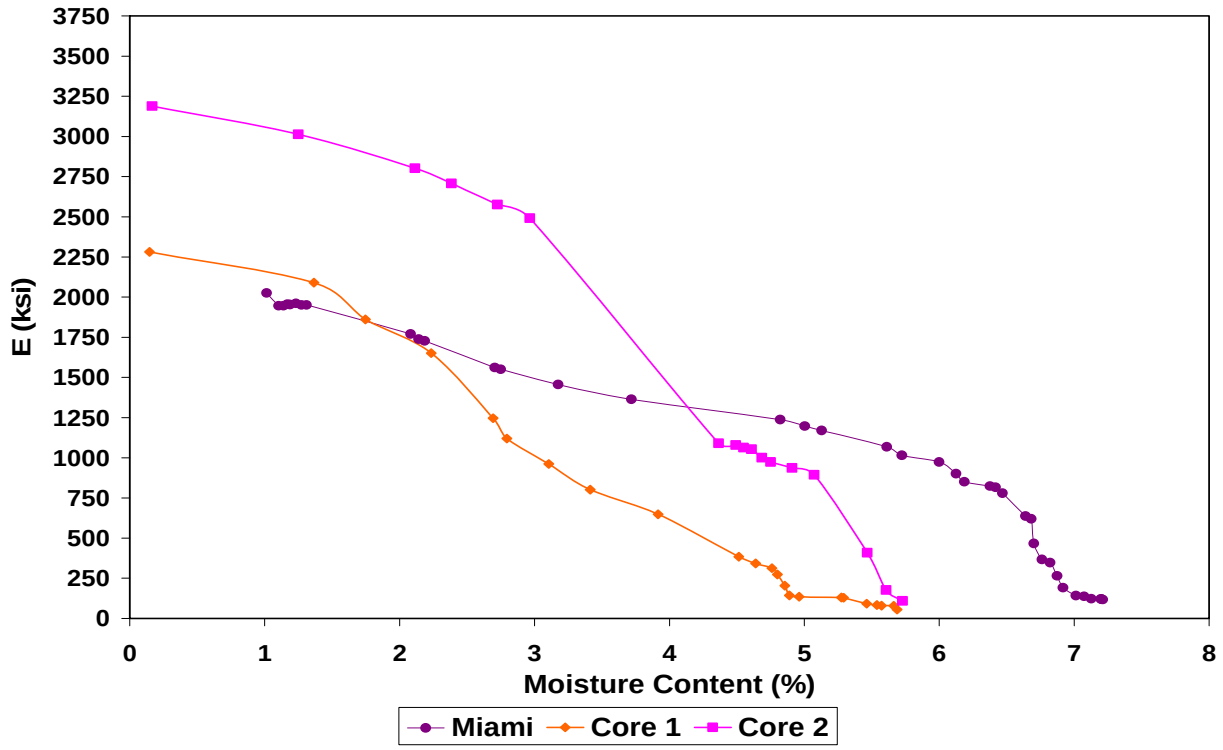

Figure 5-8. The FFRC test results for the first wetting and drying cycles on field cores and laboratory-compacted Miami limerock; Young's modulus vs. moisture content while wetting.

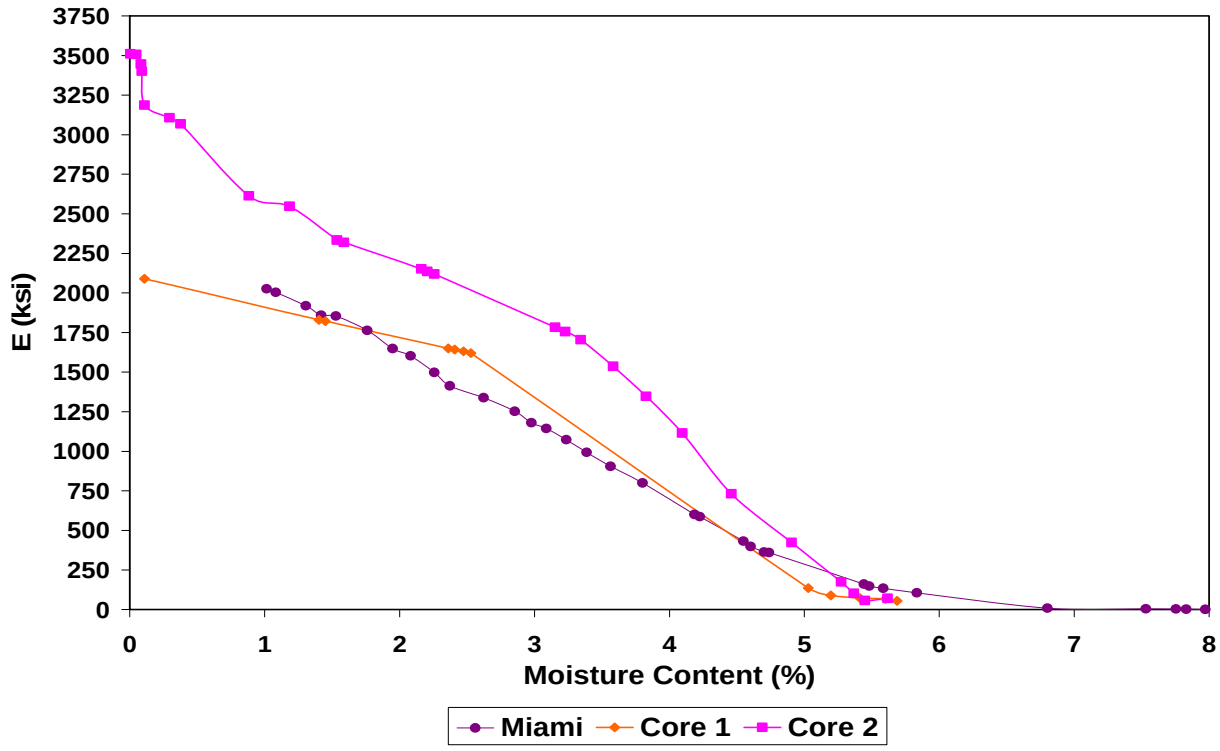

Figure 5-9. The FFRC test results for the first wetting and drying cycles on field cores and laboratory-compacted Miami limerock; Young's modulus vs. moisture content while drying.

CHAPTER 6
CONSTANT HUMIDITY EXPERIMENT

6.1 Introduction

As previously discussed, Garland and Eades (1979) have clearly demonstrated that cementation is possible in Florida limerock base materials. However, despite substantial efforts to mimick the conditions necessary for cementation, McClellan, et al. (2000) have not observed cementation. This chapter is designated to another attempt to create conditions that are favorable for the precipitation of calcite crystals, and to observe any possible calcite crystal growth parallel with the stiffness behavior in selected Florida base coarse materials.

Bricker (1971) noted that cementation in carbonate material occurs due to many factors, one of which is local pressure gradients adjacent to grain contacts. It is proposed that by controlling the relative humidity within a curing chamber such a pressure gradient will be induced and accelerate the cementation process within compacted limestone base course specimens. Desiccator cabinets of approximately 0.75 ft^3 were used as curing chambers and curing periods of 2, 7, 15 and 30 days were used to assess stiffness behavior with time via FFRC test. One sample from each source that was cured for 30 days was observed via ESEM to assess pore structure characteristics in the cured materials following the FFRC test.

6.2 Free-Free Resonant Column Testing of Laboratory Compacted Specimens

6.2.1 Specimen Preparation

Ocala, Miami, and Loxahatchee limstones were used for this specific experiment due to calcite content of these materials (Table 3-1). In addition, for comparison, a field core taken from Glades County, Florida was examined. Although it is uncertain what mine the material originated from, based on the physical characteristics and specific gravity the base course material in the Glades core appears to be Miami limestone. For materials collection and

characterization please refer to Chapter Three. The material that came from the quarry was placed into an oven to be air-dried until it became friable. Material with particle sizes greater than ¾ - inch was crushed so that the entire sample passed the ¾ - inch sieve by use of a mechanical jaw crusher. The pieces that have not been reduced to the desired size by the mechanical crushing were broken down manually until they passed the ¾ - inch sieve.

The materials were separated into portions matching the mini stockpiles from which they were collected. Each of the separate portions was thoroughly mixed with amounts of water to reach 1% wet of optimum moisture content. Immediately prior to the compaction of the materials, representative samples weighing at least a pound were taken for moisture content determination.

Materials were compacted at 1% wet of the optimum moisture content into 4-inch diameter by 8-inch height plastic cylinders because as discussed earlier FFRC testing requires an aspect ratio of 2:1 to acquire better results. It should be noted these dimensions are different from ASTM D 1557, which requires either a 4 inch or 6 inch diameter by 4.584-inch height rigid metal mold. Plastic cylinders were chosen because portions would later be sawed out for the destructive testing portion of this experiment. Compaction procedures from ASTM D 1557 had to be modified to ensure that the modified compactive effort of 56,000 ft-lbf/ft^3 was still achieved. The specimens were compacted in 9 layers with 25 blows per layer to achieve the Modified Proctor density. The 10-pound hammer and 18-inch drop were still used. Materials were compacted using a Rainhart automatic tamper at the FDOT SMO.

Two specimens were compacted for each testing variation and the resulting modulus values and moisture content reductions were averaged. The testing variations consisted of four

different time periods and three different curing humidities. In total, 24 duplicate specimens were compacted for each of the three aggregate sources.

6.2.2 FFRC Environmental Conditioning

In constant humidity environmental conditioning, the specimens were exposed to three different humidity levels for curing periods of 2, 7, 15 and 30 days to assess stiffness behavior over time. After compaction, the specimens remained in cylindrical molds and were placed in desiccator cabinets of approximately 0.75 ft^3 that are used as curing chambers for the allotted time periods. Immediately prior to resonant column testing, the specimen weight was monitored to determine the concurrent moisture content and unit mass of the specimen (ρ). The resonant column testing was monitored after each curing period. The seals of the desiccator cabinets were previously tested to ensure no leakage. To maintain a constant relative humidity in each of the chambers, different saturated salt solutions were used. It was desired to use solutions that exhibited high, medium, and low relative humidities.

Saturated salt solutions were prepared by mixing a quantity of lithium chloride ($R_H \approx$ 11%), magnesium nitrate ($R_H \approx 53\%$), or potassium sulfate ($R_H \approx 97\%$) with gently heated, distilled water. Once the solution cools, excess solids will precipitate if the solution is beyond saturation. This allows moisture from the compacted specimens to be absorbed by the saturated salt solutions until excess solids are no longer present. Approximately 250 mL of solution were used in each of the curing chambers and either replaced or remixed as necessary to ensure that solids were present. Conditions inside the curing chambers were monitored with the use of temperature and humidity gages. The temperature dependencies of the saturated salt solutions according to ASTM E 104 are presented in Table 6-1. The temperature remained at a constant 25 °C within the chambers throughout the test period.

Table 6-1. Equilibrium relative humidity values for saturated aqueous salt solutions.

Temperature (°C)	Lithium Chloride, $LiCl \cdot H_2O$	Magnesium Nitrate, $Mg(NO_3)_2 \cdot 6H_2O$	Potassium Sulfate, K_2SO_4
20	11.3 ± 0.3	54.4 ± 0.2	97.6 ± 0.5
25	11.3 ± 0.3	52.9 ± 0.2	97.3 ± 0.5
30	11.3 ± 0.2	51.4 ± 0.2	97.0 ± 0.4

6.2.3 FFRC Test Results

This section is designated to document and discuss the response of laboratory-compacted specimens of unbound aggregate that were exposed to constant humidity. The figures used in this chapter demonstrate the results of one of the replicates of each material exposed to low, medium, and high humidity. Initial measurements were taken immediately after compaction, and final measurements were taken after the allotted curing time for each specimen (i.e., 2, 7, 14, and 30 days). After testing was completed, cylinders were sealed to ensure no further loss in moisture.

Figures 6-1, 6-2, and 6-3 present the variation of Young's modulus with moisture content for low, medium, and high humidity of Ocala, Miami, and Loxahatchee, respectively. It should be noted from the figures that the small-strain modulus of all materials tested while being held at constant humidity increases with increasing time (i.e., decreasing moisture), and for all three relative humidity levels. It is also evident that the low humidity environment produces the largest change in both modulus and moisture, while the high humidity environment results in the smallest changes.

Finally, these behaviors occur under constant confinement, volume, and humidity, therefore this behavior is not due to consolidation.

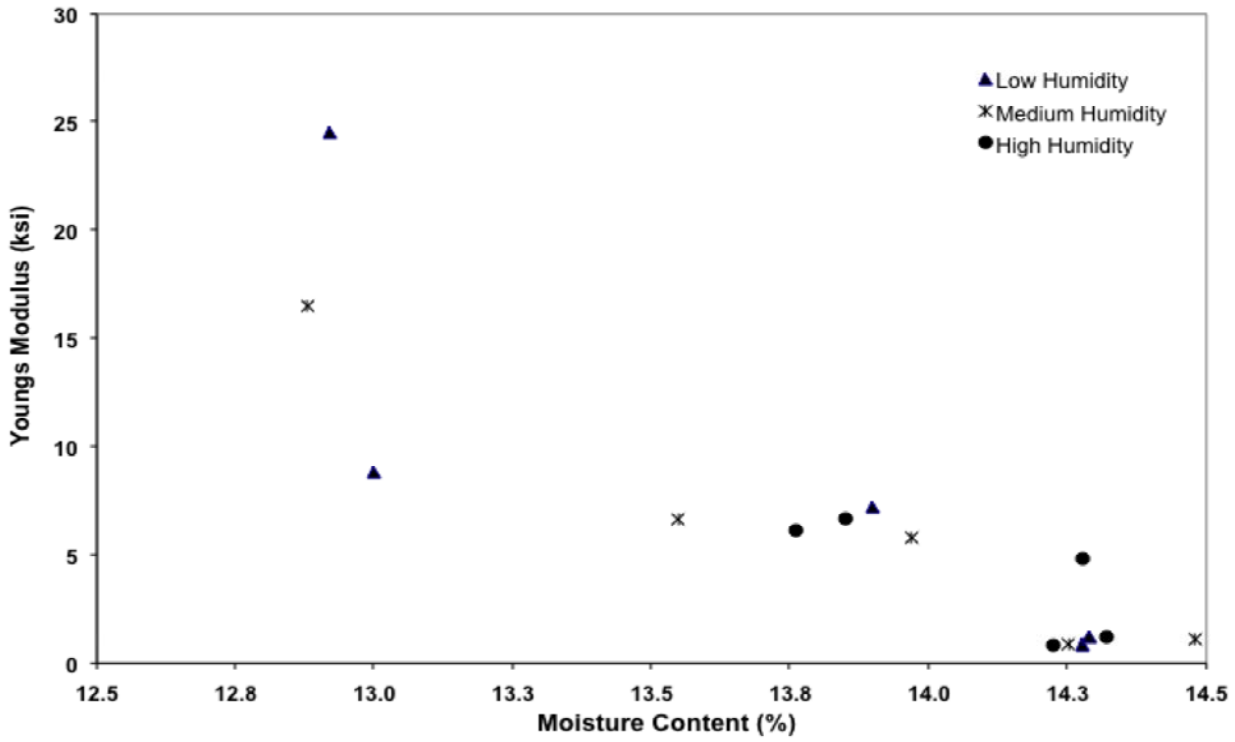

Figure 6-1. Variation of Ocala limerock Young's Modulus with moisture content as a function of humidity levels.

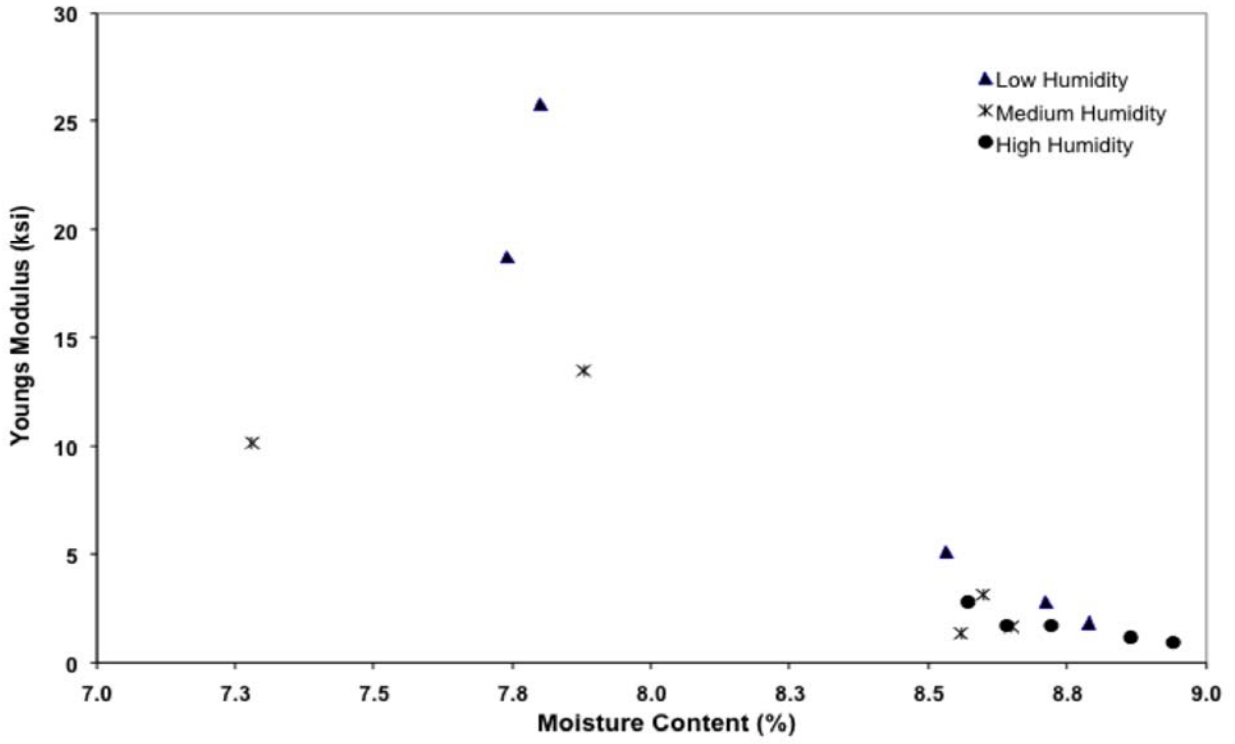

Figure 6-2. Variation of Miami limestone Young's Modulus with moisture content as a function of humidity levels.

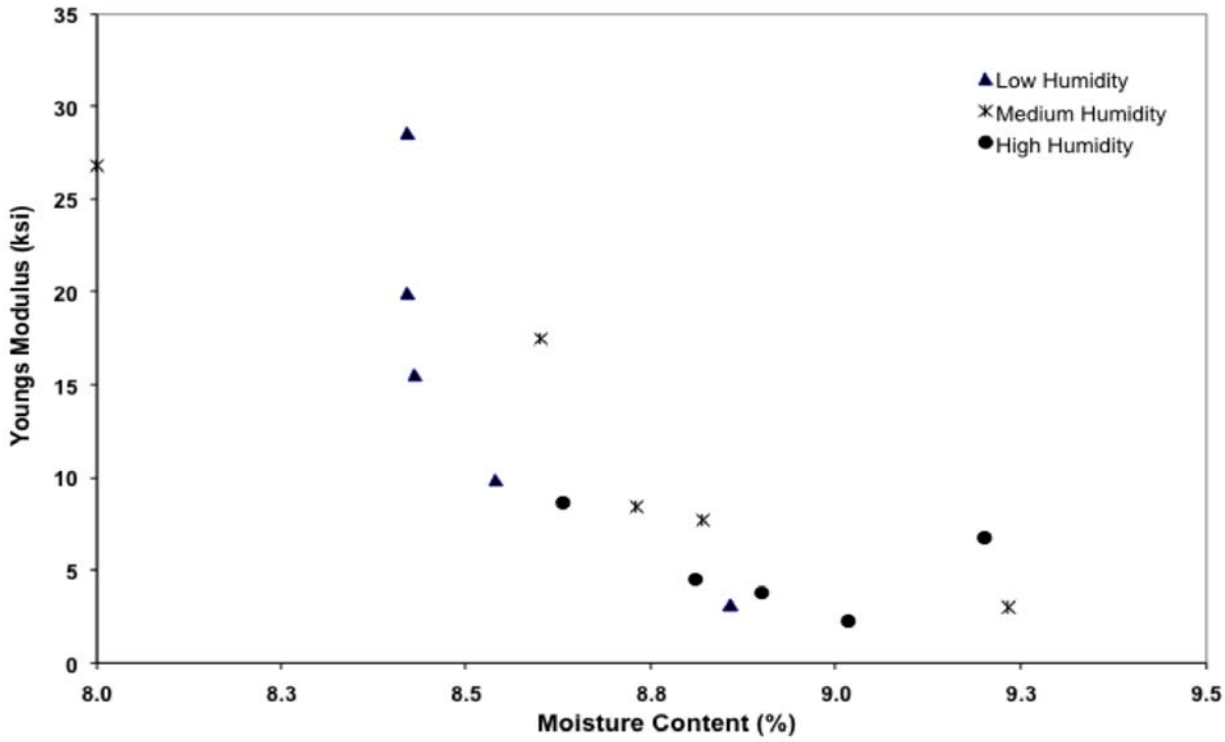

Figure 6-3. Variation of Loxahatchee shell-rock Young's modulus with moisture content as a function of humidity levels.

6.3 Scanning Electron Microscope Analysis

6.3.1 Introduction

This section is designated to discus the ESEM analysis results. ESEM techniques were used in order to see whether the moisture loss resulted in calcite cement growth, which could be responsible for the observed stiffness increase in the FFRC testing discussed in the previous section. ESEM examinations were conducted using a Hitachi S-3000 N Scanning Electron Microscope with an Energy Dispersive Spectrometer (EDS) x-ray analyzer at the UF Department of Civil and Coastal Engineering. After modulus testing, the selected specimens were cut out of the cylinder molds and prepared for ESEM analysis.

6.3.2 Specimen Preparation

Specimens from materials cured for 30 days under low relative humidity were prepared to observe with the ESEM. These samples were chosen because it was felt that these samples had

the highest potential for showing calcite cement bonding. In order to prepare samples for ESEM analysis, large slices measuring approximately 1.5-inch thick and 4-inch diameter were cut from the plastic cylinders dried in an oven. The pieces were further broken by hand into the 1 in^3 size required to fit in the ESEM mounting chamber. These samples were impregnated with a low viscosity epoxy in order to fill as many voids as possible. Epoxied samples were then cut and sanded until polished and flattened. When viewed in the ESEM, the density of the epoxy makes it appear black, allowing for easy identification of voids.

In addition to laboratory compacted specimens, a section of a field core from Glades County was examined for comparison with the laboratory compacted specimens.

6.3.3 ESEM Analysis Results

ESEM examinations of the three compacted materials and the field core were conducted in order to search for the presence of calcite crystal growth clusters. Images of 14 random points that were selected on each specimen were taken and examined for presence of calcite crystal and patterns that would suggest growth. Any calcite crystals visible at this scale were further investigated. As stated earlier, samples were polished so that the eSEM settings would not need to be reconfigured while investigating each sample and also in order to run EDS. The spectrometer identified and mapped the chemicals present for selected images.

Selected images from the analysis showing typical characteristics are presented in Figures 6-4 through 6-7 for laboratory compacted specimens, and Figures 6-8 through 6-11 for field core. The interpretation of the images is simply as follows: the light aggregates are calcium carbonate, grey aggregates are quartz, and the black areas are the intruded epoxy.

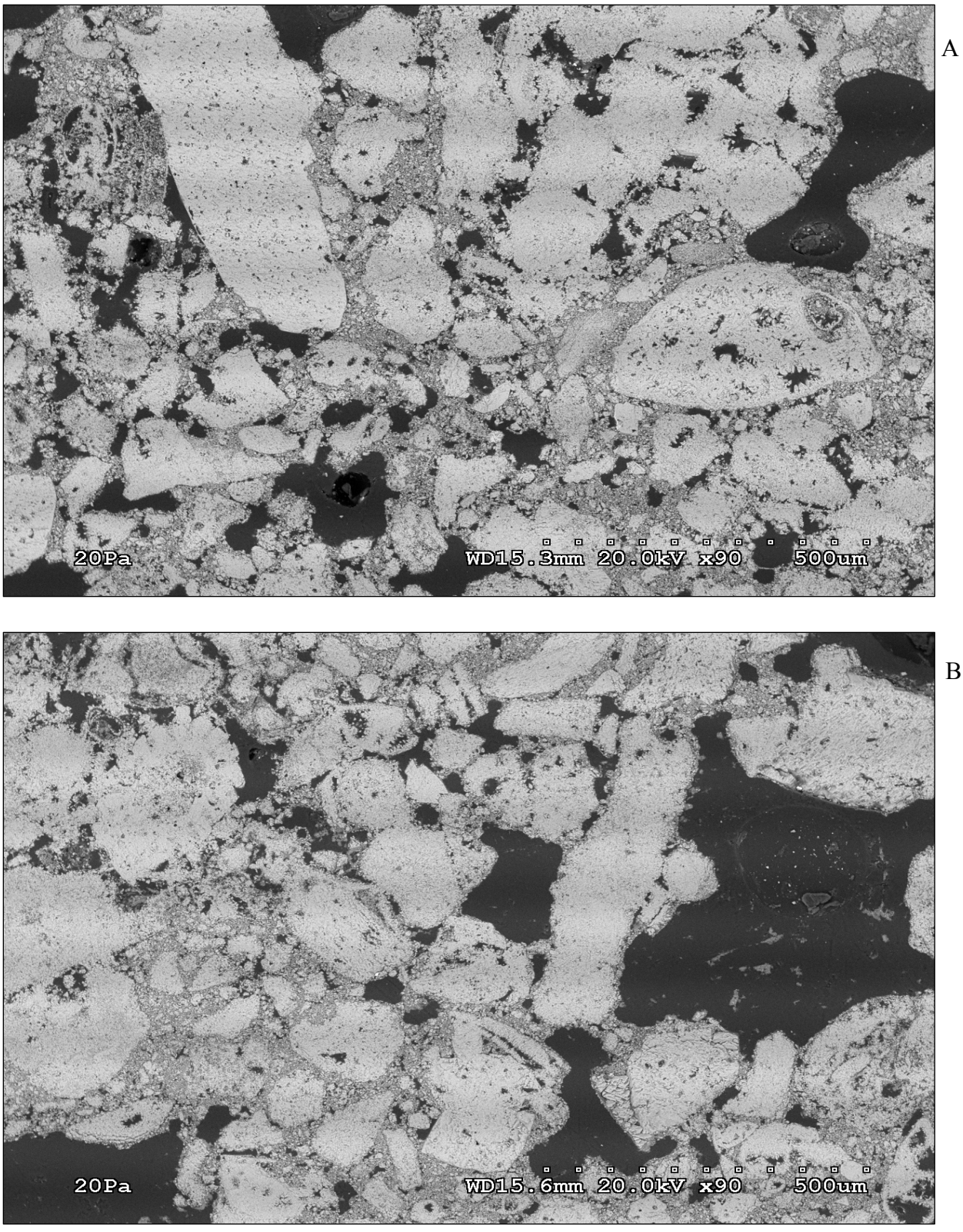

Figure 6-4. Ocala limerock typical images. A) Random point 1. B) Random point 2.

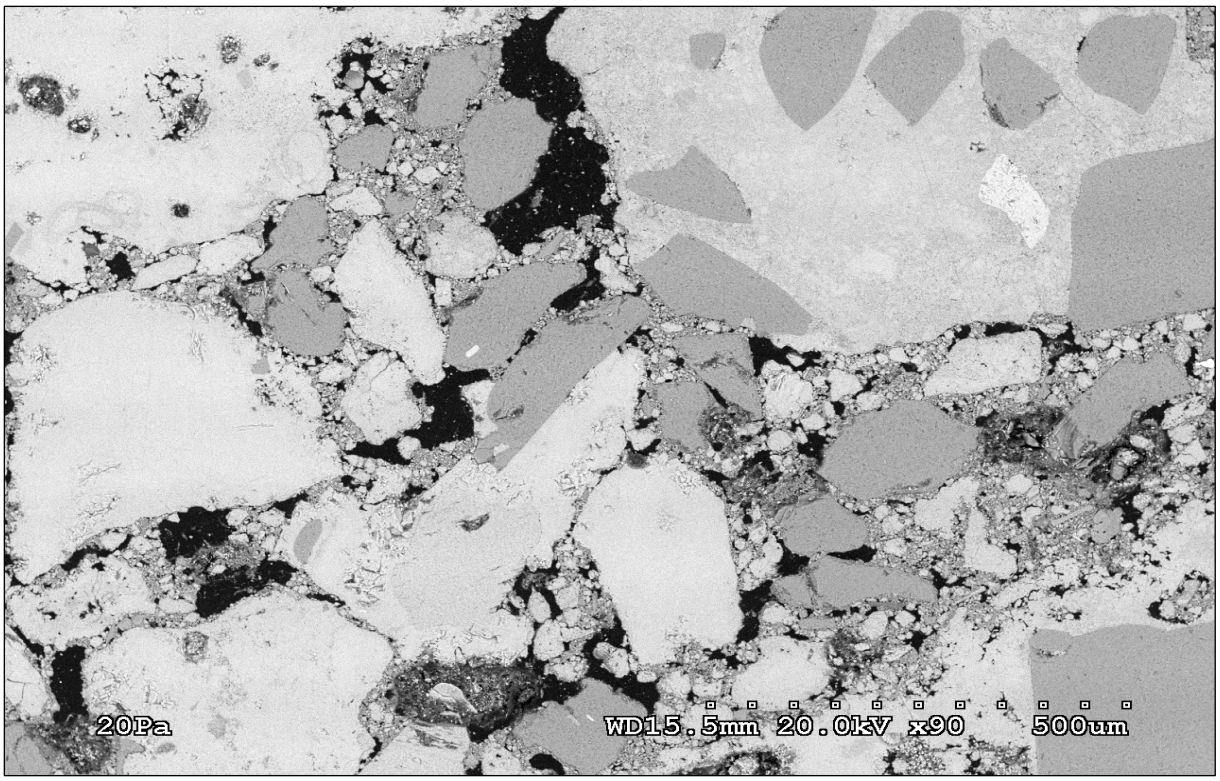

A

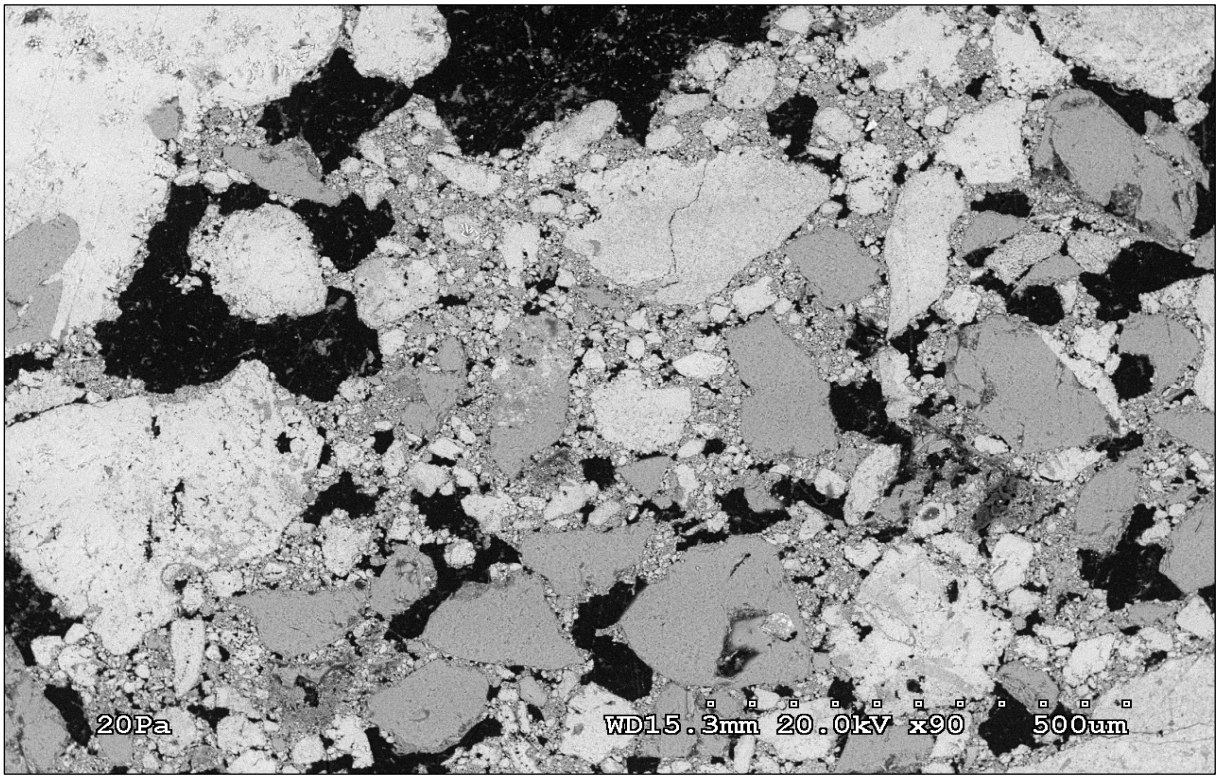

B

Figure 6-5. Miami limestone typical images. A) Random point 1. B) Random point 2.

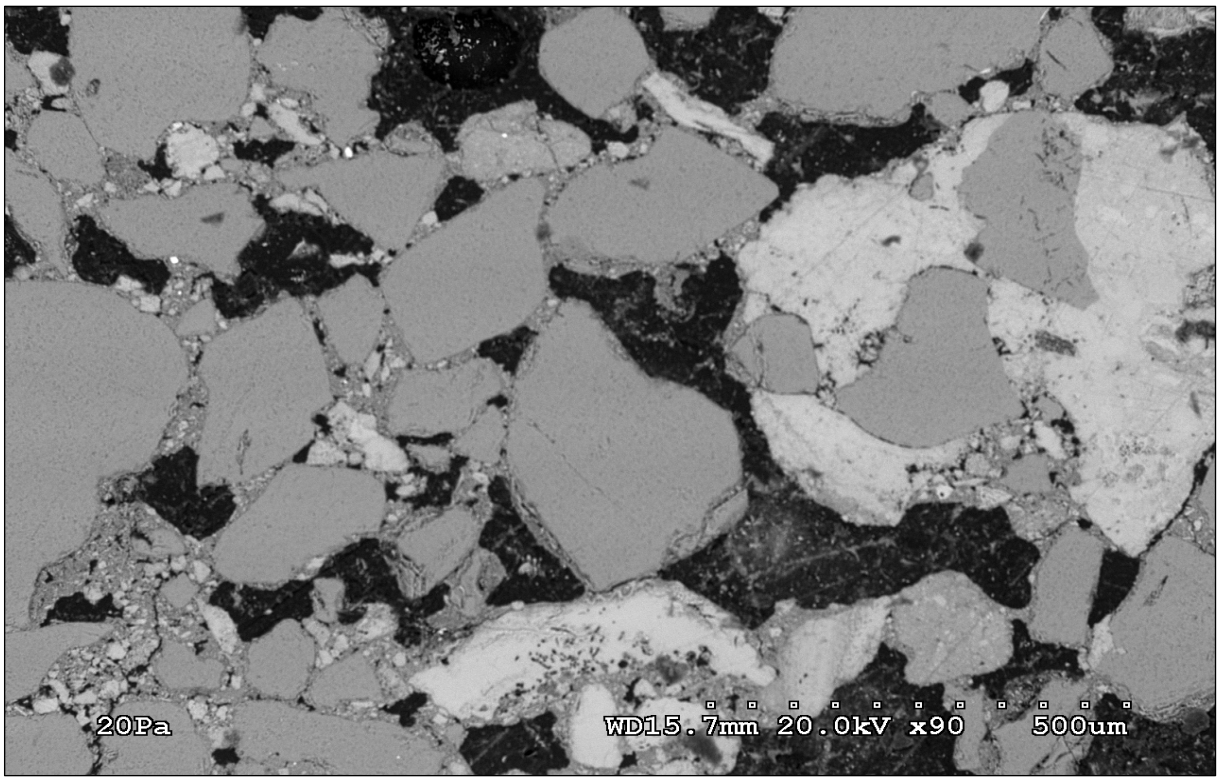

A

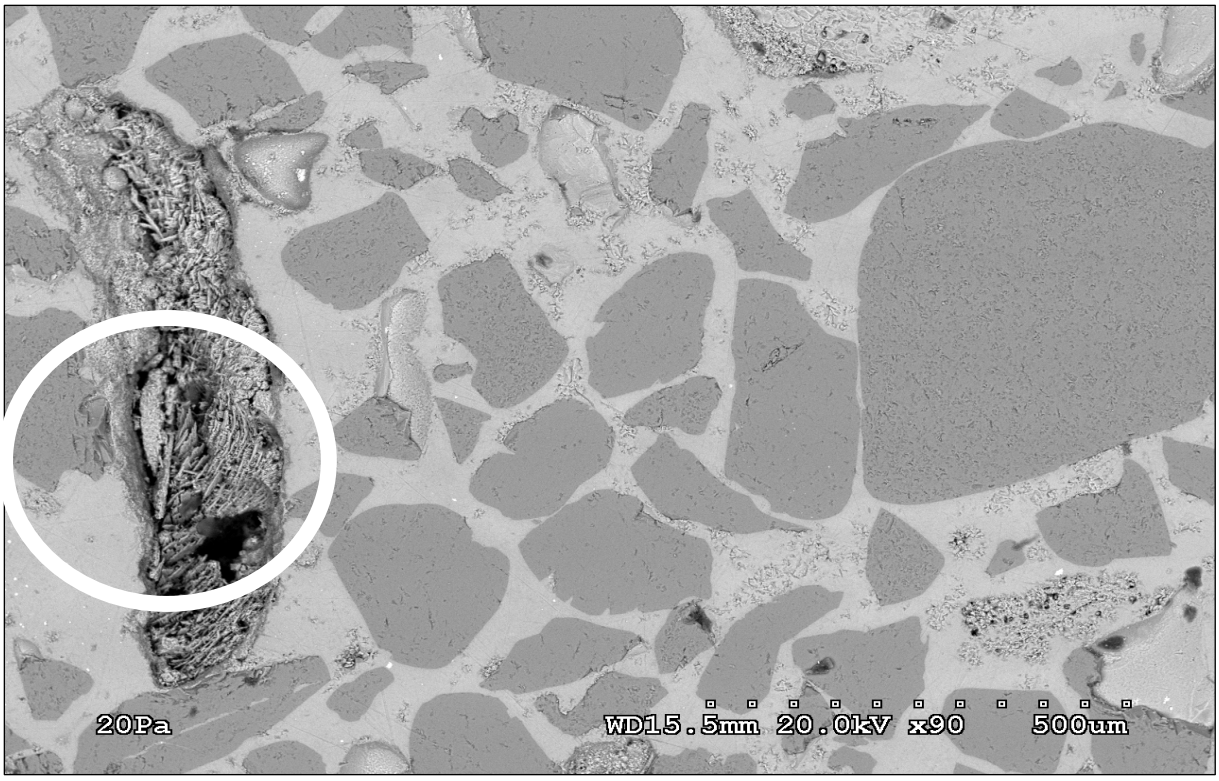

B

Figure 6-6. Loxahatchee shell-rock typical images. A) Random point 1. B) Random point 2

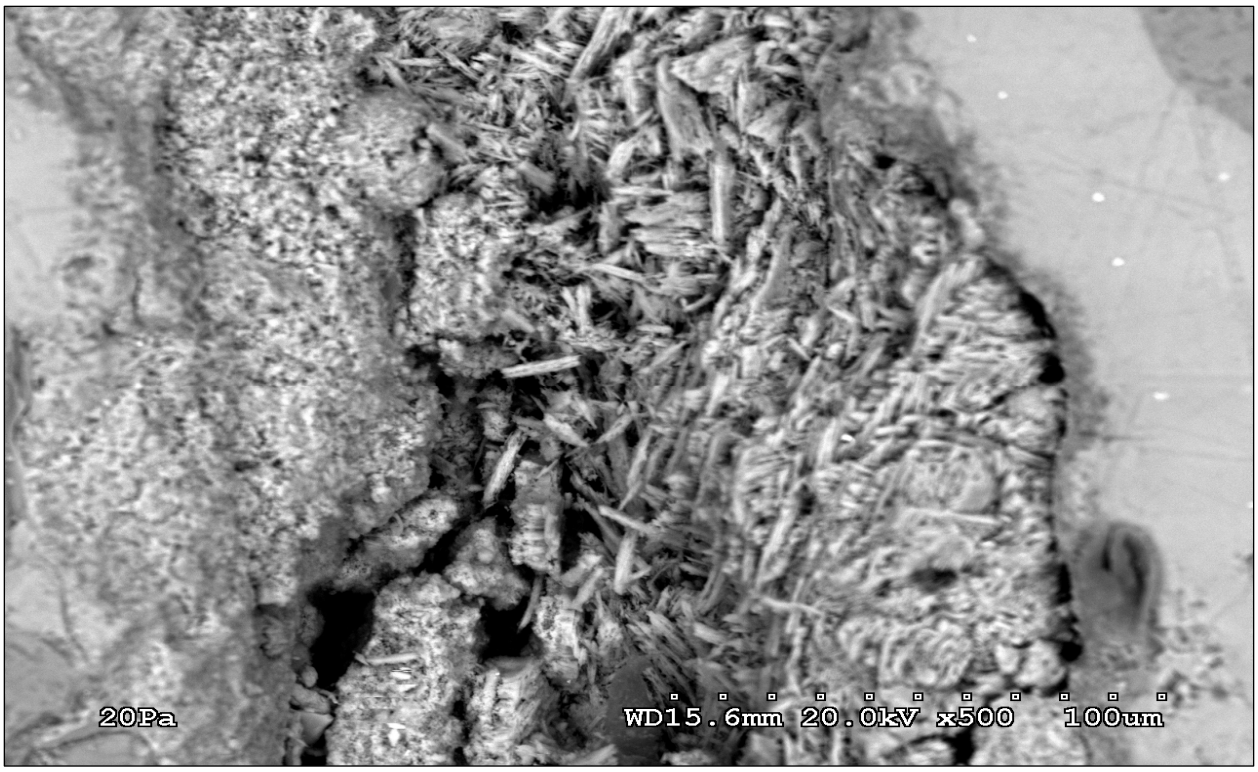

Figure 6-7. Loxahatchee shell-rock close-up of highlighted region in Figure 6-6 B.

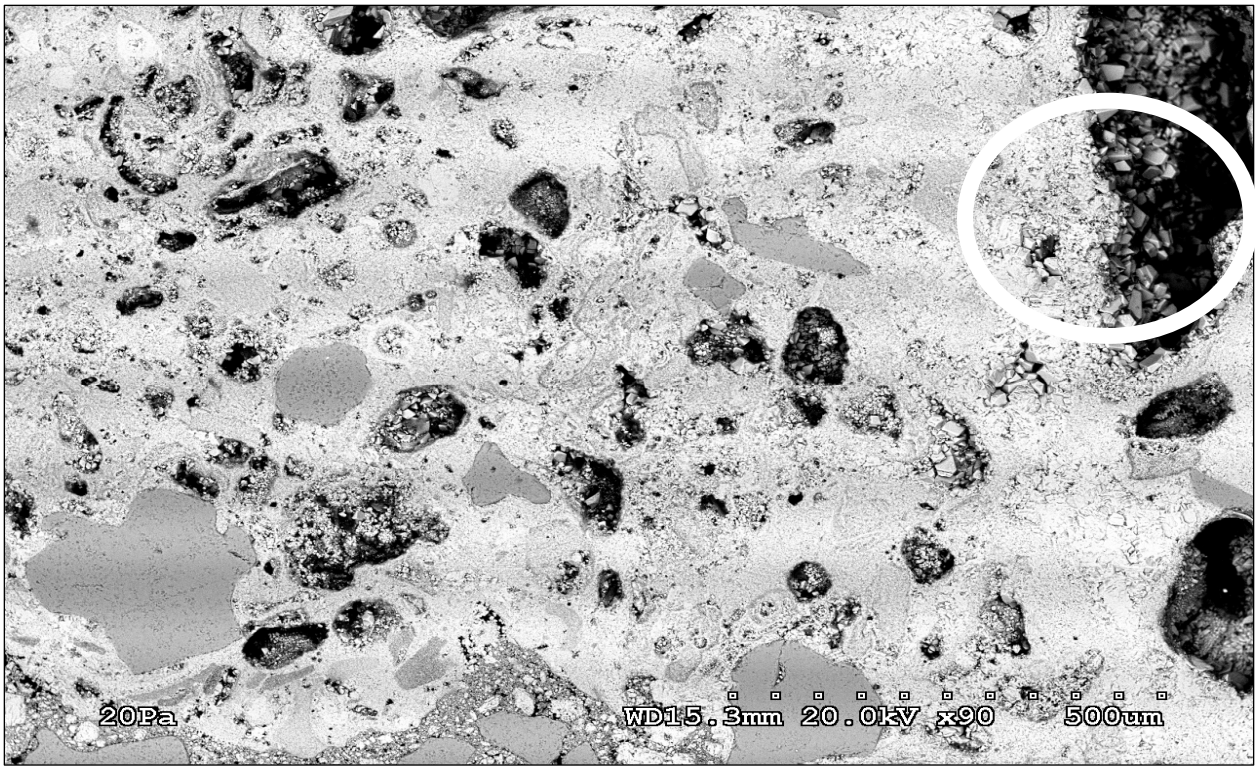

Figure 6-8. Glades core typical image showing zone of calcite crystal growth (random point 1).

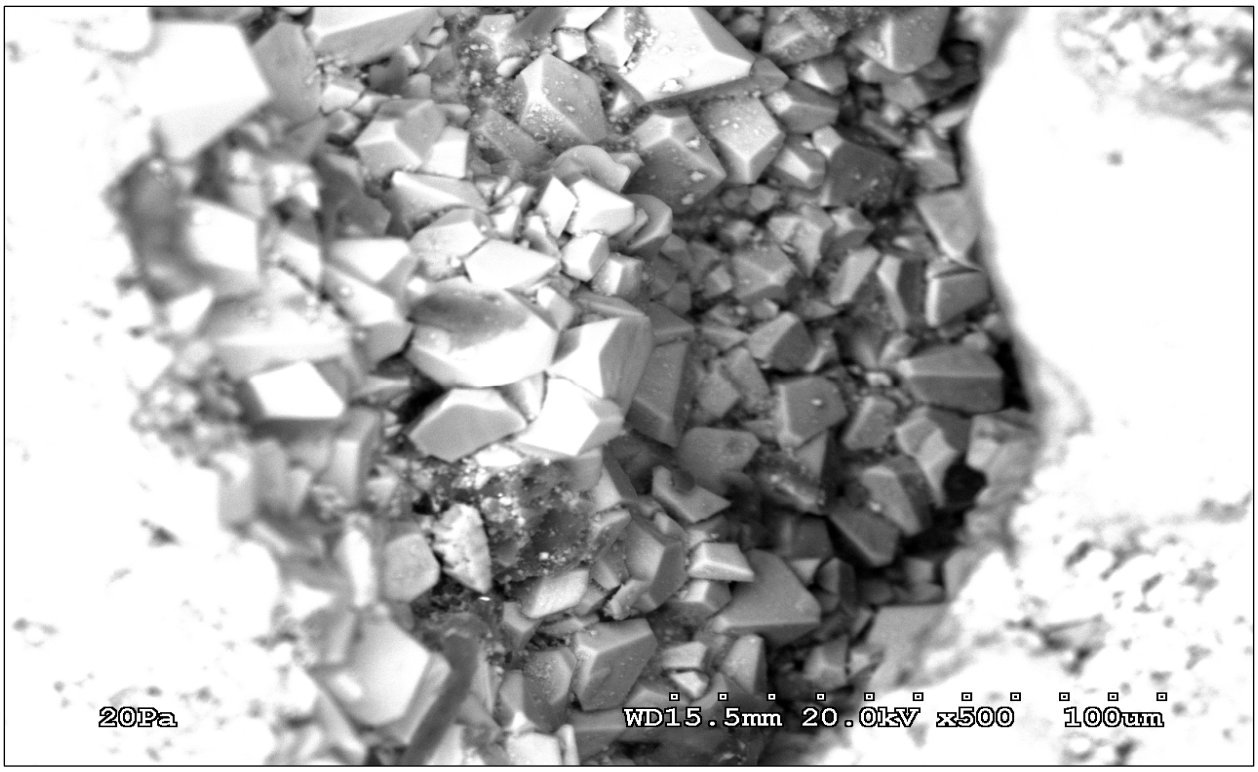

Figure 6-9. Glades core close-up of highlighted region in Figure 6-8.

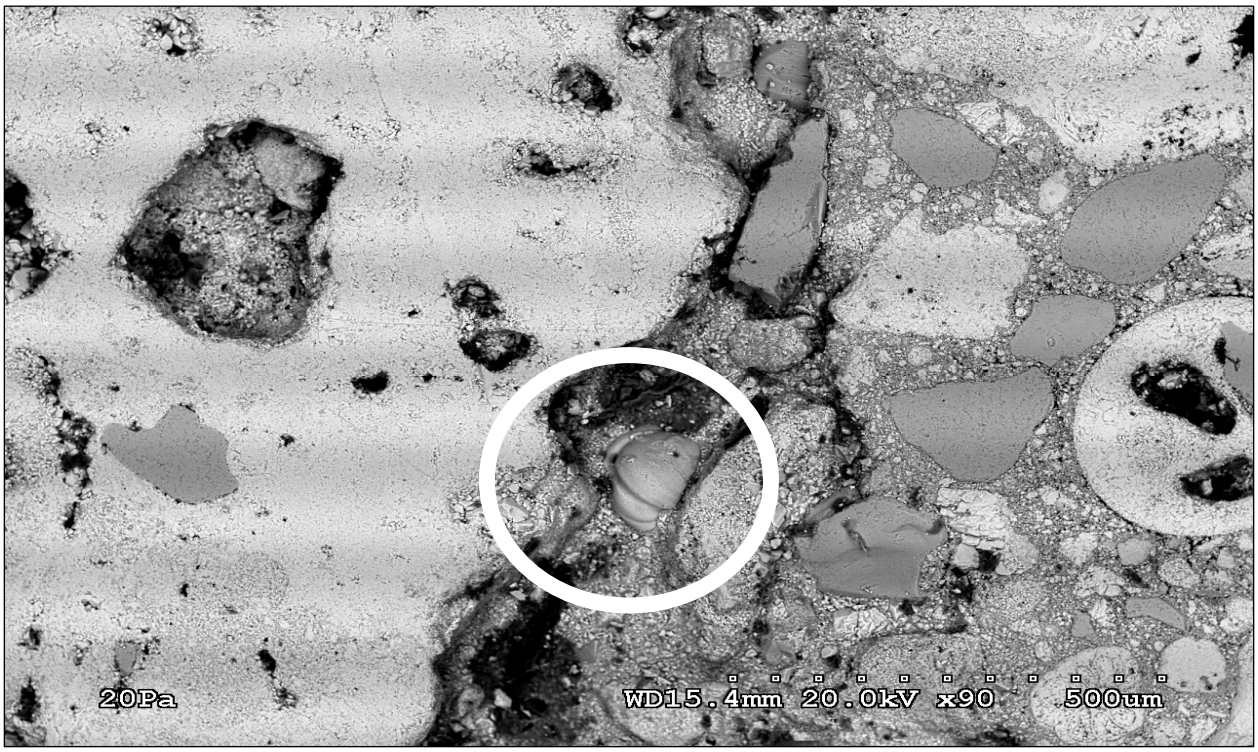

Figure 6-10. Glades core typical image showing zone of calcite crystal growth (random point 2).

Figure 6-11. Glades core close-up of highlighted region in Figure 6-10.

It should be noted from Figures 6-4 and 6-5, Ocala limerock and Miami limestone shows no sign of calcite crystal growth. Figure 6-6 B reveals a zone in the Loxahatchee shell rock containing textures related to calcite crystals. Figure 6-7 is a close-up of the area of interest in Figure 6-6 B, but reveals that the crystals are only intraparticle, and therefore would not contribute to any stiffness increase from aggregate-to-aggregate cementation.

Typically, the Glades core shows less void area than the compacted specimens. In addition, many of the Glades core images contained easy to spot, relatively large calcite crystals that appear to be growing between aggregates. Typical features of the Glades core are shown in Figures 6-8 and 6-10. Rhombohedral calcite crystals are shown filling in the pore spaces in Figures 6-9 and 6-11.

While the history of the Glades core is not available, the images presented are valuable in that they illustrate how calcite crystal growth and cementation would appear in limerock materials. In comparison, no such crystallization is observed in laboratory-compacted specimens following 30 days of curing in desiccators. Yet, significant stiffness increases were measured in these materials during these same 30 days. It is thus reasonable to suggest that the stiffening mechanism is not due to chemically-based crystallization and cementation.

6.4 Mercury Porosimetry

As part of this experiment, we also briefly experimented with the mercury porosemetry test. Mercury porosimetry characterizes a material's porosity by applying various levels of pressure to a sample immersed in mercury. In this research, mercury porosity was used to determine the pore size distribution of Florida limerock base materials. The University of Florida Particle Engineering Research Center personnel tested all materials in accordance with ASTM D 4404 using a Quantachrome Autoscan 60 Mercury Porosimeter at the UF Particle Engineering Research Center. Porosity measurements were completed on 30-day samples cured under low relative humidity. The samples were completely dried out, as any moisture will be turned into compressible water vapor. To perform an analysis, the sample is loaded into a penetrometer, which consists of a sample cup connected to a metal-clad, precision-bore, and glass sample cell ("glass capillary stem" Figure 6-12). The penetrometer is sealed and placed in a low-pressure port, where the sample is evacuated to remove air and moisture. The penetrometer's cup and the sample cell are then automatically backfilled with mercury. Excess mercury is automatically drained back into the internal reservoir; only a small amount remains in the penetrometer. As pressure on the filled penetrometer increases, mercury intrudes into the sample's pores, beginning with those pores of largest diameter. This requires that mercury move from the

capillary stem into the cup, resulting in a decreased capacitance between the now shorter mercury column inside the stem and the metal cladding on the outer surface of the stem.

The instrument automatically collects low-pressure measurements over the range of pressures specified by the operator. Then, the penetrometer is moved to the high-pressure chamber, where high-pressure measurements are taken. Data are automatically reduced using the low and high pressure data points, along with values entered by the operator, such as the weight of the sample and the weight of the penetrometer loaded with mercury.

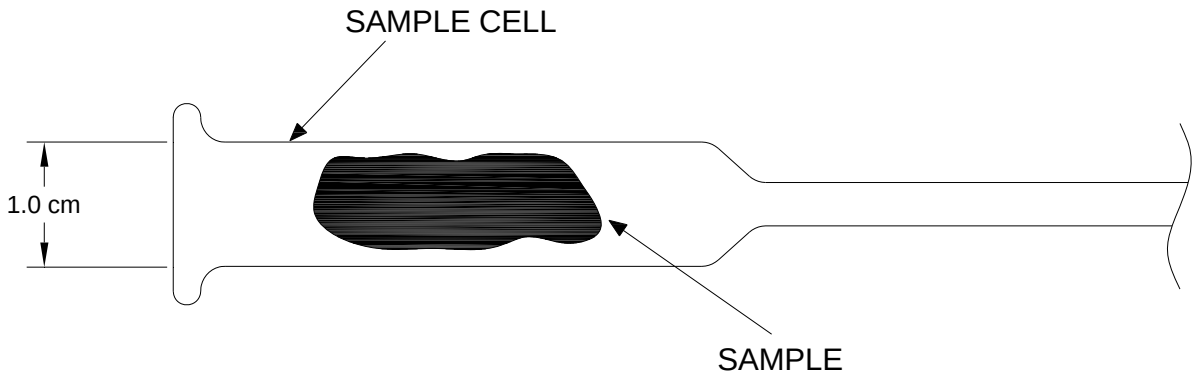

Figure 6-12. Cross-section of glass sample cell; Mercury is intruded from right side.

Representative samples were difficult to obtain since the compacted aggregate is approximately 100 cubic inches and the mercury porosimeter device accepts specimens of approximately 0.092 cubic inch. In an attempt to test representative samples, aggregate pieces were taken with finer particles attached (no "clean" aggregate).

The initial moisture content values were taken for each material during the modulus testing portion of this research. The theoretical porosity was calculated using classic weight-volume relationships. The calculations showed that the bulk porosity values of Ocala limerock, Miami limestone, and Loxahatchee shell-rock are 0.318, 0.238, and 0.266, respectively.

Mercury Porosimeter testing gave further insight into the void structure of the compacted limestone. Mercury porosimetry is able to give distributions of pore sizes while bulk porosity measurements do not. The mercury porosimetry test is capable of giving measurements accurate to diameters ranging between 3.6 nm and 100 μm.

The mercury porosemetry results are shown below in Figure 6-13. The figure displays cumulative porosity on the vertical axis versus pore diameter on the horizontal, and for pore sizes between approximately 3.6 nm and 100 μm as noted above. At a given pore diameter, the cumulative porosity presents the normalized volume of pores (i.e., the porosity) equal or larger in size than the given diameter. The shape of the diagram is indicative of the distribution of pore sizes within the specimen. It should be noted that the flat portions of the plot ranging between 10^{-6} and 10^{-5} meters are due to testing inaccuracies caused by switching between the low-and high-pressure chambers. In addition, it should be noted that the cumulative porosity at the smallest pore size indicated is smaller than the bulk porosity values presented previously. The bulk porosity was determined from measurements on the complete 4-inches by 8-inches cylinders of materials, where as the cumulative porosity was determined via mercury porosimetry measurements on a much smaller sample, and thus does not represent the value of the largest pores in the material, i.e., larger than 100 μm.

It is clear from the figure that indeed the pore size distribution is different between the four materials. For the lab specimens, the Miami material reaches a plateau at the smallest pore diameter, whereas the Ocala material plateaus at the largest pore diameter. This suggests that the Miami material has the smallest pores available within the pore volume. On the other hand, the Ocala material has the largest number of pores between 10^{-6} and 10^{-7} m, since this graph is very steep in this region. This has implications for material behavior: smaller pore sizes produce

largest suction values, i.e., negative pore pressure. This could explain the differences in small-strain stiffness upon drying between the different materials.

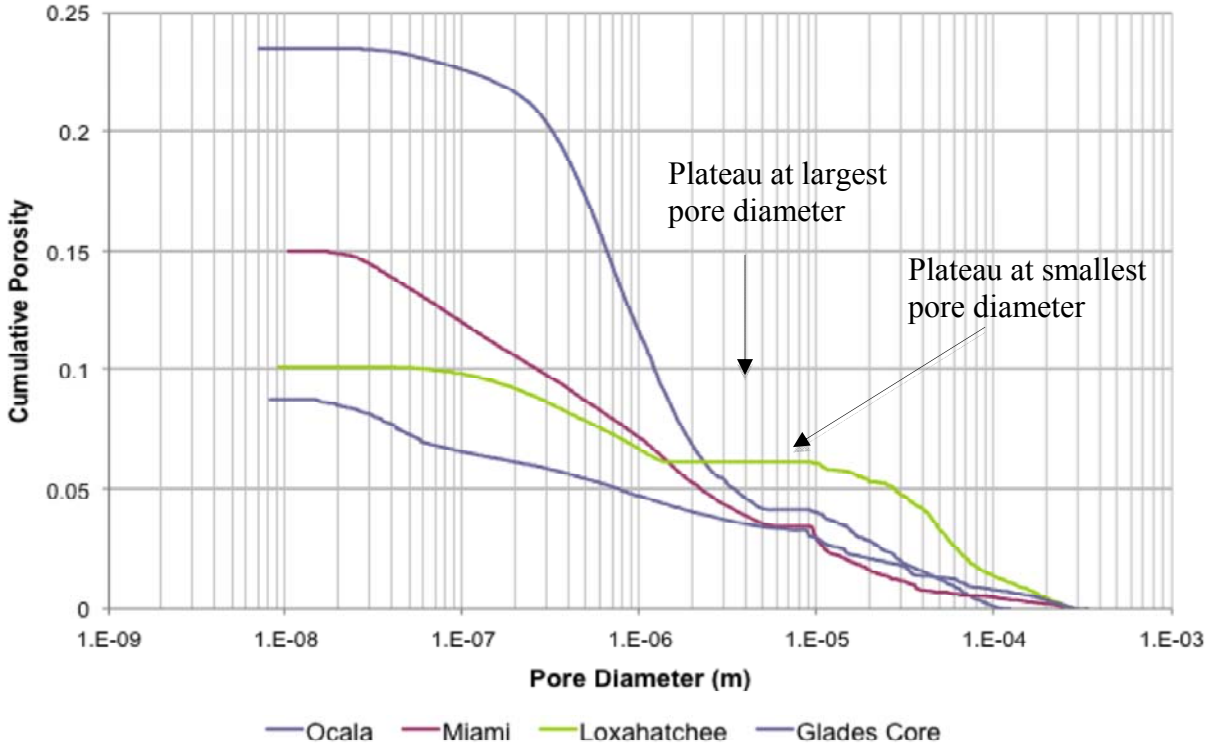

Figure 6-13. Mercury porosimeter results for 30-day specimens and Glades core.

CHAPTER 7
RESILIENT MODULUS (M_R) TEST RESULTS

7.1 Resilient Modulus (M_R) Testing of Laboratory Compacted Specimens

7.1.1 Introduction

As discussed previously, the FFRC test is an effective means for studying the influence of specimen conditioning or material response, as the test is non-destructive and simple to complete. However, the large-strain resilient modulus is thought to be more indicative of material response under actual traffic loading. Thus, the FDOT SMO conducted a limited parallel study to investigate the material responses to conditioning via the M_R test.

This chapter will document and discuss the response of laboratory-compacted specimens of unbound aggregate that are exposed to environmental conditioning discussed in Chapter 4. The figures used in this chapter demonstrate comparisons of the resilient modulus test results of three replicates of each material exposed to environmental conditioning. Comparisons of the response between the different materials will be presented for each condition. The variation of the resilient modulus with bulk stress of three replicates of each material, per condition, and the variation of the resilient modulus with bulk stress corresponding to various moisture content levels of each material, per replicate, is presented in Appendix I.

7.1.2 Resilient Modulus Test Conditions

The details of samples, such as dimensions, number of samples, and specimen preparation parameters that are used in M_R testing were discussed in Chapter 4. In this section, conditions applied to each replicate of each material are presented.

7.1.2.1 Newberry and Ocala

The following conditions were applied to three replicates of each material. As designated by the FDOT SMO, condition 1 represents optimum moisture condition.

Conditions 2, 3, and 3B represent outdoor ambient condition. Conditions 4 and 5 represent wetting and drying conditions.

- Condition 1: Sample is packed to optimum moisture and tested via M_R.
- Condition 2: Sample is packed to optimum moisture and then set outside for 7 days prior to M_R testing.
- Condition 3: Sample from condition 2 put back outside for 7 additional days (14 total) prior to M_R testing.
- Condition 3B: Sample from condition 3 put back outside for 7 additional days (21 total) prior to M_R testing.
- Condition 4: Sample is packed to optimum moisture and then dried in oven at 110 ºF for 2 days before testing.
- Condition 5: Sample from condition 4 is soaked for 4 days and then re-tested.

7.1.2.2 Loxahatchee and Miami

The following conditions were applied to three replicates of each material. As designated by the FDOT SMO, condition 1 represents optimum moisture condition. Conditions 2, 3, and 3B represent outdoor ambient condition. Conditions 4 through 10 represent wetting and drying conditions.

- Condition 1: Sample is packed to optimum moisture and tested via M_R.
- Condition 2: Sample is packed to optimum moisture and then set outside for 7 days prior to M_R testing.
- Condition 3: Sample from condition 2 put back outside for 7 additional days (14 total) prior to M_R testing.
- Condition 3B: Sample from condition 3 put back outside for 7 additional days (21 total) prior to M_R testing.
- Condition 4: Sample is packed to optimum moisture and then dried in 110 ºF oven for 2 days before M_R testing.
- Condition 5: Sample from condition 4 soaked for 4 days and then re-tested.
- Condition 6: Sample from condition 5 dried in 110 ºF oven for 2 days and then re-tested.
- Condition 7: Sample from condition 6 soaked for 4 days and then re-tested.
- Condition 8: Sample from condition 7 dried in 110 ºF oven for 2 days and then re-tested.
- Condition 9: Sample from condition 8 soaked for 4 days and then re-tested.

- Condition 10: Sample from condition 9 dried in 110 ºF oven for 2 days and then re-tested.

7.1.2.3 Georgia

The following conditions were applied to two replicates for optimum moisture and outdoor ambient conditions, and one replicate for oven drying condition. Condition 1 represents optimum moisture condition. Conditions 2, 3, and 4 represent outdoor ambient condition. Condition 5 represents oven drying condition.

- Condition 1: Sample is packed to optimum moisture and tested via M_R.
- Condition 2: Sample from condition 1 set outside for 2 days prior to M_R testing.
- Condition 3: Sample from condition 2 put back outside for 5 additional days (7 total) prior to M_R testing.
- Condition 4: Sample from condition 3 put back outside for 7 additional days (14 total) prior to M_R testing.

7.2 Response of Laboratory Compacted Specimens to Environmental Conditioning

This section will introduce the response of laboratory-compacted specimens of unbound aggregate that are exposed to optimum moisture, outdoor ambient, and wetting and drying cycles. Please note that resilient modulus tests with time at constant optimum moisture content were not conducted in this study. However, McClellan et al. (2000) indicate that aging of specimens at constant optimum moisture for up to 28-days had no observable effect on resilient modulus.

7.2.1 Optimum Moisture

Sample preparation for the FFRC and M_R tests was similar and discussed in detail in Chapter 4. Figure 7-1 presents variation of the resilient modulus with bulk stress for three replicates of each material. The bulk stress used here is the sum of the confining stress and the actual applied cyclic stress (deviator stress). The procedure to find the resilient modulus includes fifteen loading sequences (100 cycles per sequence) with a combination of five levels of confining pressures (3, 5, 10, 15, and 20 psi) and varying levels of deviator stress.

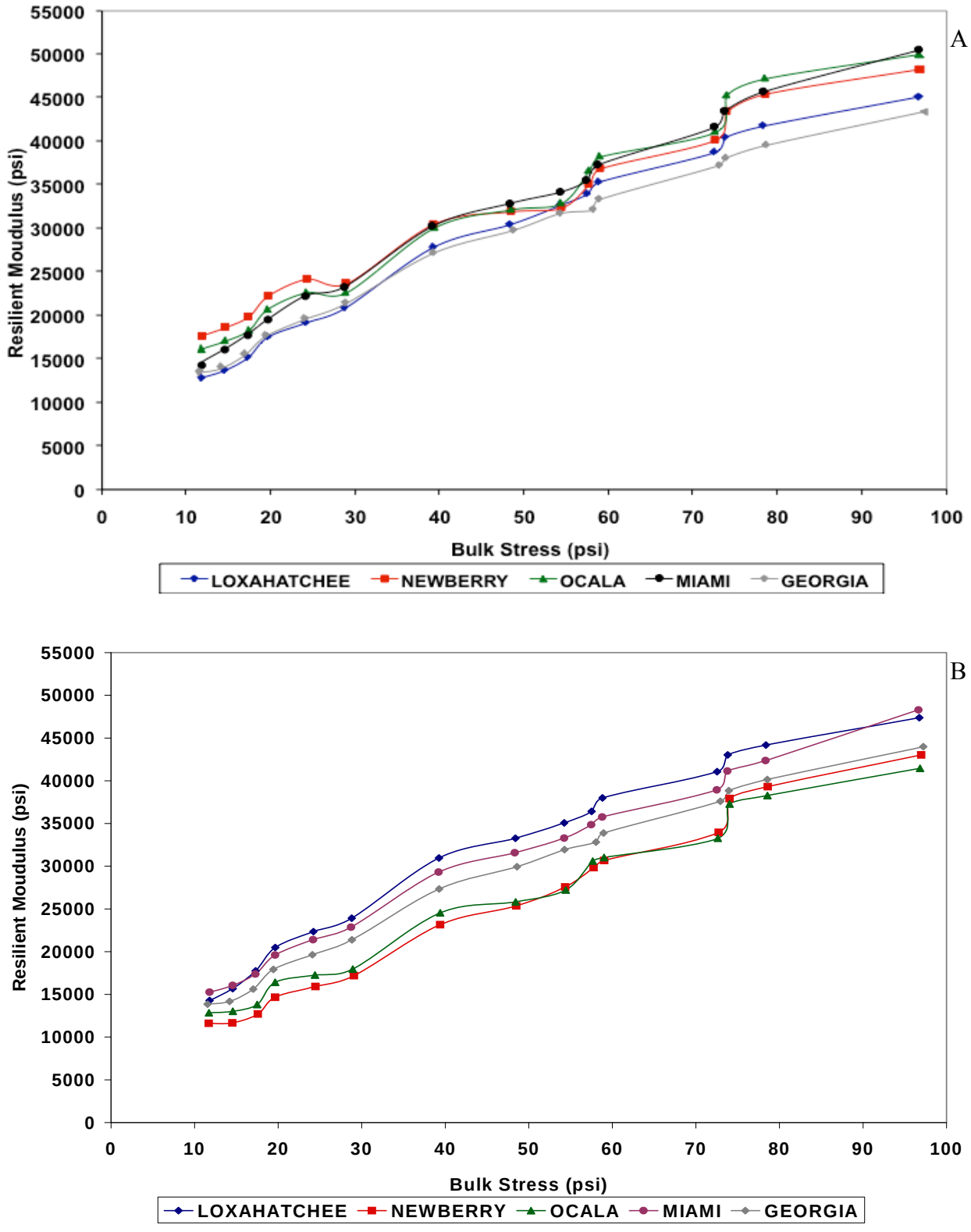

Figure 7-1. Variation of resilient modulus with bulk stress. A) Replicate 1. B) Replicate 2. C) Replicate 3.

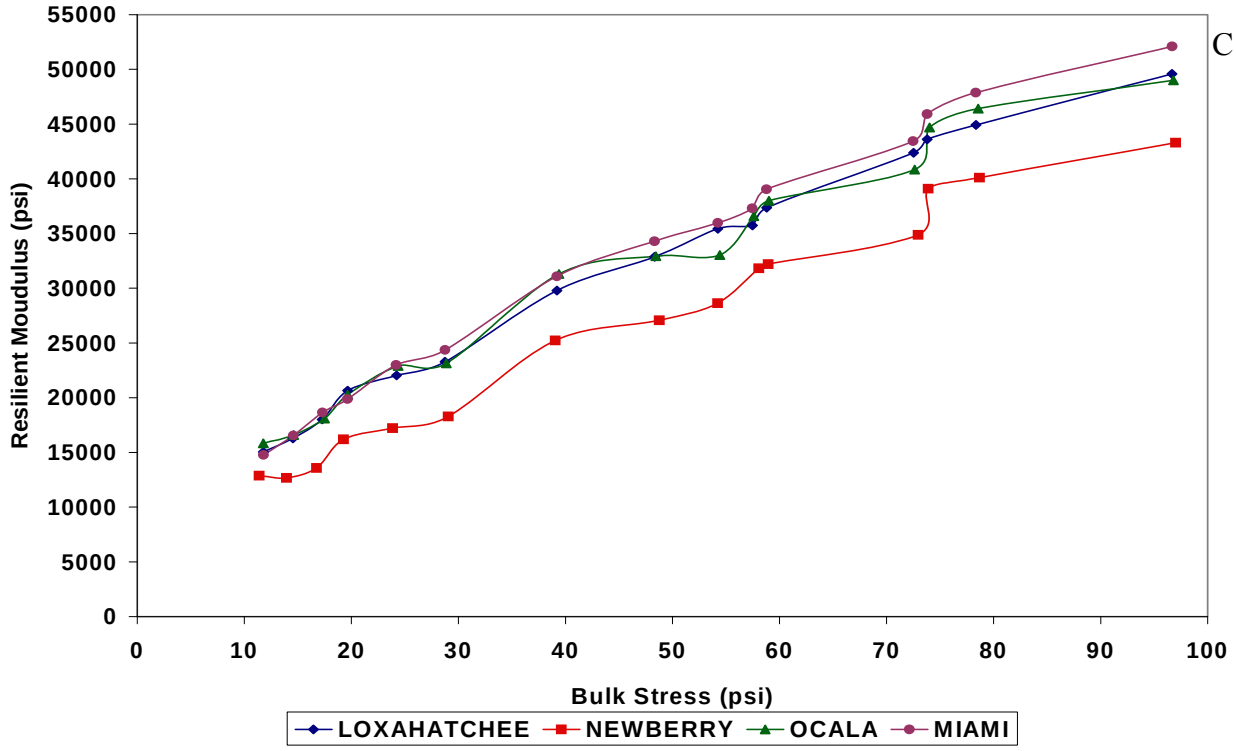

Figure 7-1. Continued.

It can be easily seen from the figures that the resilient modulus increases with an increase of bulk stress while at constant moisture. This behavior may be explained as when the bulk stress increases, the normal contact forces between particles increases, which results in better interlocking and frictional characteristics.

7.2.2 Drying

In this section, the influence of removal of water (drying) on the materials is discussed. The results were produced by placement of the specimens in outdoor shade environment and low-heat oven. As anticipated, both environmental conditioning methods produced relatively slow drying behavior and this behavior is depicted in the figures. Based on the material behavior observed under free-free resonant column testing (the results produced by placement of the specimen in ambient conditions either on laboratory bench or in outdoor shade environments are

almost identical) preparation for laboratory ambient environment of materials was deemed unnecessary.

7.2.2.1 Outdoor Ambient

Figures 7-2, 7-3, and 7-4 present resilient modulus test results for each of the five materials while being exposed to outdoor ambient air for replicate 1, 2, and 3, respectively. Figures 7-2 A, 7-3 A, and 7-4 A demonstrate that placement of specimens initially at optimum moisture content (time = 0) in outdoor shade drives water out from each replicate of each material. Variation of resilient modulus at a representative bulk stress of 20 psi (M_R (20)) with moisture content as the material dries from optimum water content, both in arithmetic scale, is presented in Figures 7-2 C, 7-3 C, and 7-4 C for each replicate of every material. Variation of M_R (20) with time in days, both in arithmetic scales are presented in Figures 7-2 B, 7-3 B, and 7-4 B for each replicate of every material. In Florida, the typical value of bulk stress is 20 psi for base course that corresponds to a commonly used asphalt concrete thickness of 2 to 4 inches.

It should be noted from the Figures 7-2 C, 7-3 C, and 7-4 C that for all replicates, the materials undergoes a notable increase, almost more than double, in resilient modulus as water is lost. The moisture content and modulus change occurs continually for 21 days, and all five materials demonstrate similar trends, but as was in the FFRC test, the rate of change and magnitude of the effect are different between materials. It should be noted that the Georgia granite changes the most, while change in Newberry limerock is the smallest.

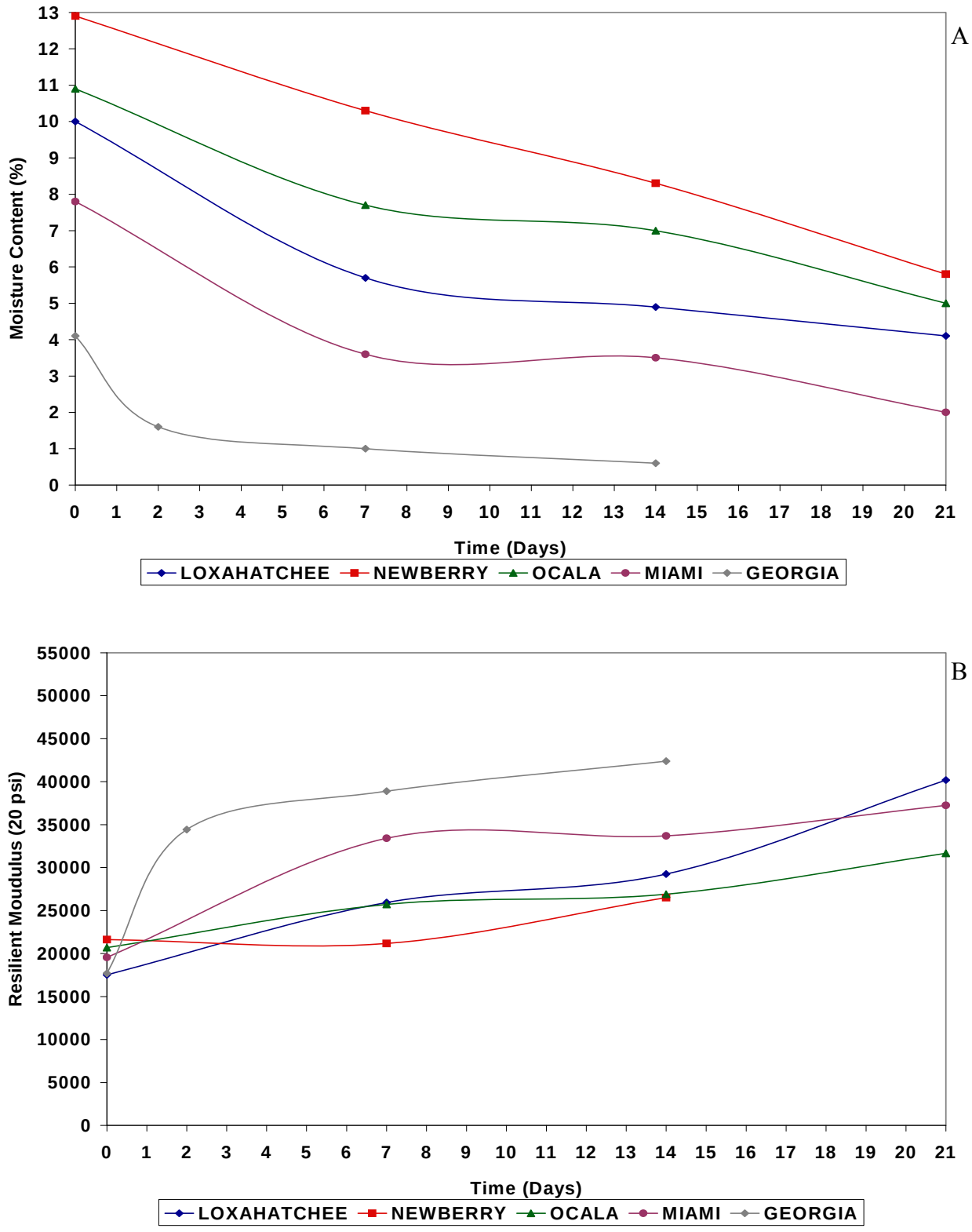

Figure 7-2. The resilient modulus test results of replicate 1.

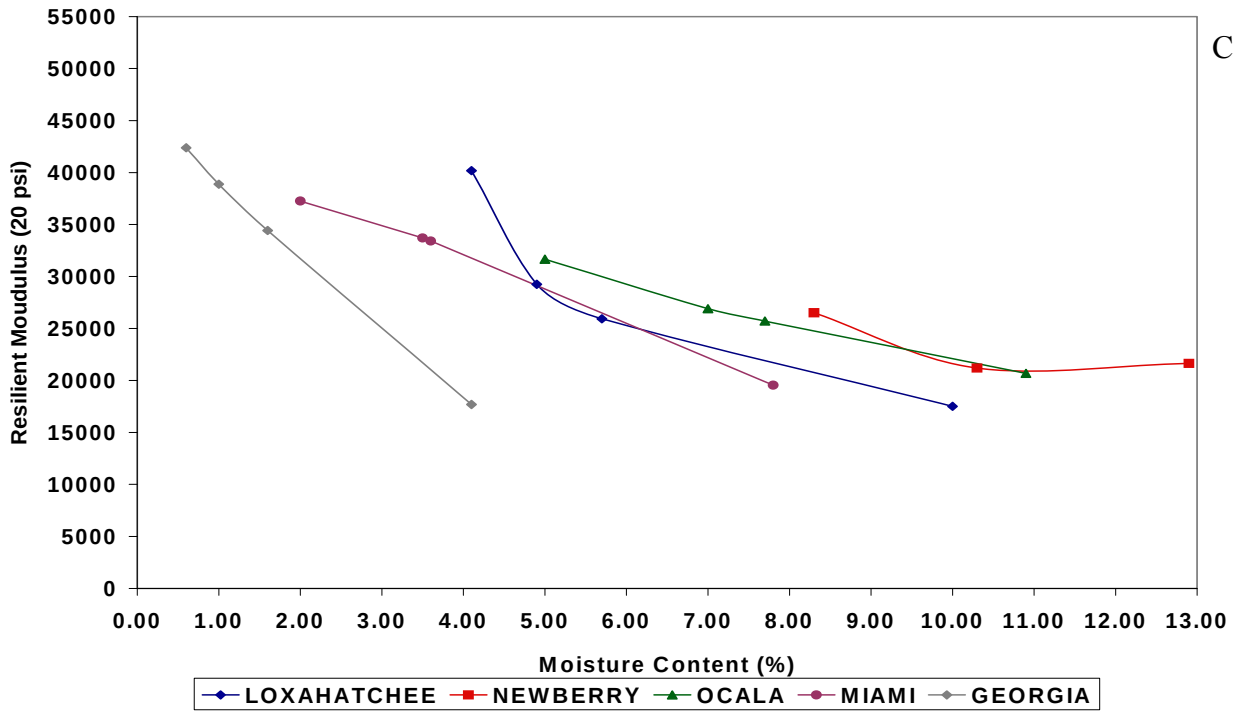

Figure 7-2. Continued.

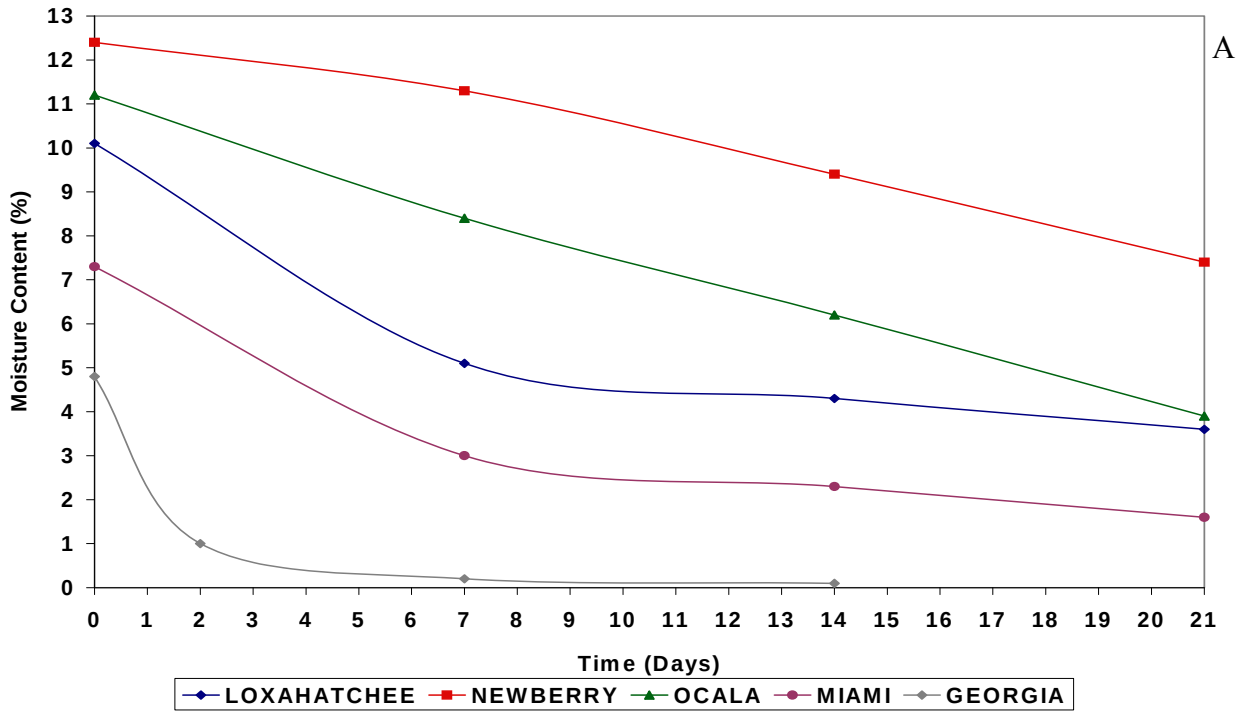

Figure 7-3. The resilient modulus test results of replicate 2.

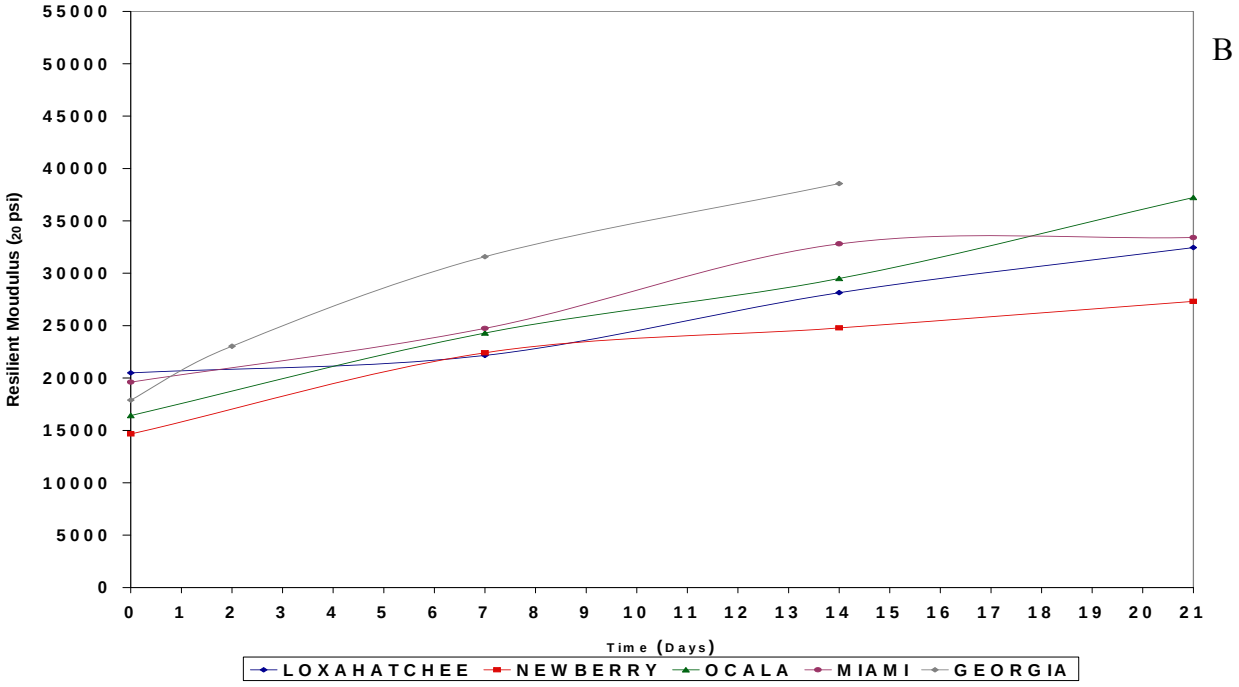

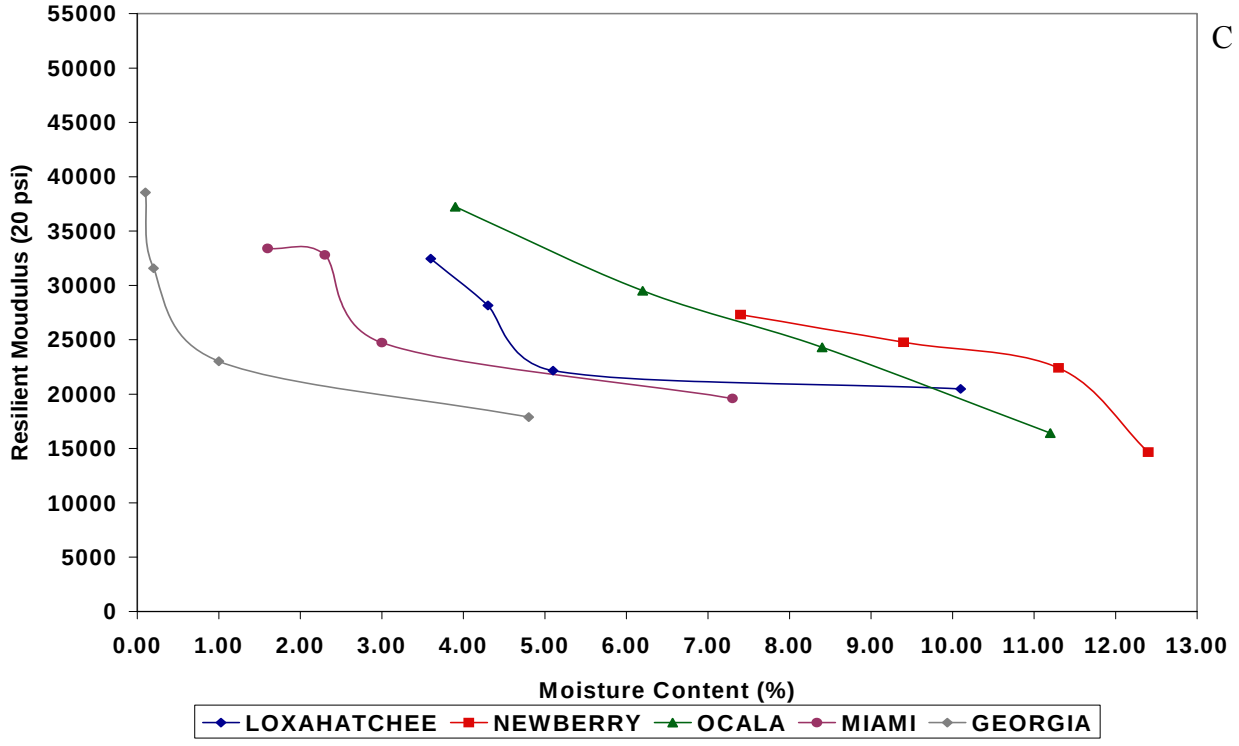

Figure 7-3. Continued.

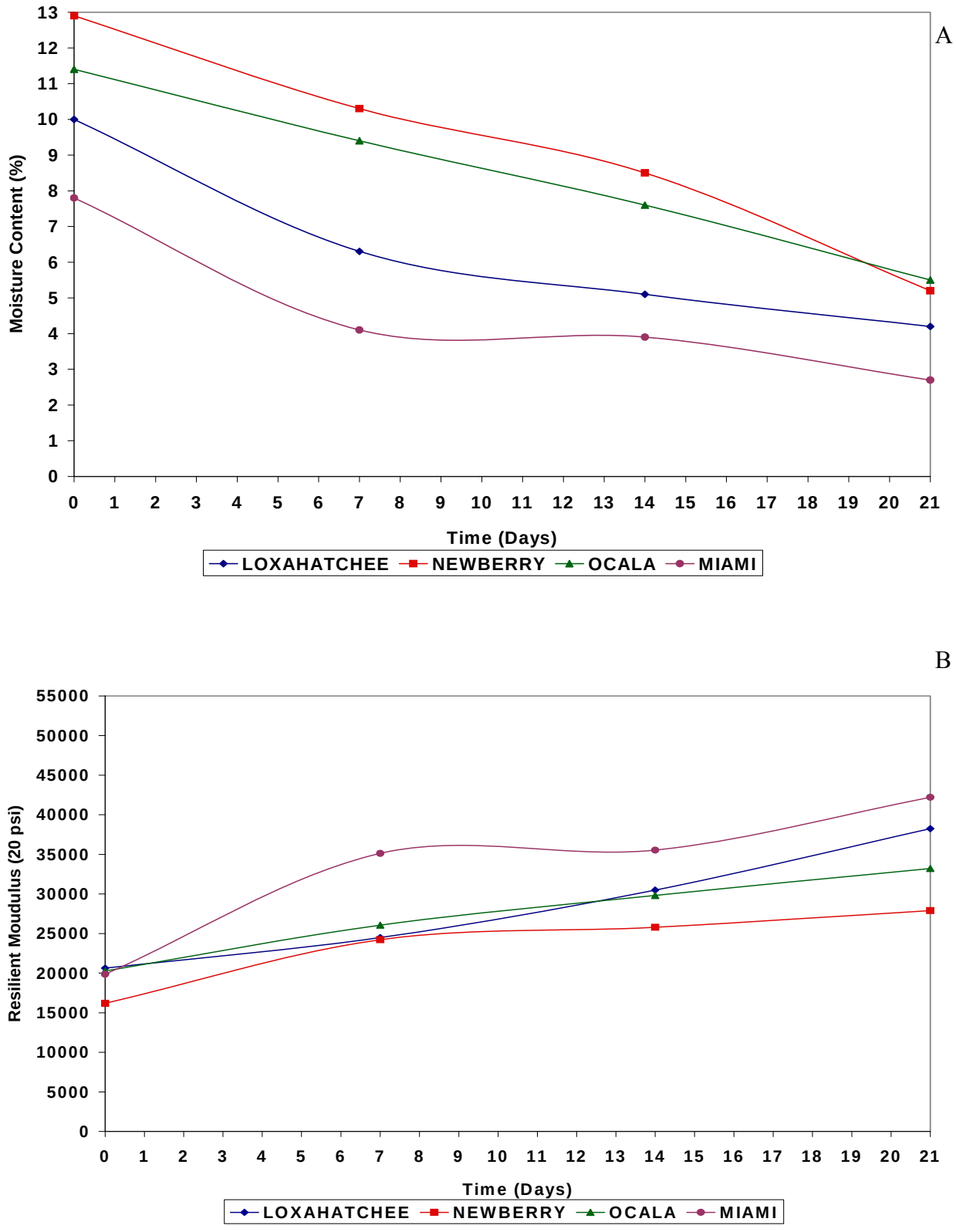

Figure 7-4. The resilient modulus test results of replicate 3.

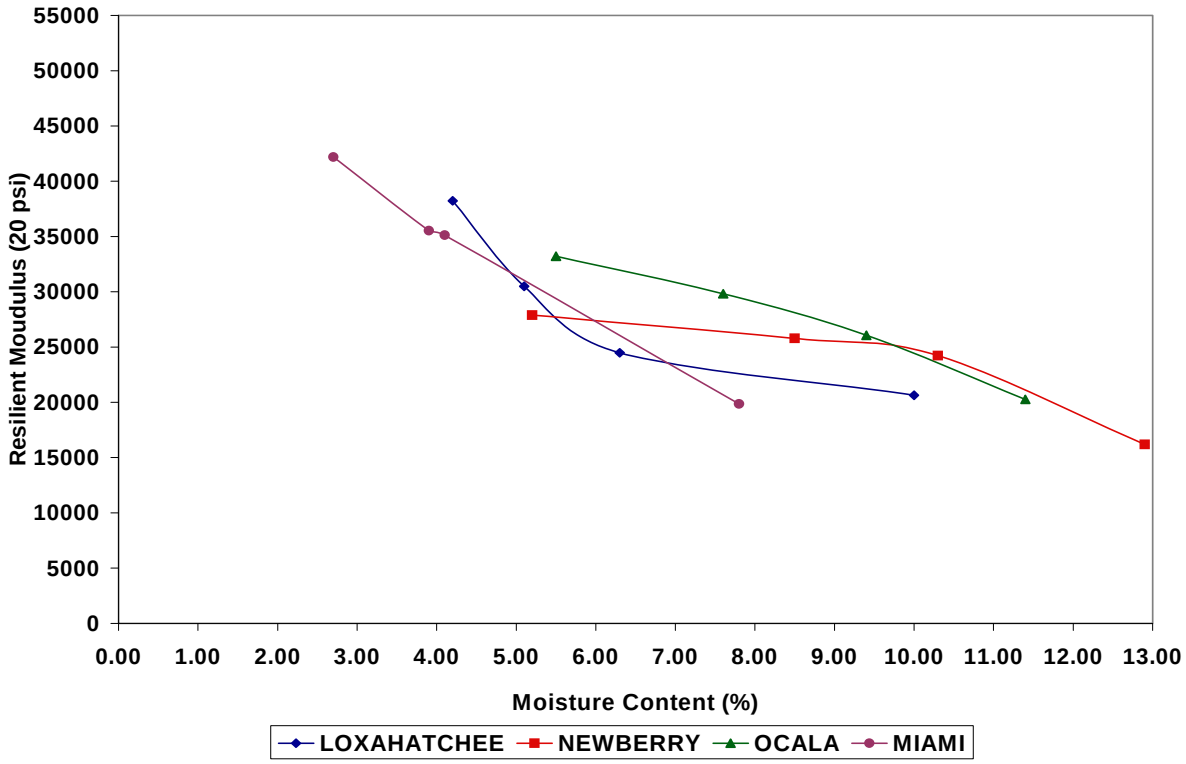

Figure 7-4. Continued.

7.2.2.2 Oven Drying

As described in Chapter 4, the specimens were put in an oven at low heat (110 ºF) for relatively slow drying, and the specimens underwent several oven drying processes during wetting and drying cycles. Influence of oven drying on the material response is shown for replicates 1, 2, and 3 in Figures 7-5, 7-6, and 7-7, respectively. As clearly demonstrated, the modulus increases in Figures 7-5 B, 7-6 B, and 7-7 B corresponds directly with the moisture reductions in Figures 7-5 A, 7-6 A, and 7-7 A.

If the outdoor ambient and oven drying results are compared, it can be noted clearly that any type of drying produces a notable increase in resilient modulus. It should also be noted that in drying, all five materials demonstrate similar trends, but the rate of change and magnitude of the effect are different between materials, and the resilient modulus of Ocala and Newberry limerock (almost identical) changes the most. This would suggest that the hypothesized suction

mechanism has more effect on resilient modulus of Ocala and Newberry. Remember that the effect was more pronounced at small-strain for Miami and Loxahatchee.

7.2.3 Wetting

For wetting, the specimens were put in water tanks to observe the influence of addition of water, and the influence of wetting on the material response is shown for replicates 1, 2, and 3 in Figures 7-5, 7-6, and 7-7, respectively. Placement of a nearly dry specimen in a soaking tank allows the material to slowly absorb water, and this is demonstrated as the increasing trends in Figures 7-5 A, 7-6 A, and 7-7 A. The decreasing trends in Figures 7-5 B, 7-6 B, and 7-7 B represent the corresponding decrease in resilient modulus as water is absorbed. As with the tests during drying, all five materials demonstrate similar trends, but the rate of change and the magnitude of the effect are different between materials. Figures 7-5, 7-6, and 7-7 also reveal that the drying and wetting responses of a given material does not follow the same relationship. It should be noted that in Figure 7-6 B and Figure 7-7 B the second drying cycles show illogical behavior of a decrease in resilient modulus during drying. This is assumed to be a technical error or a clerical error during recording of data.

7.2.4 Wetting and Drying Cycles

This section will describe the observed response due to repeated application of drying and then wetting. The materials were subjected to cycles of drying and wetting, as much as the stability of the materials allowed. It is noted that the material response appears to be reasonably repeatable. Subsequent responses to drying and wetting are similar to the initial response. This suggests that the underlying mechanism for the response is largely reversible.

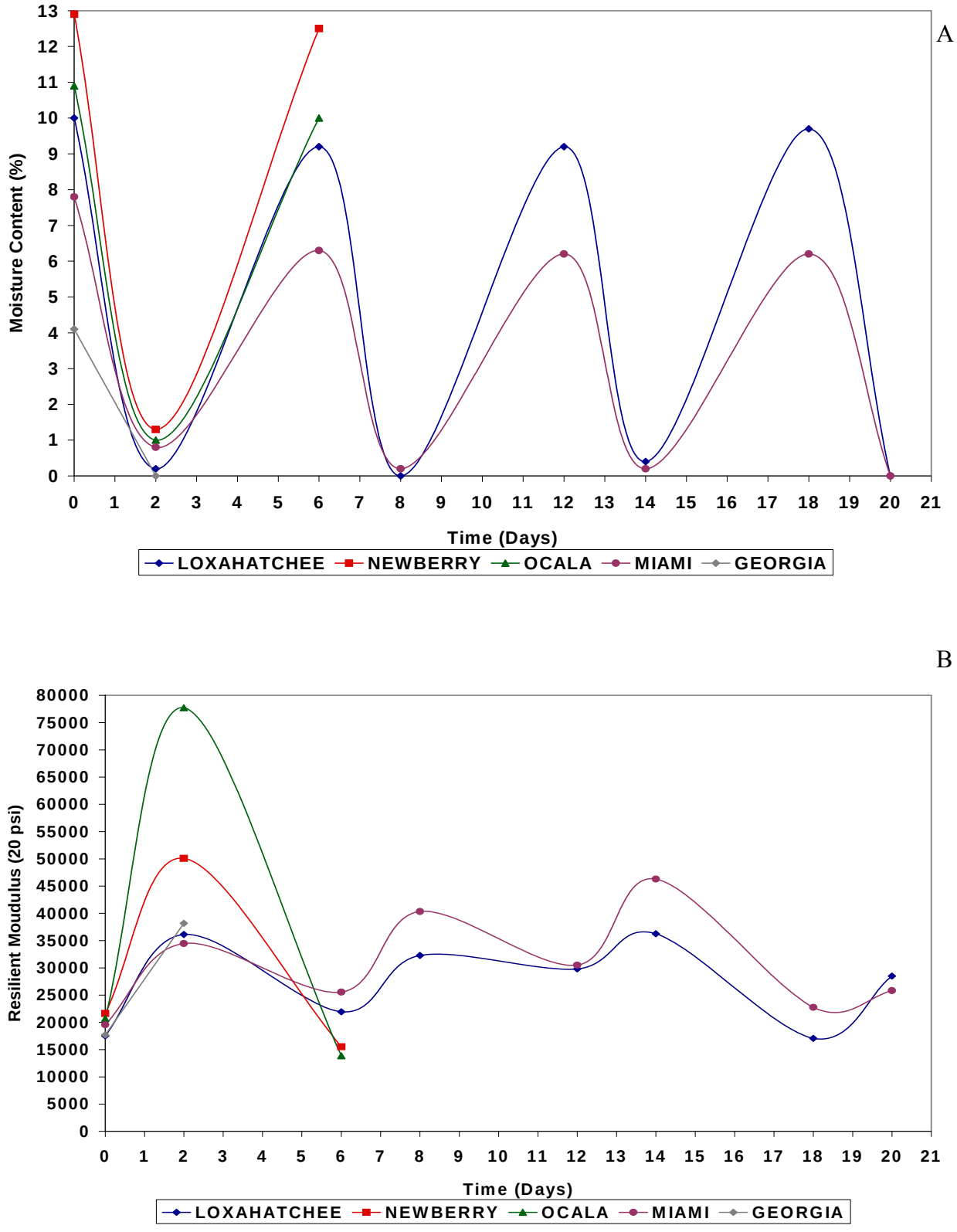

Figure 7-5. The resilient modulus test results of replicate 1 for wetting and drying.

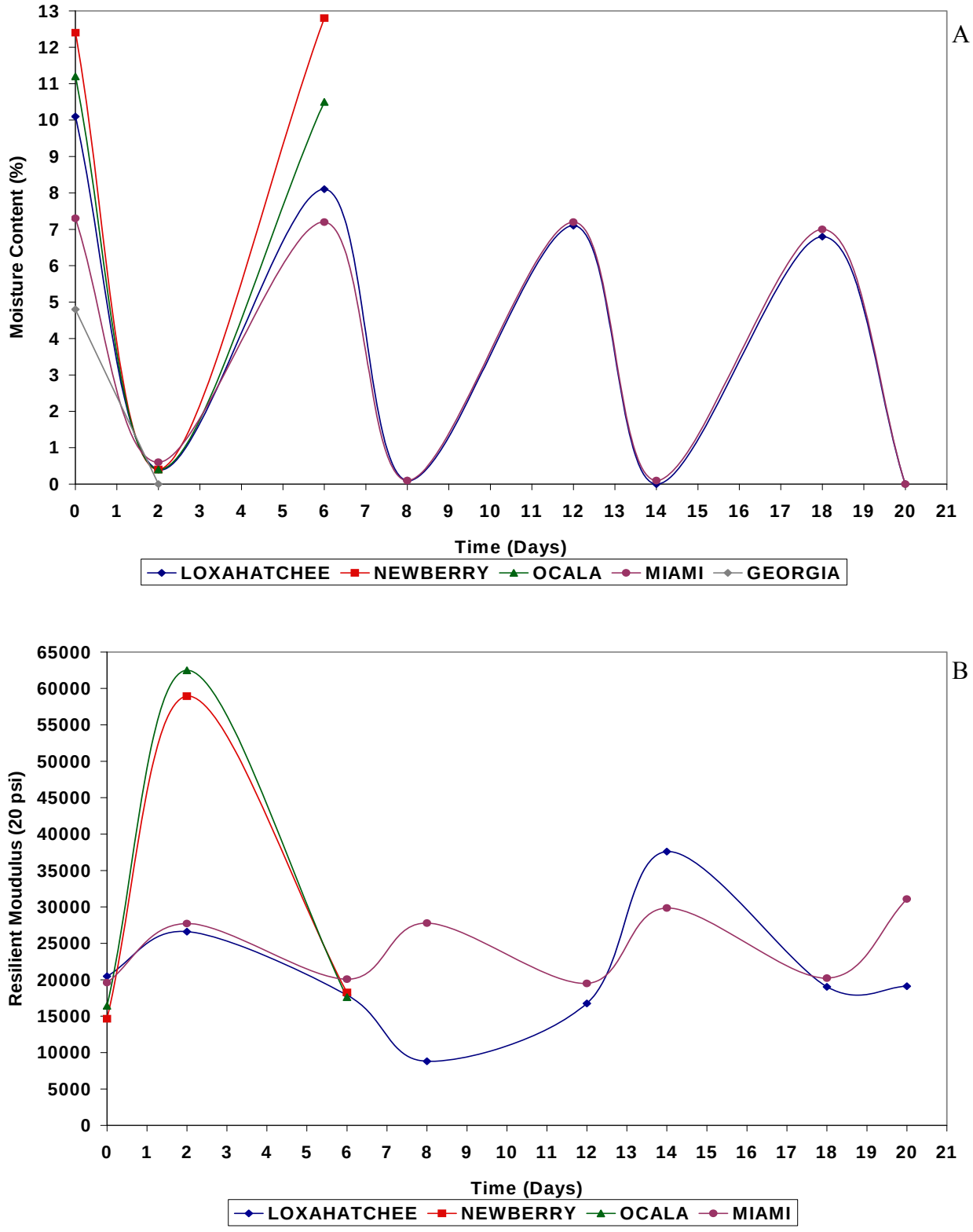

Figure 7-6. The resilient modulus test results of replicate 2 for wetting and drying.

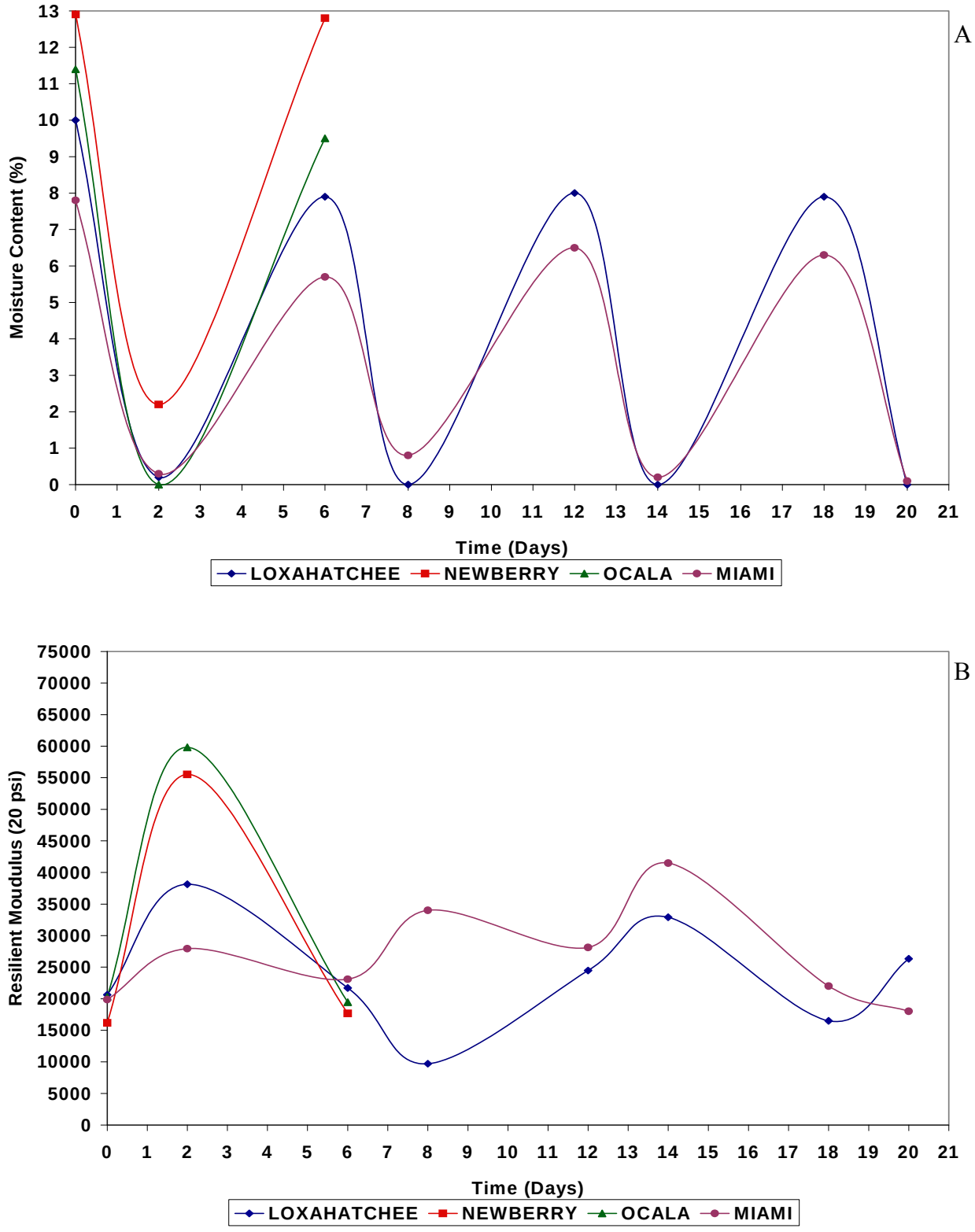

Figure 7-7. The resilient modulus test results of replicate 3 for wetting and drying.

7.3 Comparisons of M_R Test Results and FFRC Test Results for Drying Samples

This section is dedicated to compare and discuss the differences or similarities in material responses to FFRC test and M_R test. Both test results showed increase in modulus for all materials while there is a loss in moisture. Another significant behavior observed was that these responses are largely reversible, such that the increased modulus decreases to the modulus at optimum moisture, if not lower, when water is added. These behaviors indicate that the hypothesized mechanism, which is the increase in modulus is due to the effective confining stress created by negative pore water pressure (suction) in the material, is plausible. Figure 7-8 shows variation of Young's modulus (E, ksi) and resilient modulus (M_R, ksi) at a bulk stress of 20 psi for same material with moisture content, in arithmetic scale. Because the variation of M_R with moisture content is not easily observed in this figure, the data were replotted in Figure 7-9. Here, modulus ratio is plotted on logarithmic vertical axis, or the modulus at any time (E, M_R) divided by the modulus at maximum dry density and optimum moisture content immediately following compaction (E_{opt}, M_{Ropt}). Several observations are apparent from these figures, including:

- It is interesting to note that the small-strain Young's modulus (E) and the resilient modulus (M_R) at 20-psi bulk stress at optimum moisture content are nearly the same. This could be of practical value for future investigations.
- However, it is readily noted that the change in Young's modulus with drying is much more dramatic. As described by Cho and Santamarina (2001), the effective confinement due to suction is maintained at small-strain, whereas the resilient modulus test produces larger strains that break the influence of suction. Despite this difference, it is still noted that drying can produce a change in resilient modulus of approximately double.
- For the limerock materials, the change in Young's modulus with drying is many orders of magnitude, with Loxahatchee, Newberry, and Ocala changing by nearly a factor of 100, and Miami by nearly 1000. However, it is interesting to note that the change in Georgia granite is comparatively only about a factor of 10. Clearly, the effects of suction at small strain are more significant on the limerock materials.

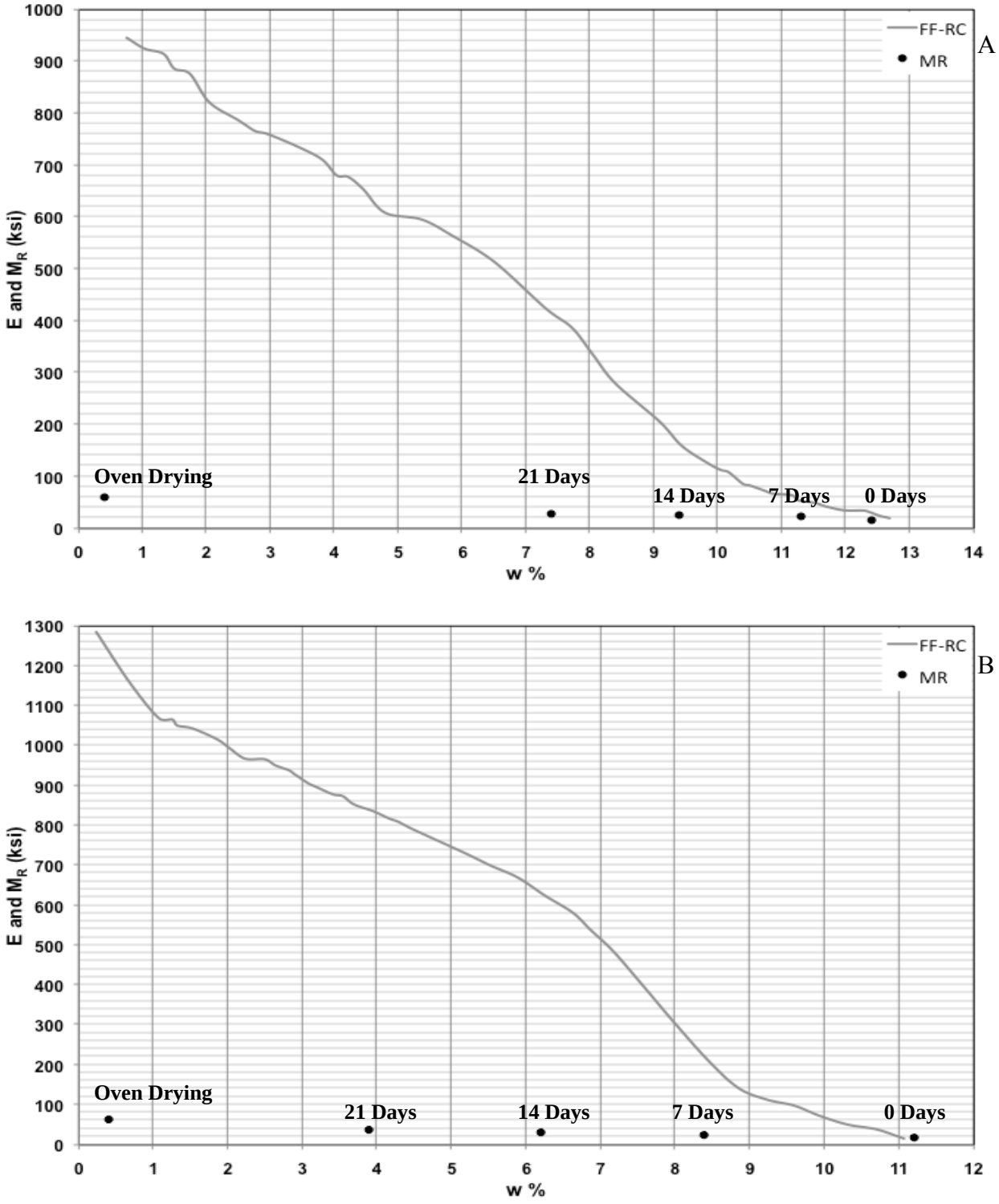

Figure 7-8. Variations of Young's modulus and resilient modulus with moisture content. A) Newberry. B) Ocala. C) Loxahatchee. D) Miami. E) Georgia.

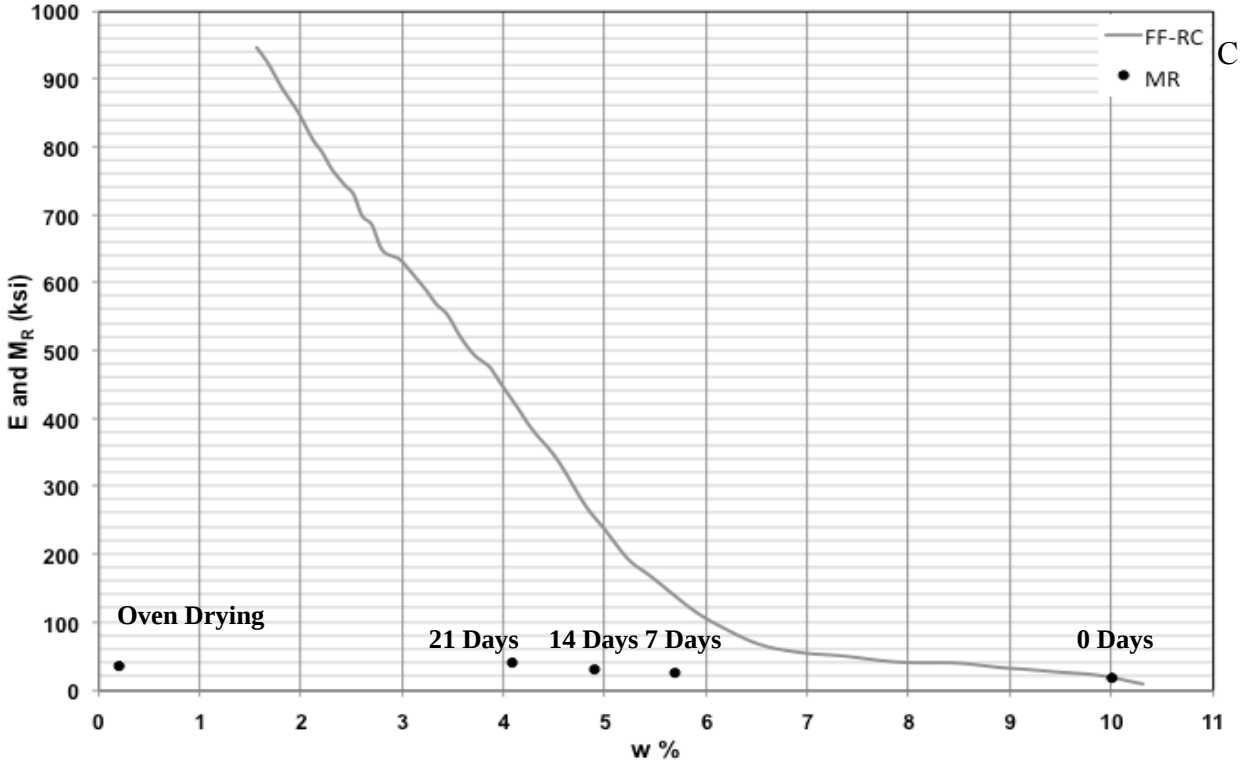

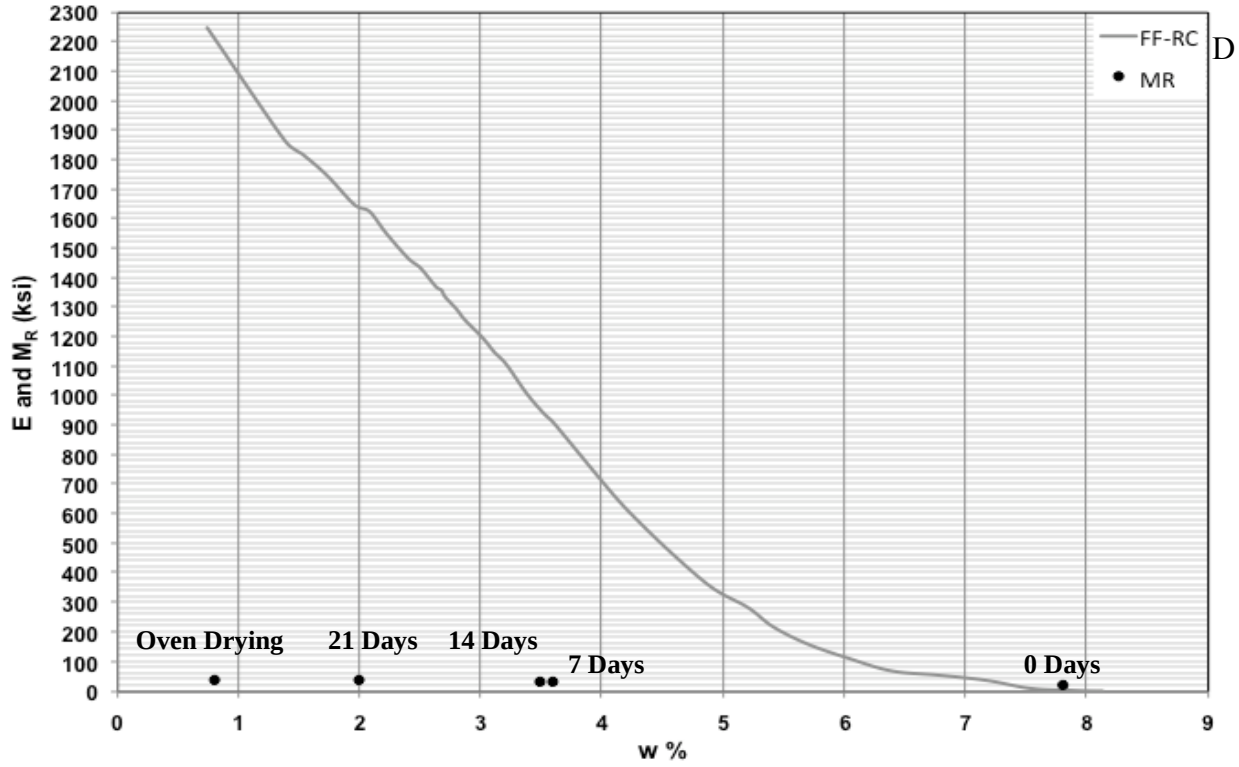

Figure 7-8. Continued.

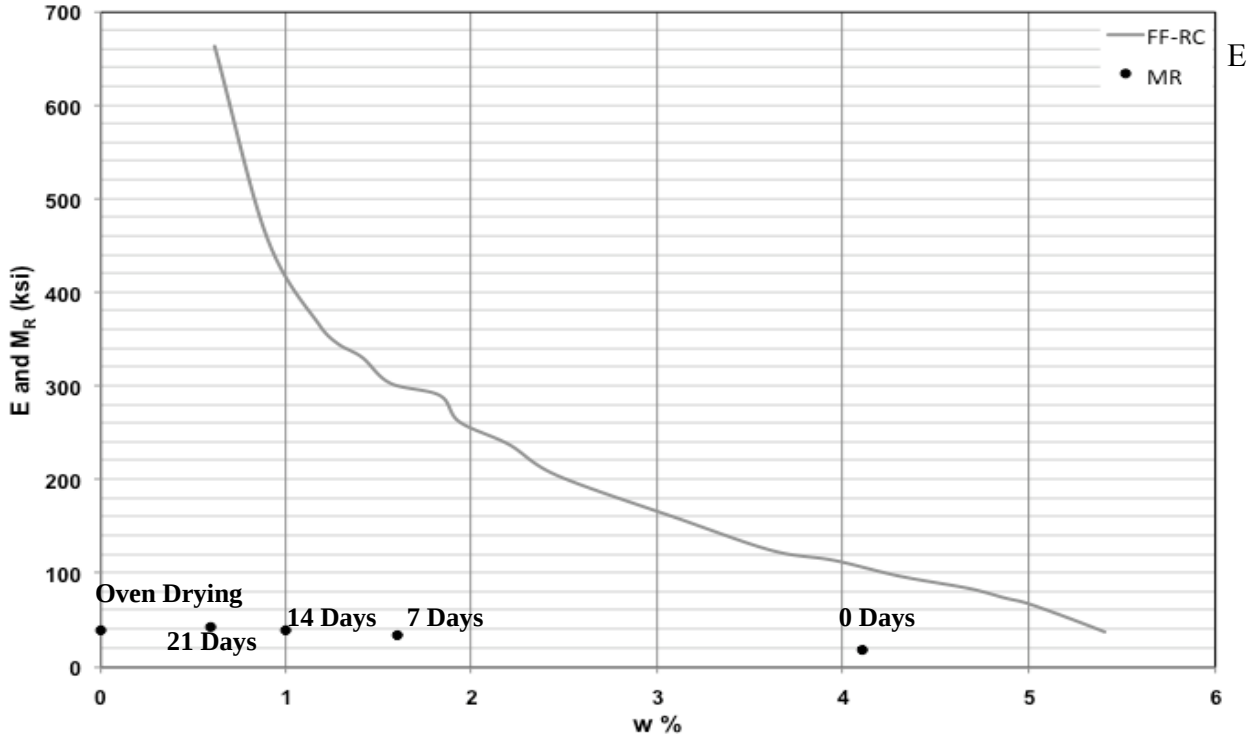

Figure 7-8. Continued.

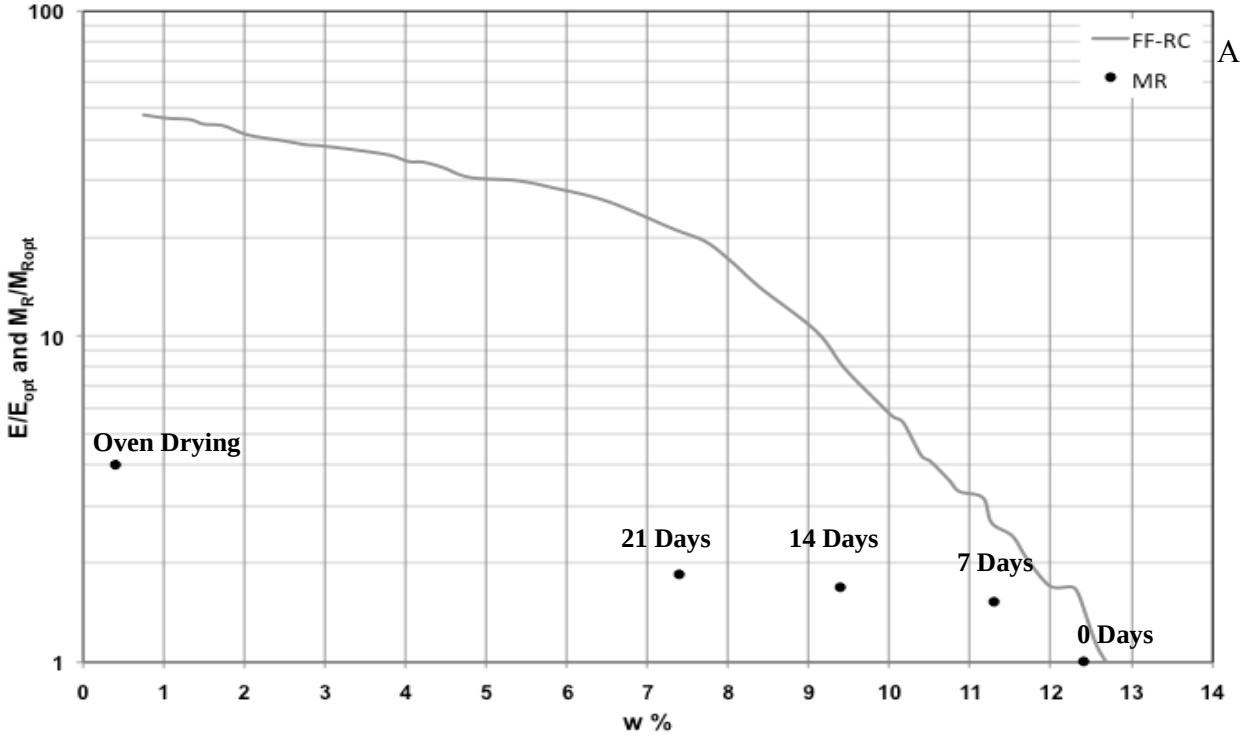

Figure 7 9. Variations of normalized Young's modulus and resilient modulus with moisture content. A) Newberry. B) Ocala. C) Loxahatchee. D) Miami. E) Georgia.

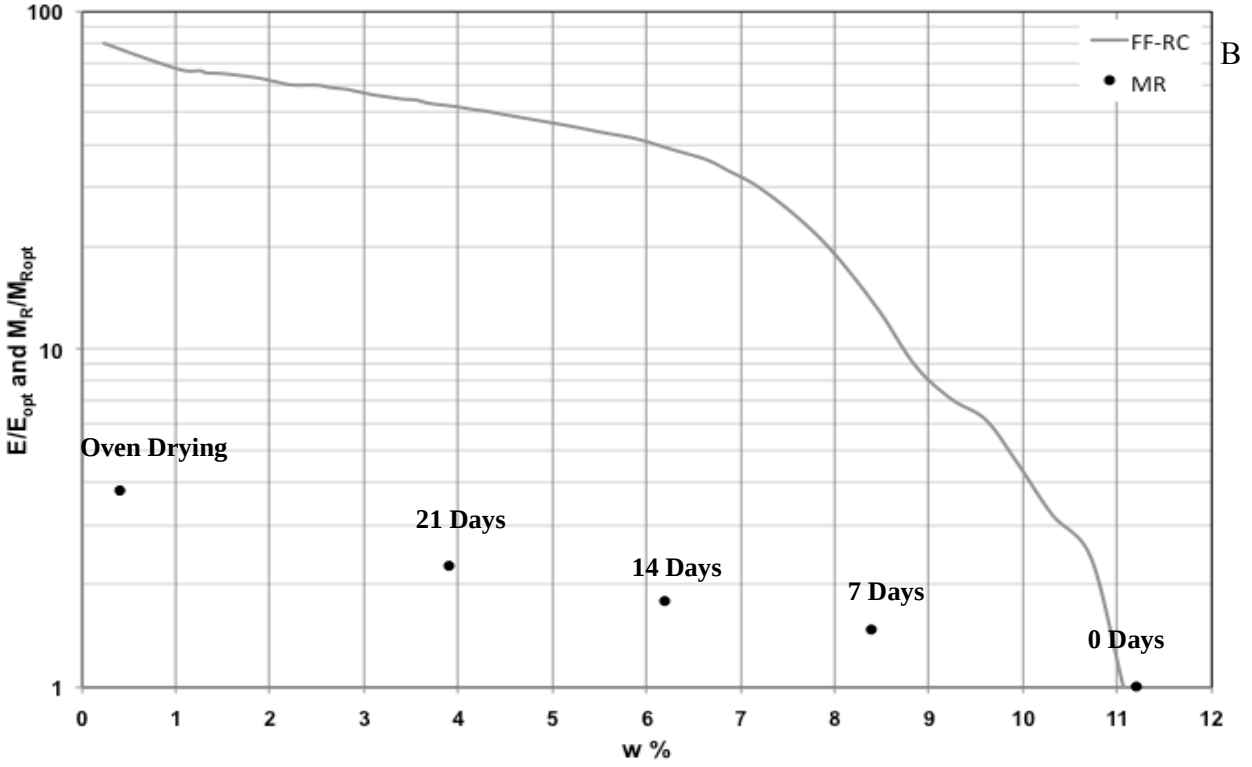

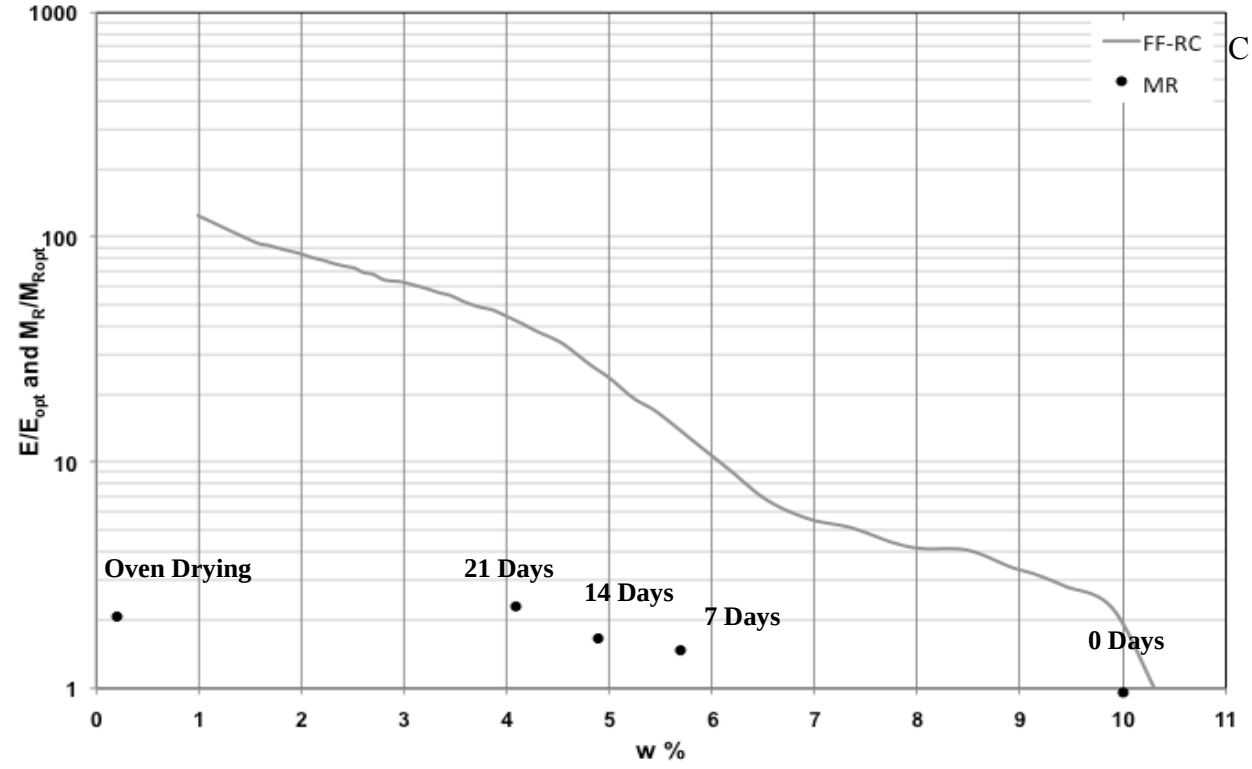

Figure 7-9. Continued.

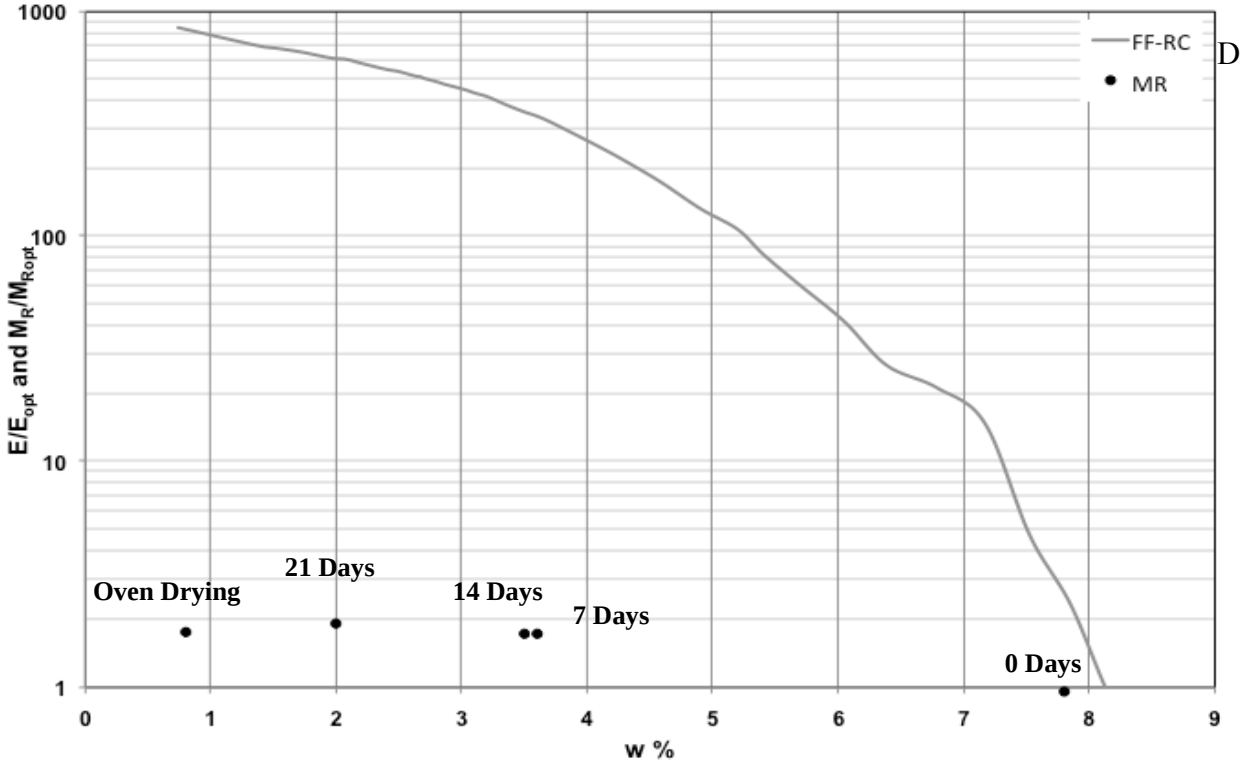

D

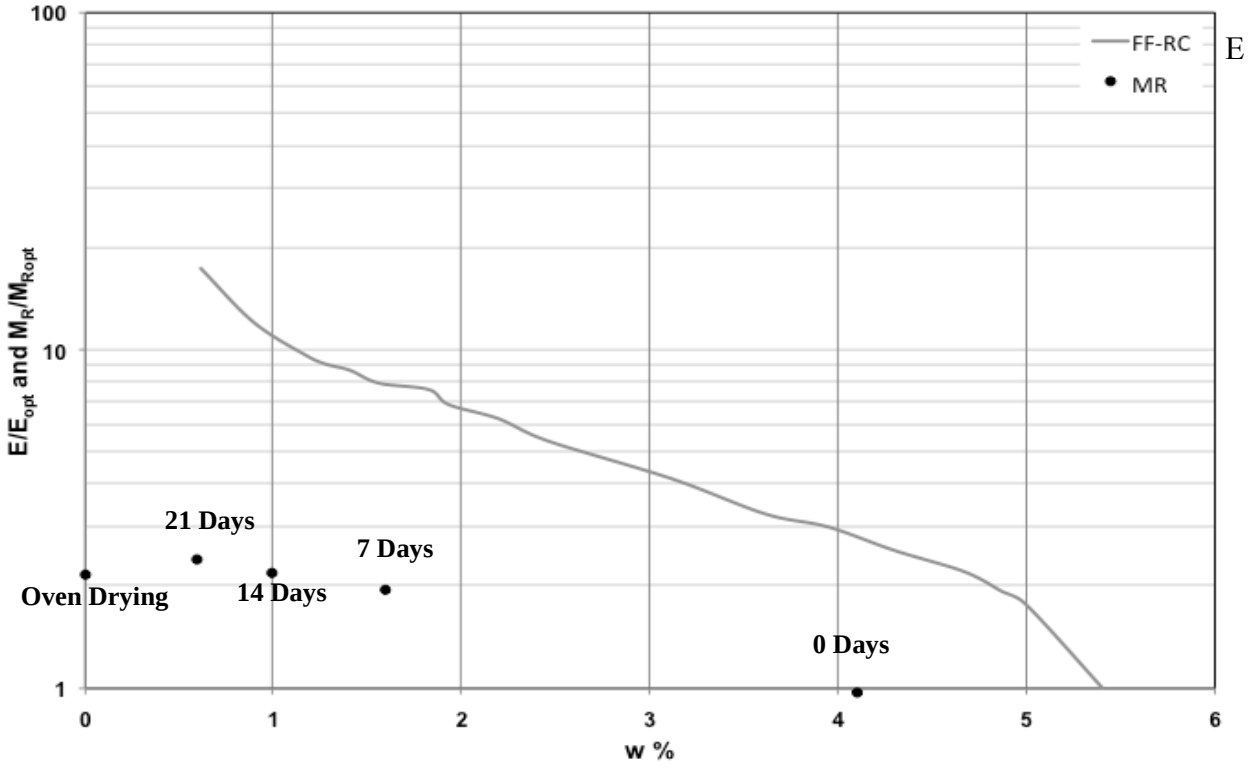

E

Figure 7-9. Continued.

CHAPTER 8
RECOMMENDATIONS FOR PAVEMENT DESIGN

8.1 Introduction

The primary objective of the research reported herein is to identify, document, and recommend practical methodologies to supplement existing and future pavement design procedures with a protocol that incorporates expected stiffness and strength gains in Florida base materials. The review of relevant literature and the presentation of laboratory test results in Chapters 2 through 7 have provided significant documentation of the expected mechanical behavior of Florida base materials. The following sections will recommend a methodology for incorporating these findings into pavement design practice.

8.2 Mechanistic-Empirical Pavement Design Guide

National Cooperative Highway Research Program (NCHRP) Project 1-37A has produced "Guide for Mechanistic-Empirical Design of New and Rehabilitated Pavement Structures," referred to herein as the M-E PDG. The national intent is to seek adoption of this guide by the American Association of State Highway and Transportation Officials (AASHTO) for the design of pavement systems. As documented in Chapter 1, FDOT existing practice for incorporating stiffness and strength gains of Florida base materials is accomplished via an increased layer coefficient. However, it is expected that future pavement design will be based on the new M-E PDG, and thus recommendations for incorporating the findings of the research reported herein into pavement design practice will focus on use of this new guide. With regard to unbound base materials, the following three items are of significant importance within the M-E PDG:

1. Two pavement response models are available for the design of flexible pavement systems: a traditional, multi-layered, linear elastic analysis (LEA), and an advanced, nonlinear, two-dimensional, finite element analysis program (FEA). For the LEA

response model, the primary input for the base material is one effective linear elastic resilient modulus, while the FEA model is able to account for the nonlinear stress-strain behavior of unbound base and subgrade materials.

2. Base material characterization inputs are defined at three levels designated as Levels 1, 2, and 3. In general, the base material inputs include resilient modulus, Poisson's ratio, plasticity index, particle size distribution, maximum dry unit weight and optimum water content, specific gravity of solids, saturated hydraulic conductivity, degree of saturation, and the coefficient of lateral earth pressure. Discussion herein will focus on resilient modulus characterization. Level 1 is intended to characterize the nonlinear resilient modulus behavior for use in the FEA response model. Here, the nonlinear behavior is modeled via a constitutive relationship between resilient modulus and in situ stress state. The constitutive equation includes three coefficients (k_1, k_2, and k_3) that are determined via regression modeling of resilient modulus values measured in the laboratory for multiple stress states. The expected M-E PDG inputs for Level 1 are the three coefficients, k_1, k_2, and k_3. Level 2 is intended to characterize the stress-strain response via one effective, linear elastic, resilient modulus value that will be used in the LEA response model. This one value can be determined directly from laboratory testing, or indirectly via correlations between resilient modulus and other mechanical and index properties. Like Level 2, Level 3 is intended to characterize the stress-strain response via one effective, linear elastic, resilient modulus value that will be used in the LEA response model. However, for Level 3, this one value is determined via correlations between resilient modulus and the AASHTO or Unified classification of the material.

3. The M-E PDG can account for the widely recognized and significant effects of moisture on the resilient modulus characteristics of unbound base materials. To begin, it is recommended that the resilient modulus inputs at Levels 1, 2, and 3 all be determined and specified at the optimum moisture content and maximum dry unit weight condition for the material. As a first option, the M-E PDG will utilize the Enhanced Integrated Climatic Model (EICM) to estimate variation in resilient modulus based on changing moisture and temperature profiles through the pavement structure. For these predictions, the EICM utilizes many of the input parameters listed above, e.g., particle size distribution, specific gravity, and saturated hydraulic conductivity. In lieu of using the EICM, it is also possible to directly enter seasonal (e.g., monthly) variation in resilient modulus or resilient modulus parameters. Finally, it is also possible to ignore the effects of moisture, and use a constant resilient modulus for analysis and design.

8.3 Florida Pavement Design

The research documented herein provides significant evidence that the stiffness and strength changes in Florida base materials at typical field moisture contents are governed by the effects of suction or negative pore water pressure. This phenomenon is reversible and determined by the amount of moisture in the material. In comparison with the Georgia granite graded aggregate base, the effects of suction at small strain are accentuated in the Florida limestone base materials, and thus consideration of this phenomenon appears especially warranted. In fact, this moisture-driven mechanism can be accounted for in the M-E PDG as described above. The principles of unsaturated soil mechanics (e.g., suction, negative pore pressure) are used directly in the EICM to estimate variation in resilient modulus as a result of changes in moisture. Thus, the M-E PDG can be used directly and immediately for pavement

design in Florida, and it can account for some of the mechanical behavior of Florida base materials documented herein. As recommended by the M-E PDG, determination of resilient modulus or resilient modulus parameters should be determined at optimum moisture conditions, and then adjustment of the mechanical behavior is made internally based upon calculated changes in moisture.

8.4 Recommendations for Future Research

The research described herein has significantly advanced understanding of the mechanical behavior of Florida base materials. Used in conjunction with the M-E PDG, a rational means is available to account for changes observed in the mechanical behavior during service. However, it should also be recognized that the process is not perfect, and several fundamental issues remain to be understood and incorporated, including:

- The effects of suction are shown herein to be significantly dependent on the level of strain; the effects are very substantial at small strain, while there is less effect at larger strain. This research has documented the effects at two strain levels: very small or elastic strain levels via the free-free resonant column test, and at a higher level of strain in the nonlinear range of the material via the resilient modulus test. However, a real pavement system will experience a wide range of strains under wheel loading, yet the effects of suction are revealed herein at only two strain levels. The effects of suction over a wide range of strains should be determined. Further, the effects of suction modeled in the M-E PDG are assumed to be independent of strain, and are based upon the strain at which the resilient modulus is determined. Given the very significant influence that level of strain has on the suction effects, it would appear that an improved procedure is warranted for capturing the combined effects of suction and strain on pavement response. In reality, it would appear that a significant horizontal

gradient in modulus must exist as distance from the wheel load changes, particularly for materials that are drier than optimum moisture, where the effects of suction are significant. This stiffness gradient could have a significant influence on the cracking behavior of flexible pavement surface layers.

- The effects of suction accounted for in the M-E PDG are modeled via the EICM. The EICM includes a means to predict changes in moisture and temperature in a pavement structure, and a means to adjust the resilient modulus based upon changes in moisture. Both of these procedures incorporate empirical relationships between fundamental parameters (e.g., soil water characteristic curve, resilient modulus) and index parameters of the material (e.g., particle size distribution, specific gravity, degree of saturation). It is widely recognized that Florida limestone base materials are unique, thus it should be established that the EICM empirical relationships are applicable to Florida materials.

CHAPTER 9
CLOSURE

9.1 Summary of Findings

An investigation of characteristics of unbound aggregates used for base material in the state of Florida was performed to study the mechanical properties, to observe and document stiffness changes with time and under varying environmental conditions, and to identify potential mechanisms causing these changes. Small-strain moduli of laboratory-compacted specimens were investigated via FF-RC test to determine the stiffness properties of each material under various conditions. Five aggregate sources were selected from those commonly used in Florida. Mines in Newberry, Ocala, and Miami where chosen to represent lime-rock sources from northern, central, and southern Florida, respectively. In addition, a limestone-based shell-rock from Loxahatchee, FL, and a granite-based graded aggregate from Georgia were included in the study. Sampling of each of these materials was conducted following standard FDOT procedures. In addition to the fresh samples, two intact field cores exposed to cycles of wetting and drying similar to the laboratory-compacted specimens were investigated. Following construction, specimens of each material were exposed to one of four conditions as follows: ambient, constant moisture, oven drying, and wetting. Finally, the SMO investigated these same fresh materials via the resilient modulus test. The following are the findings of these investigations:

- While being held at constant moisture, the small-strain modulus of all materials tested is not constant, but increases with increasing time. The rate of modulus increase with time decreases with time. That is, the largest change occurs early, and then gradually diminishes. While the general trend of increasing modulus with time is common to all materials tested, the rate of increase is considerably different. The Miami lime-rock displays a very significant increase with time, while the increase for the Georgia granite is relatively small.
- Placement of the specimens in either ambient condition (laboratory bench or outdoor shade environments) or in an oven slowly drives water from the material. As the water is lost due to drying exposure, the materials undergo a dramatic increase in small-strain modulus. The moisture content and modulus change occurs most significantly at the beginning of drying

exposure, after which the rate of change decreases with increasing time. As with the tests at constant moisture, all five materials demonstrate similar trends, but the rate of change and the magnitude of the effect are different between materials. Once again the Miami lime-rock changes the most, while the change in Georgia granite is smallest.

- Placing specimens in a water tank allows the material to slowly absorb water, leading to an increase in moisture content in the material. The increase in moisture content causes the materials to undergo a dramatic decrease in small-strain modulus. The moisture content and modulus change occurs most significantly at the beginning of exposure, after which the rates decrease with increasing time. As with the tests during drying, all five materials demonstrate similar trends, but the rate of change and the magnitude of the effect are different between materials.

- The drying and wetting responses of a given material do not follow the same relationships. Rather, there is a hysteretic phenomenon whereby a different modulus is measured while drying to certain moisture content than while wetting to the same moisture content.

- With respect to cycles of drying and wetting, it is observed that the material response is repeatable. Subsequent responses to drying and wetting are very similar to the initial response. It is observed that these trends are displayed for the Florida lime-rock and shell-rock materials, and for the granite-based graded aggregate from Georgia.

- As for the two intact field cores, it is observed that the response of the field cores appear very similar to that of the fresh, laboratory compacted specimens. Even after 10 years of service, the softening while wetting followed by a return to high stiffness when nearly dry appears to be very repeatable and reversible. The response of field cores is similar to that of a laboratory compacted specimen of material from the same general source in south Florida, and aging has not significantly altered the material response.

- Curing compacted specimens with different relative humidity (low, medium, high) resulted in stiffness increases for each material type. Materials cured under low relative humidity conditions showed the greatest increase in stiffness, while materials cured under high relative humidity conditions showed the lowest stiffness increase.

- Although all materials showed an increase in stiffness, ESEM analysis did not reveal the presence of calcite crystals, except for a slight amount in the field samples.

- The pore size distribution is different between the four Florida materials. The Miami material has the smallest pores available within the pore volume. On the other hand, the Ocala material has the largest number of pores between 10^{-6} and 10^{-7} m.

- The resilient modulus increases with an increase of bulk stress at optimum moisture.

- The removal of water leads to a notable increase in the larger-strain resilient modulus. The rate of change and magnitude of the effect are different between materials as was observed with the small-strain modulus. It should be noted that the Georgia granite changes the most, while the change in Newberry lime-rock is the smallest.

- As water is added to the materials, the larger-strain resilient modulus decreases in all materials. All five materials demonstrate similar trends, but the rate of change and the magnitude of the effect are different between materials.

- As with the small-strain modulus, the drying and wetting responses of a given material do not follow the same relationship. Rather, there is a hysteretic phenomenon whereby a different modulus is measured while drying to certain moisture content than while wetting to the same moisture content. With respect to cycles of drying and wetting, it is observed that the material response is repeatable. Subsequent responses to drying and wetting are very similar to the initial response.

- It is observed that the small-strain modulus is much larger than the resilient modulus, indicating a stiffness reduction with increased strain.

- Removal of water causes a larger relative change in small-strain modulus than in resilient modulus. However, the addition of water reduces the increase in small-strain and resilient modulus back to the values obtained at optimum moisture.

9.2 Conclusions

The stiffness or modulus of an unbound aggregate base material is not constant, but is significantly influenced by changes in time, moisture, and stress. The evidence suggests that these changes can be explained by the science of unsaturated soil mechanics: changes in moisture or moisture distribution results in changes in internal pore pressure, which affect the effective confining pressure constraining the material. The influence of this phenomenon is observed but is not as dramatic at higher strain.

Based upon these results it appears that a pavement design process based on resilient modulus for the base material should account for changes in moisture content anticipated in the base during the life of the pavement structure. The authors are aware that a procedure to account for the effects of moisture changes and other seasonal effects on the resilient modulus of base materials has been implemented in the new Mechanistic-Empirical (M-E) Pavement Design Guide. It is thus recommended that this procedure be utilized in conjunction with the findings reported herein to design pavements in Florida. The guide can be used directly and immediately for pavement design in Florida, and it can account for some of the mechanical behavior of

Florida base materials documented herein. As recommended by the guide, determination of resilient modulus or resilient modulus parameters should be conducted at optimum moisture conditions, and then adjustment of the mechanical behavior is made within the design procedure based upon calculated changes in moisture.

APPENDIX A
GRAIN SIZE DISTRIBUTION AND MATERIAL PROPERTIES

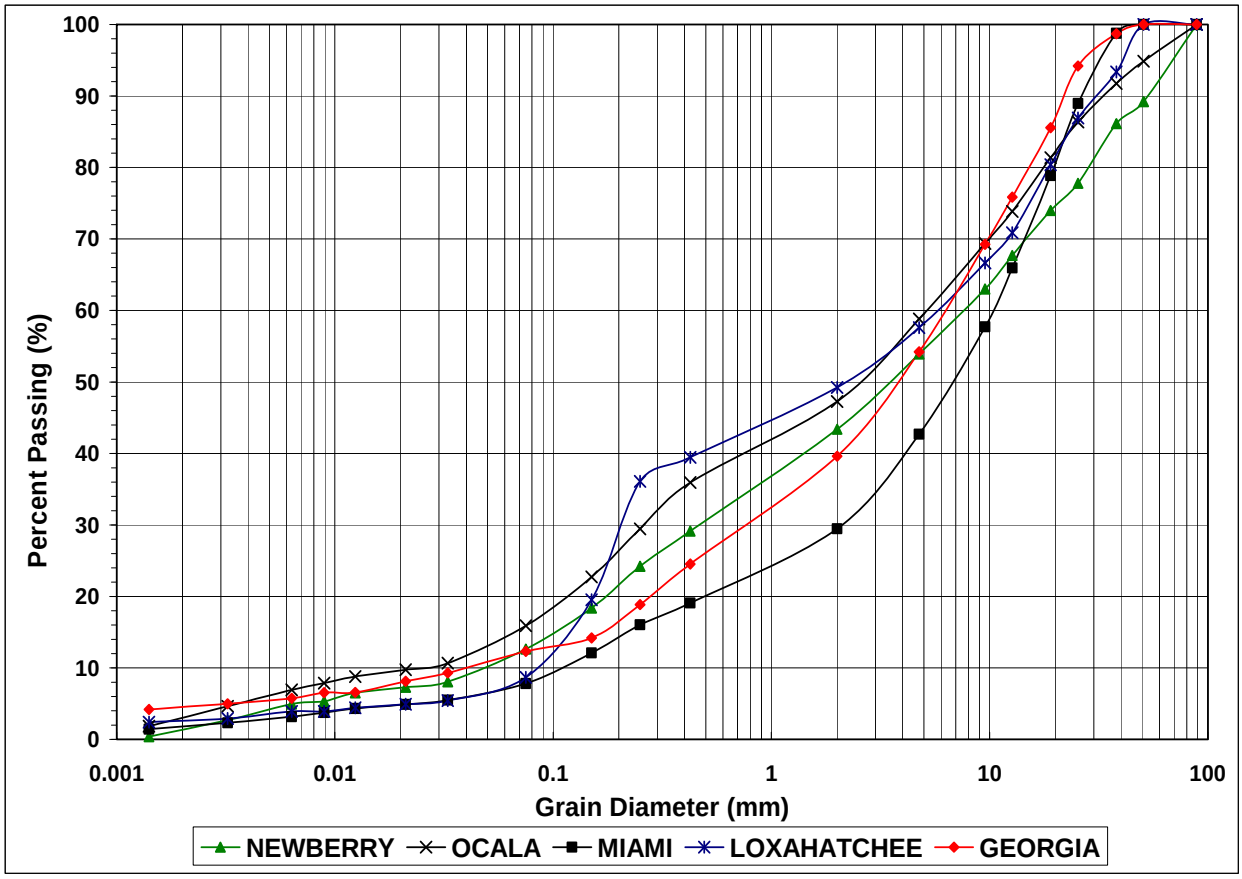

Figure A-1. Grain size distribution of materials collected from the 2nd mini-stockpiles (replicates) of each source.

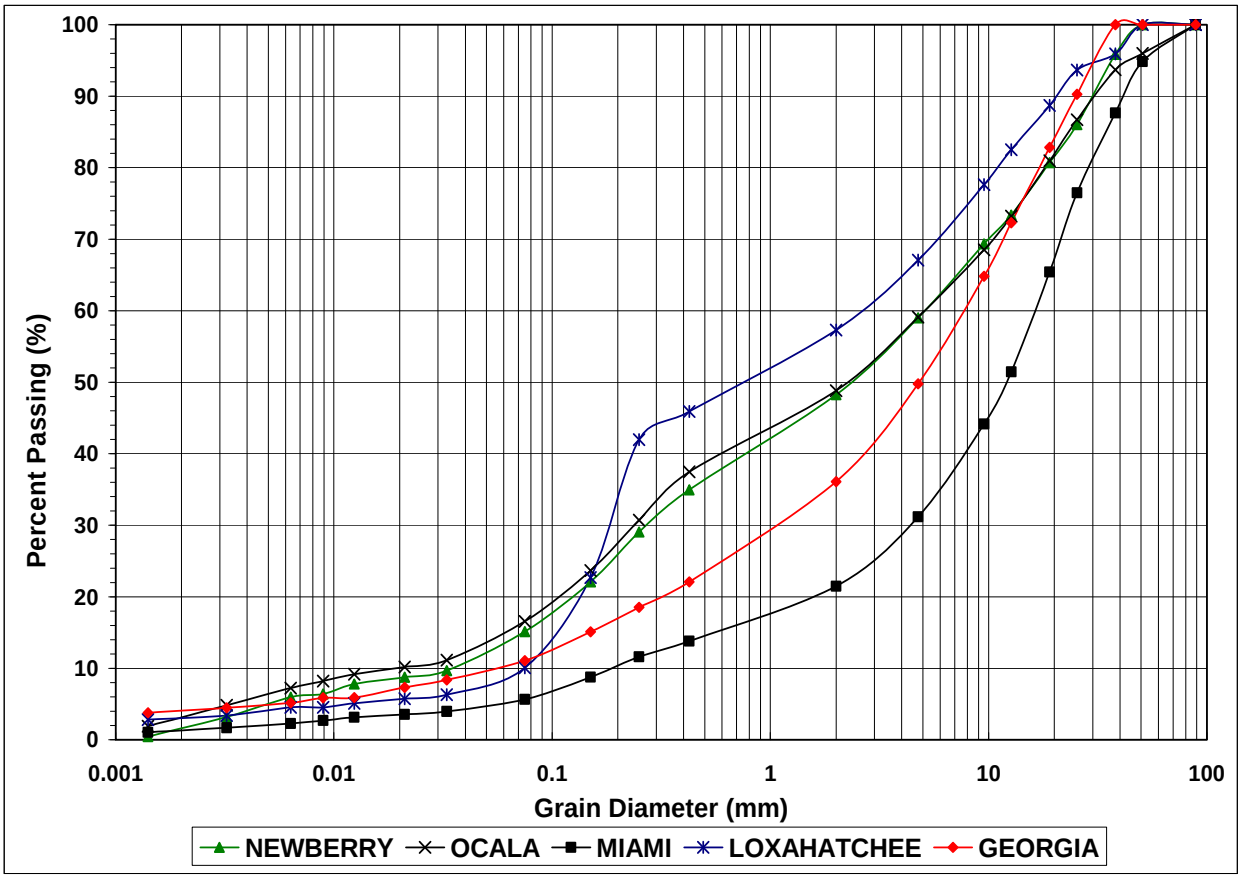

Figure A-2. Grain size distribution of materials collected from the 3rd replicates of each source.

Table A-1. Material parameters of 2nd replicates.

Parameter	Material				
	Georgia Granite	Loxahatchee Shell Rock	Miami Limerock	Newberry Limerock	Ocala Limerock
Unified Classification	GW-GM	GP-GM	GW-GM	GM	GM
D_{50} (mm) Mean Grain Size	5.00	0.75	12.00	2.40	2.40
D_{10} (mm) Effective Grain Size	0.05	0.075	0.2	0.035	0.02
Cu-The Uniformity Coefficient	156	34.7	90	142.9	250
Cz-The Coefficient of Curvature	3.103	0.185	5.625	0.386	0.625
Specific Gravity	2.7000	2.7091	2.7072	2.7196	2.7203
Void Ratio at Optimum	0.1889	0.403	0.285	0.456	0.399
Plastic Limit	NP	NP	NP	NP	NP
Plasticity Index	NP	NP	NP	NP	NP
Liquid Limit	NP	NP	NP	NP	NP

Table A-2. Material parameters of 3rd replicates.

Parameter	Material				
	Georgia Granite	Loxahatchee Shell Rock	Miami Limerock	Newberry Limerock	Ocala Limerock
Unified Classification	GW-GM	GP-GM	GW-GM	GM	GM
D_{50} (mm) Mean Grain Size	3.80	2.00	6.85	3.50	2.60
D_{10} (mm) Effective Grain Size	0.04	0.085	0.11	0.05	0.02
Cu-The Uniformity Coefficient	160	69.4	100	150	250
Cz-The Coefficient of Curvature	2.316	0.080	3.306	0.540	0.625
Specific Gravity	2.7000	2.7091	2.7072	2.7196	2.7203
Void Ratio at Optimum	0.189	0.395	0.280	0.459	0.400
Plastic Limit	NP	NP	NP	NP	NP
Plasticity Index	NP	NP	NP	NP	NP
Liquid Limit	NP	NP	NP	NP	NP

APPENDIX B
NEWBERRY INDIVIDUAL SMALL-STRAIN MODULUS TEST RESULTS

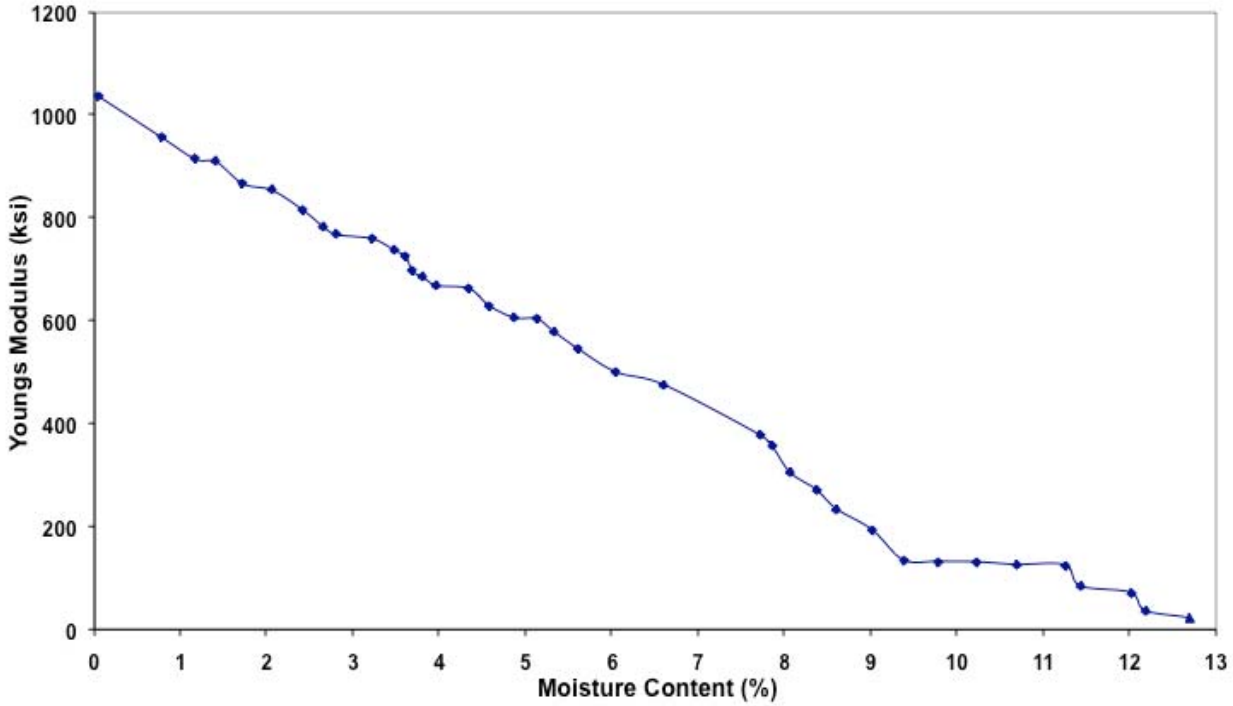

Figure B-1. Variation of Young's modulus with moisture content, replicate 1, outdoor ambient.

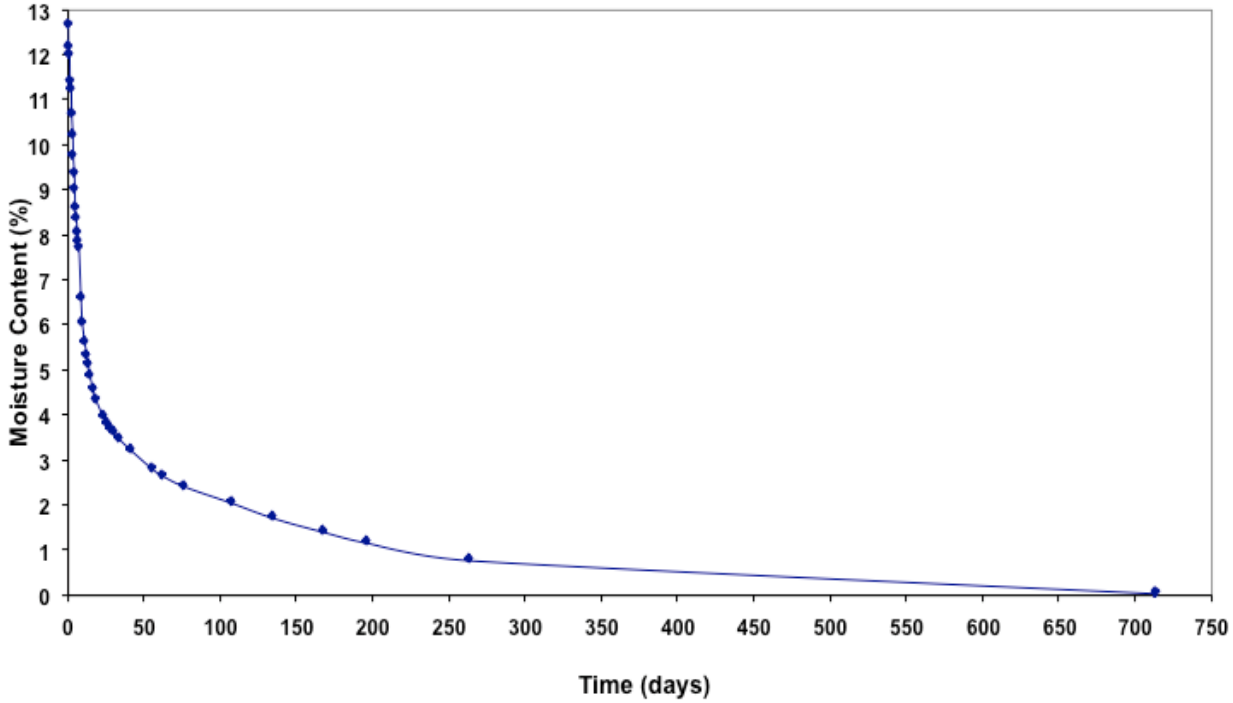

Figure B-2. Variation of moisture content with time, replicate 1, outdoor ambient.

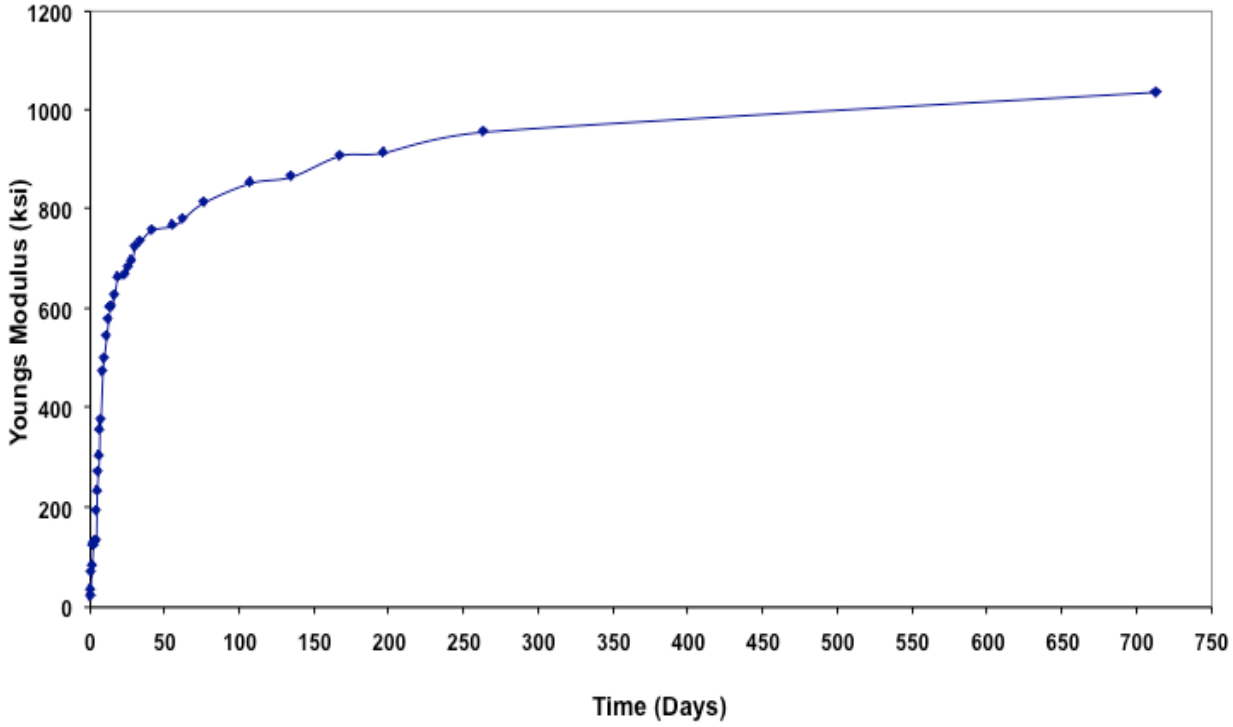

Figure B-3. Variation of Young's modulus with time, replicate 1, outdoor ambient.

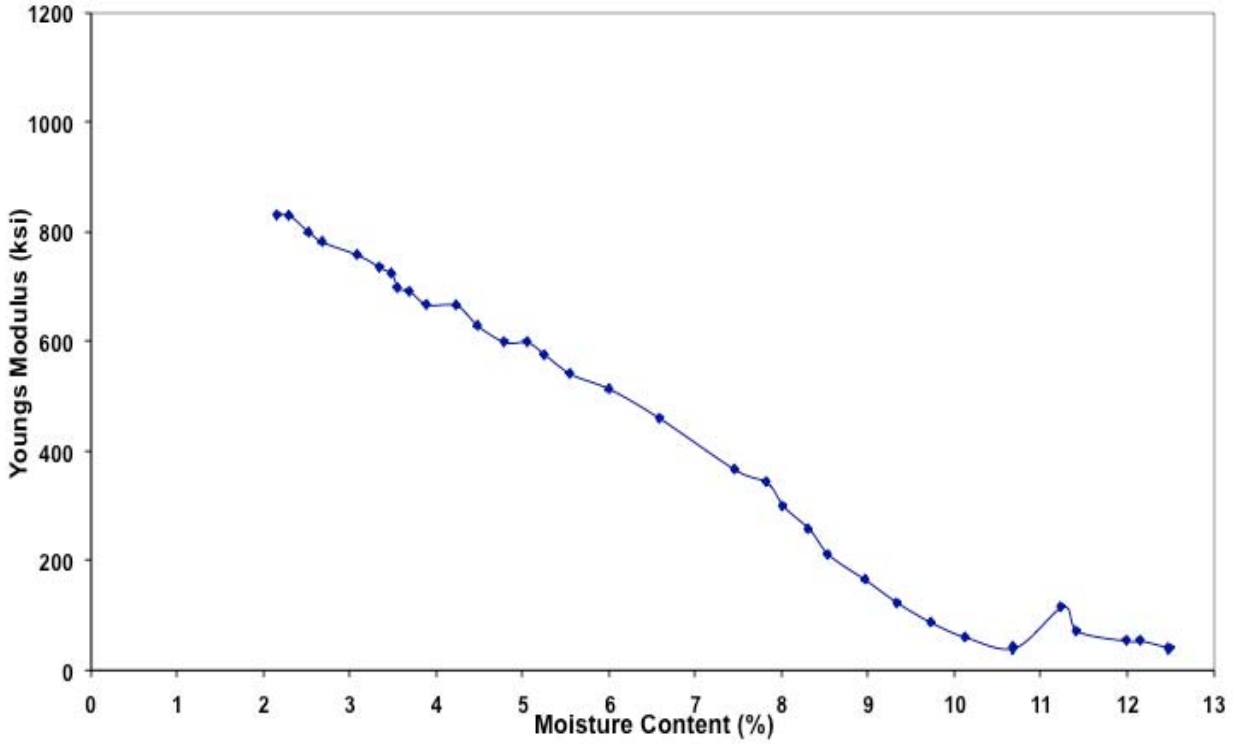

Figure B-4. Variation of Young's modulus with moisture content, replicate 2, outdoor ambient.

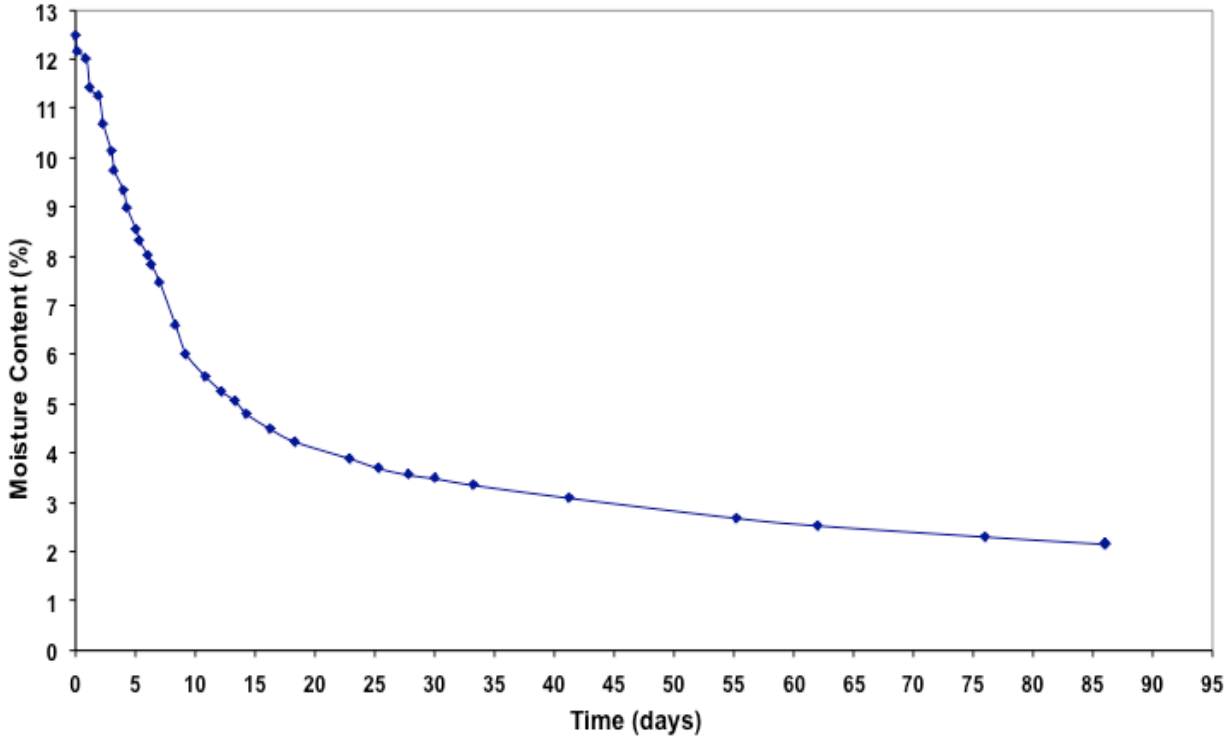

Figure B-5. Variation of moisture content with time, replicate 2, outdoor ambient.

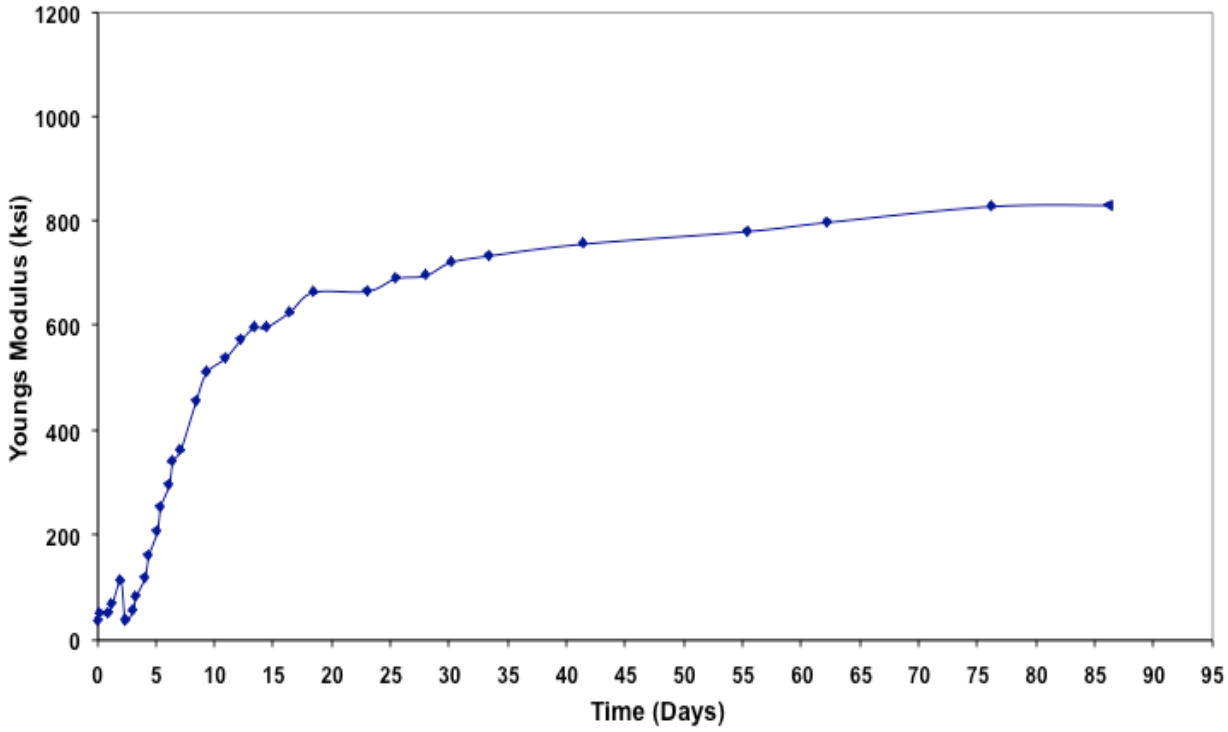

Figure B-6. Variation of Young's modulus with time, replicate 2, outdoor ambient.

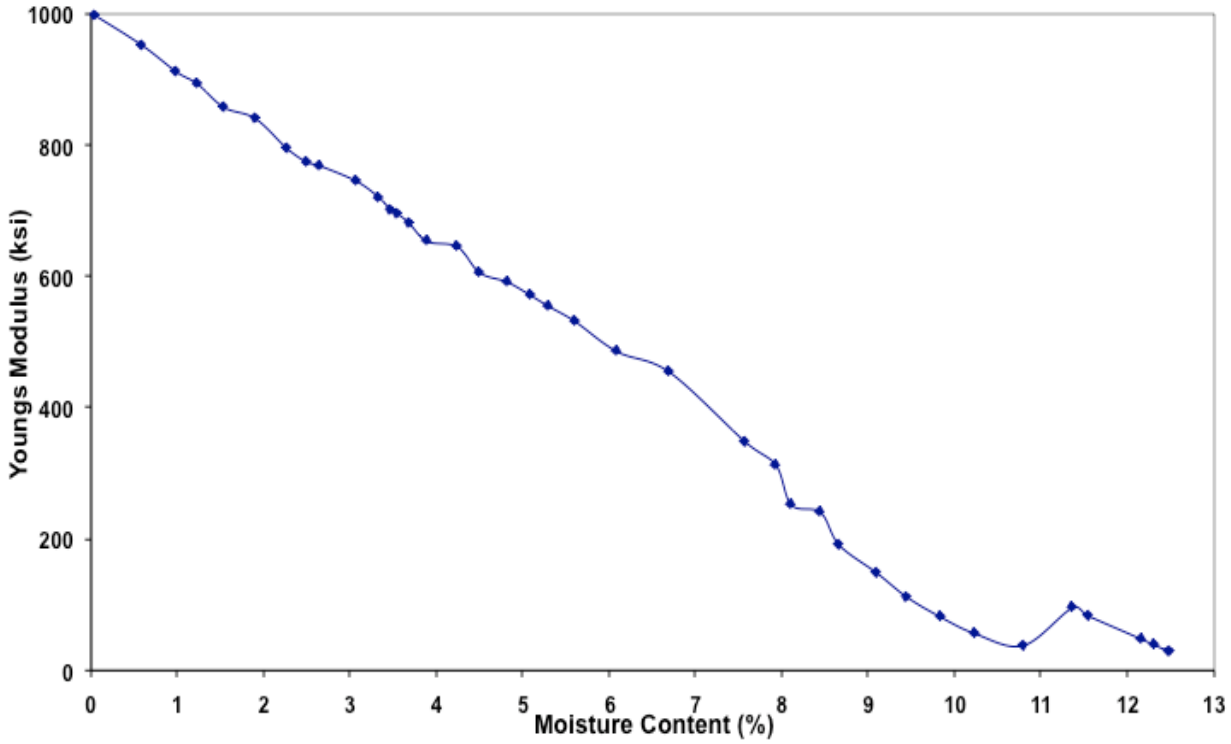

Figure B-7. Variation of Young's modulus with moisture content, replicate 3, outdoor ambient.

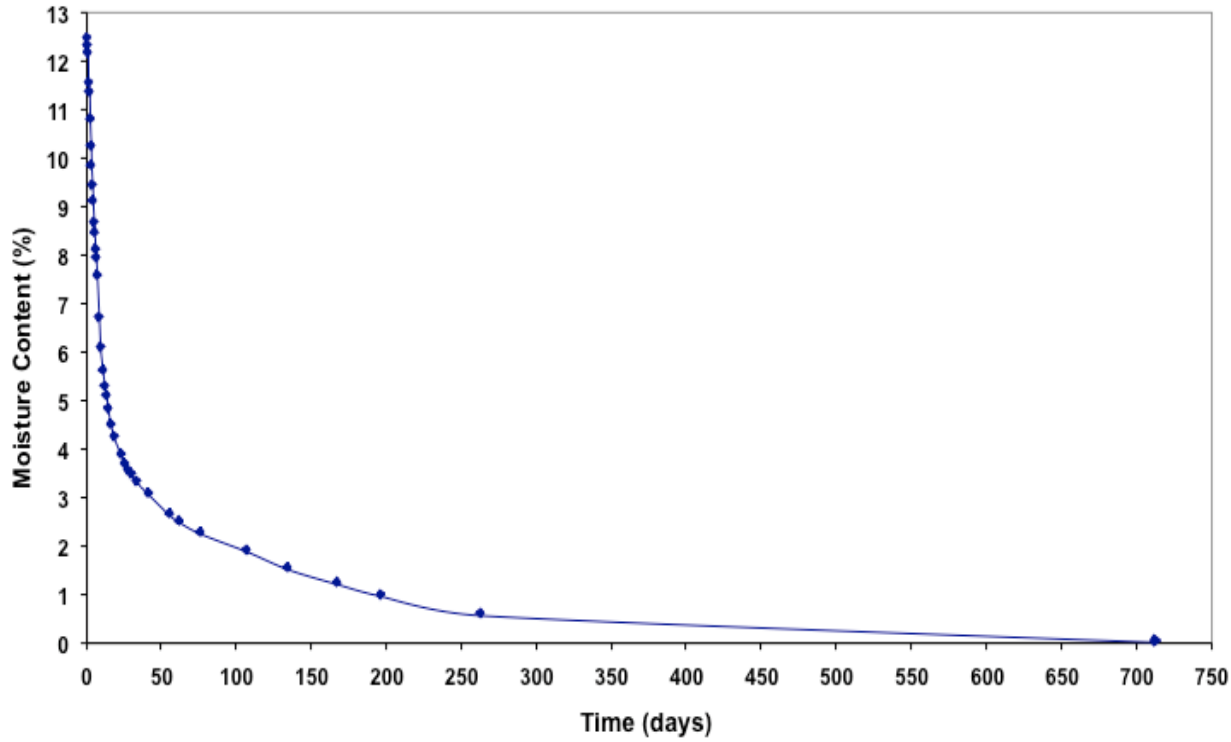

Figure B-8. Variation of moisture content with time, replicate 3, outdoor ambient.

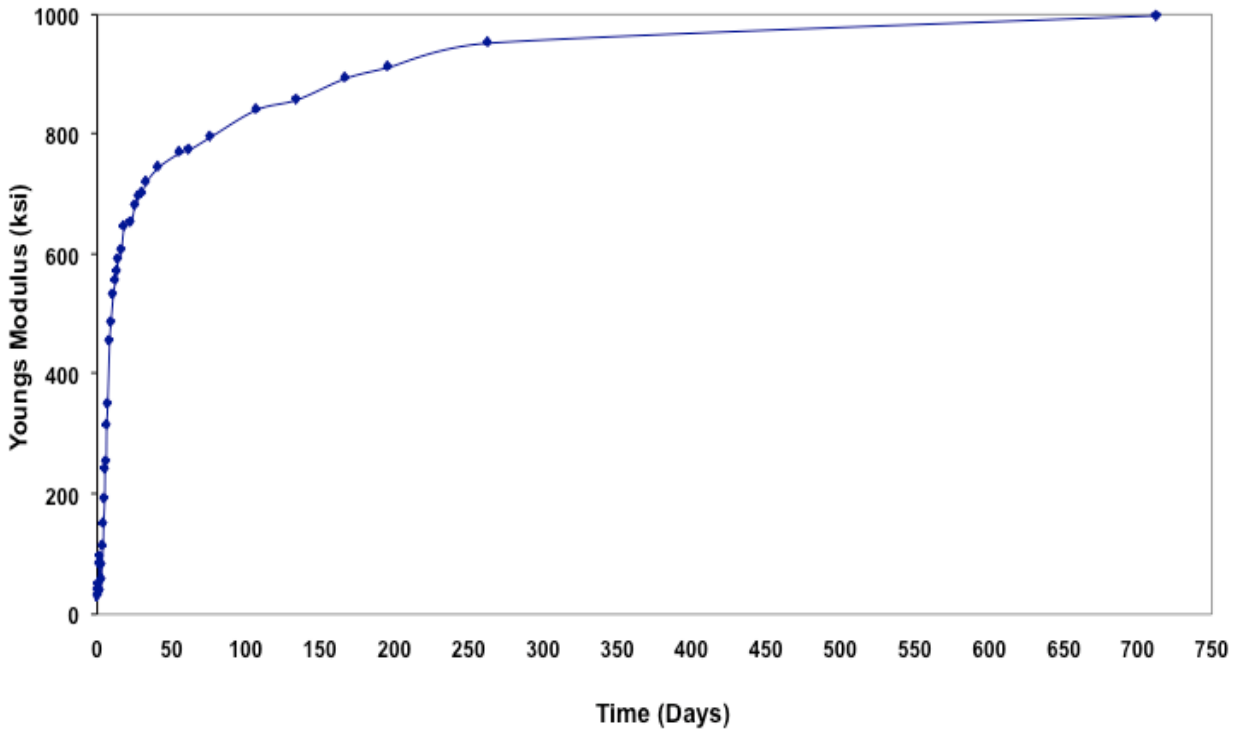

Figure B-9. Variation of Young's modulus with time, replicate 3, outdoor ambient.

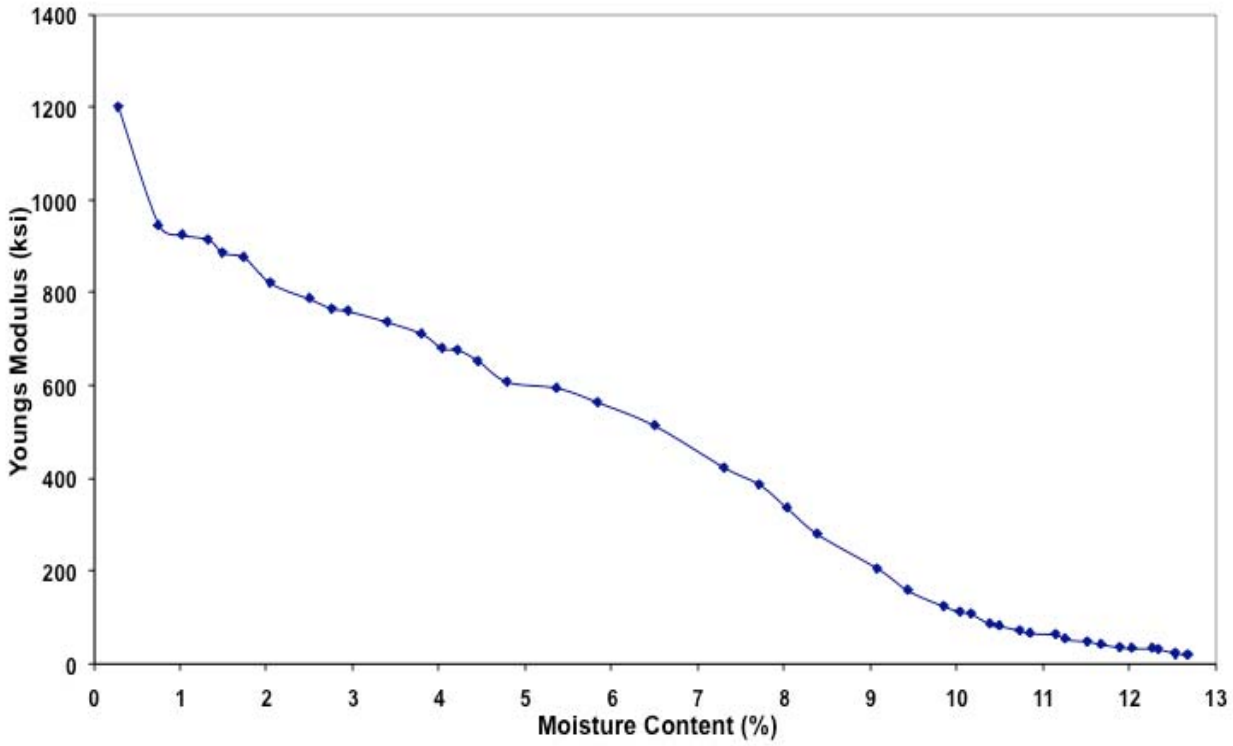

Figure B-10. Variation of Young's modulus with moisture content, replicate 1, laboratory ambient.

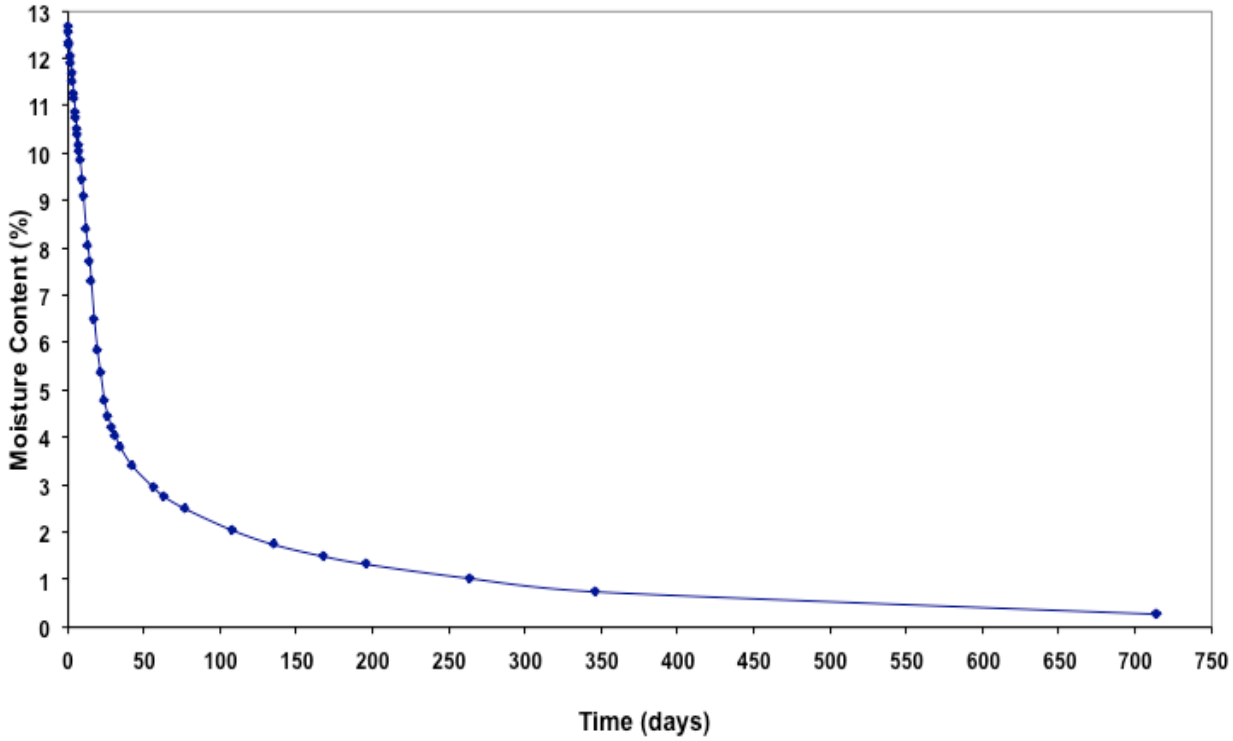

Figure B-11. Variation of moisture content with time, replicate 1, laboratory ambient.

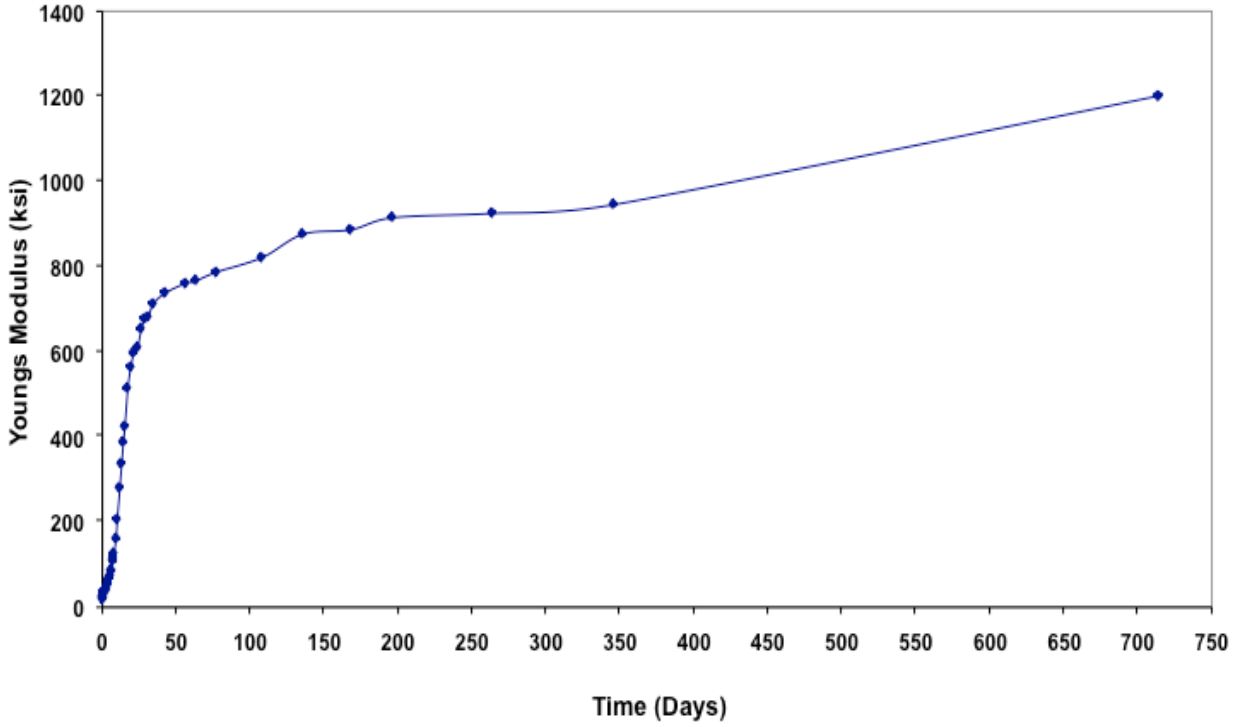

Figure B-12. Variation of Young's modulus with time, replicate 1, laboratory ambient.

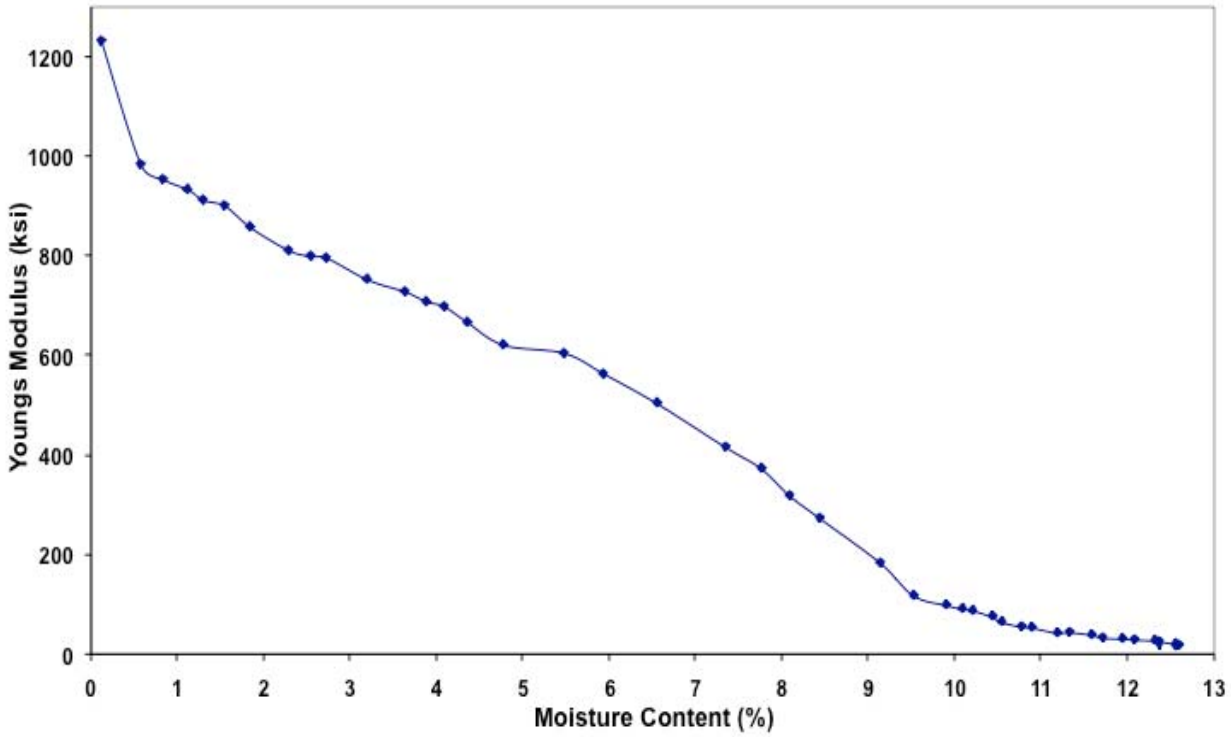

Figure B-13. Variation of Young's modulus with moisture content, replicate 2, laboratory ambient.

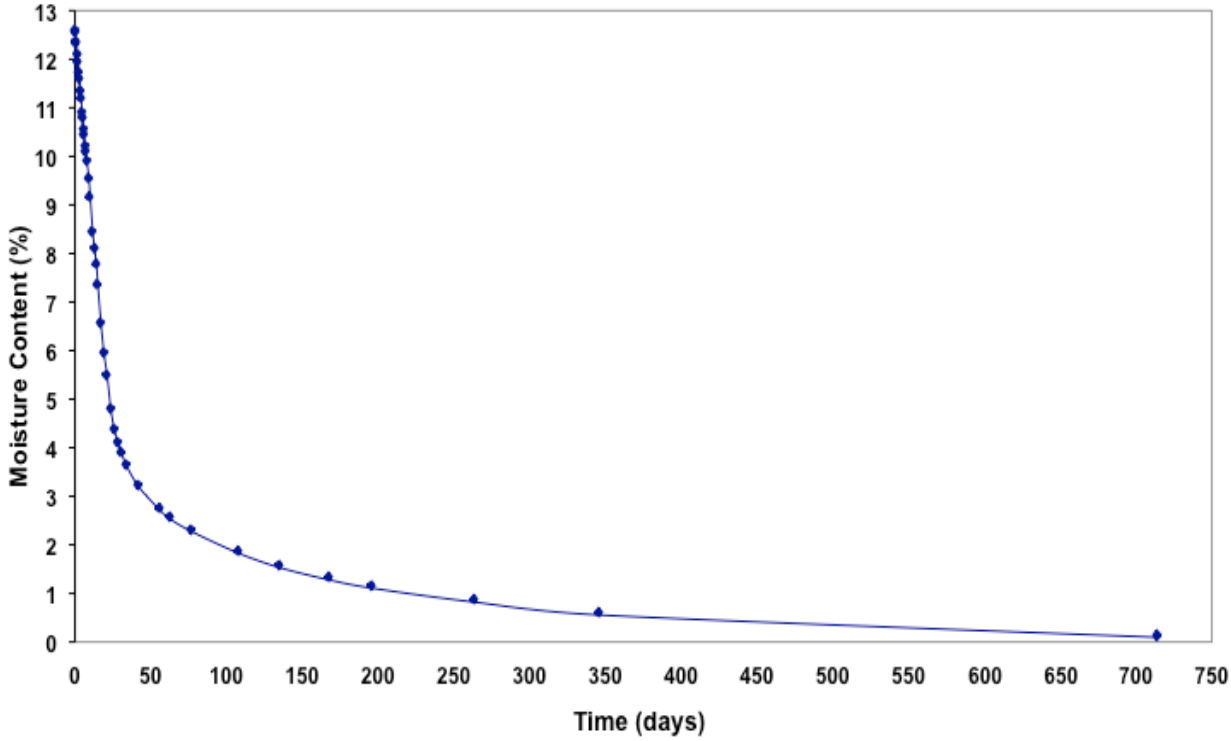

Figure B-14. Variation of moisture content with time, replicate 2, laboratory ambient.

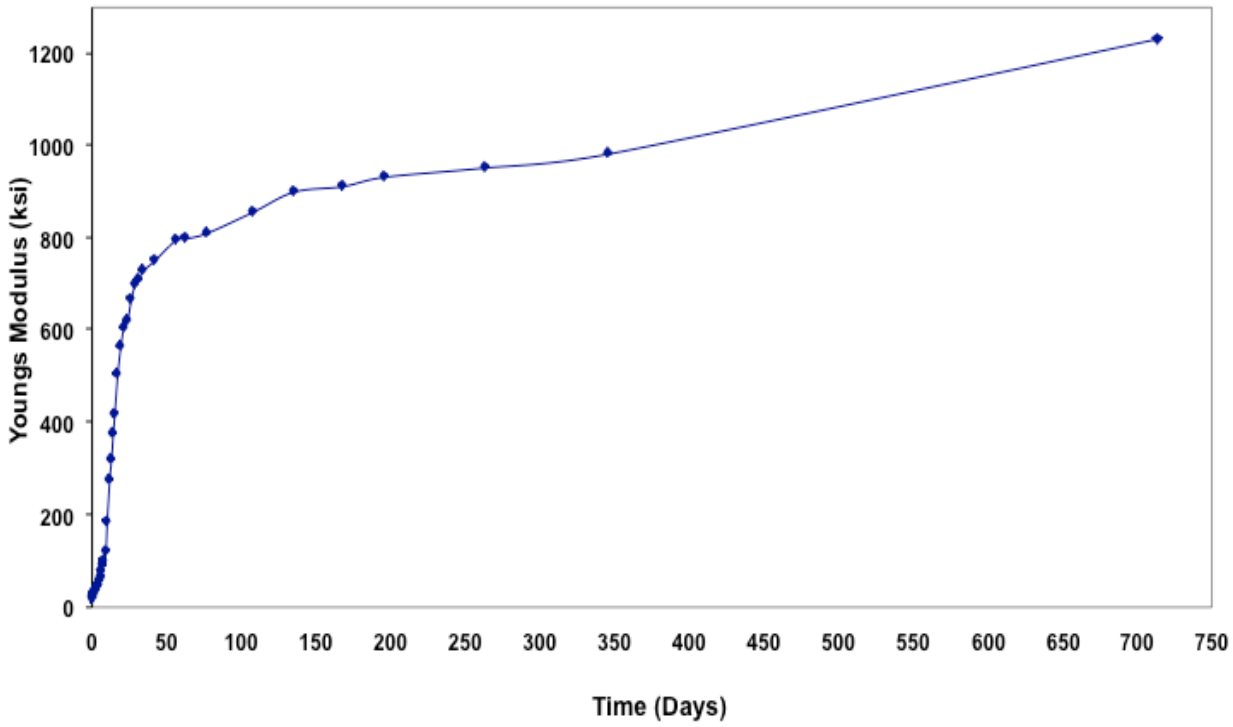

Figure B-15. Variation of Young's modulus with time, replicate 2, laboratory ambient.

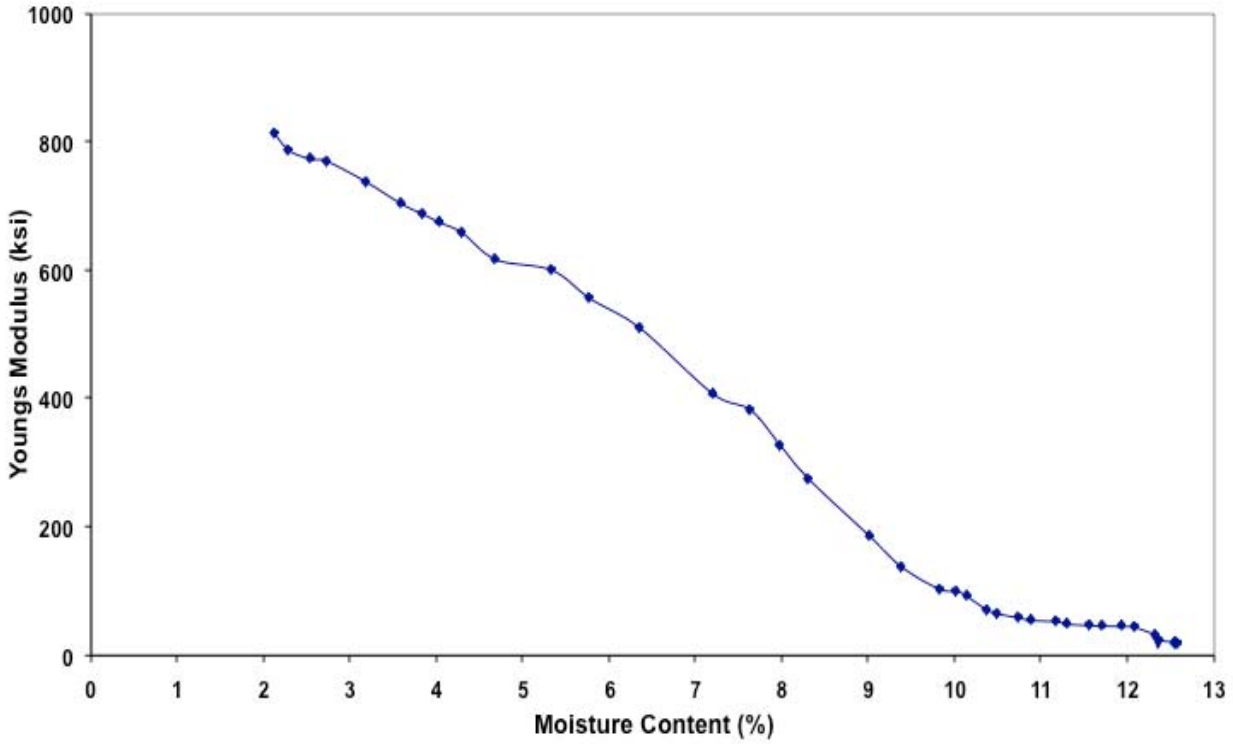

Figure B-16. Variation of Young's with moisture content, replicate 3, laboratory ambient.

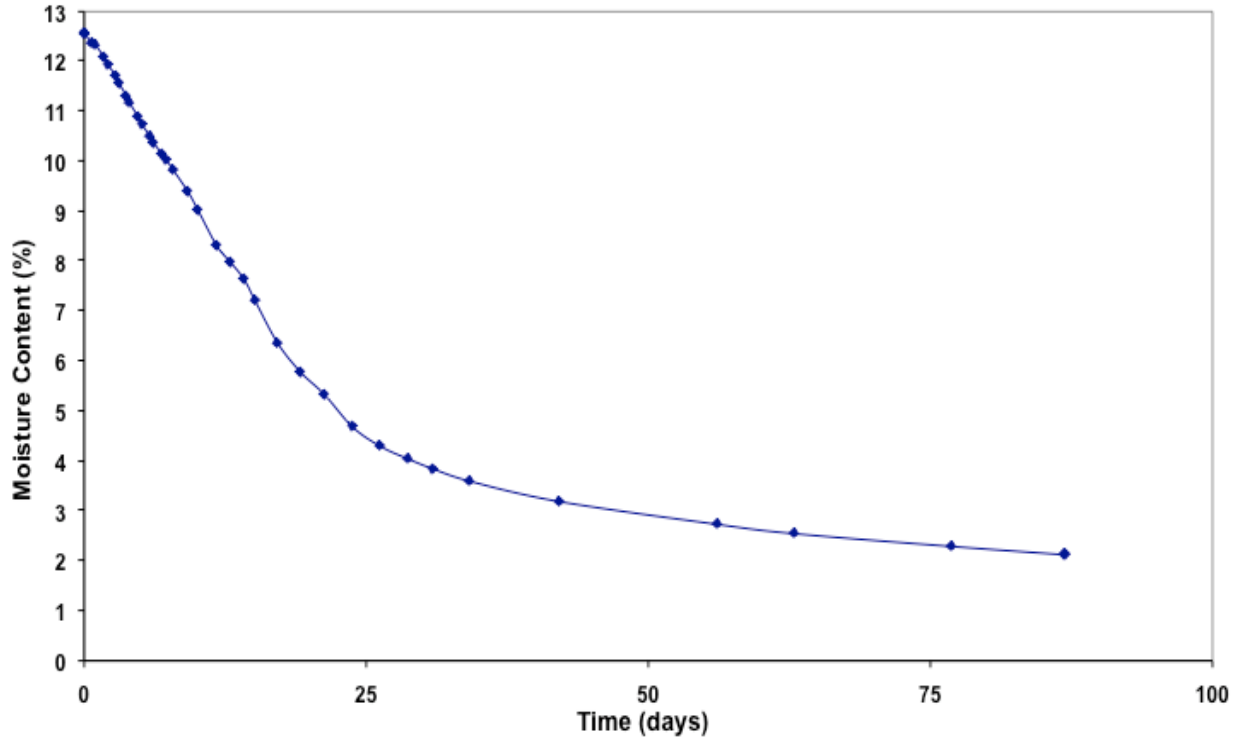

Figure B-17. Variation of moisture content with time, replicate 3, laboratory ambient.

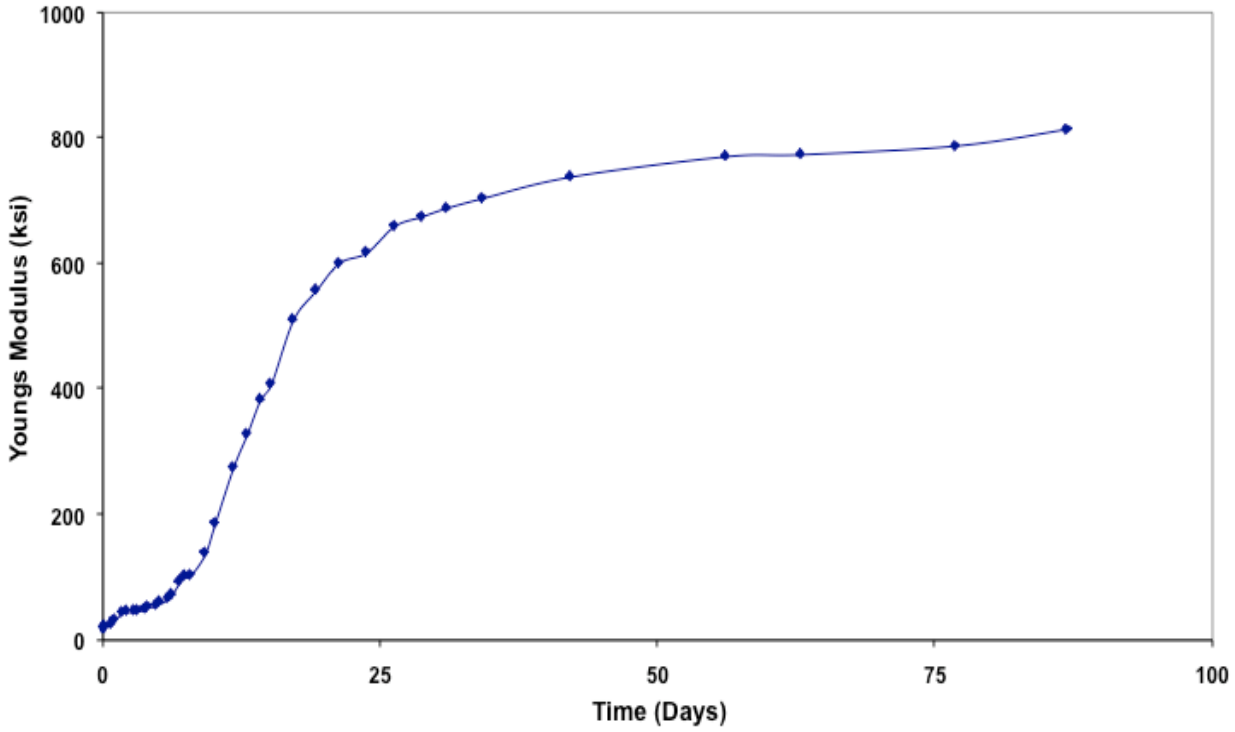

Figure B-18. Variation of Young's modulus with time, replicate 3, laboratory ambient.

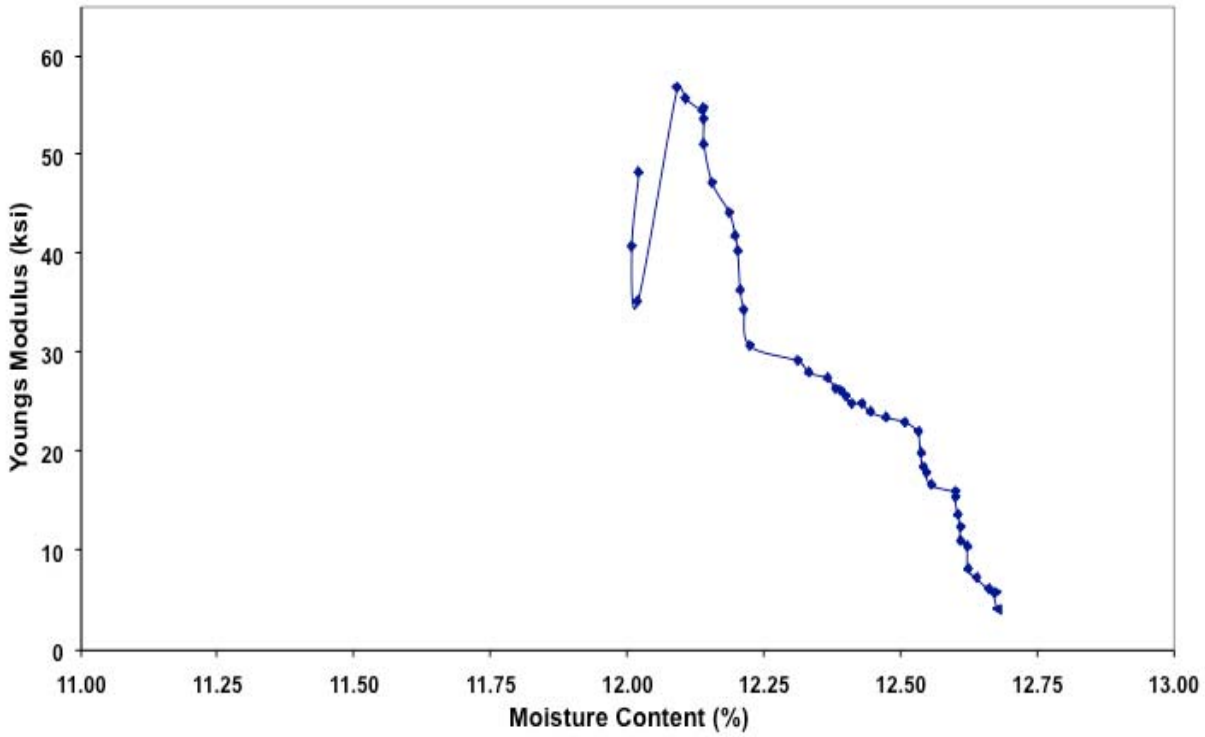

Figure B-19. Variation of Young's modulus with moisture content, replicate 1, constant moisture.

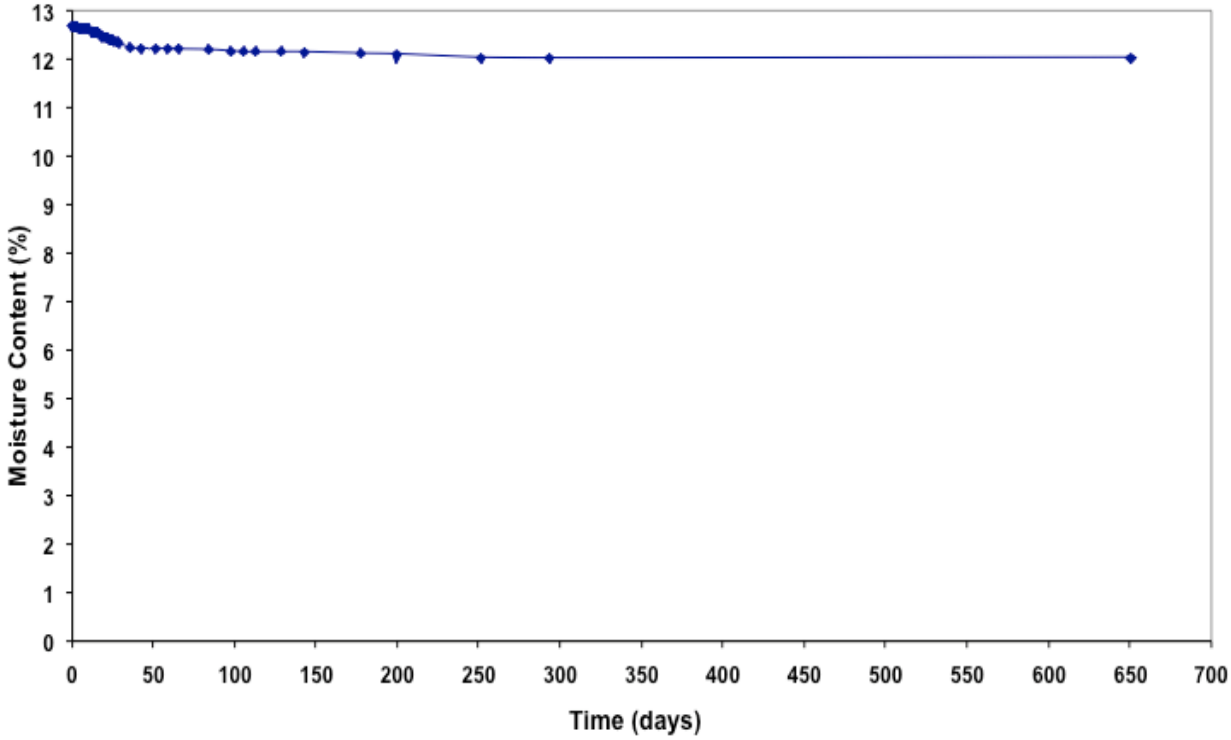

Figure B-20. Variation of moisture content with time, replicate 1, constant moisture.

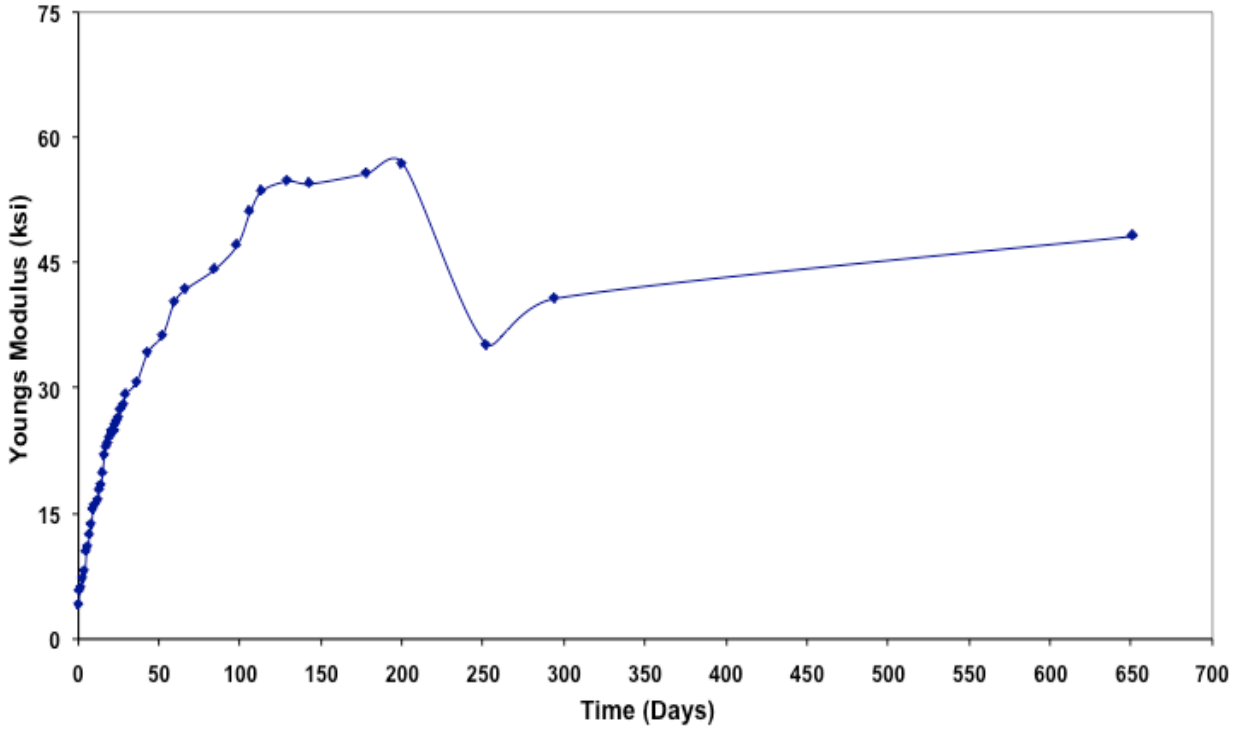

Figure B-21. Variation of Young's modulus with time, replicate 1, constant moisture.

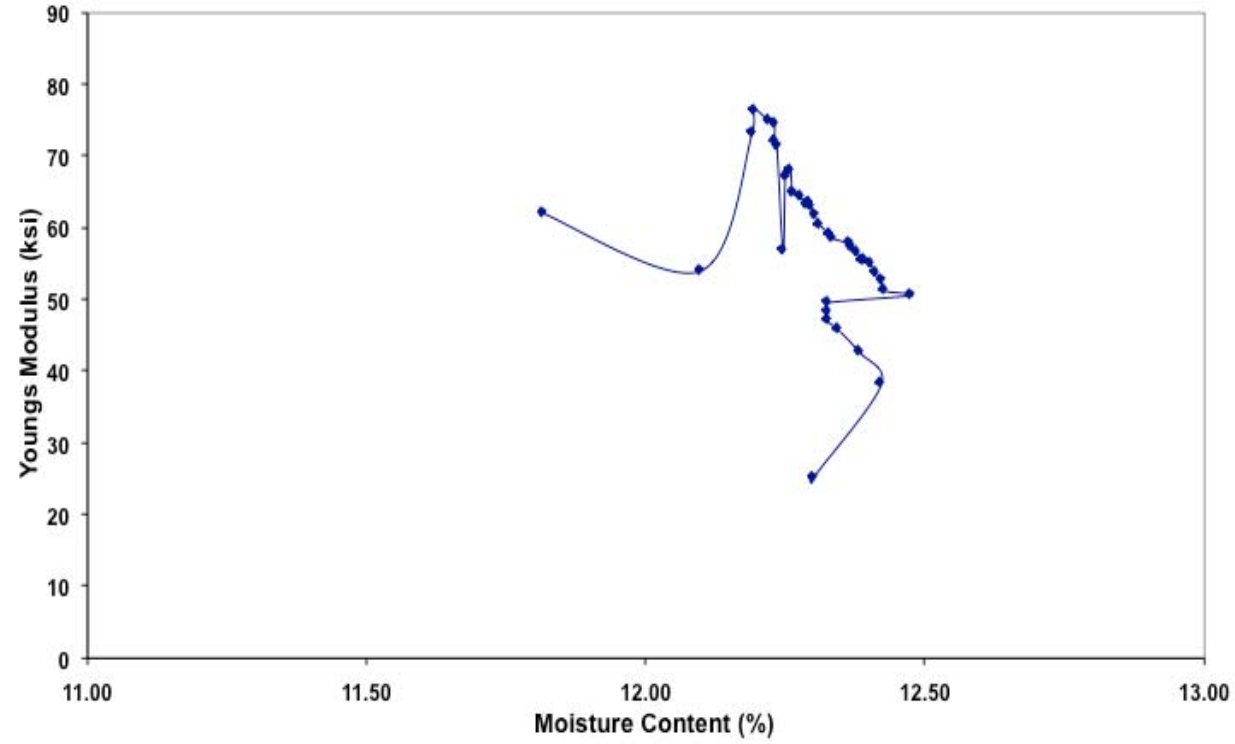

Figure B-22. Variation of Young's modulus with moisture content, replicate 2, constant moisture.

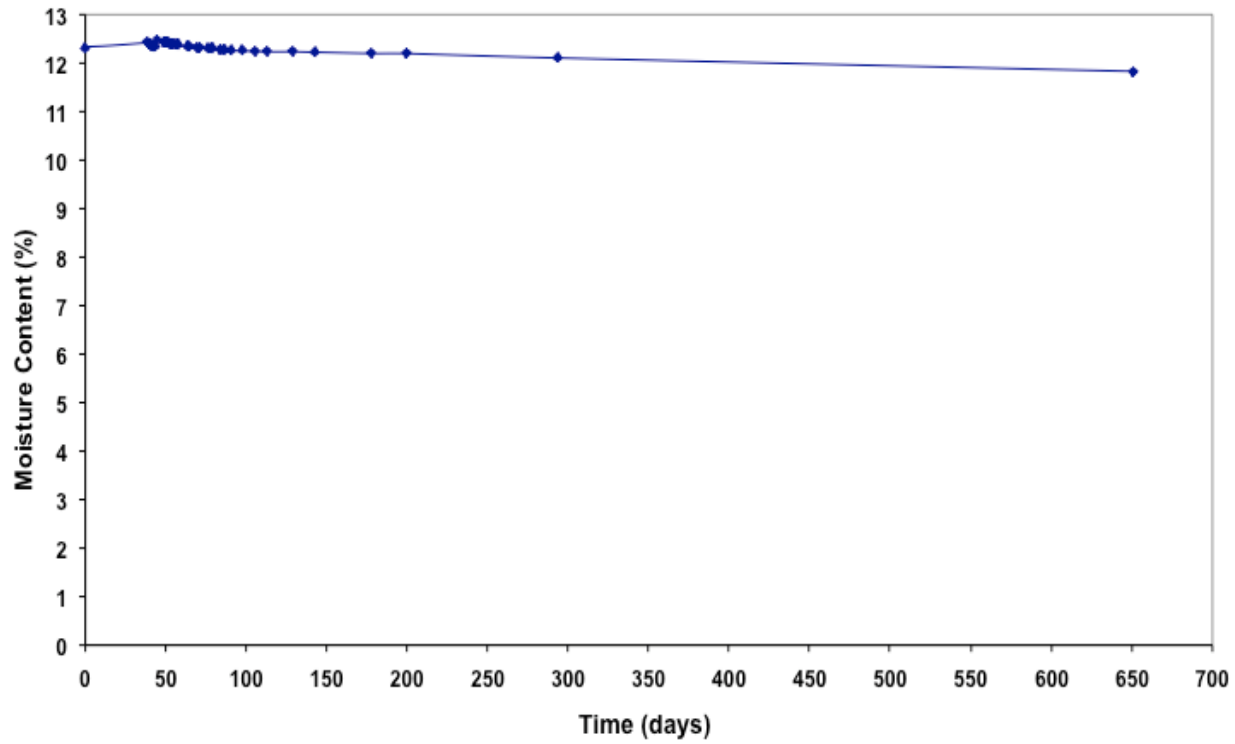

Figure B-23. Variation of moisture content with time, replicate 2, constant moisture.

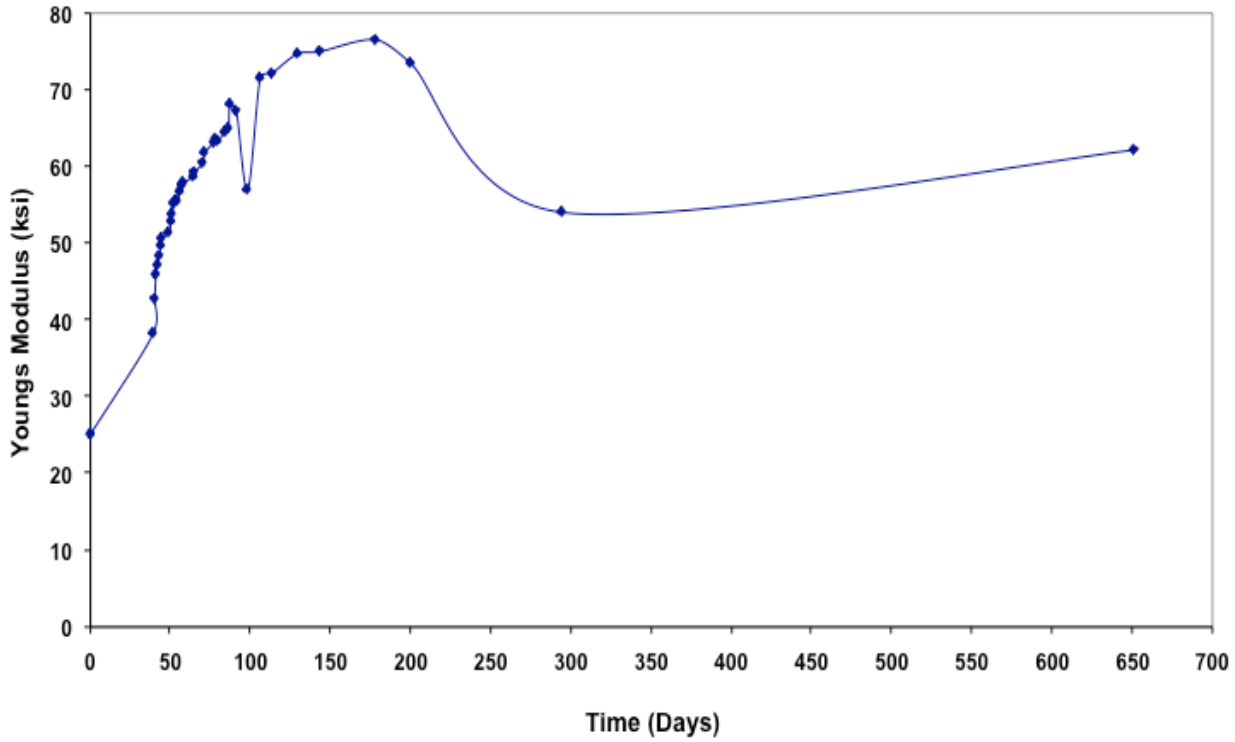

Figure B-24. Variation of Young's modulus with time, replicate 2, constant moisture.

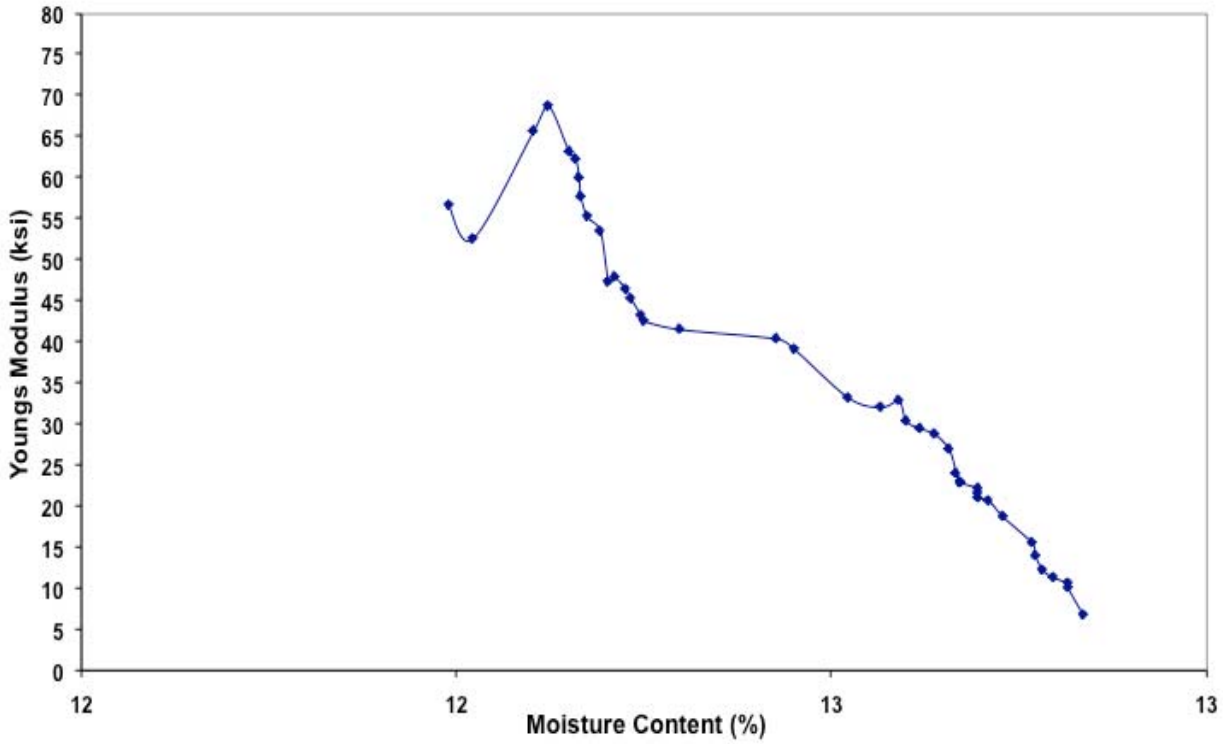

Figure B-25. Variation of Young's modulus with moisture content, replicate 3, constant moisture.

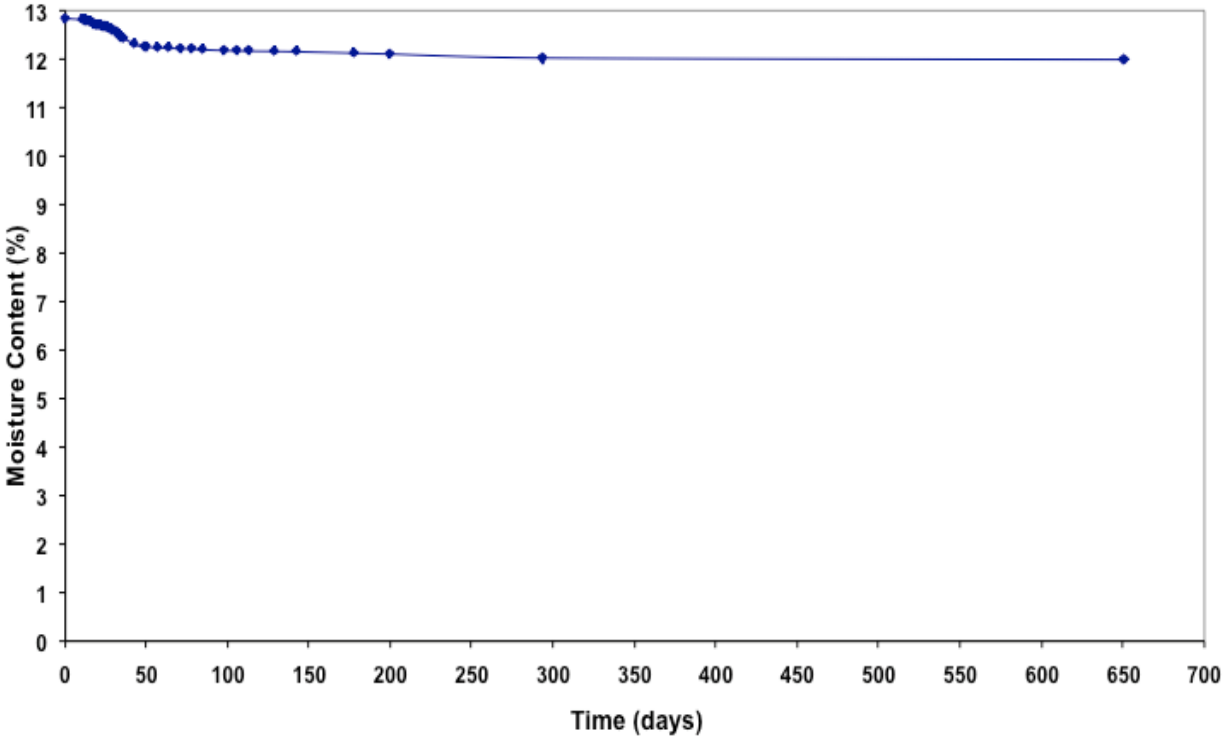

Figure B-26. Variation of moisture content with time, replicate 3, constant moisture.

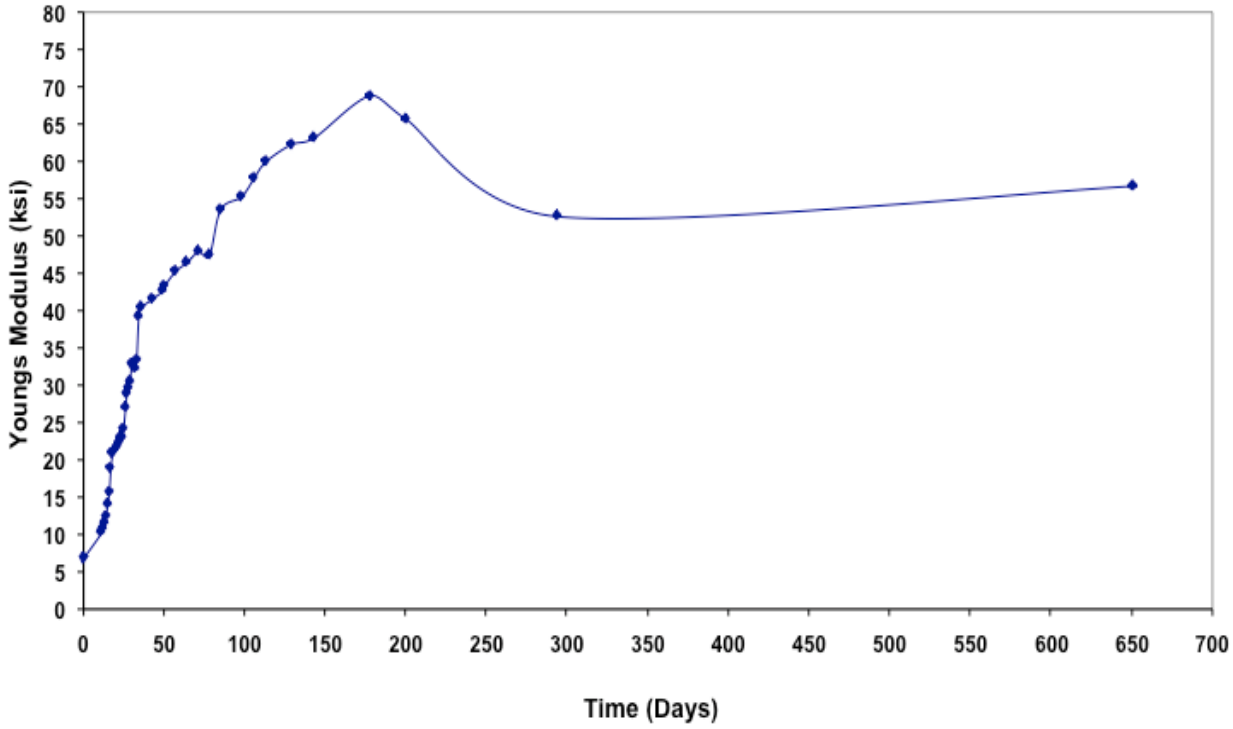

Figure B-27. Variation of Young's modulus with time, replicate 3, constant moisture.

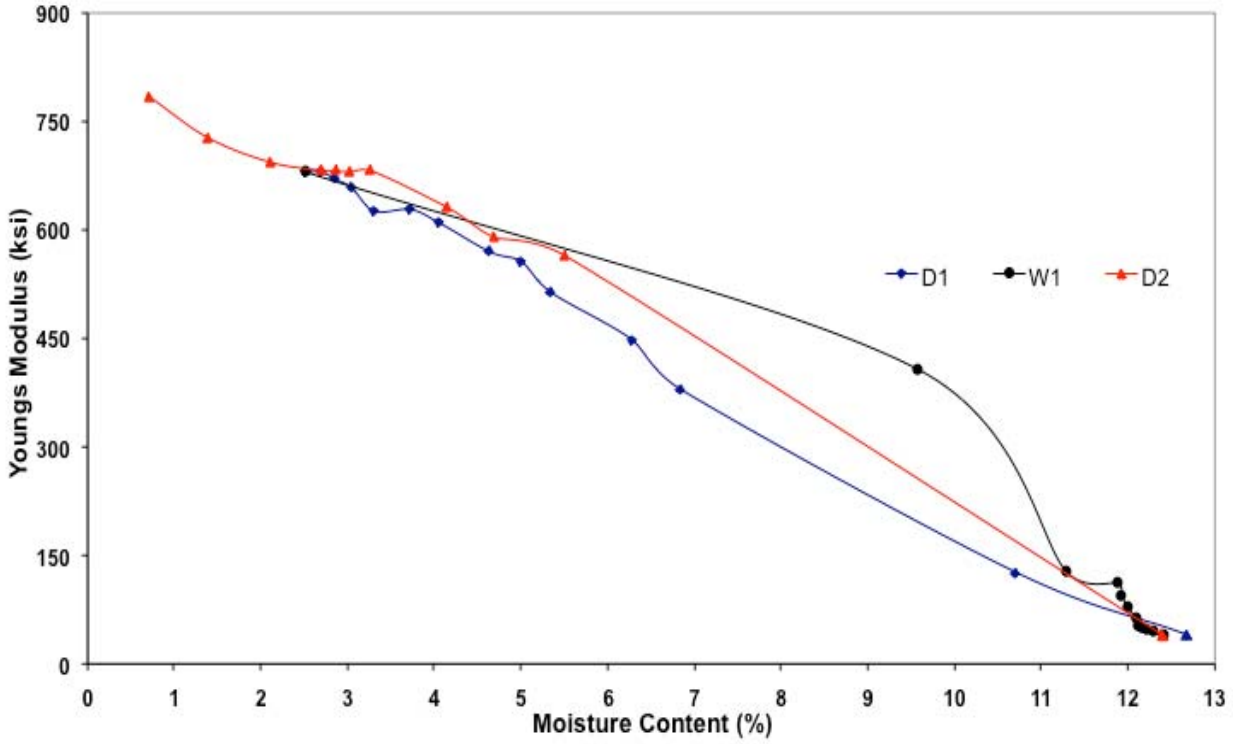

Figure B-28. Variation of Young's modulus with moisture content, replicate 1, wetting and drying.

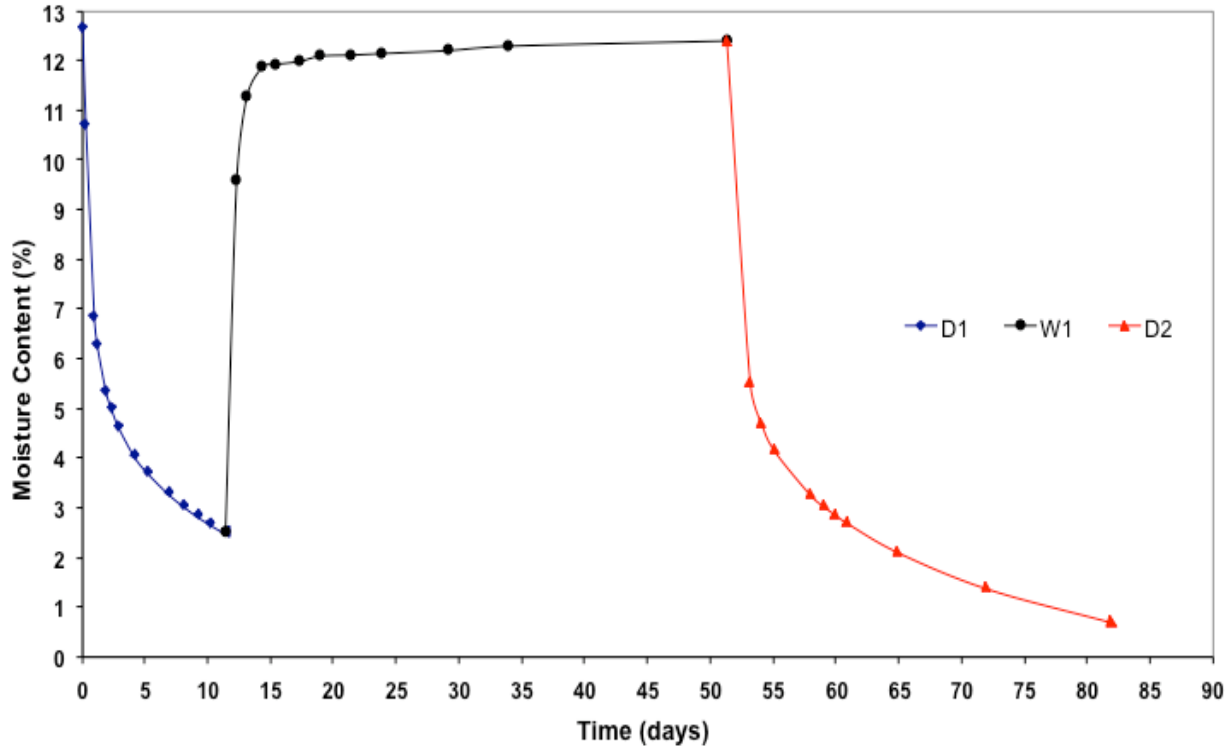

Figure B-29. Variation of moisture content with time, replicate 1, wetting and drying.

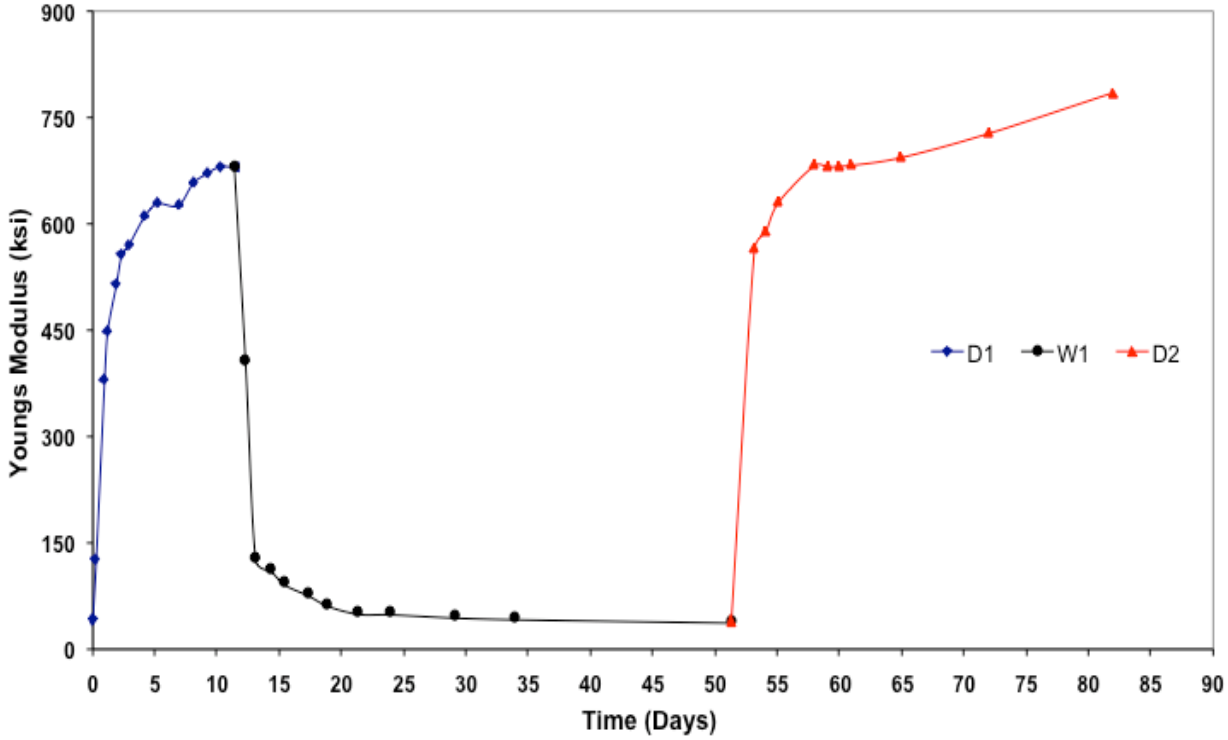

Figure B-30. Variation of Young's modulus with time, replicate 1, wetting and drying.

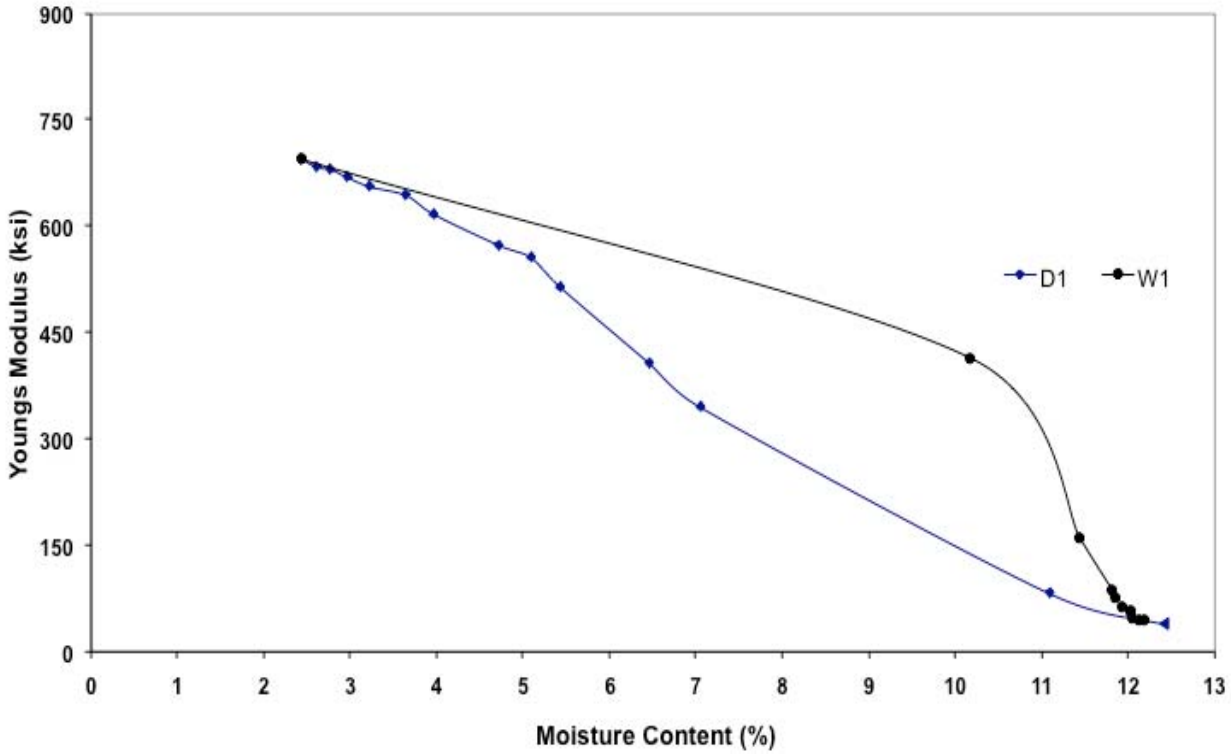

Figure B-31. Variation of Young's modulus with moisture content, replicate 2, wetting and drying.

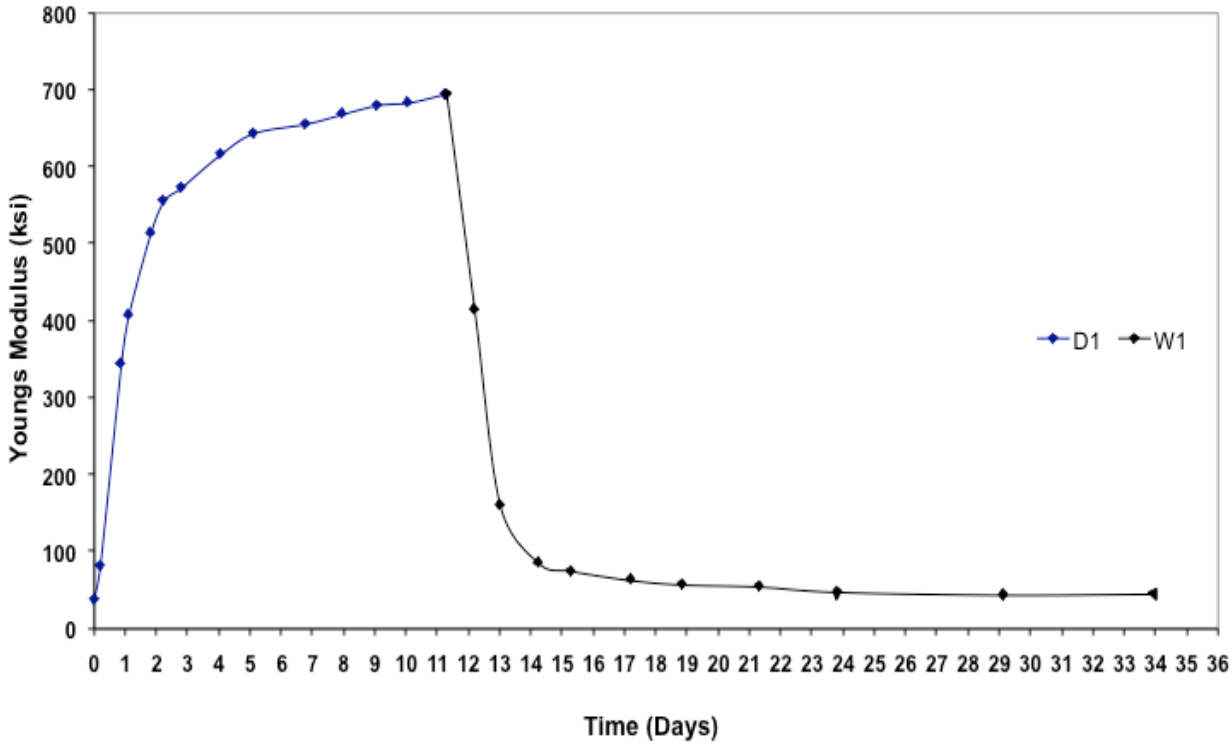

Figure B-32. Variation of Young's modulus with time, replicate 2, wetting and drying.

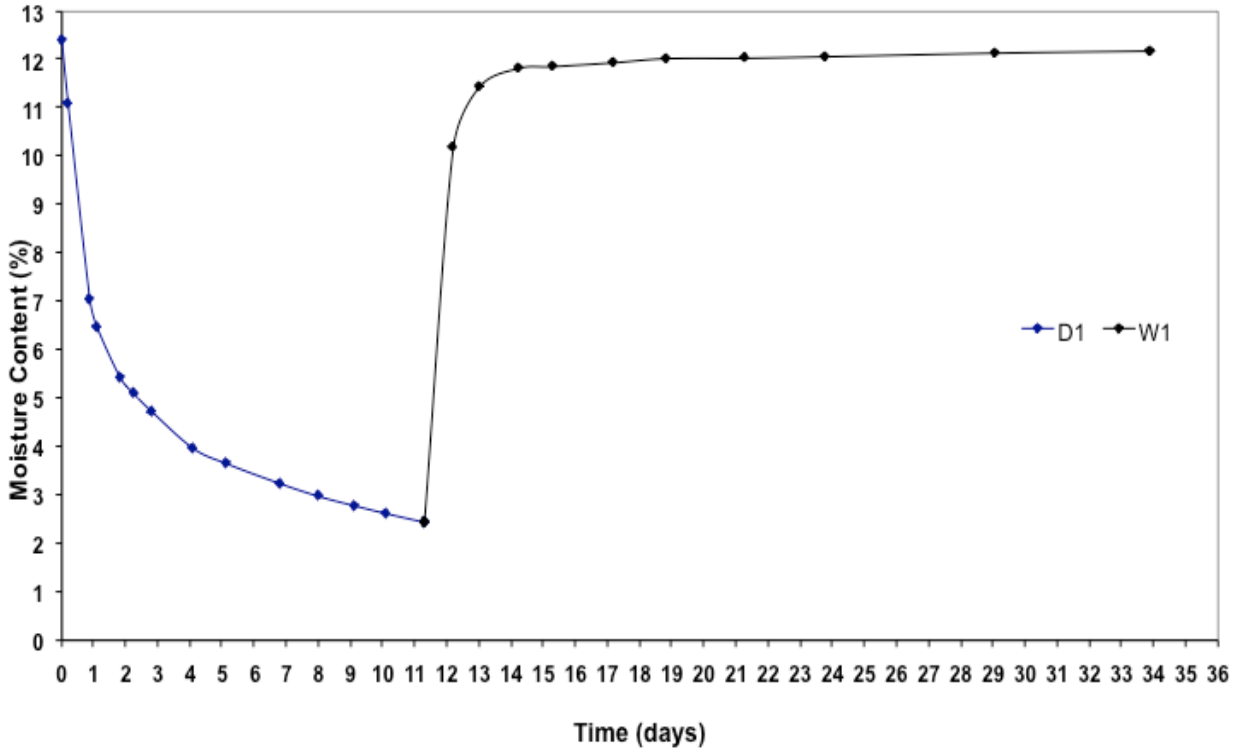

Figure B-33. Variation Moisture Content with Time, replicate 2, wetting and drying.

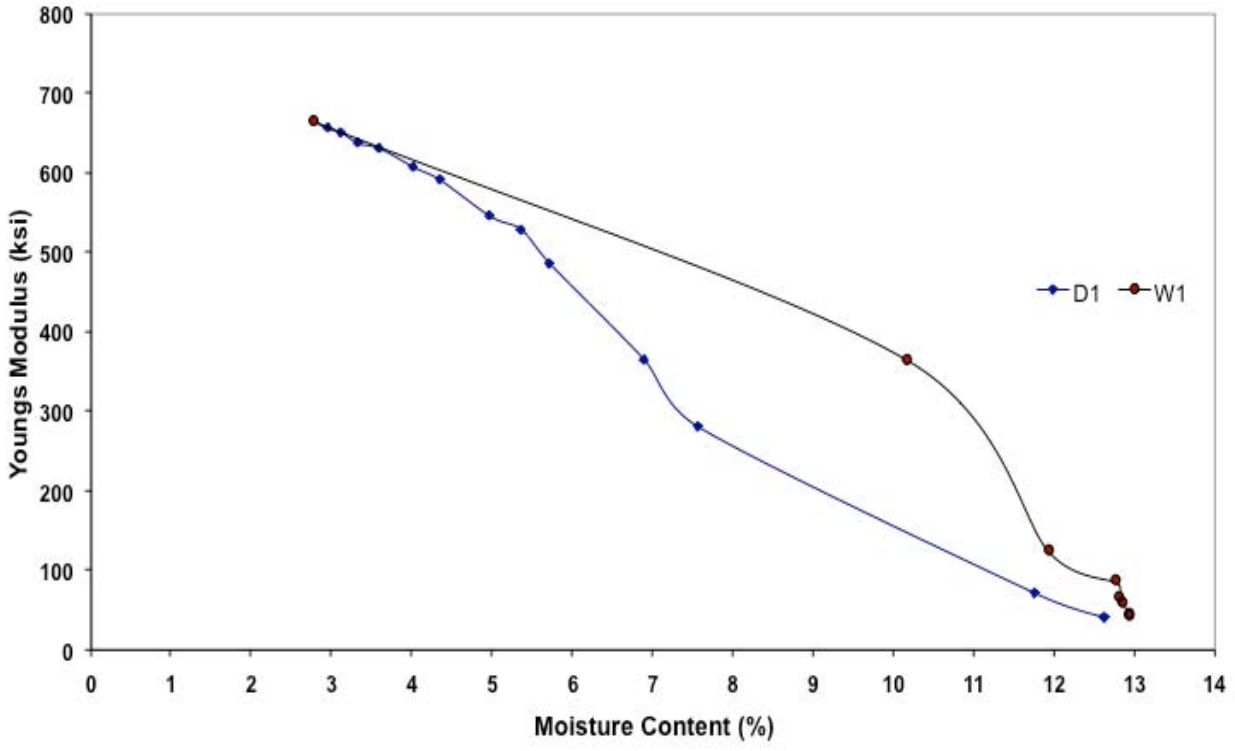

Figure B-34. Variation of Young's modulus with moisture content, replicate 3, wetting and drying.

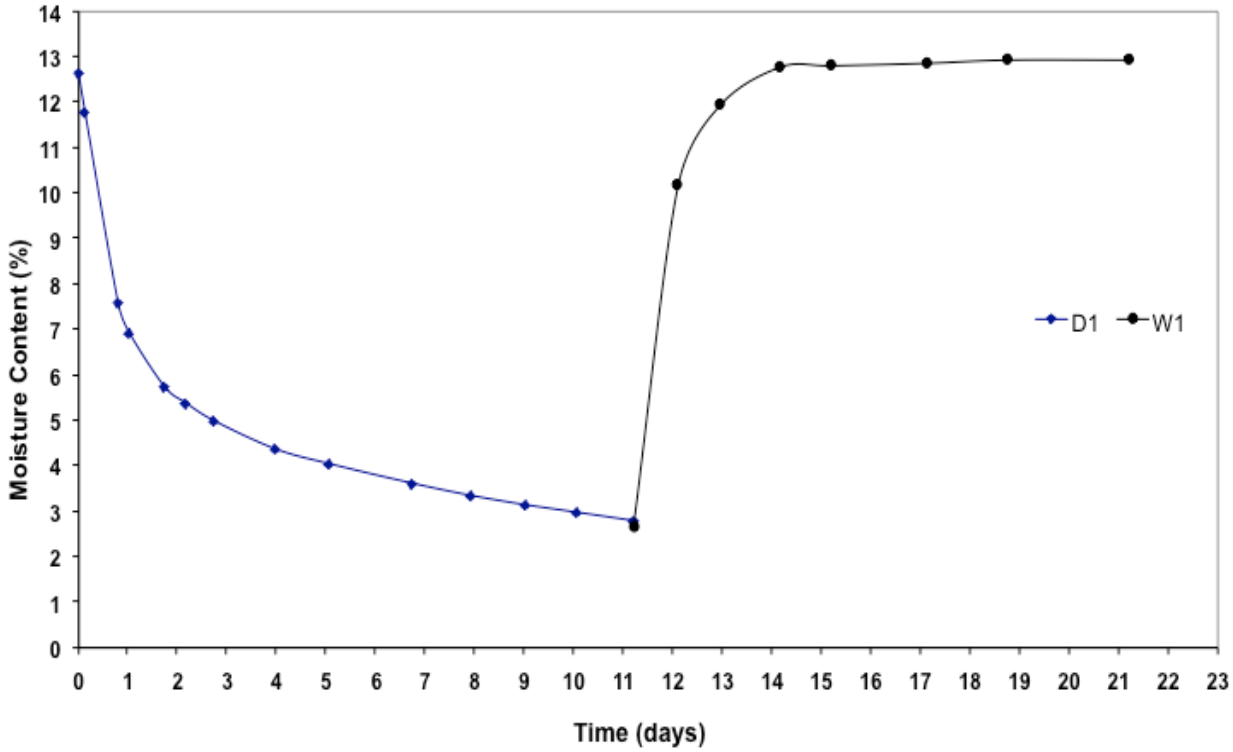

Figure B-35. Variation of moisture content with time, replicate 3, wetting and drying.

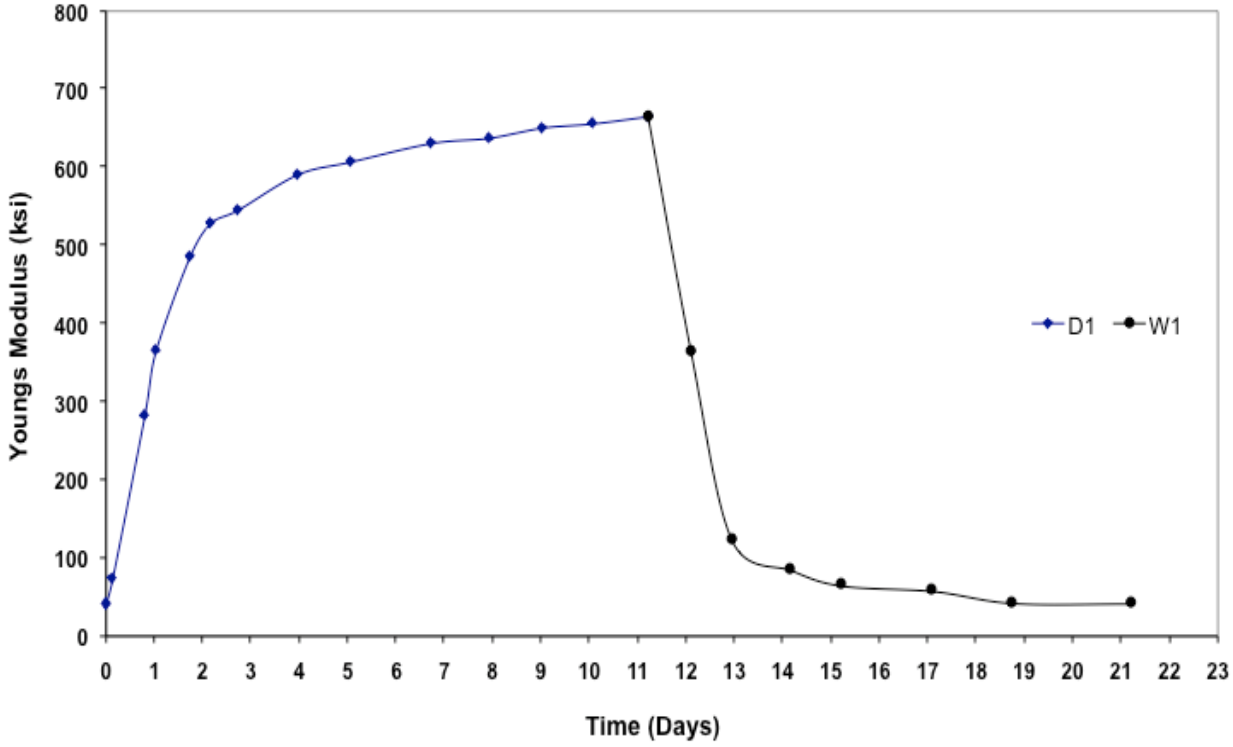

Figure B-36. Variation of Young's modulus with time, replicate 3, wetting and drying.

APPENDIX C
OCALA INDIVIDUAL SMALL-STRAIN MODULUS TEST RESULTS

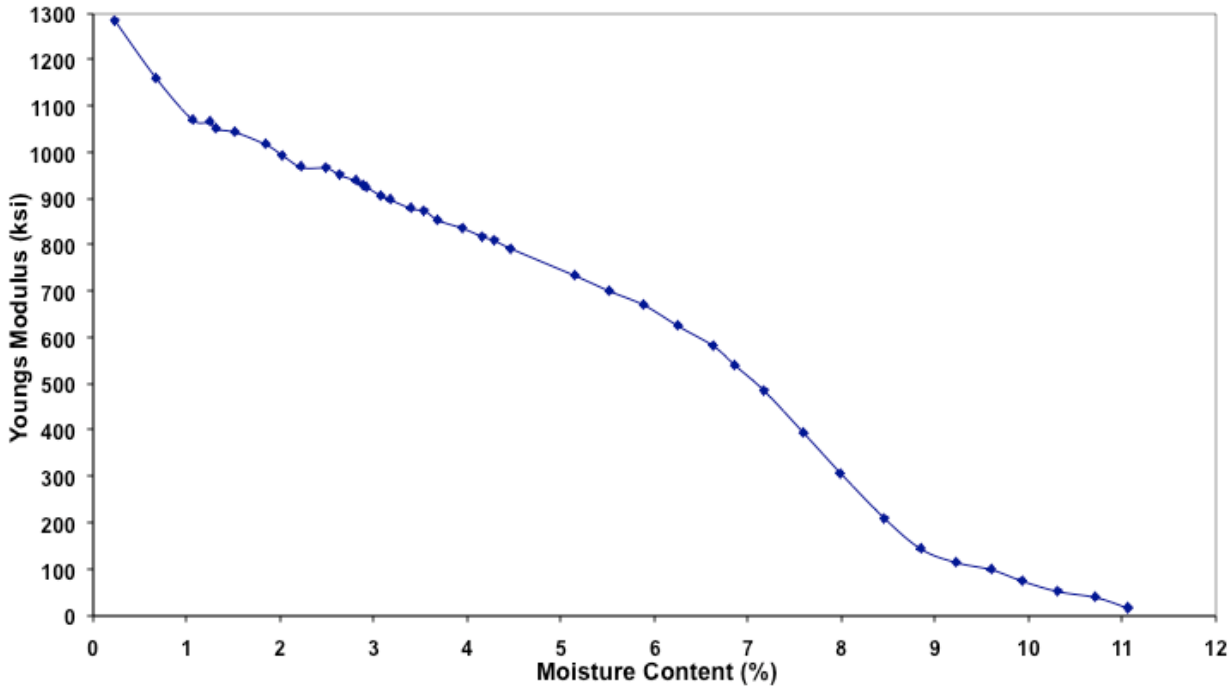

Figure C-1. Variation of Young's modulus with moisture content, replicate 1, laboratory ambient.

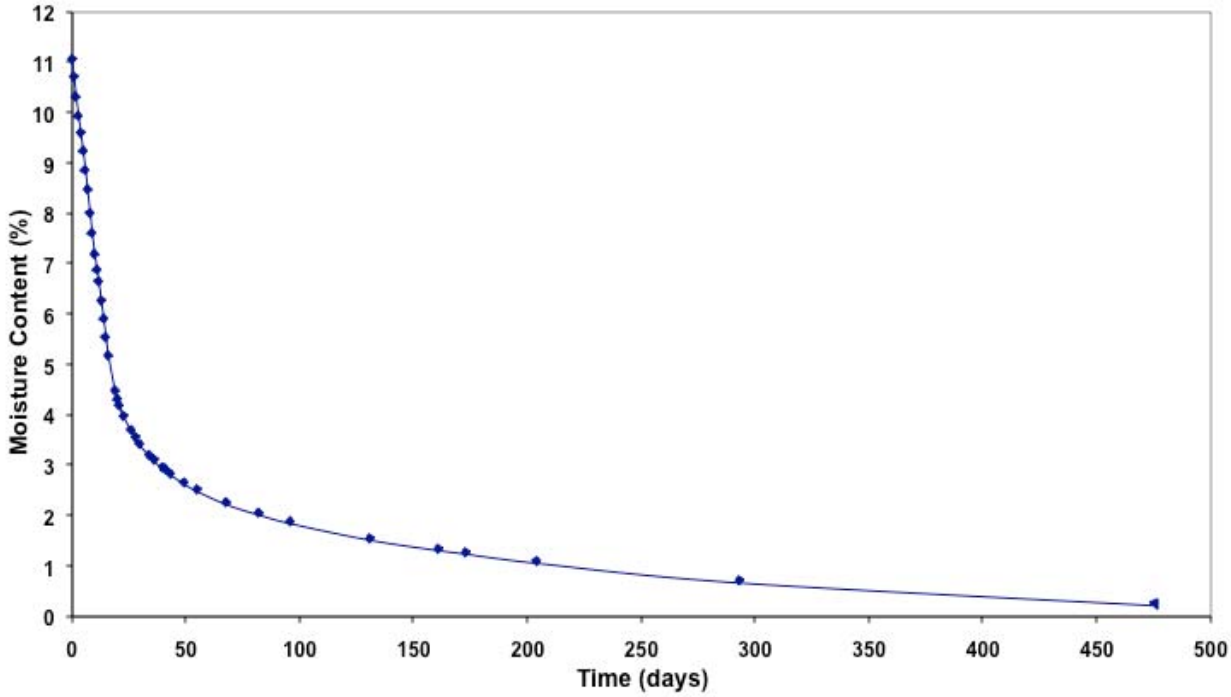

Figure C-2. Variation of moisture content with time, replicate 1, laboratory ambient.

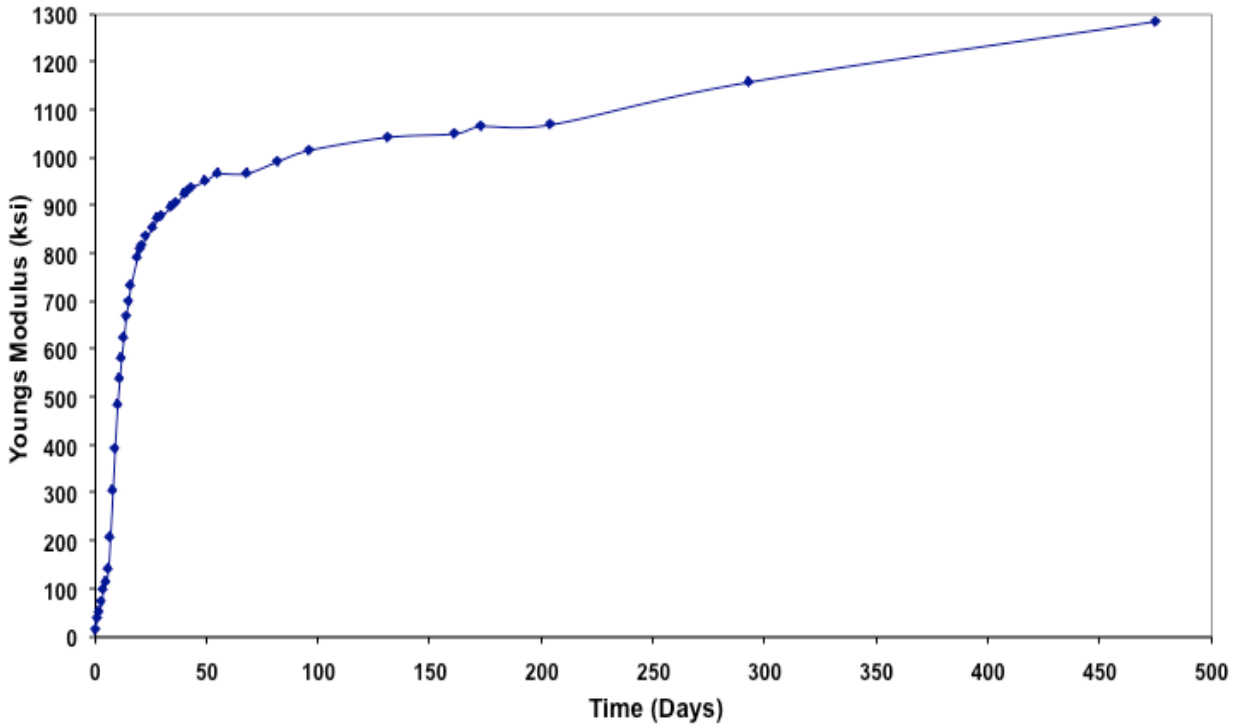

Figure C-3. Variation of Young's modulus with time, replicate 1, laboratory ambient.

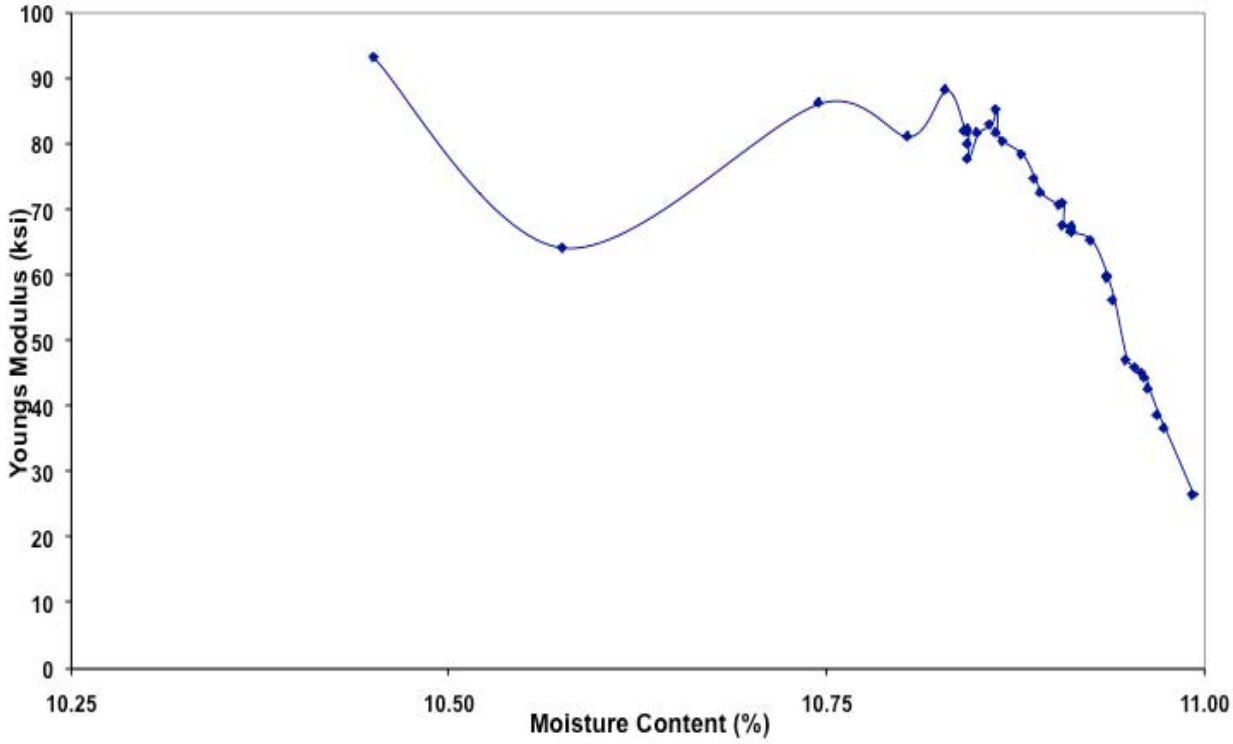

Figure C-4. Variation of Young's modulus with moisture content, replicate 1, constant moisture.

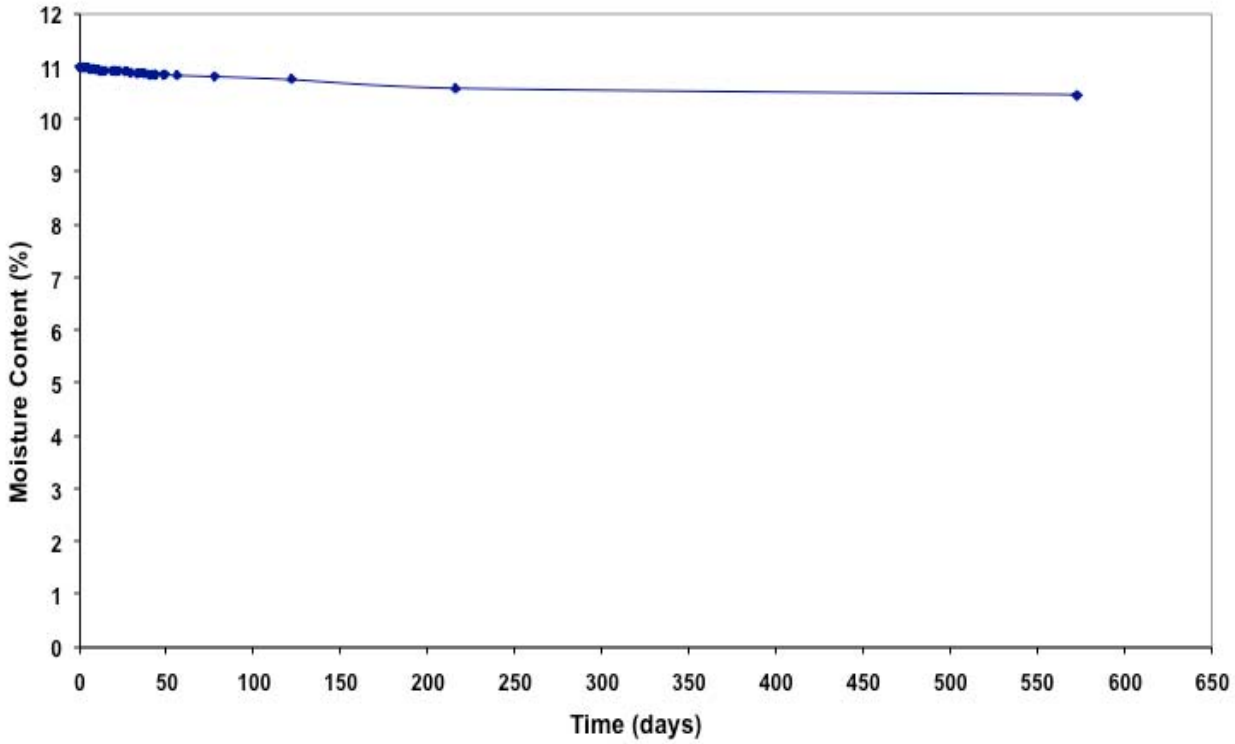

Figure C-5. Variation of moisture content with time, replicate 1, constant moisture.

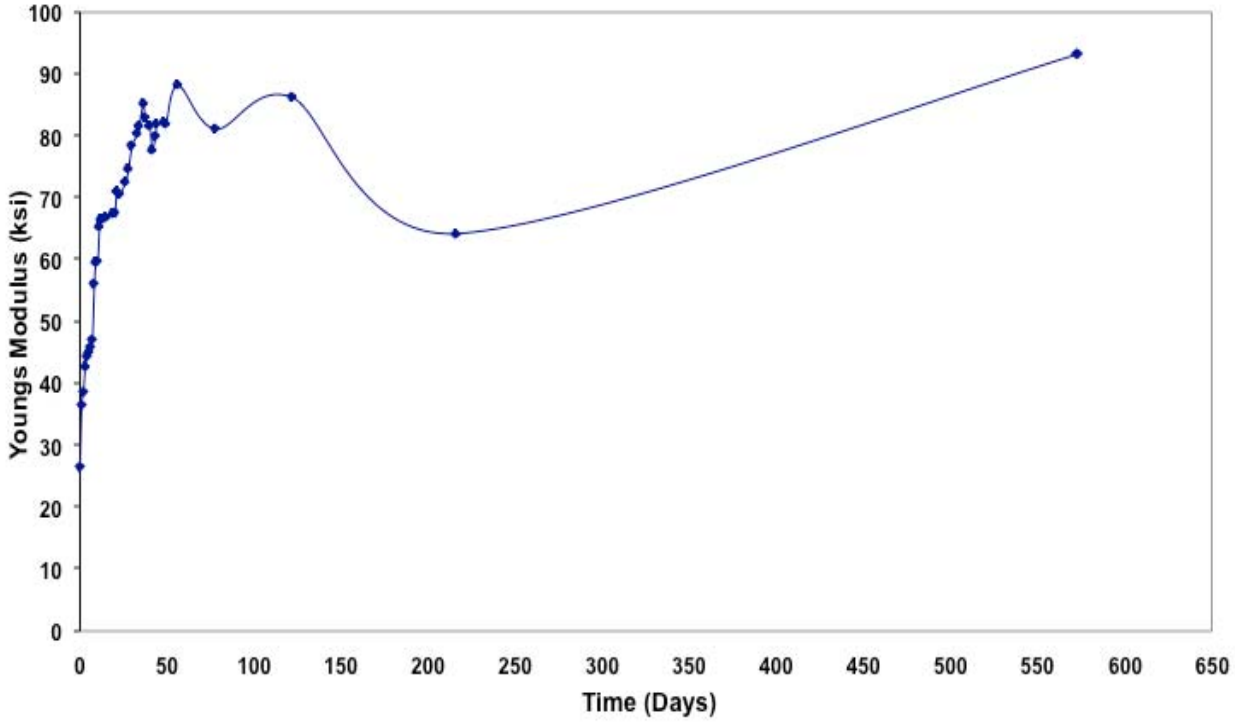

Figure C-6. Variation of Young's modulus with time, replicate 1, constant moisture.

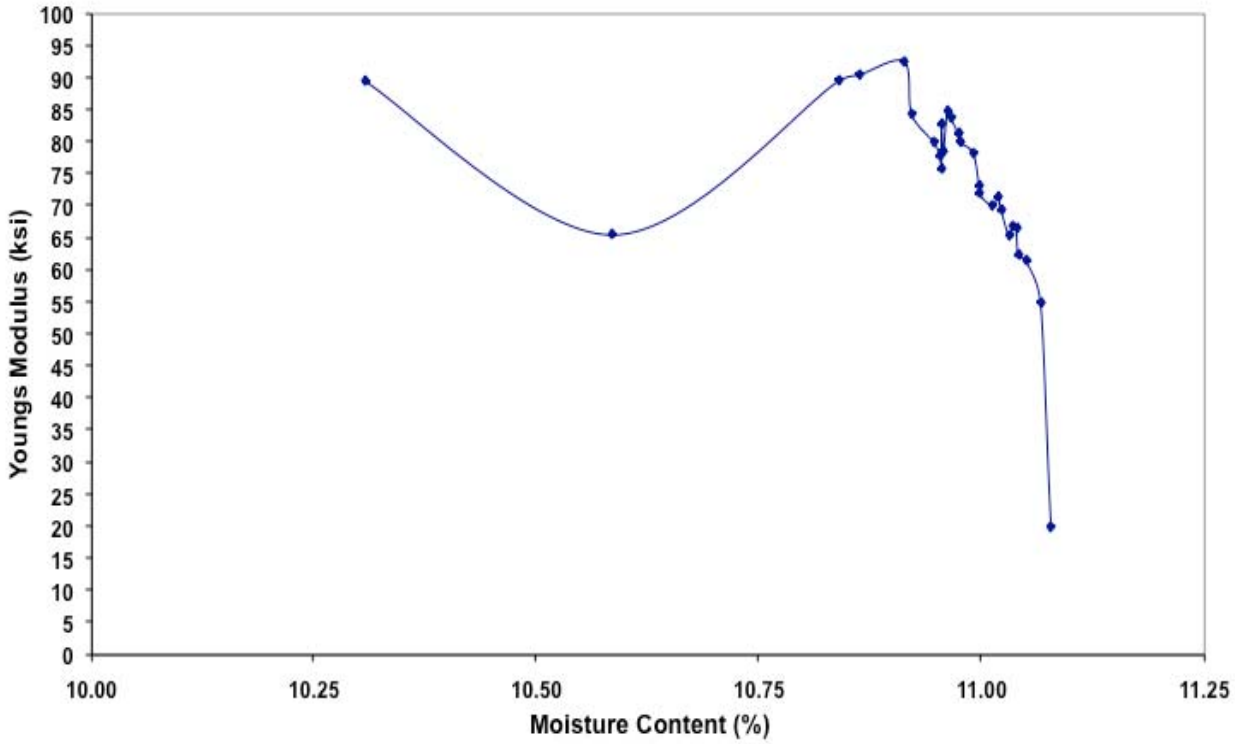

Figure C-7. Variation of Young's modulus with moisture content, replicate 2, constant moisture.

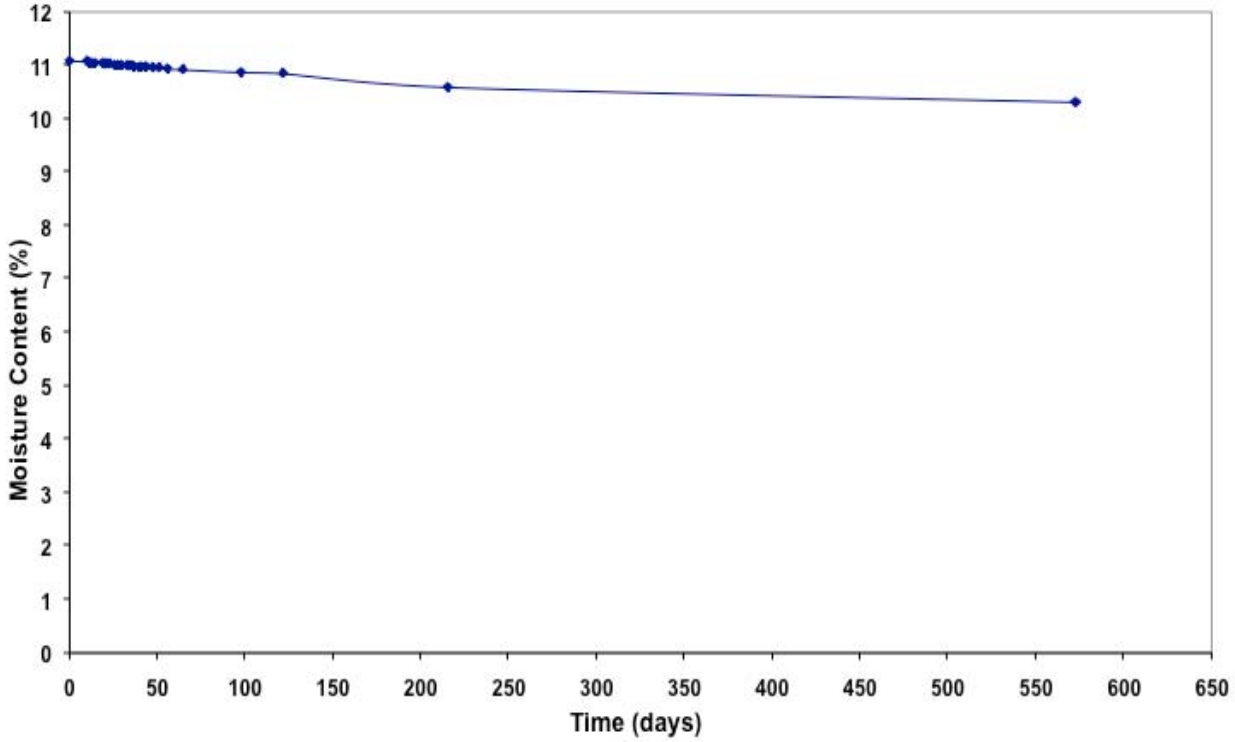

Figure C-8. Variation of moisture content with time, replicate 2, constant moisture.

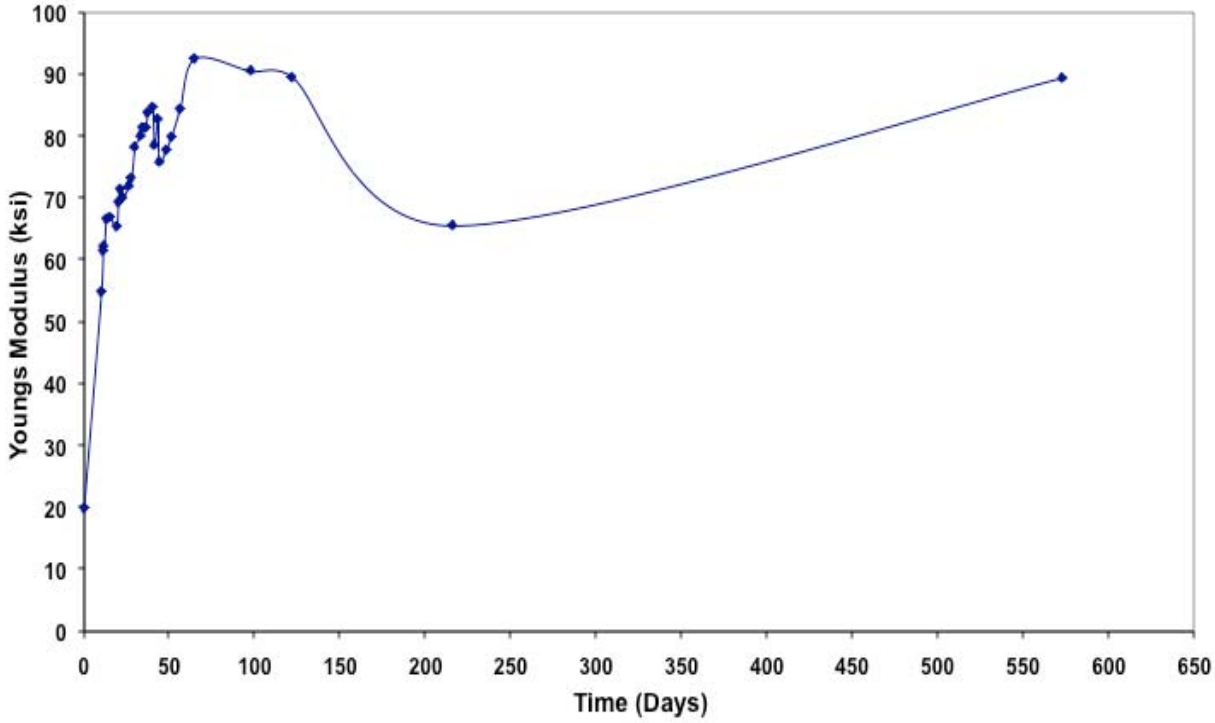

Figure C-9. Variation of Young's modulus with time, replicate 2, constant moisture.

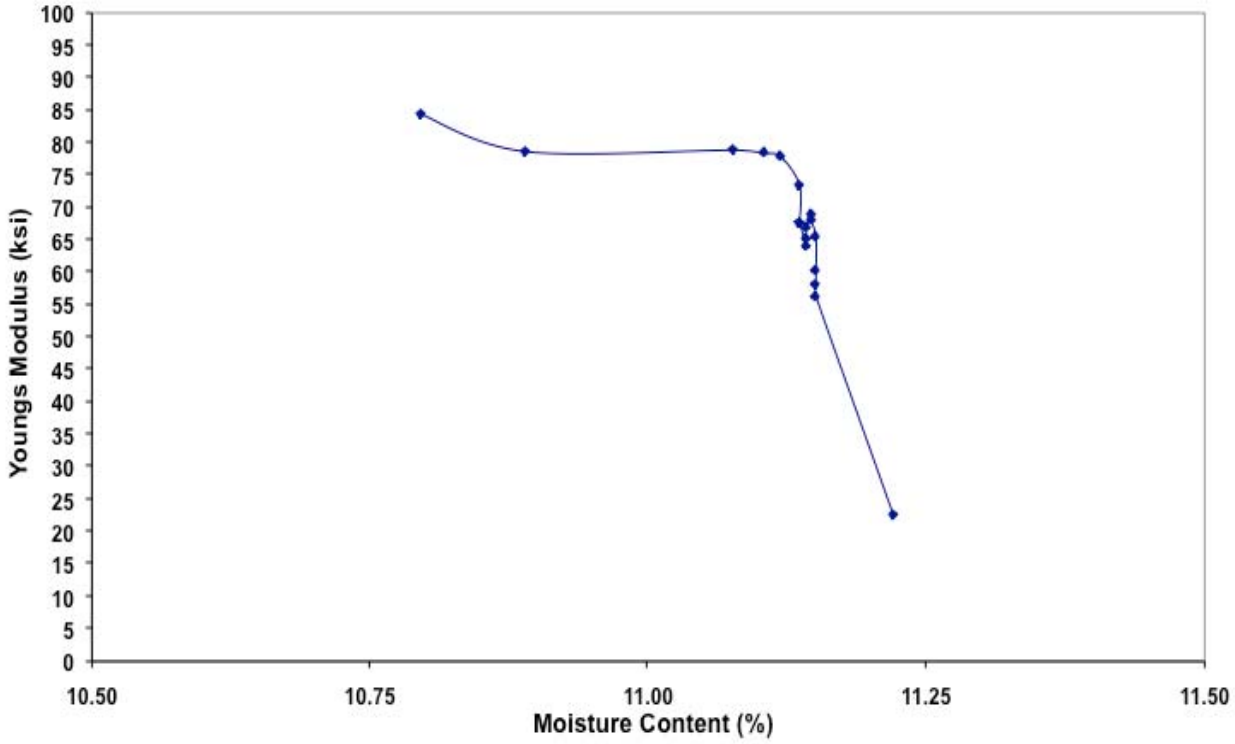

Figure C-10. Variation of Young's modulus with moisture content, replicate 3, constant moisture.

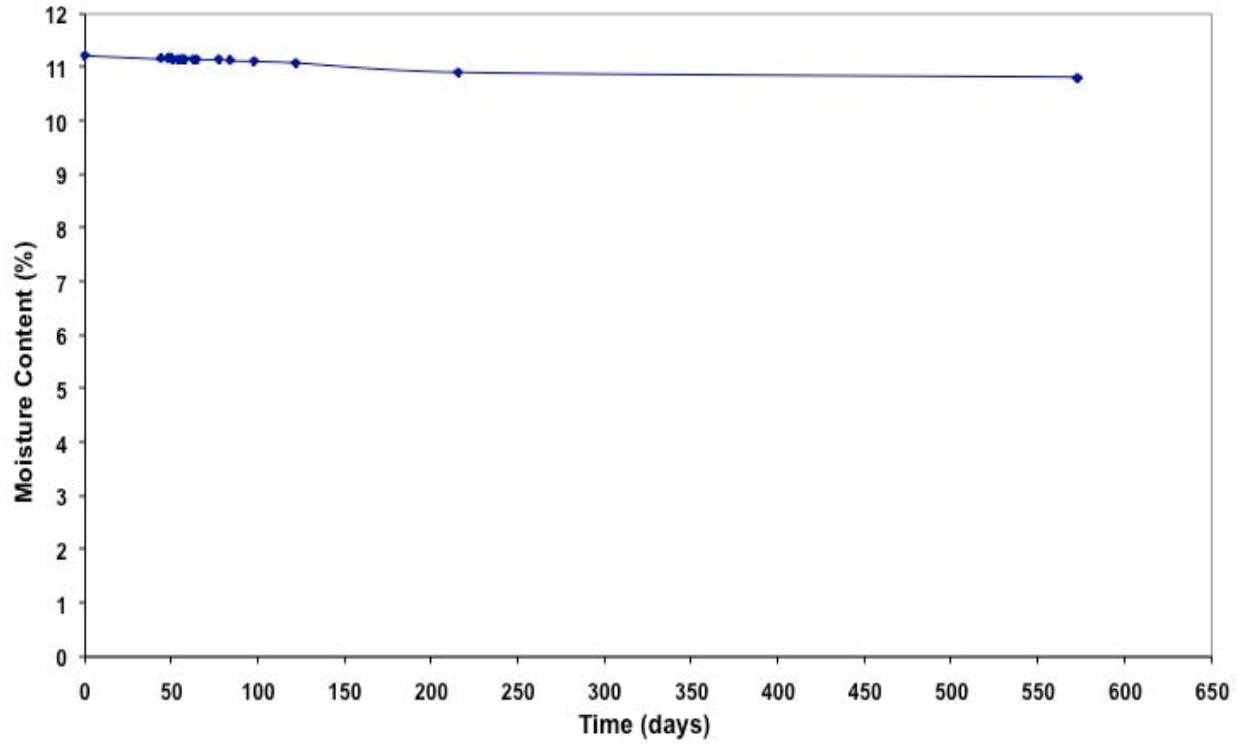

Figure C-11. Variation of moisture content with time, replicate 3, constant moisture.

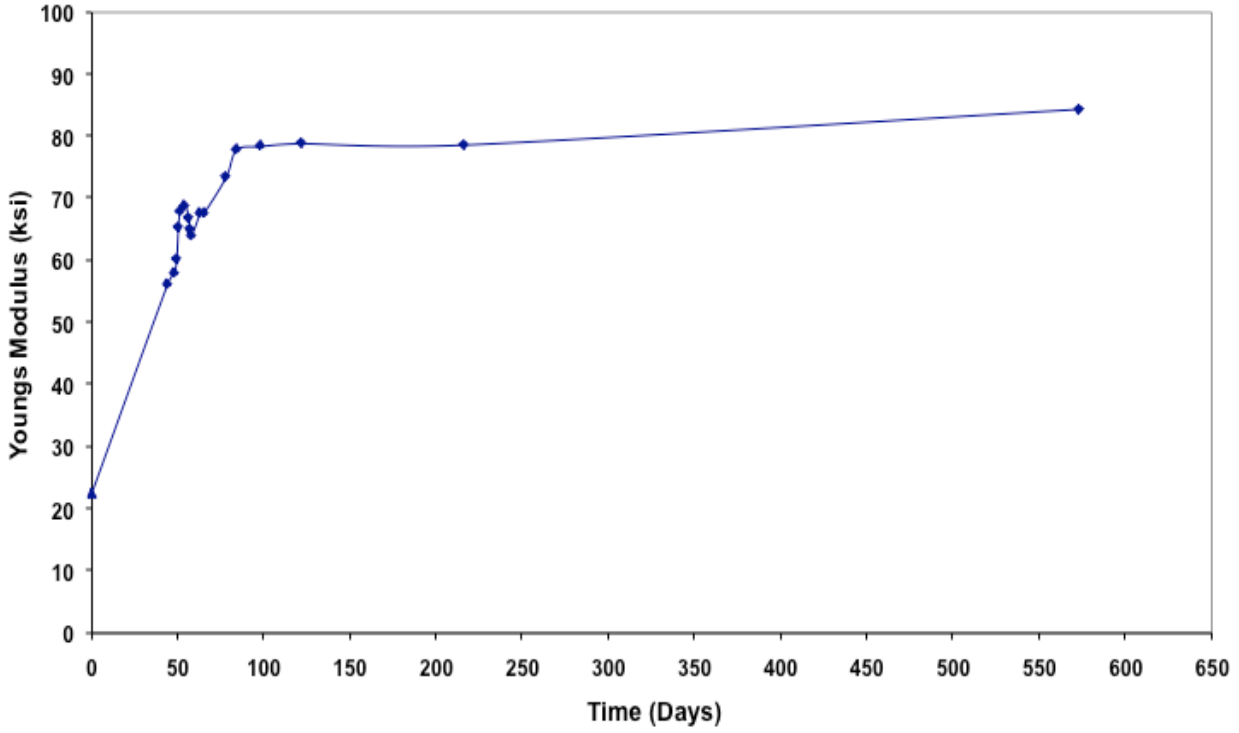

Figure C-12. Variation of Young's modulus with time, replicate 3, constant moisture.

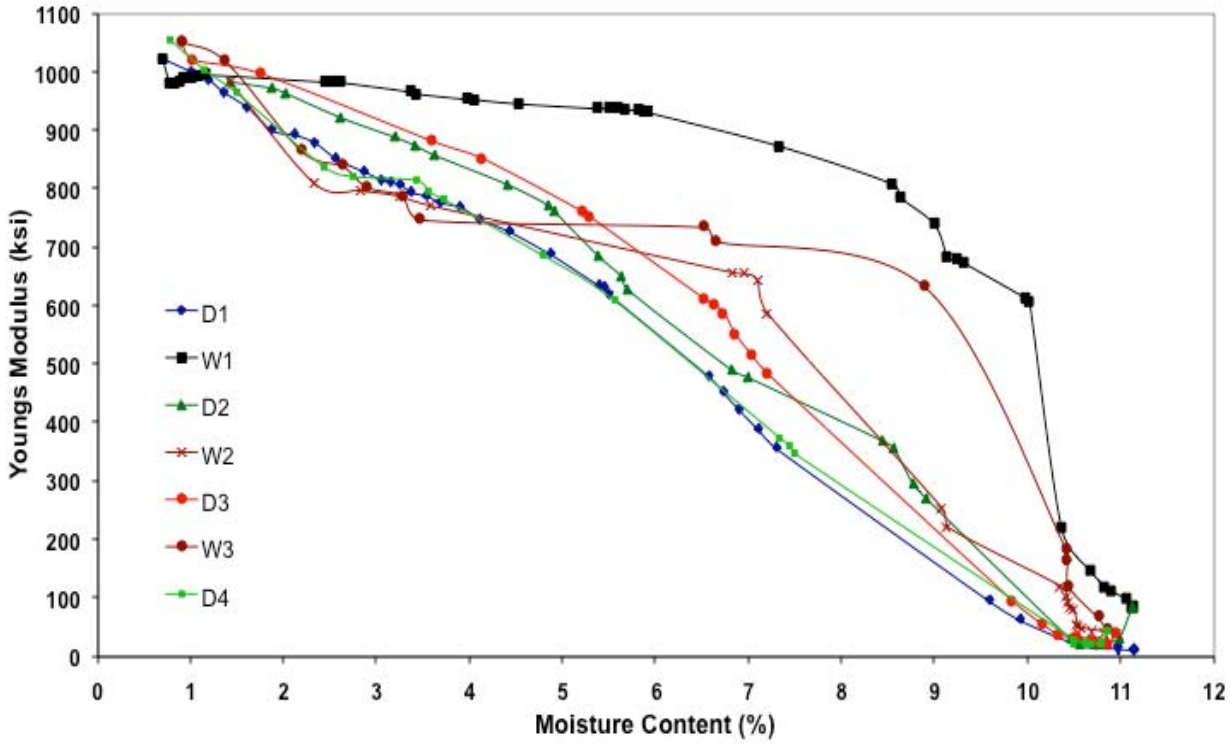

Figure C-13. Variation of Young's modulus with moisture content, replicate 1, wetting and drying.

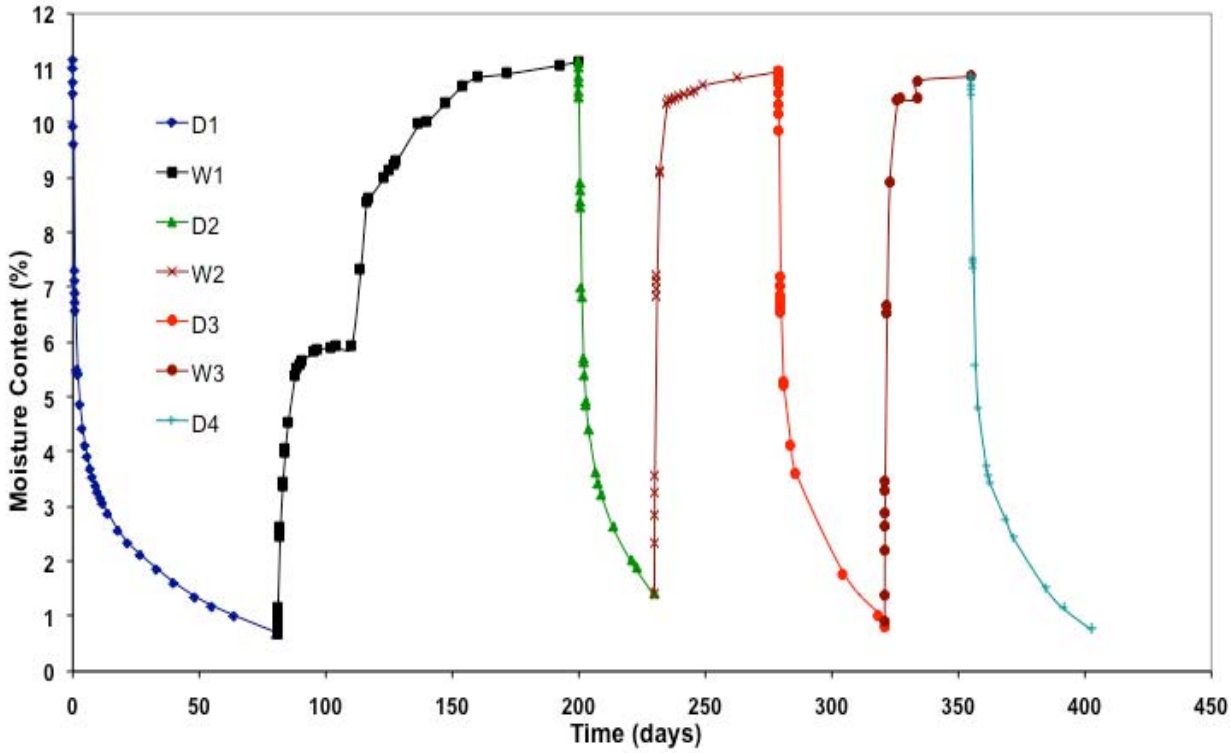

Figure C-14. Variation of moisture content with time, replicate 1, wetting and drying.

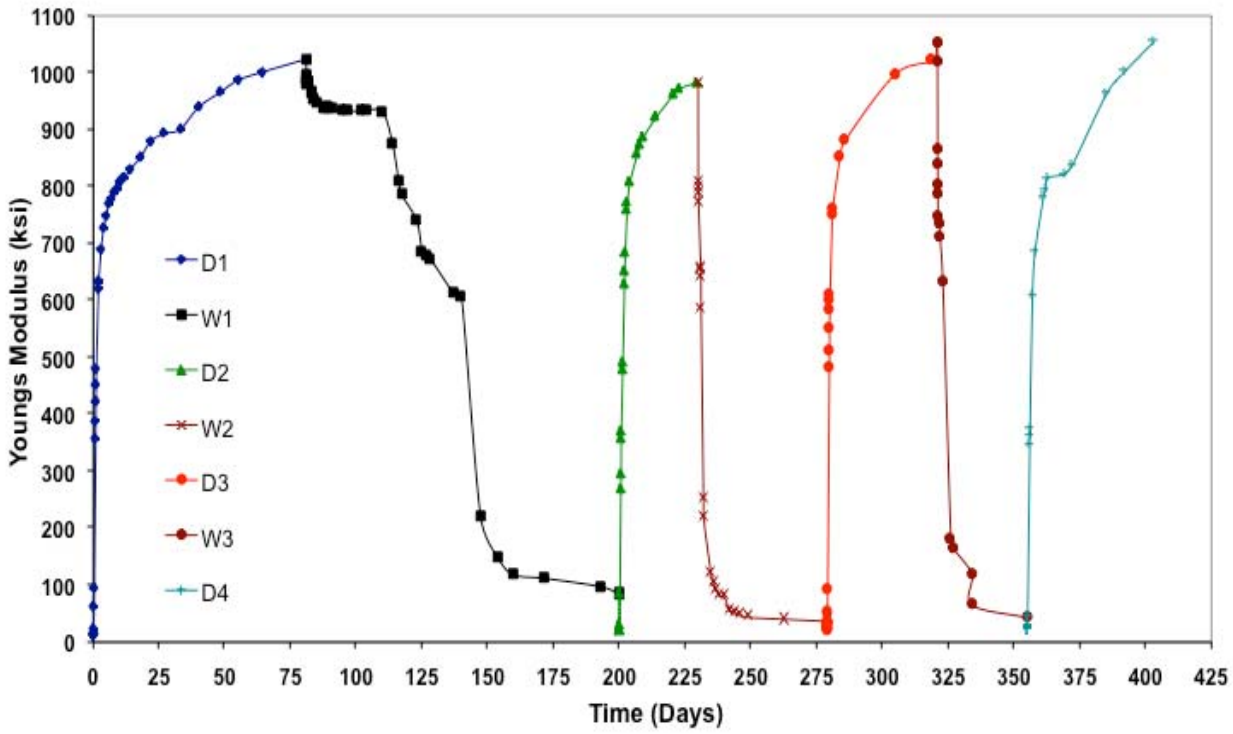

Figure C-15. Variation of Young's modulus with time, replicate 1, wetting and drying.

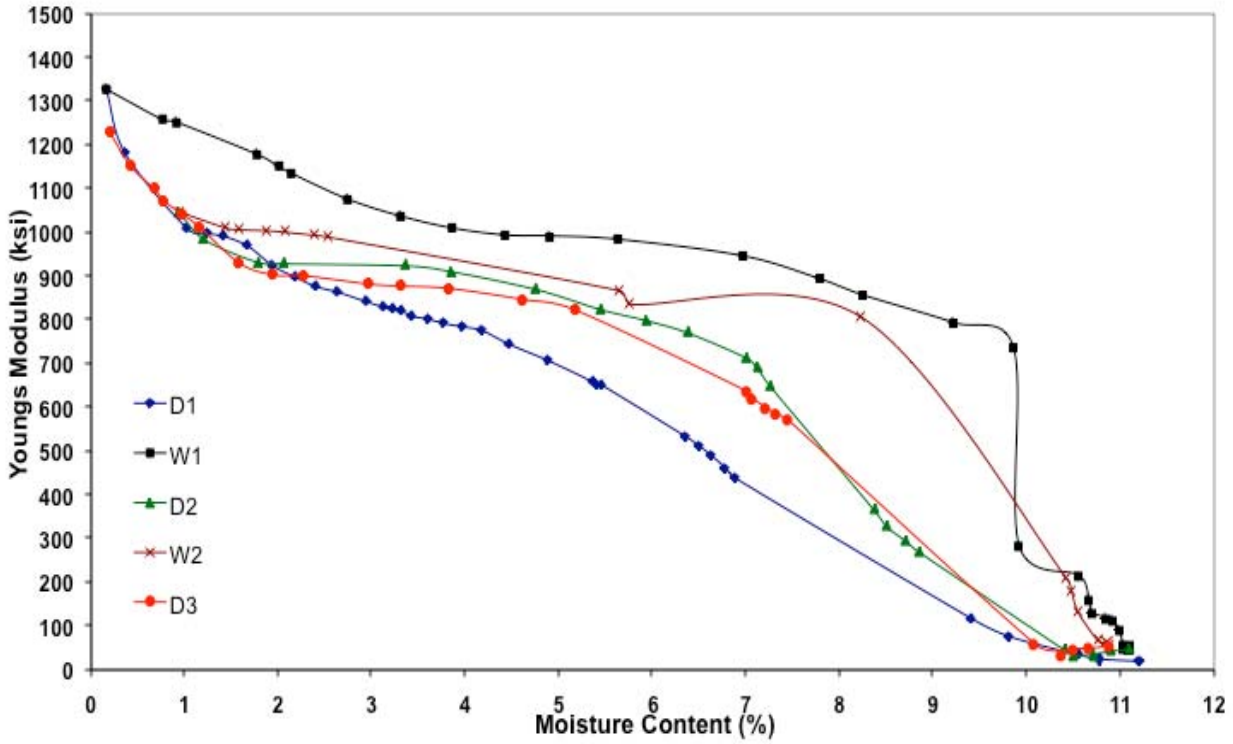

Figure C-16. Variation of Young's with Moisture Content, replicate 2, wetting and drying.

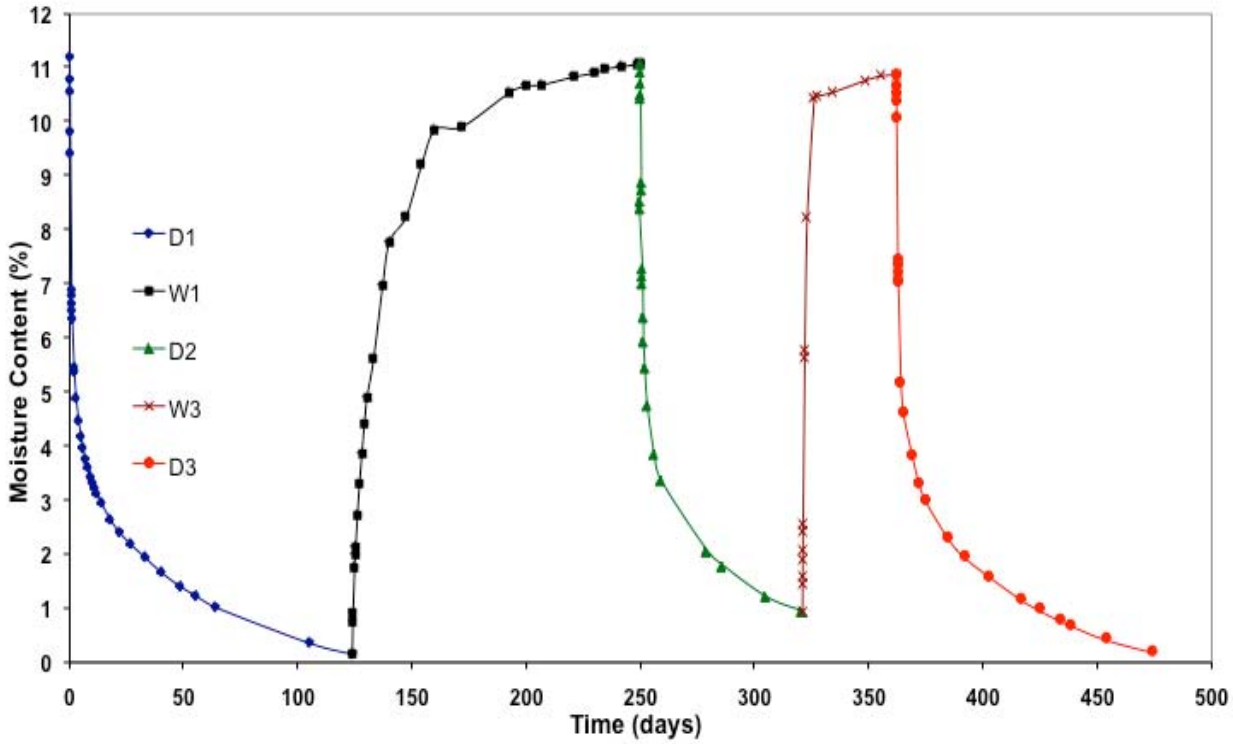

Figure C-17. Variation of moisture content with time, replicate 2, wetting and drying.

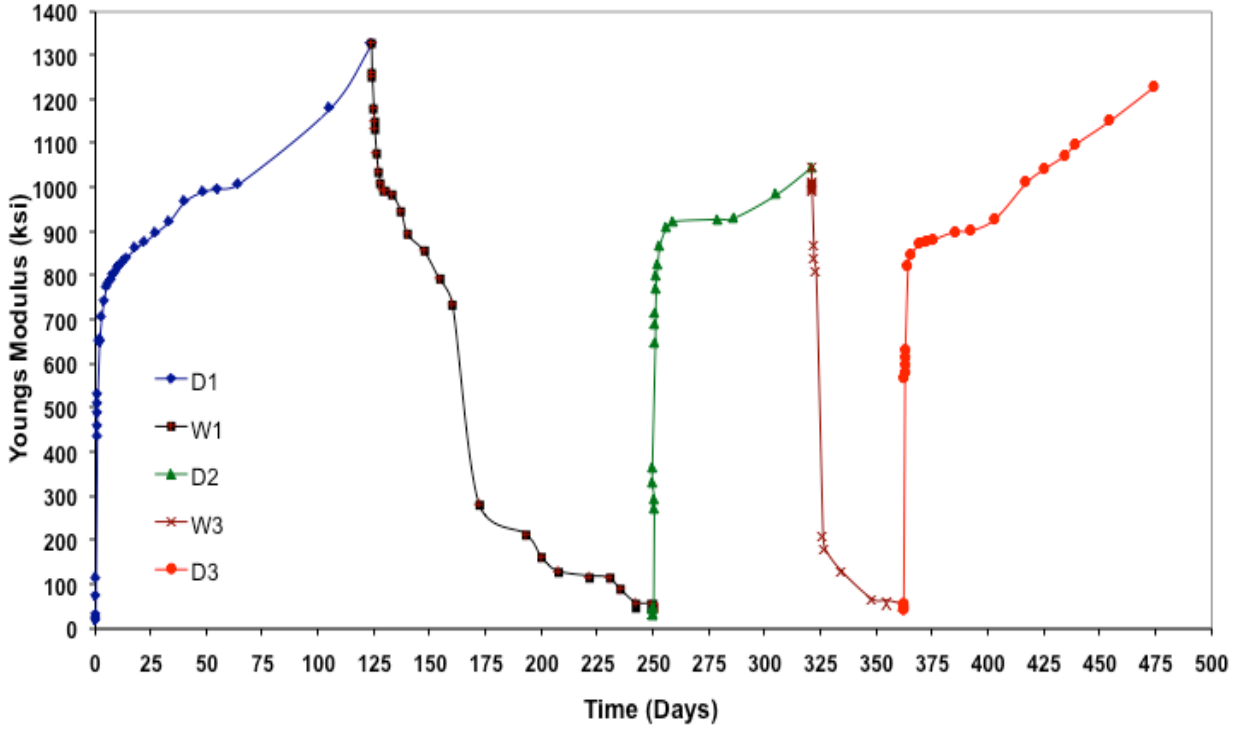

Figure C-18. Variation of Young's modulus with time, replicate 2, wetting and drying.

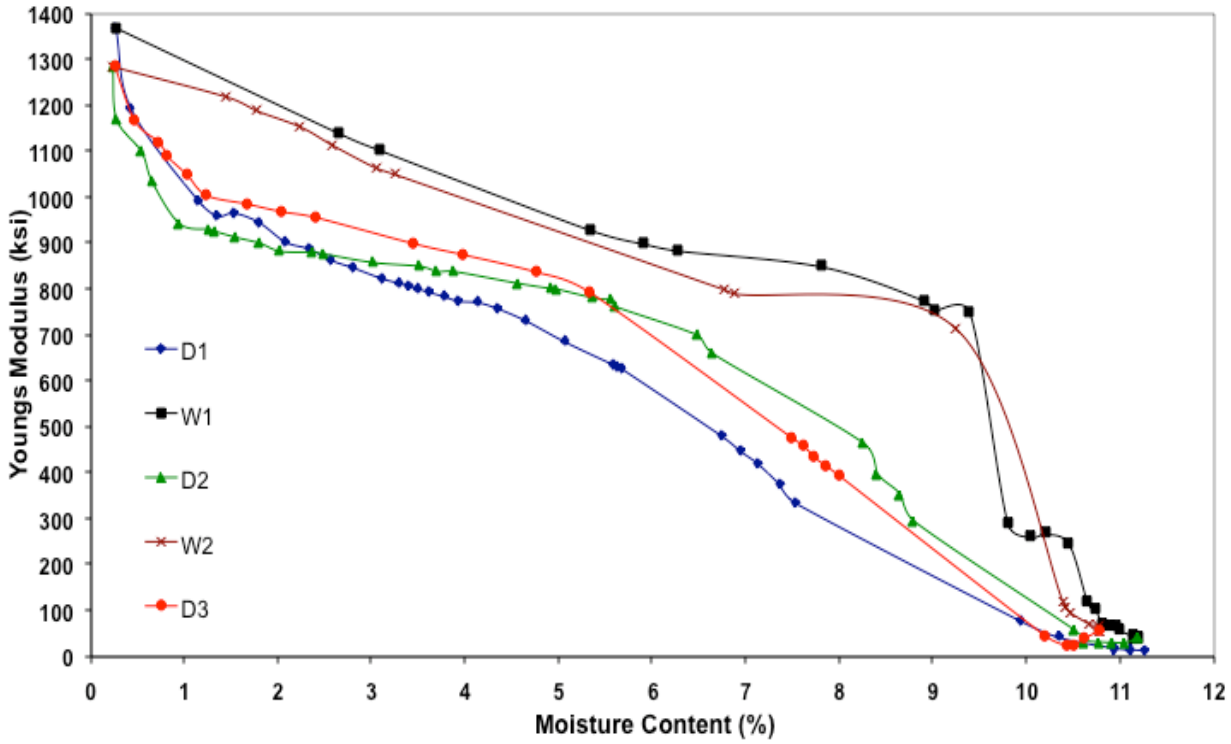

Figure C-19. Variation of Young's modulus with moisture content, replicate 3, wetting and drying.

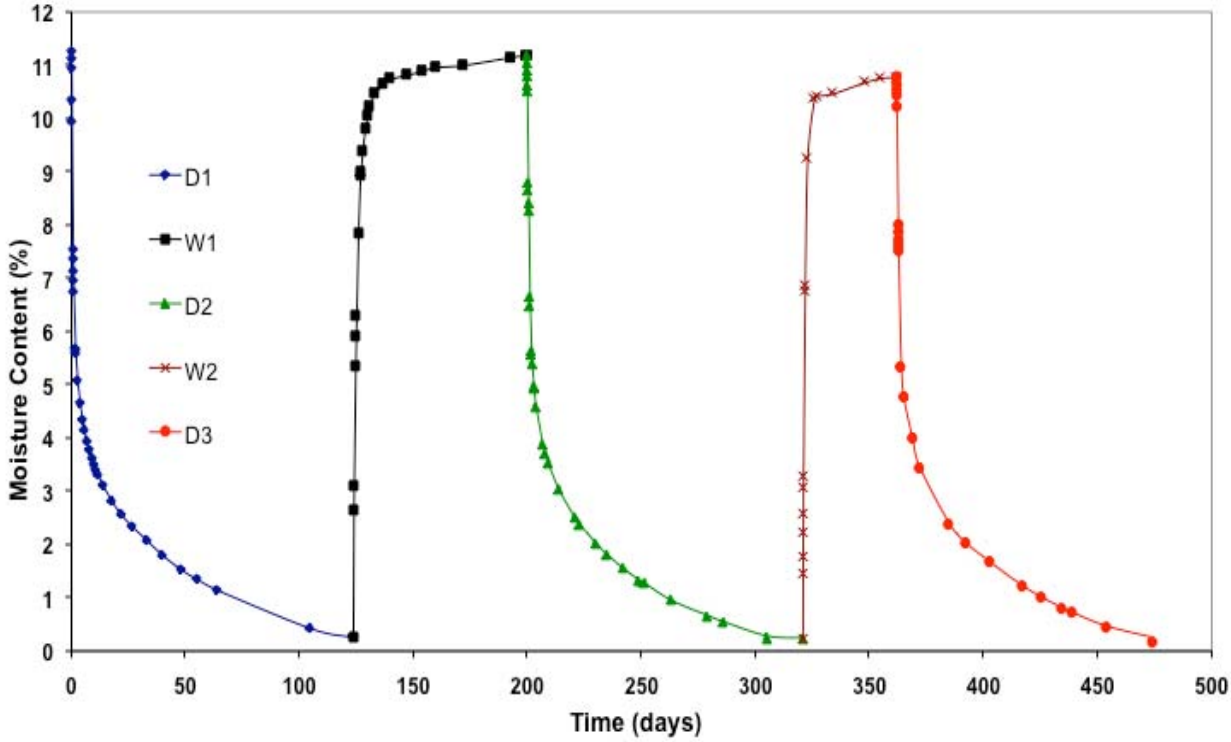

Figure C-20. Variation of moisture content with time, replicate 3, wetting and drying.

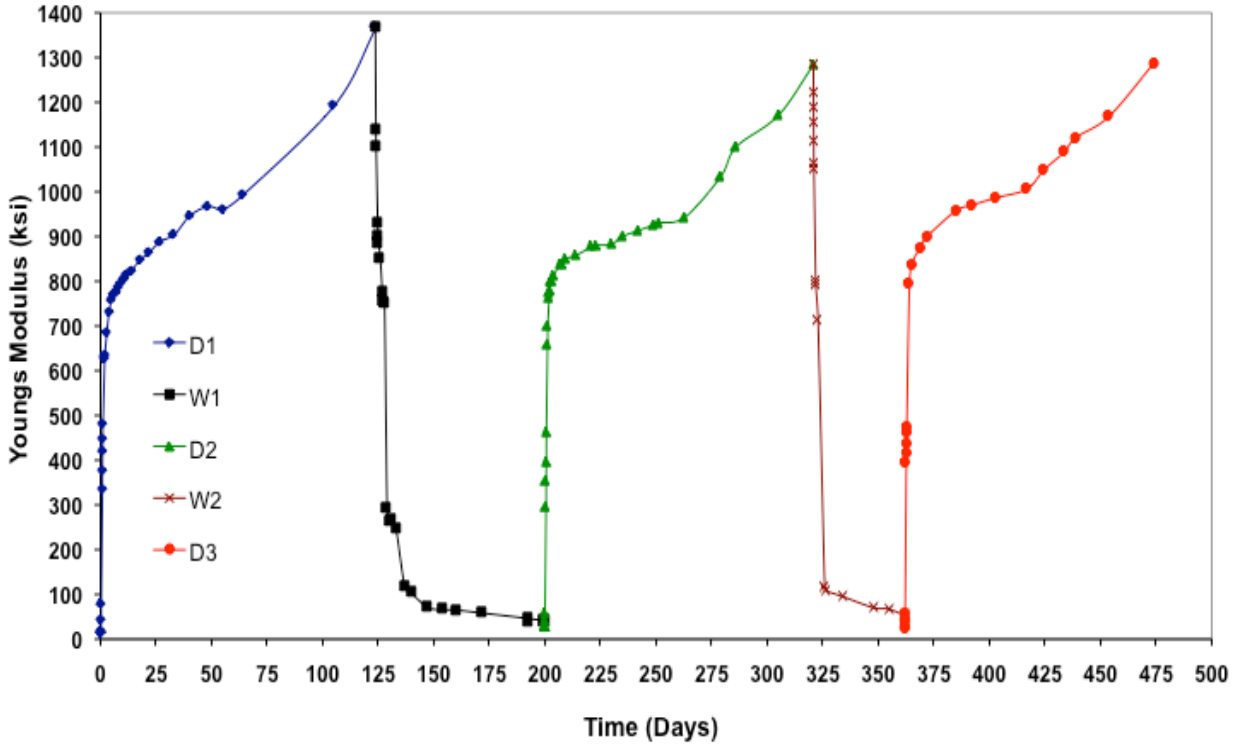

Figure C-21. Variation of Young's modulus with time, replicate 3, wetting and drying.

APPENDIX D
LOXAHATCHEE INDIVIDUAL SMALL-STRAIN MODULUS TEST RESULTS

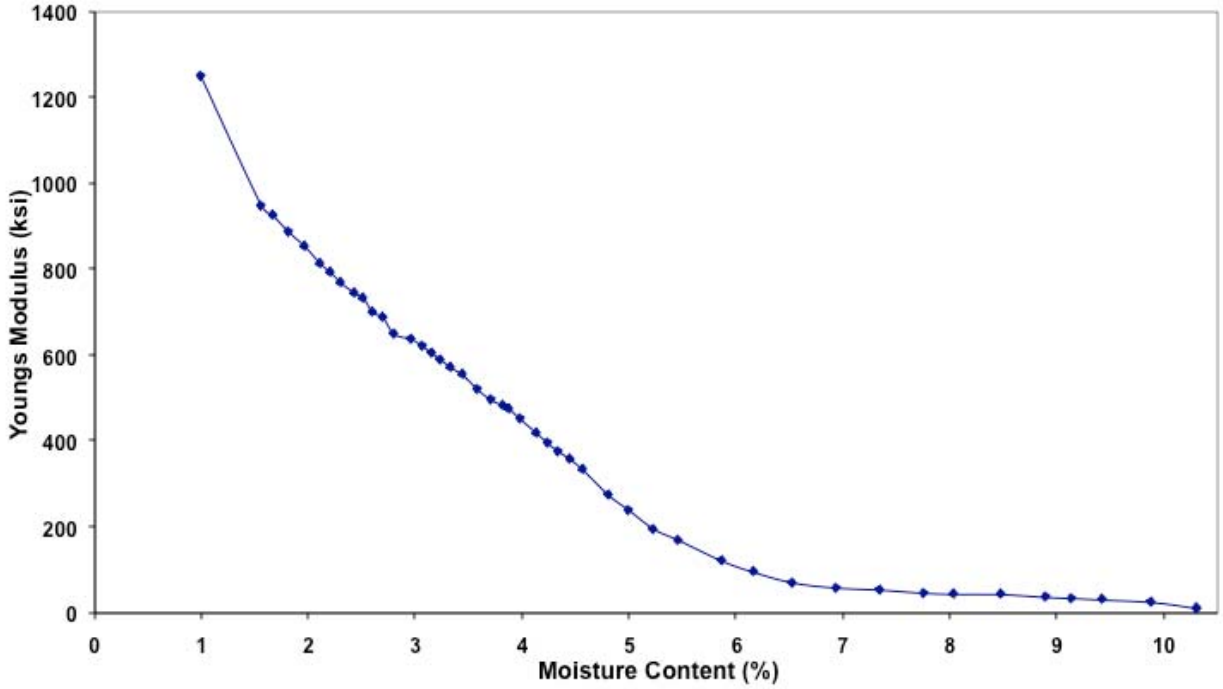

Figure D-1. Variation of Young's modulus with moisture content, replicate 1, laboratory ambient.

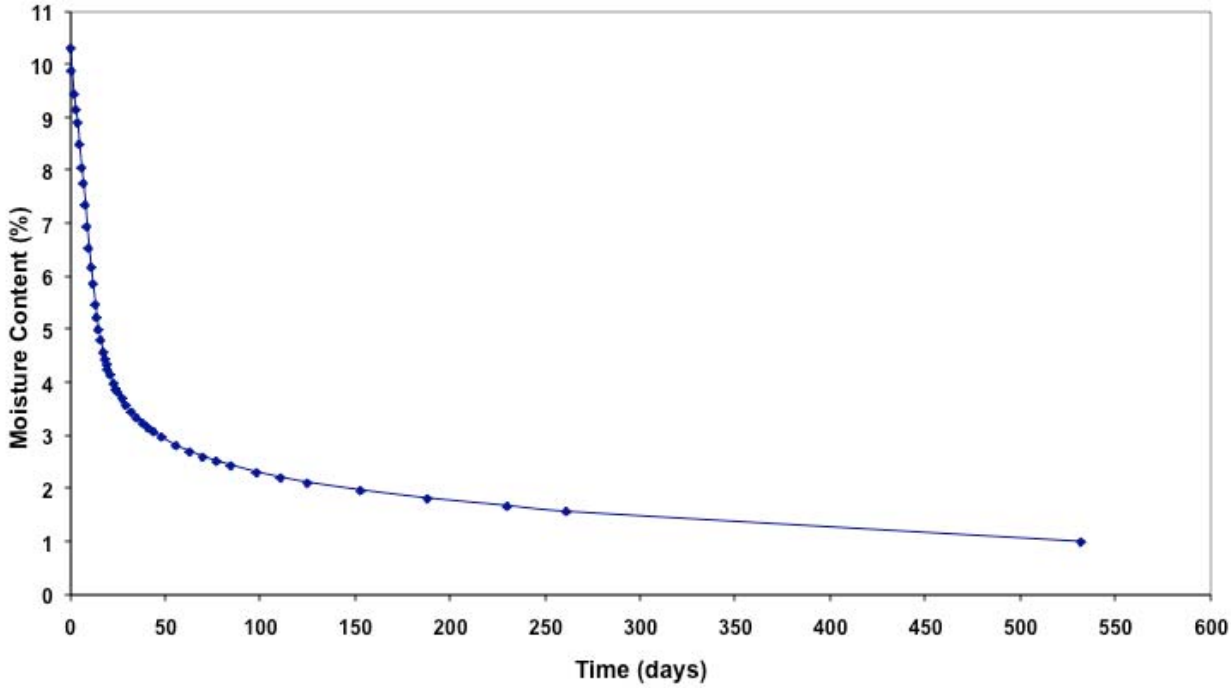

Figure D-2. Variation of moisture content with time, replicate 1, laboratory ambient.

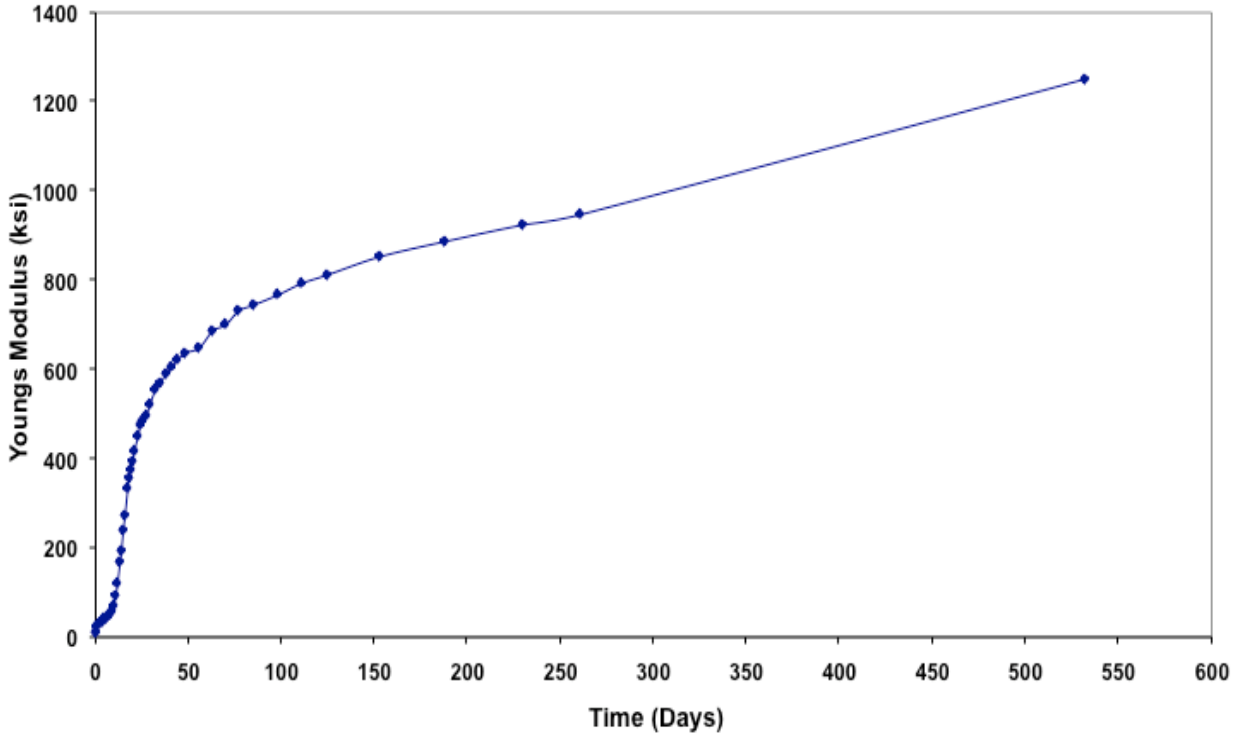

Figure D-3. Variation of Young's modulus with time, replicate 1, laboratory ambient.

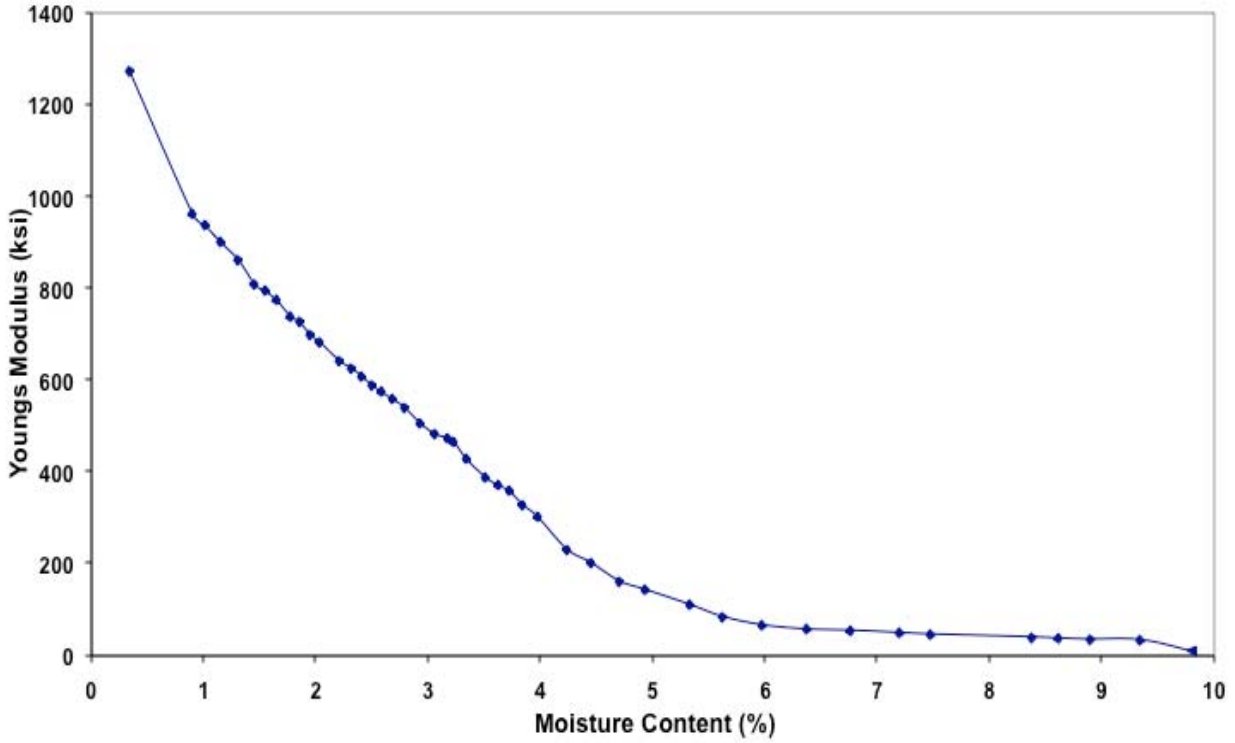

Figure D-4. Variation of Young's modulus with moisture content, replicate 2, laboratory ambient.

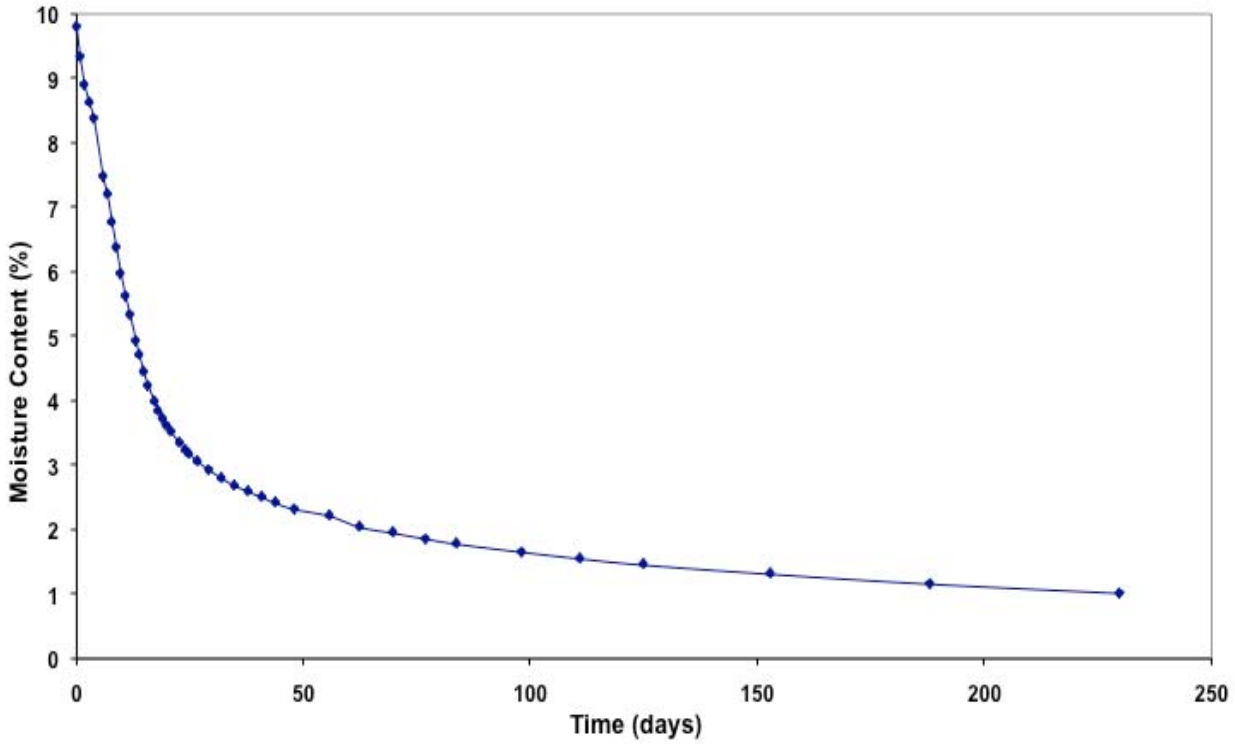

Figure D-5. Variation of moisture content with time, replicate 2, laboratory ambient.

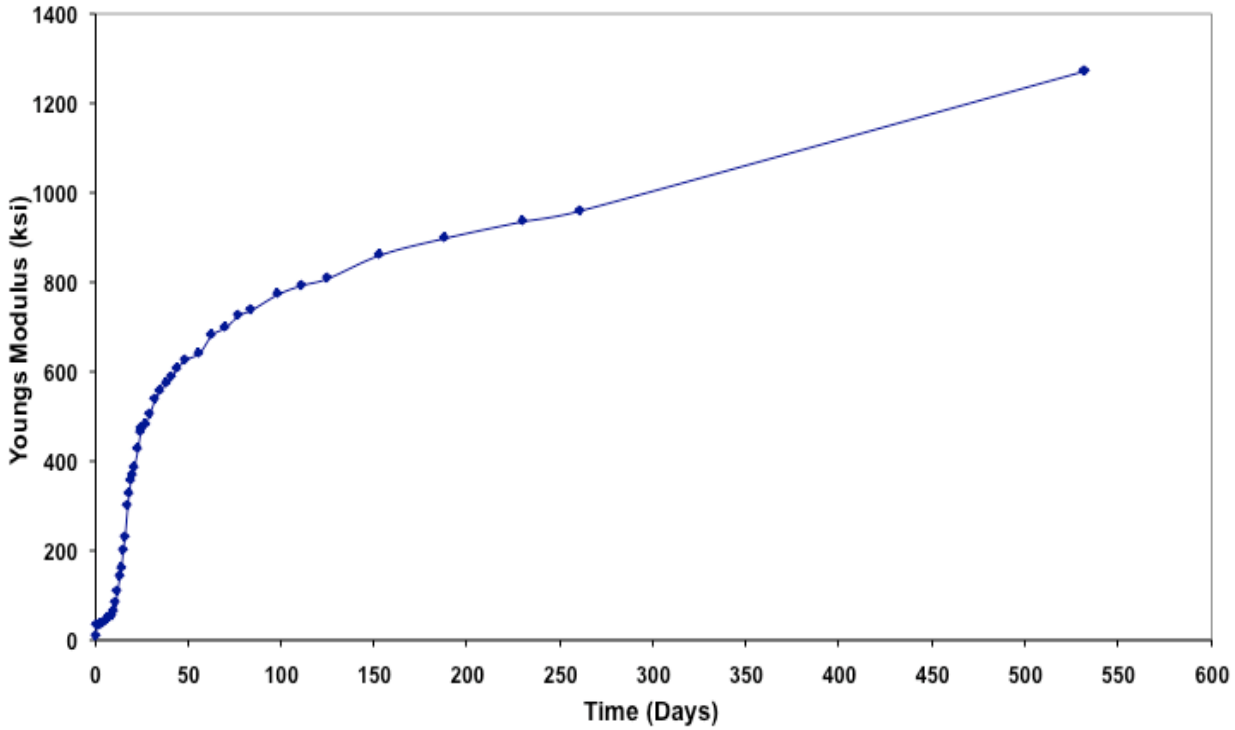

Figure D-6. Variation of Young's modulus with time, replicate 2, laboratory ambient.

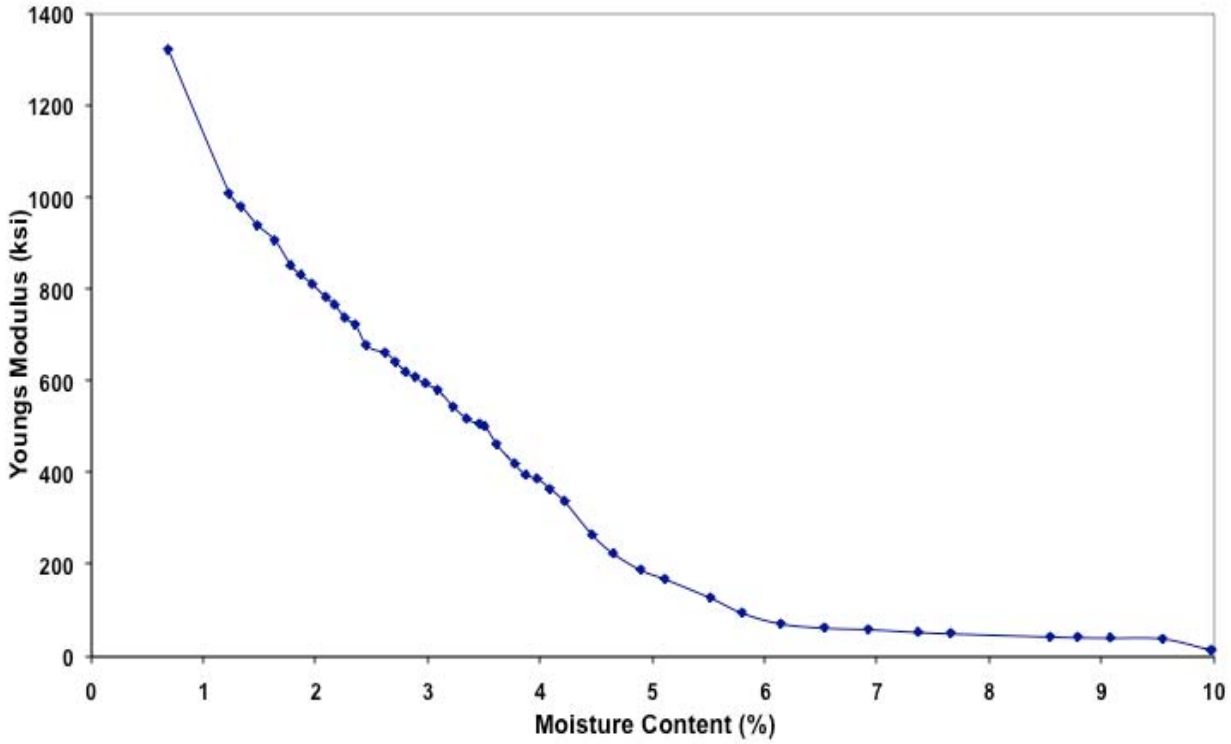

Figure D-7. Variation of Young's modulus with moisture content, replicate 3, laboratory ambient.

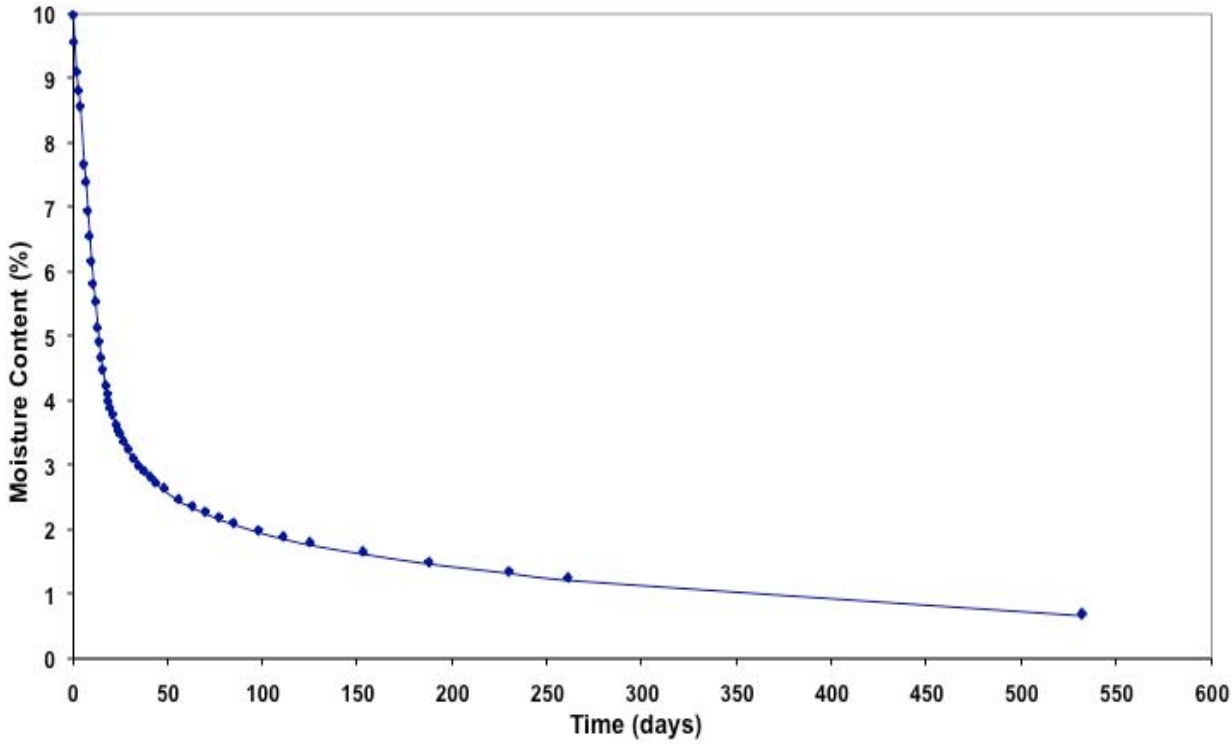

Figure D-8. Variation of moisture content with time, replicate 3, laboratory ambient.

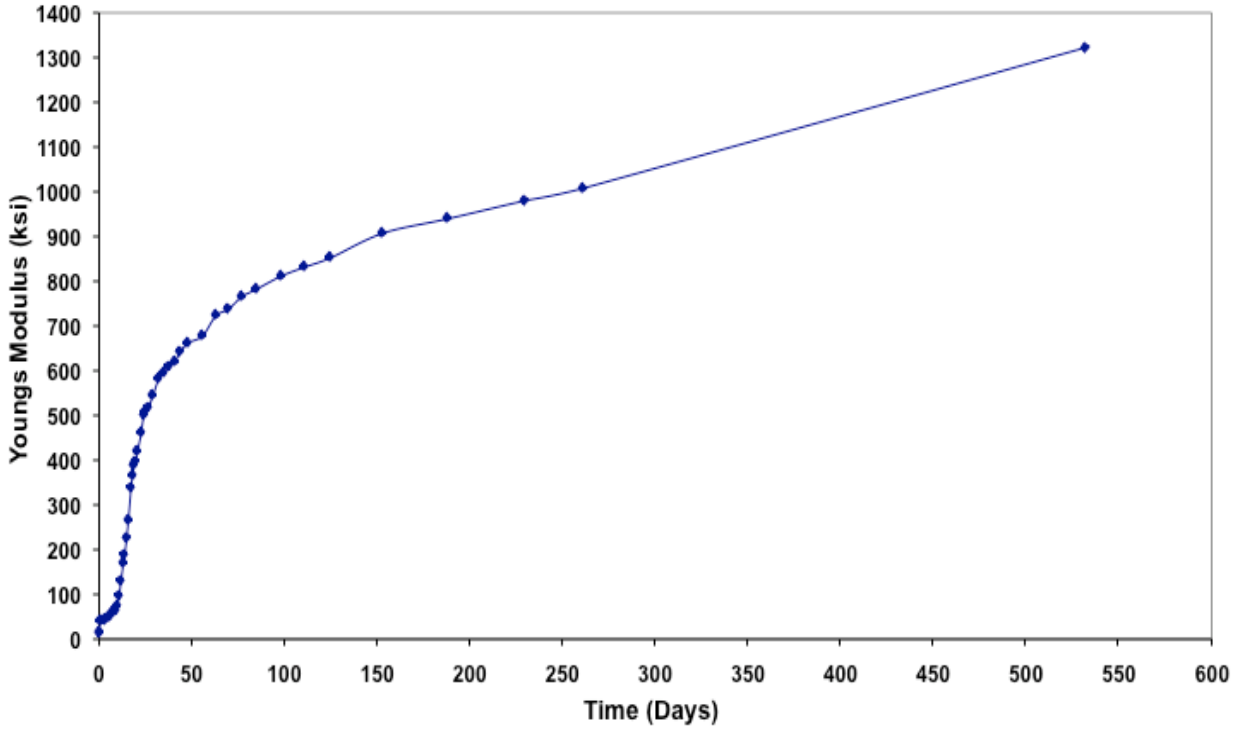

Figure D-9. Variation of Young's modulus with time, replicate 3, laboratory ambient.

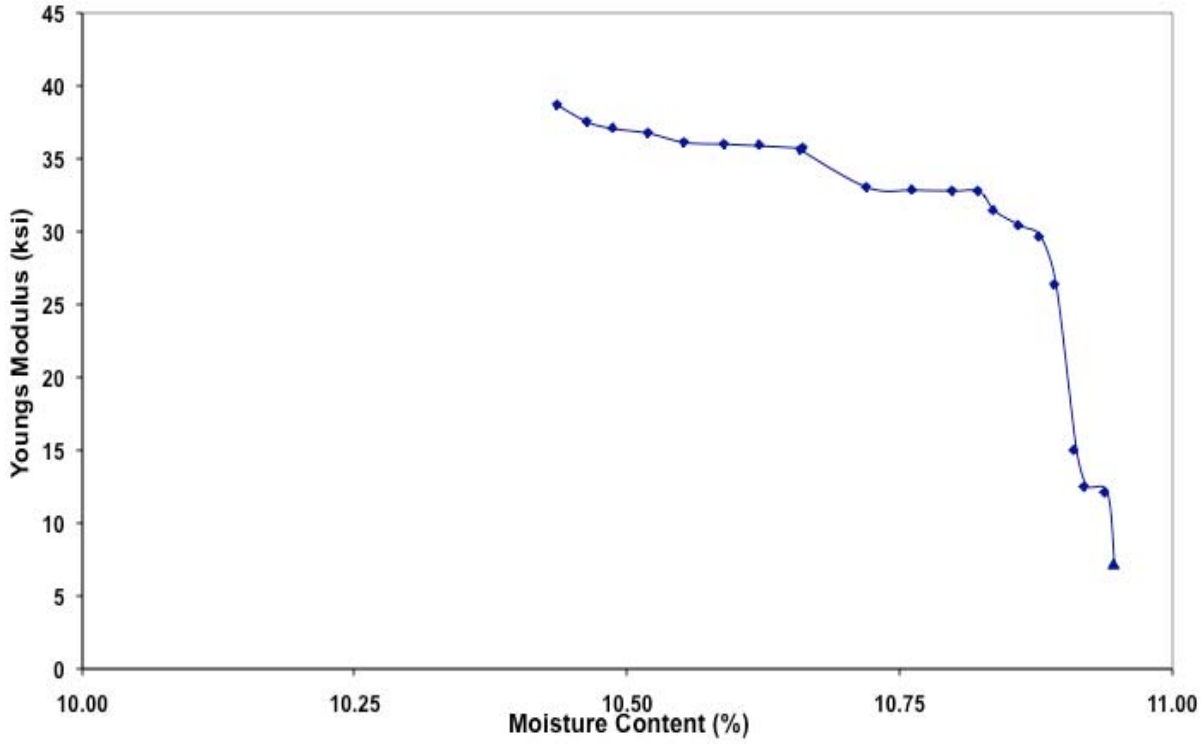

Figure D-10. Variation of Young's modulus with moisture content, replicate 1, constant moisture.

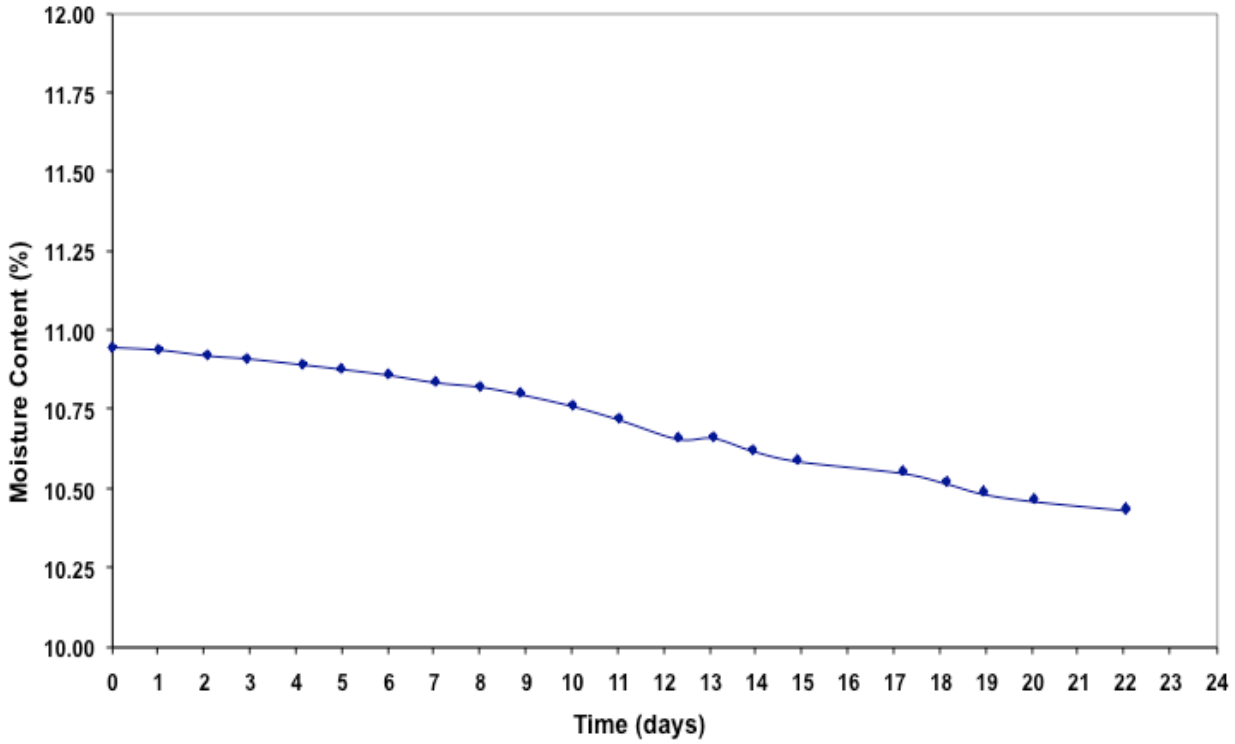

Figure D-11. Variation of moisture content with time, replicate 1, constant moisture.

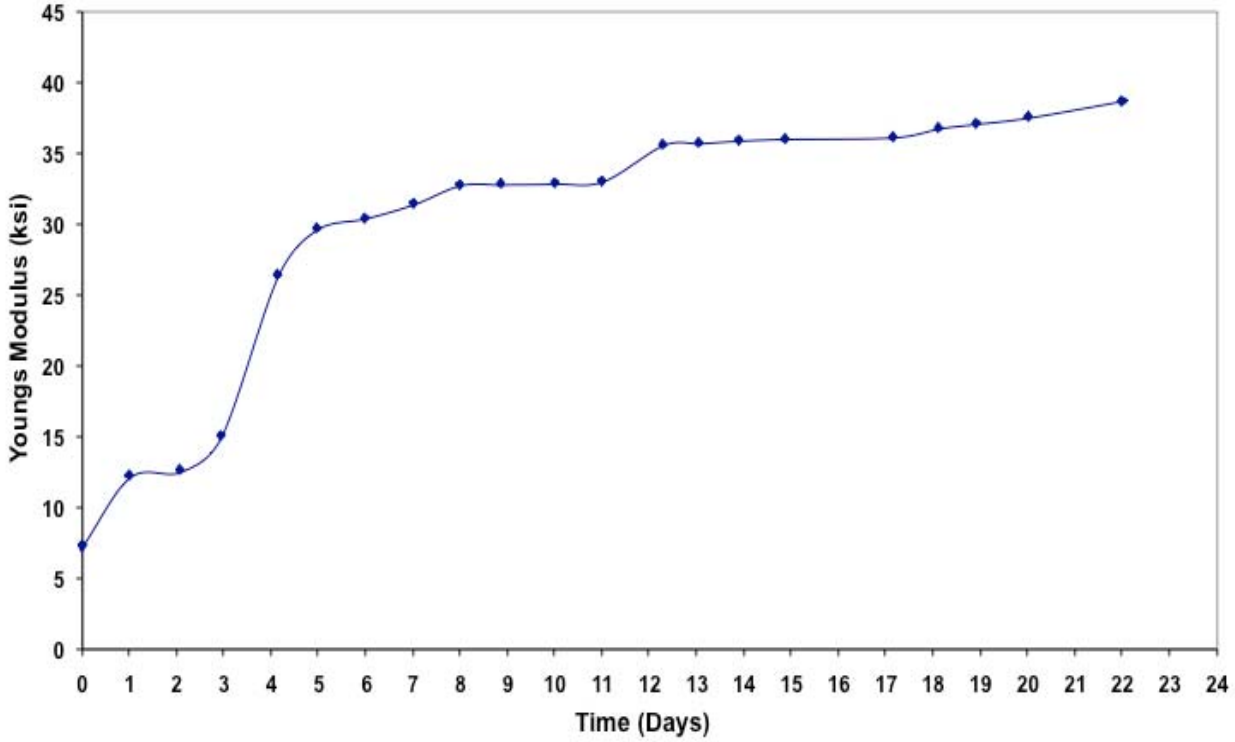

Figure D-12. Variation of Young's modulus with time, replicate 1, constant moisture.

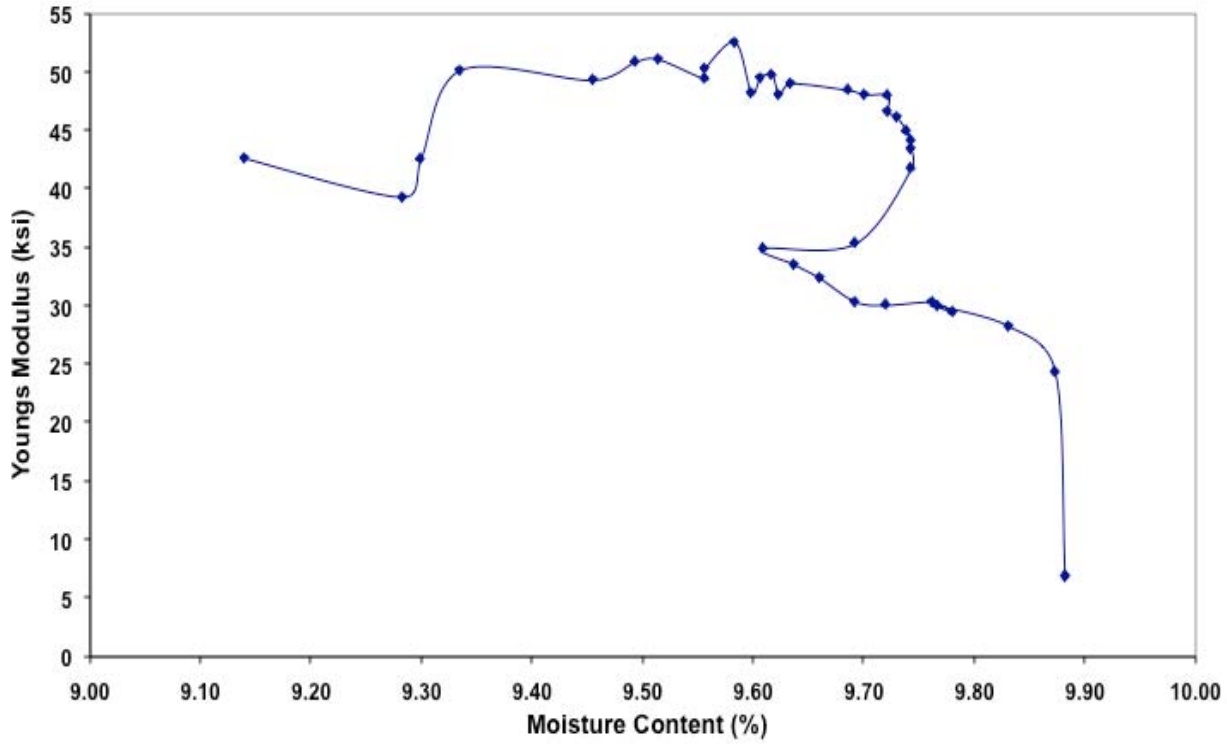

Figure D-13. Variation of Young's modulus with moisture content, replicate 2, constant moisture.

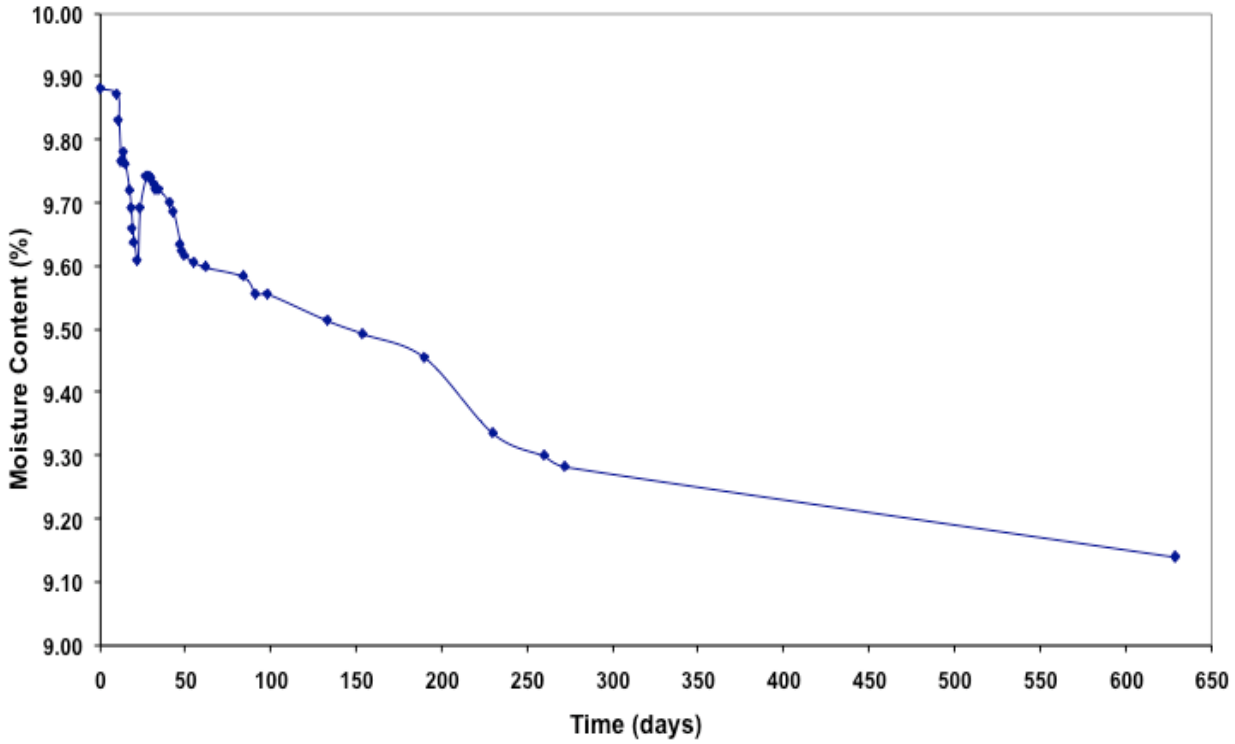

Figure D-14. Variation of moisture content with time, replicate 2, constant moisture.

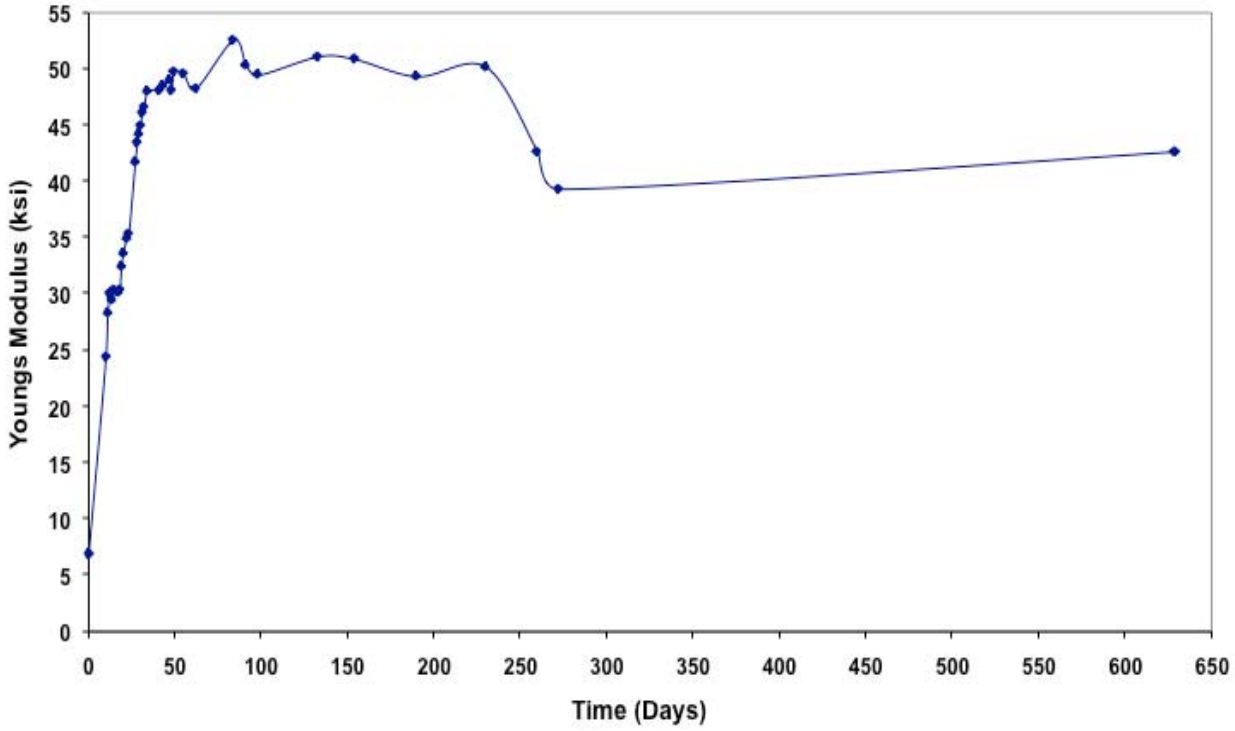

Figure D-15. Variation of Young's modulus with time, replicate 2, constant moisture.

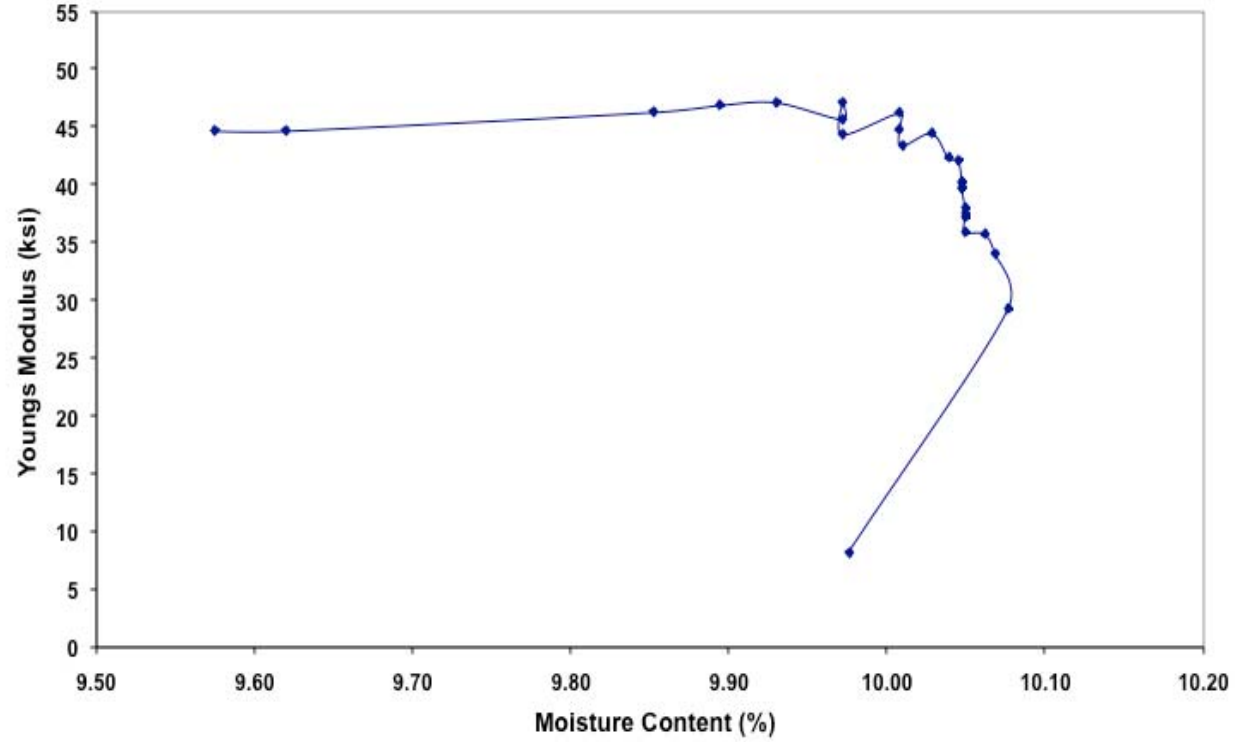

Figure D-16. Variation of Young's with moisture content, replicate 3, constant moisture.

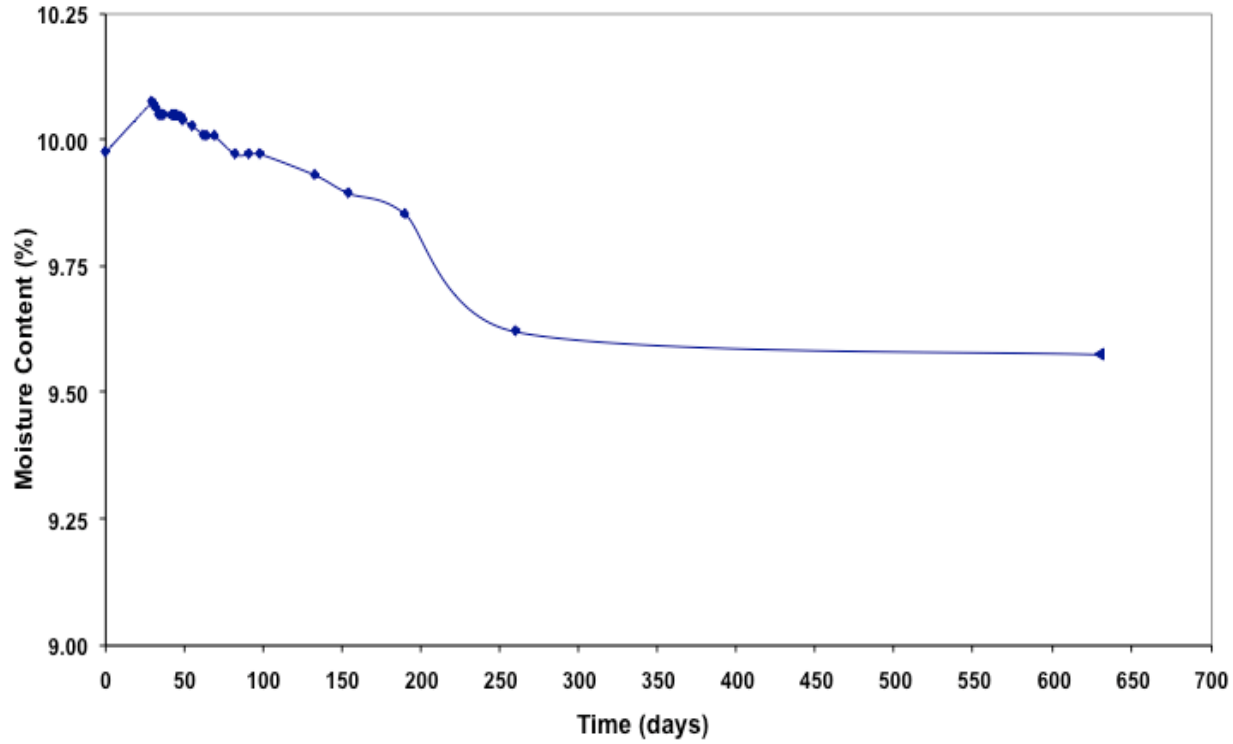

Figure D-17. Variation of moisture content with time, replicate 3, constant moisture.

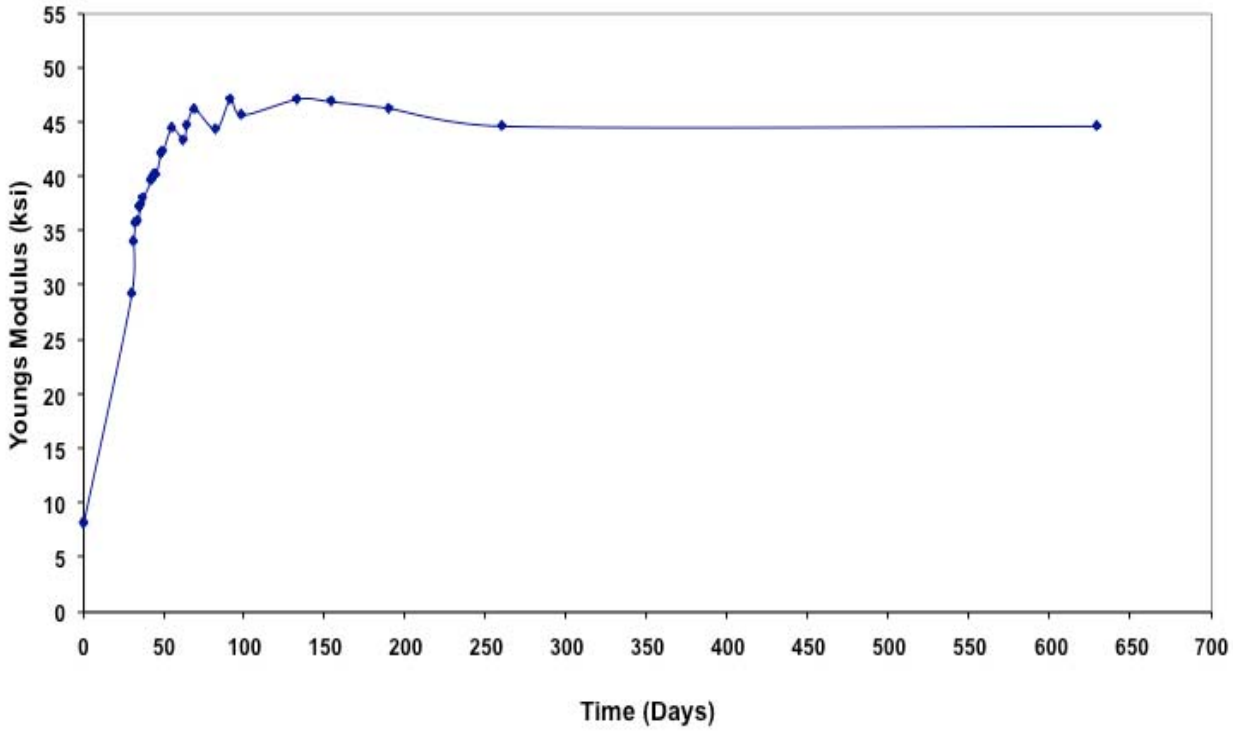

Figure D-18. Variation of Young's modulus with time, replicate 3, constant moisture.

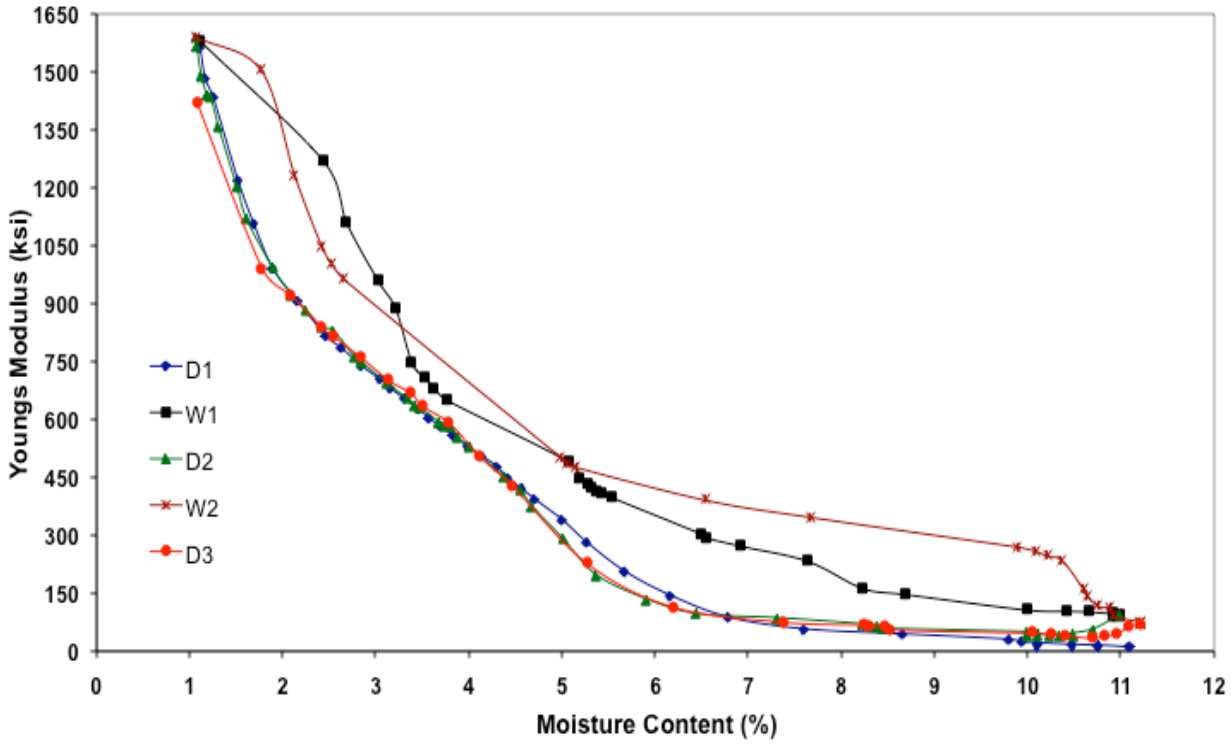

Figure D-19. Variation of Young's modulus with moisture content, replicate 1, wetting and drying.

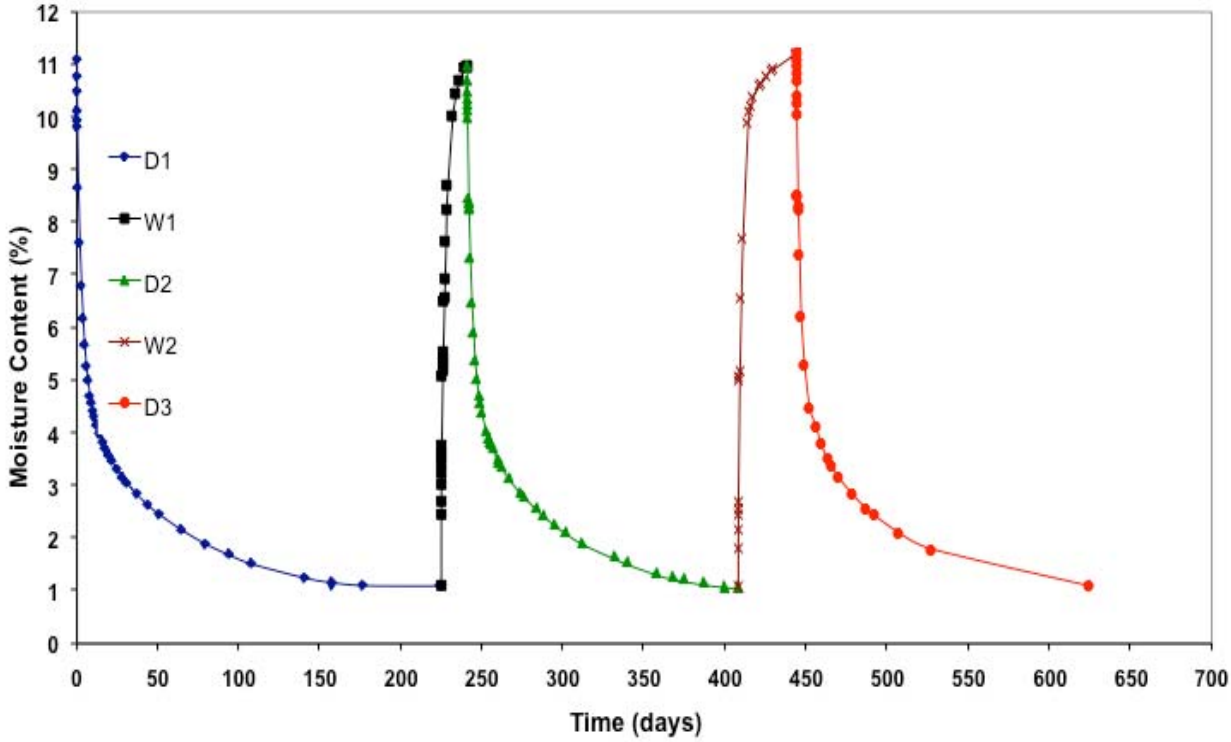

Figure D-20. Variation of moisture content with time, replicate 1, wetting and drying.

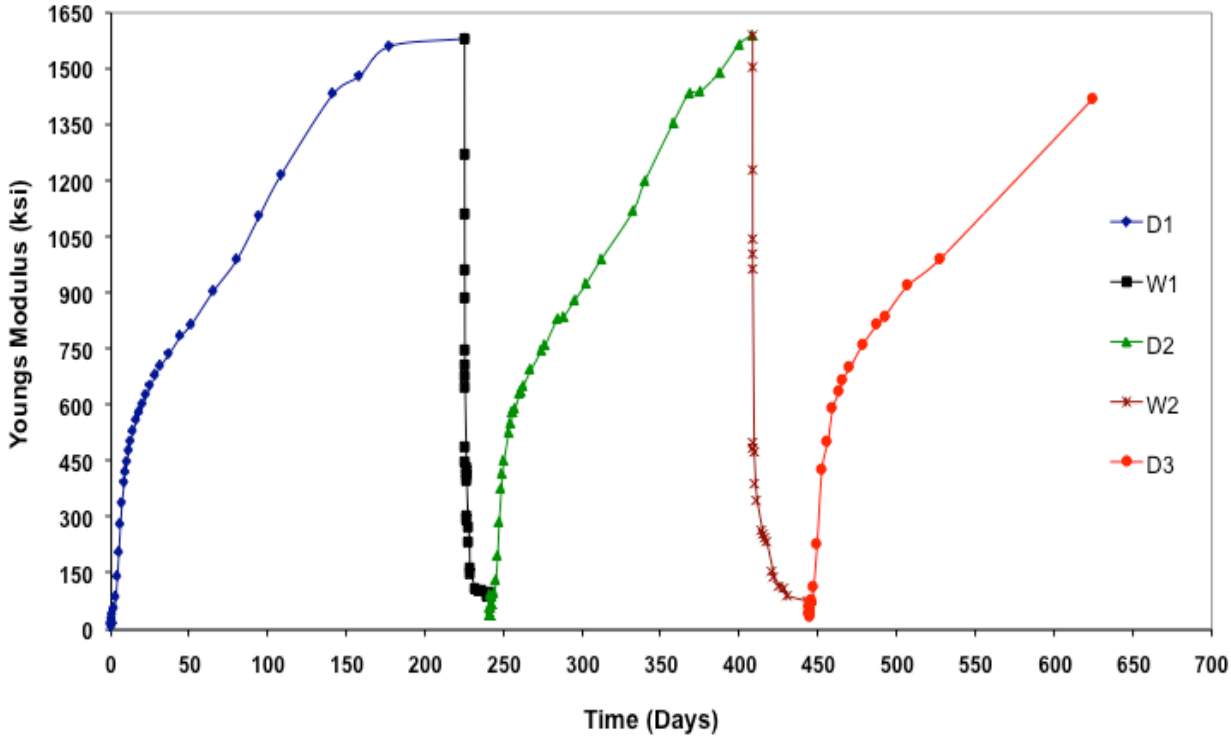

Figure D-21. Variation of Young's modulus with time, replicate 1, wetting and drying.

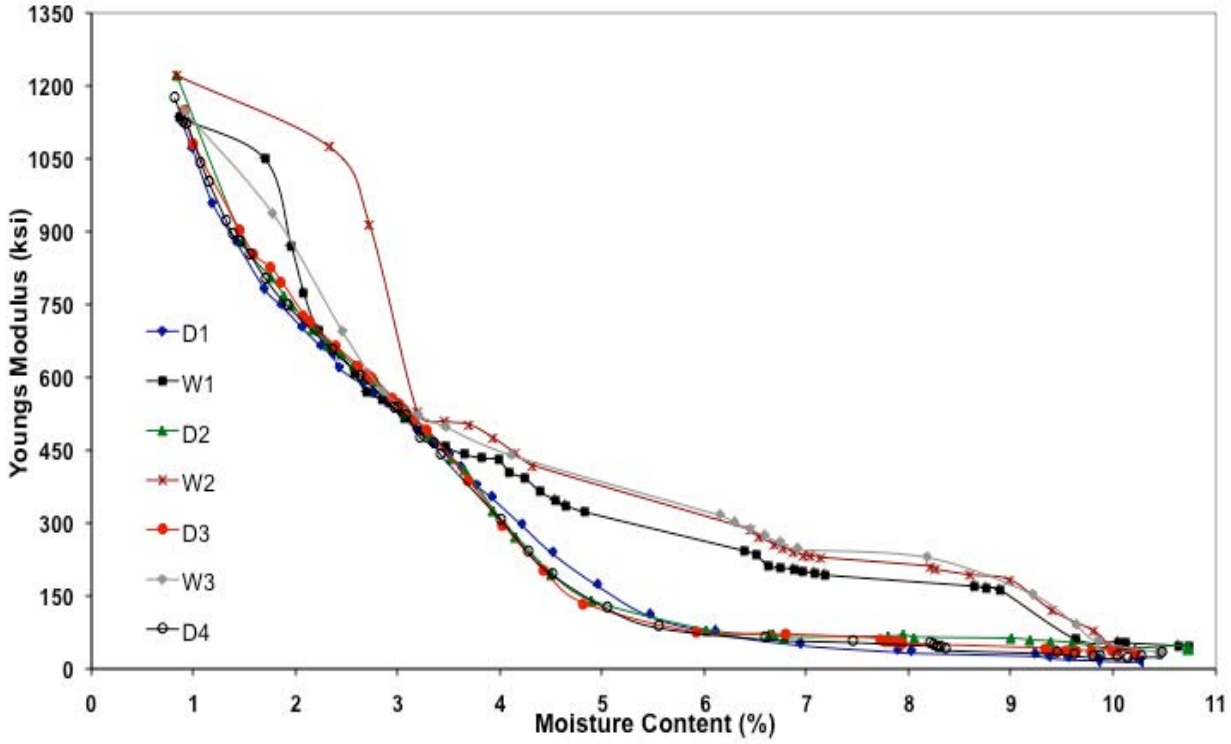

Figure D-22. Variation of Young's modulus with moisture content, replicate 2, wetting and drying.

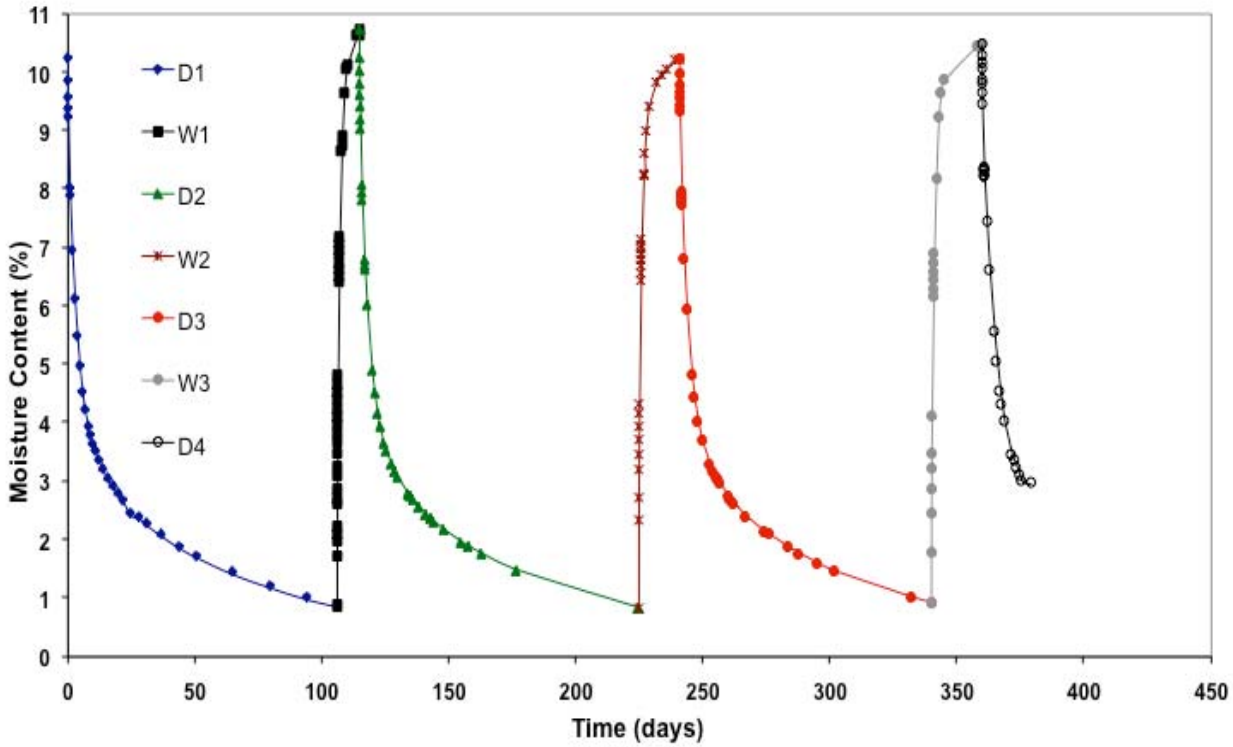

Figure D-23. Variation of moisture content with time, replicate 2, wetting and drying.

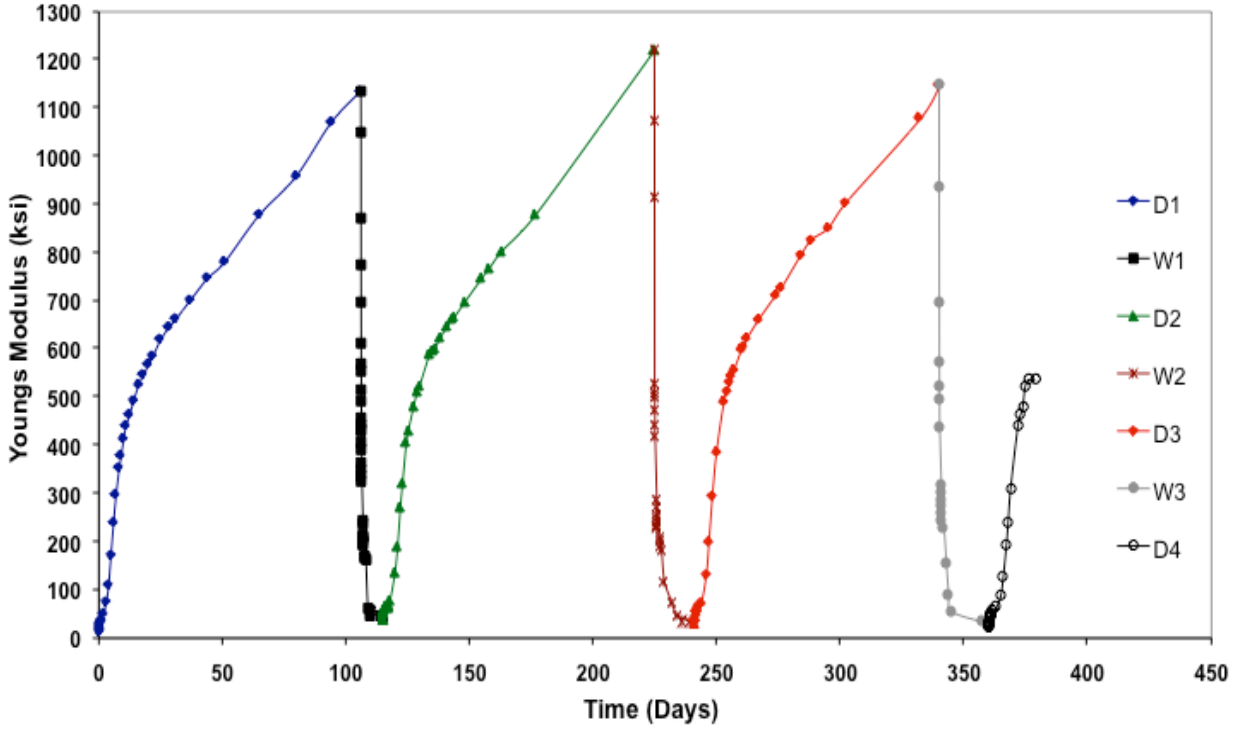

Figure D-24. Variation of Young's modulus with time, replicate 2, wetting and drying.

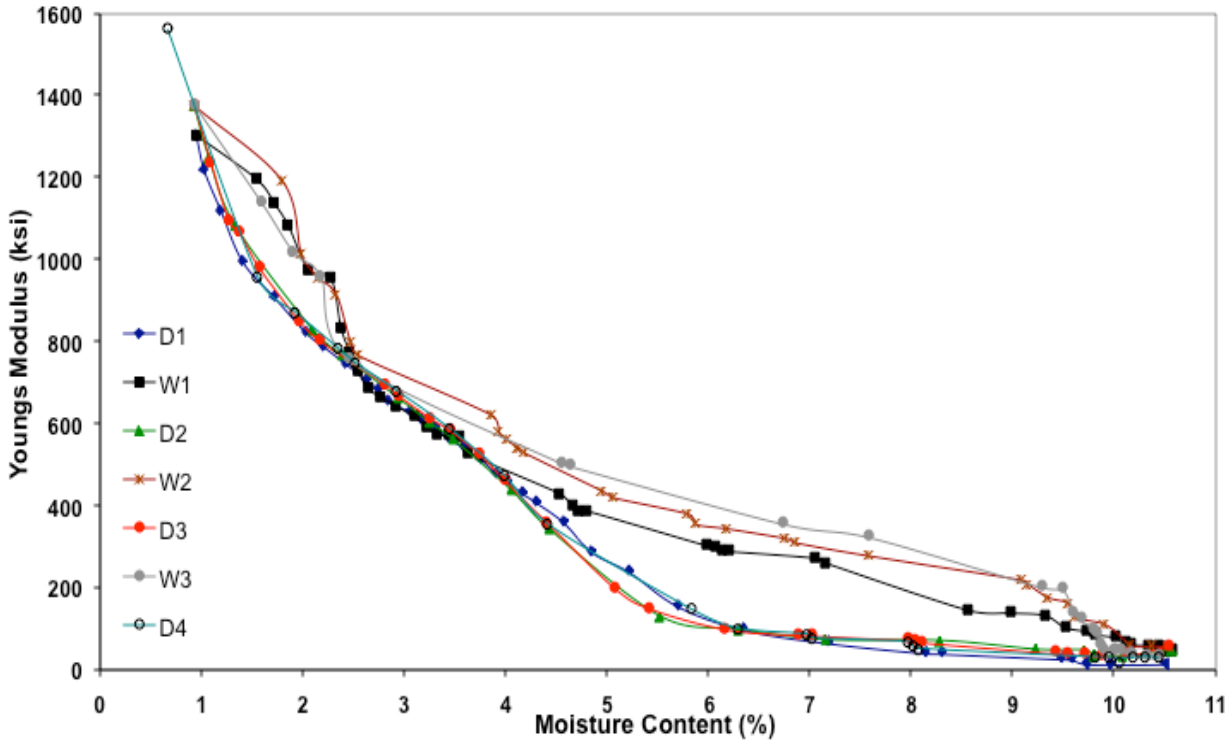

Figure D-25. Variation of Young's modulus with moisture, content, replicate 3, wetting and drying.

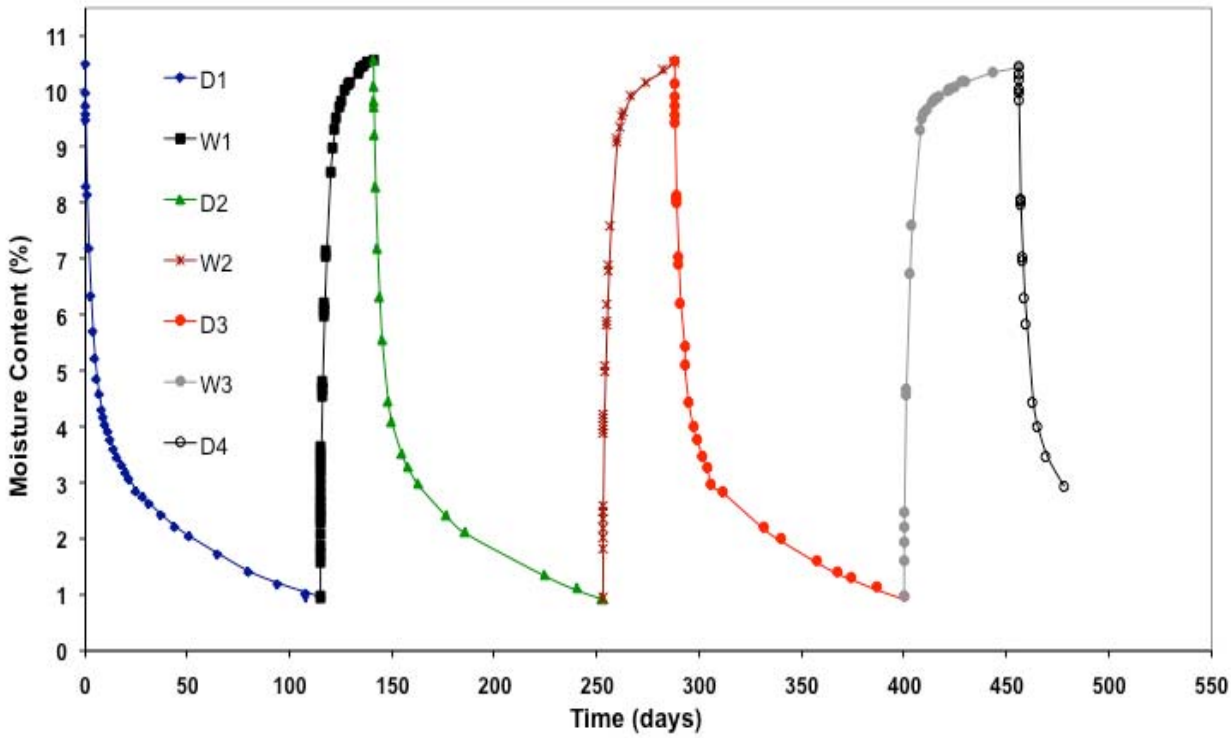

Figure D-26. Variation of moisture content with time replicate 3, wetting and drying.

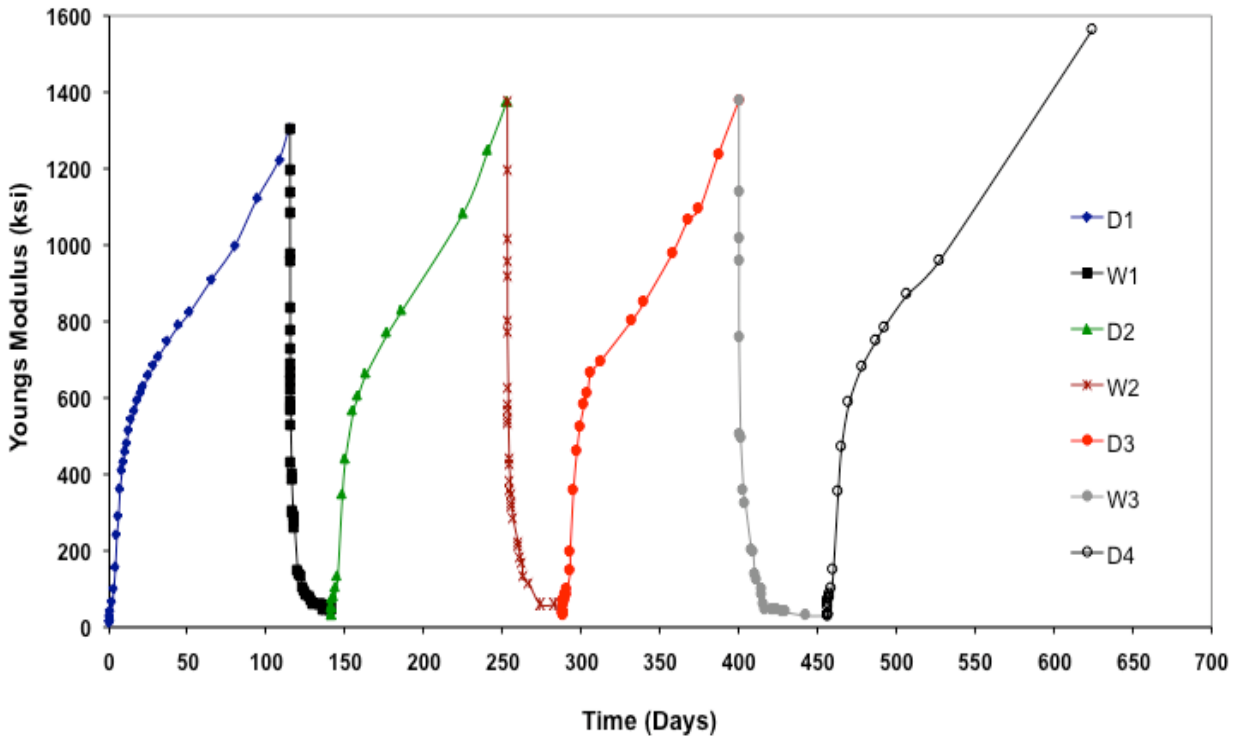

Figure D-27. Variation of Young's modulus with time replicate 3, wetting and drying.

APPENDIX E
MIAMI INDIVIDUAL SMALL-STRAIN MODULUS TEST RESULTS

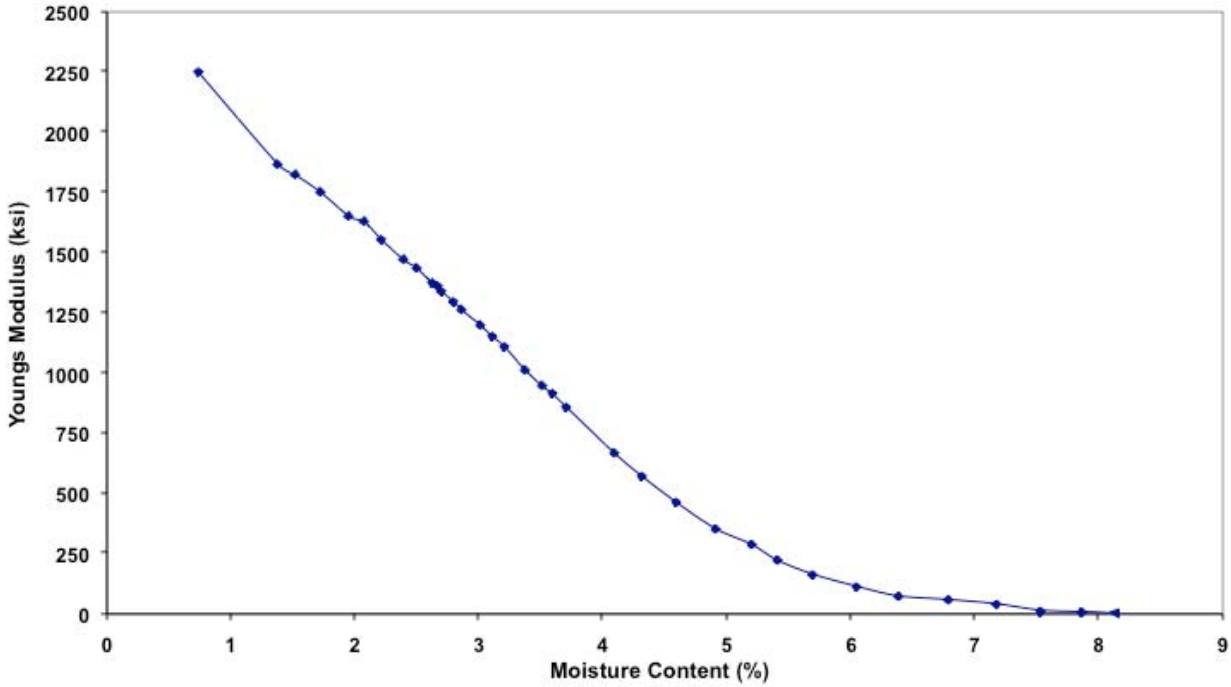

Figure E-1. Variation of Young's modulus with moisture content, replicate 1, laboratory ambient.

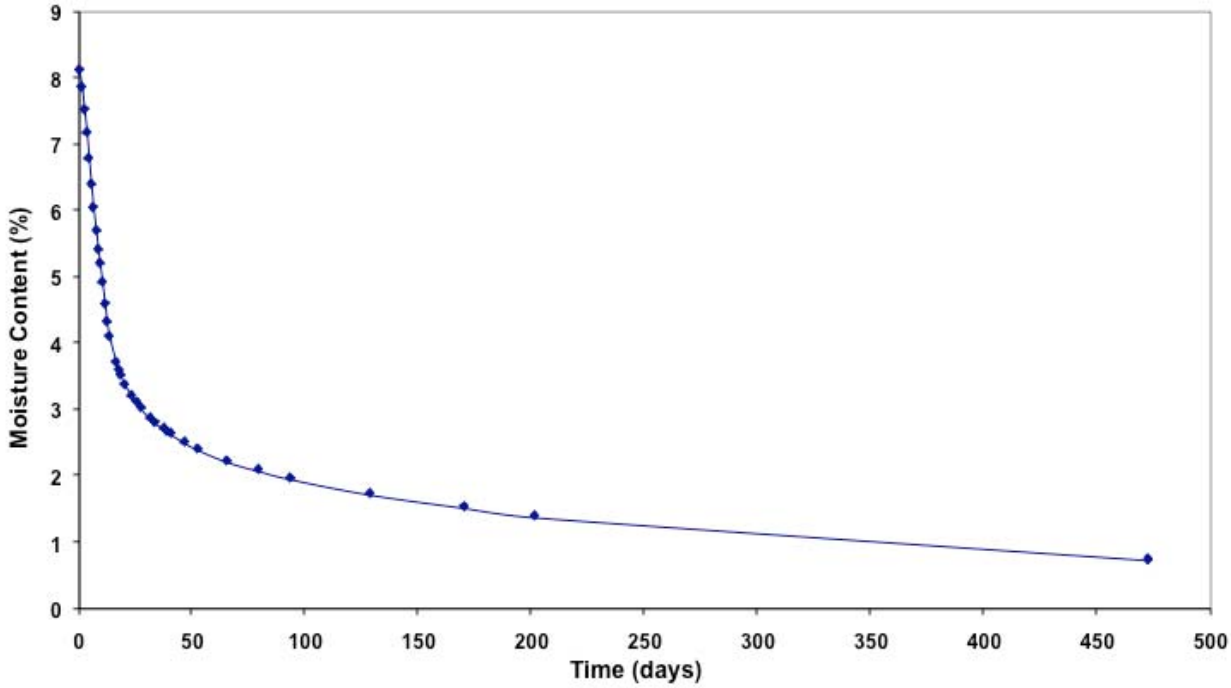

Figure E-2. Variation of Moisture content with time, replicate 1, laboratory ambient.

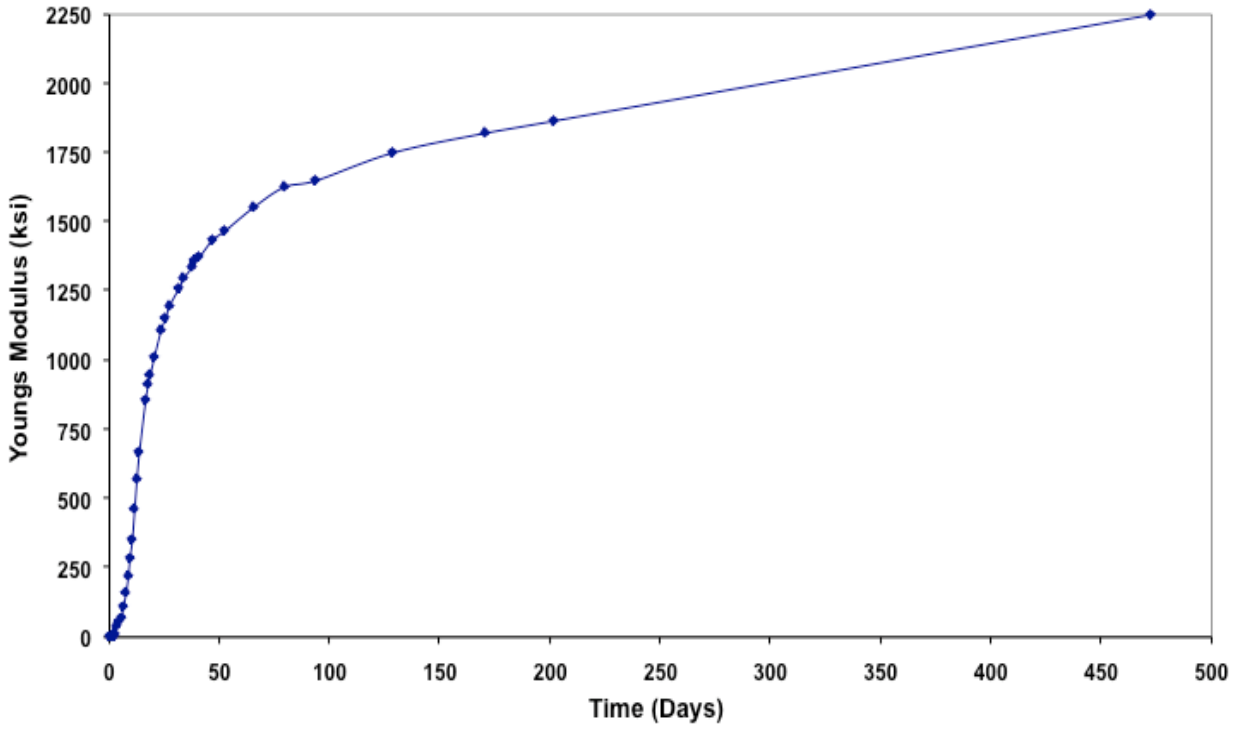

Figure E-3. Variation of Young's Modulus with time, replicate 1, laboratory ambient.

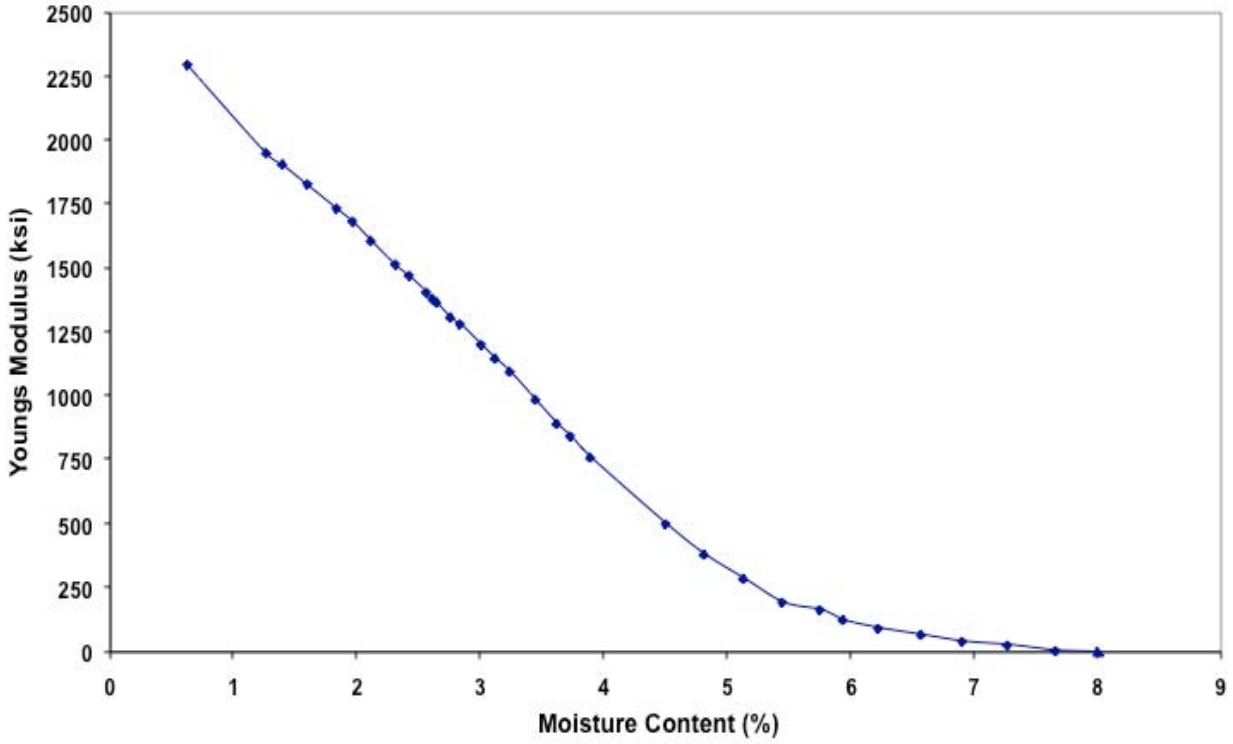

Figure E-4. Variation of Young's modulus with moisture content, replicate 2, laboratory ambient.

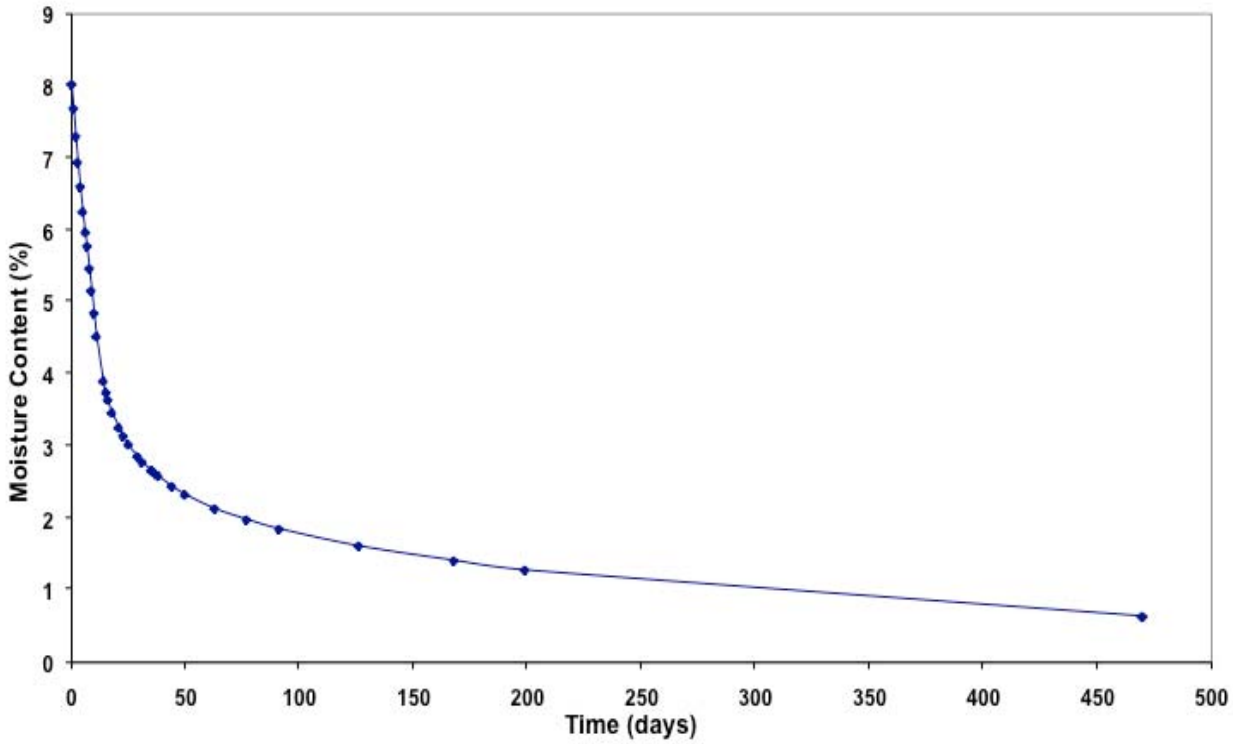

Figure E-5. Variation of moisture content with time, replicate 2, laboratory ambient.

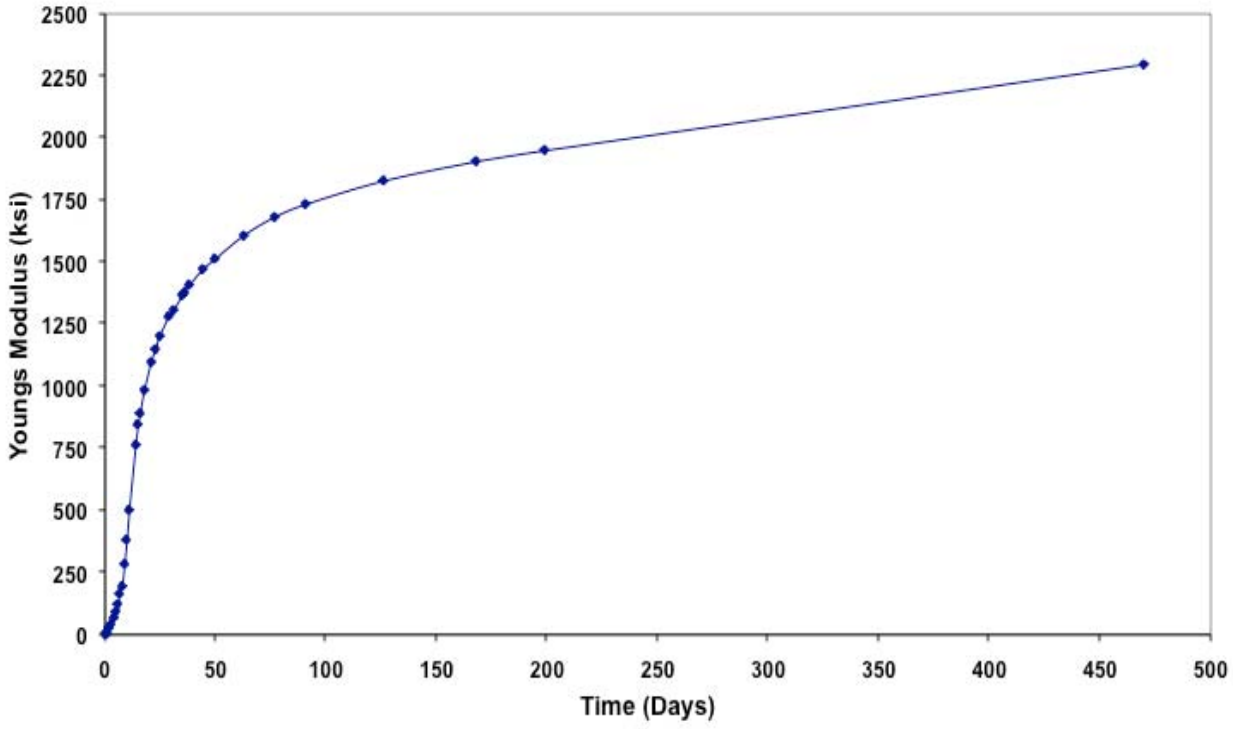

Figure E-6. Variation of Young's modulus with time, replicate 2, laboratory ambient.

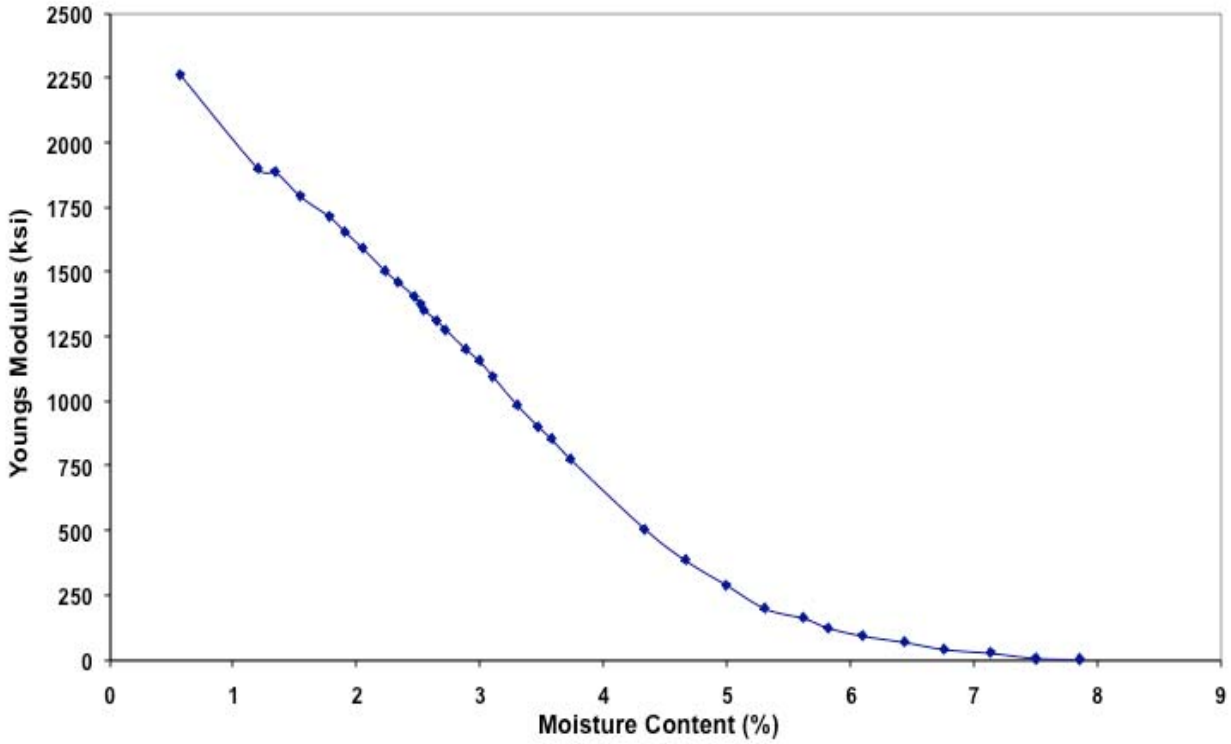

Figure E-7. Variation of Young's modulus with moisture content, replicate 3, laboratory

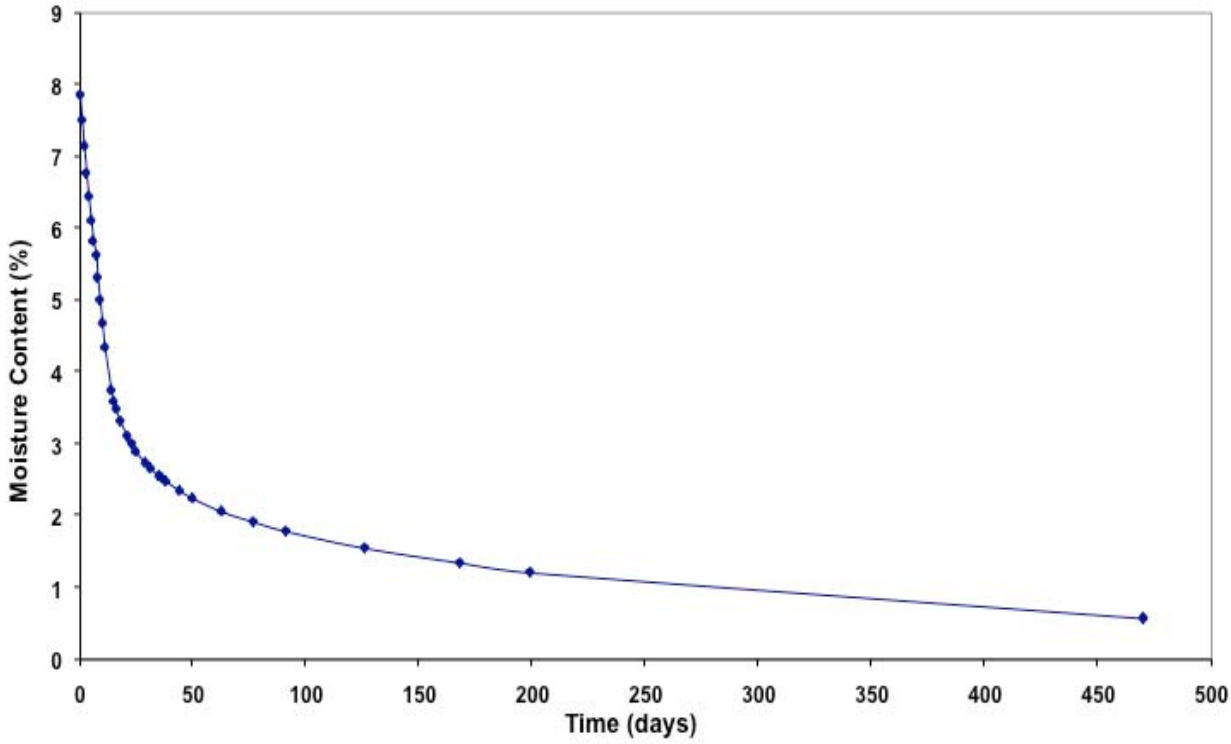

ambient.

Figure E-8. Variation of moisture content with time, replicate 3, laboratory ambient.

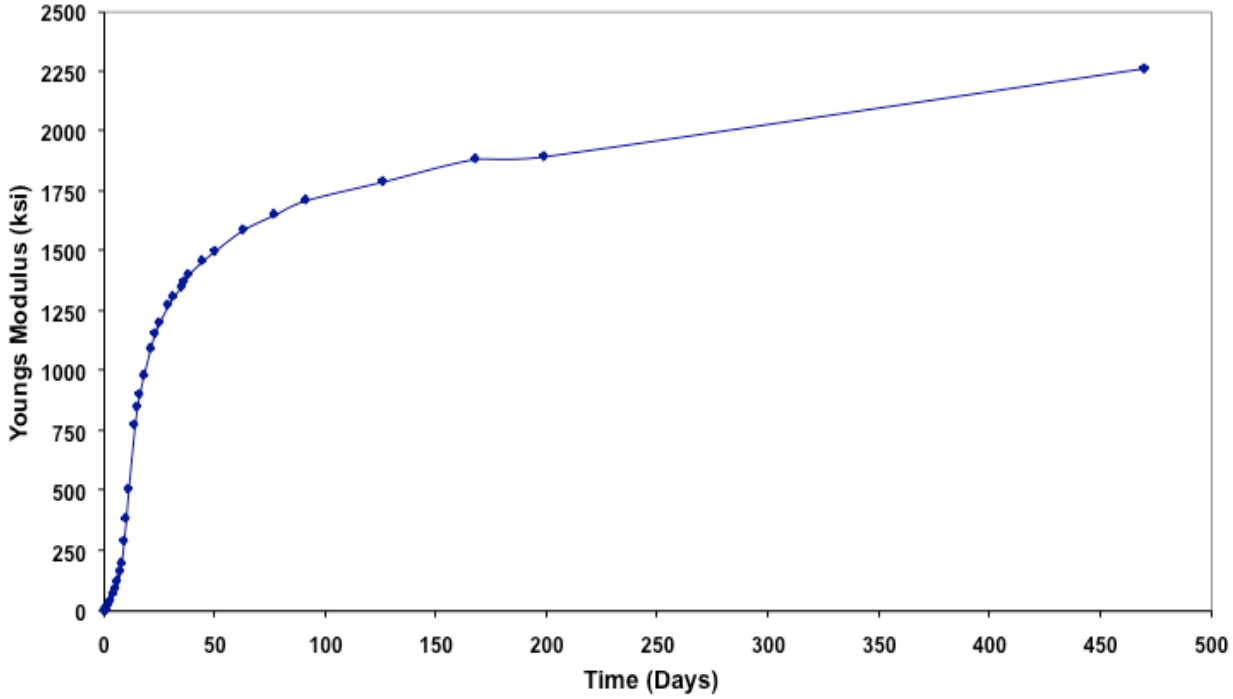

Figure E-9. Variation of Young's modulus with time, replicate 3, laboratory ambient.

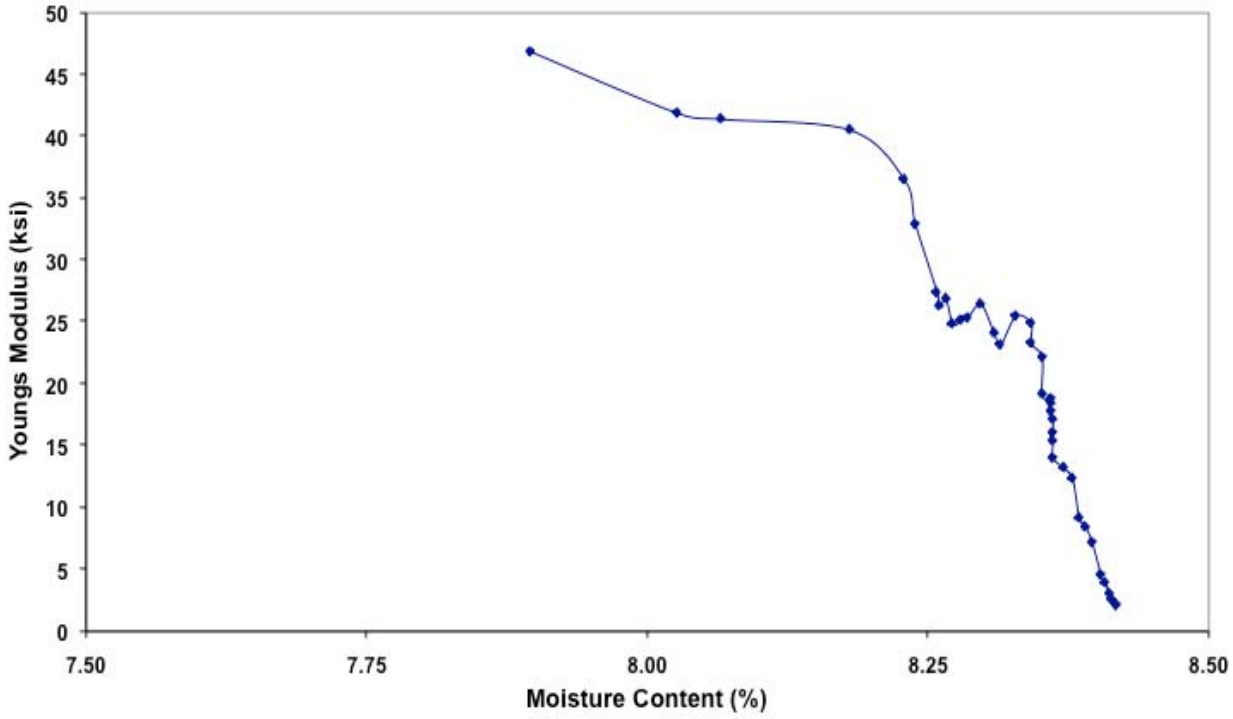

Figure E-10. Variation of Young's modulus with moisture content, replicate 1, constant moisture.

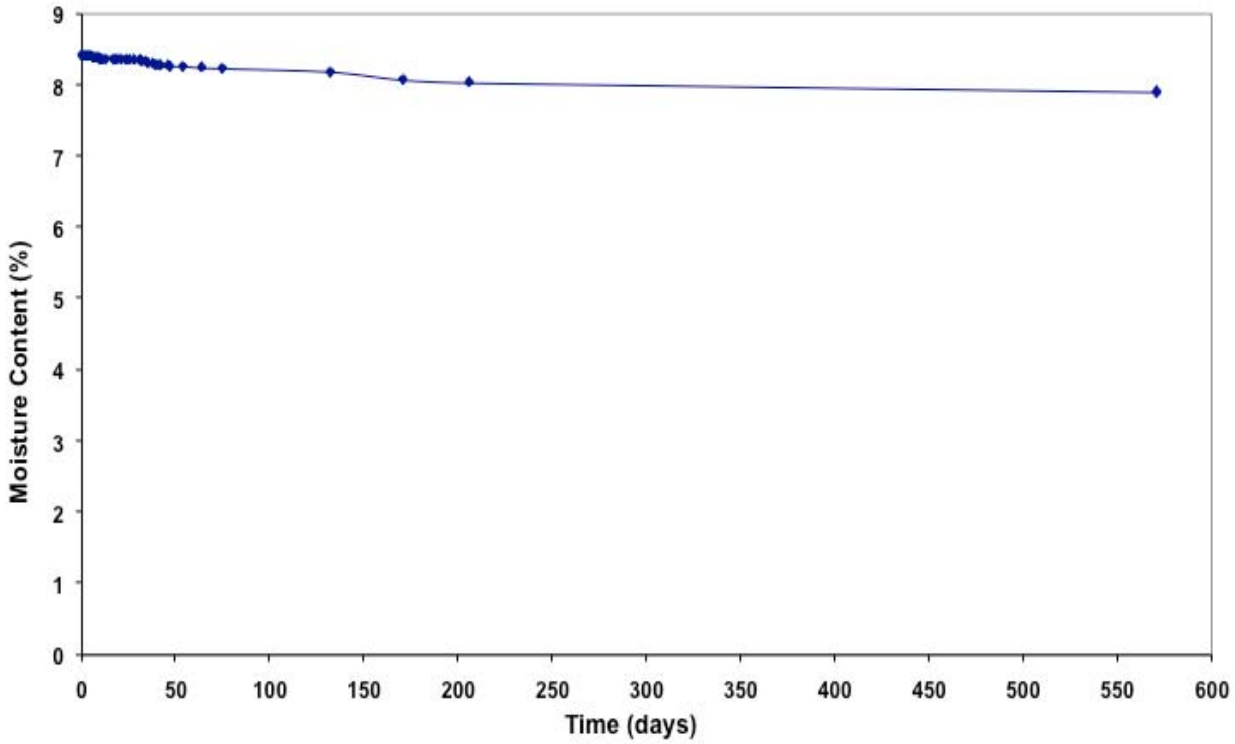

Figure E-11. Variation of moisture content with time, replicate 1, constant moisture.

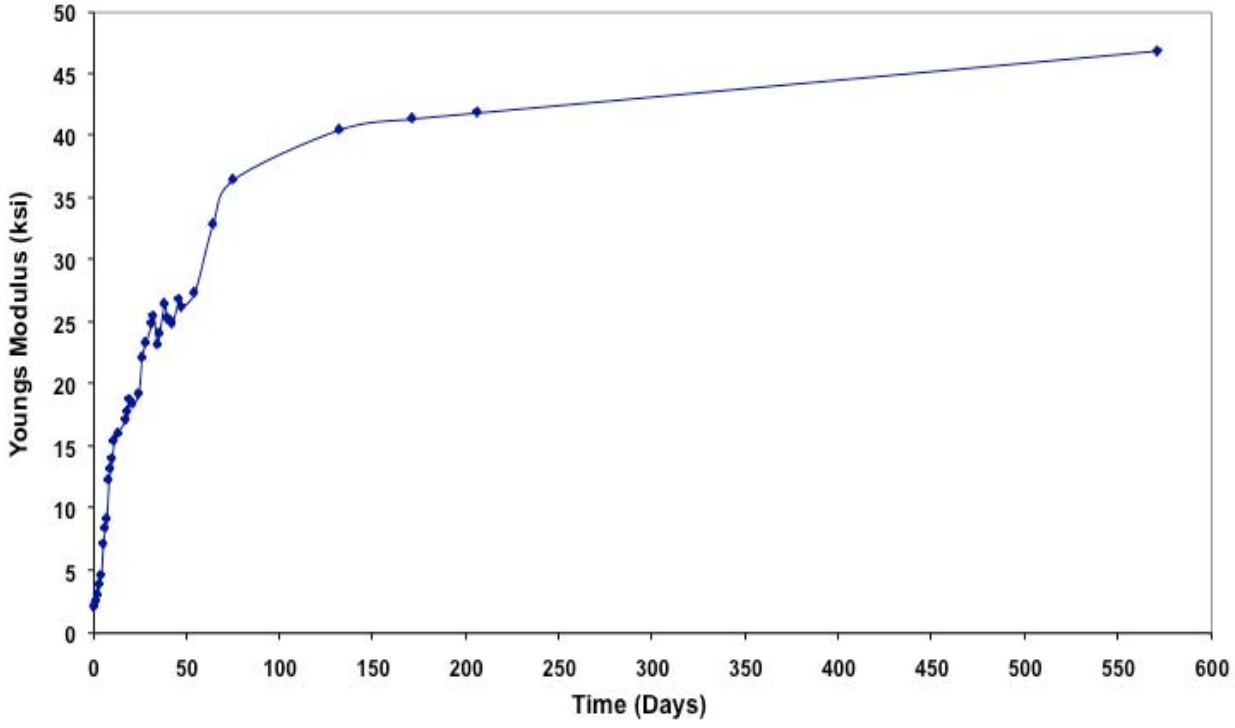

Figure E-12. Variation of Young's modulus with time, replicate 1, constant moisture.

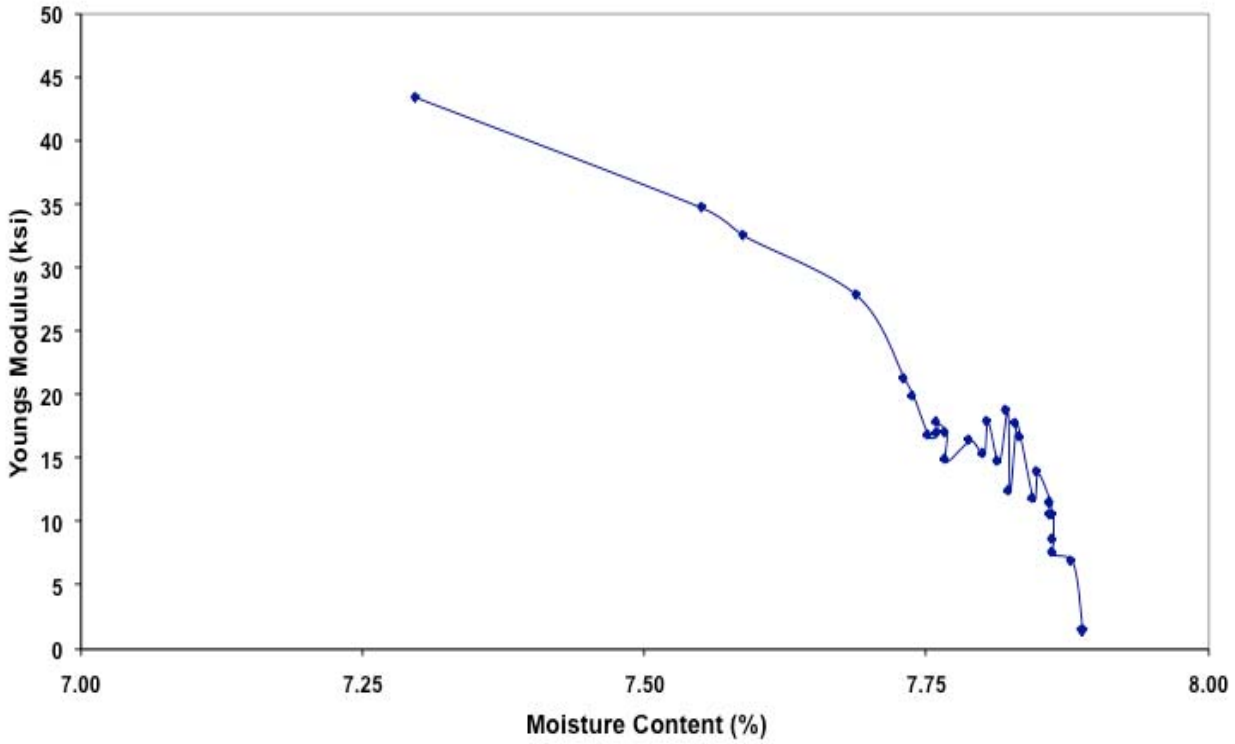

Figure E-13. Variation of Young's modulus with moisture content, replicate 2, constant moisture.

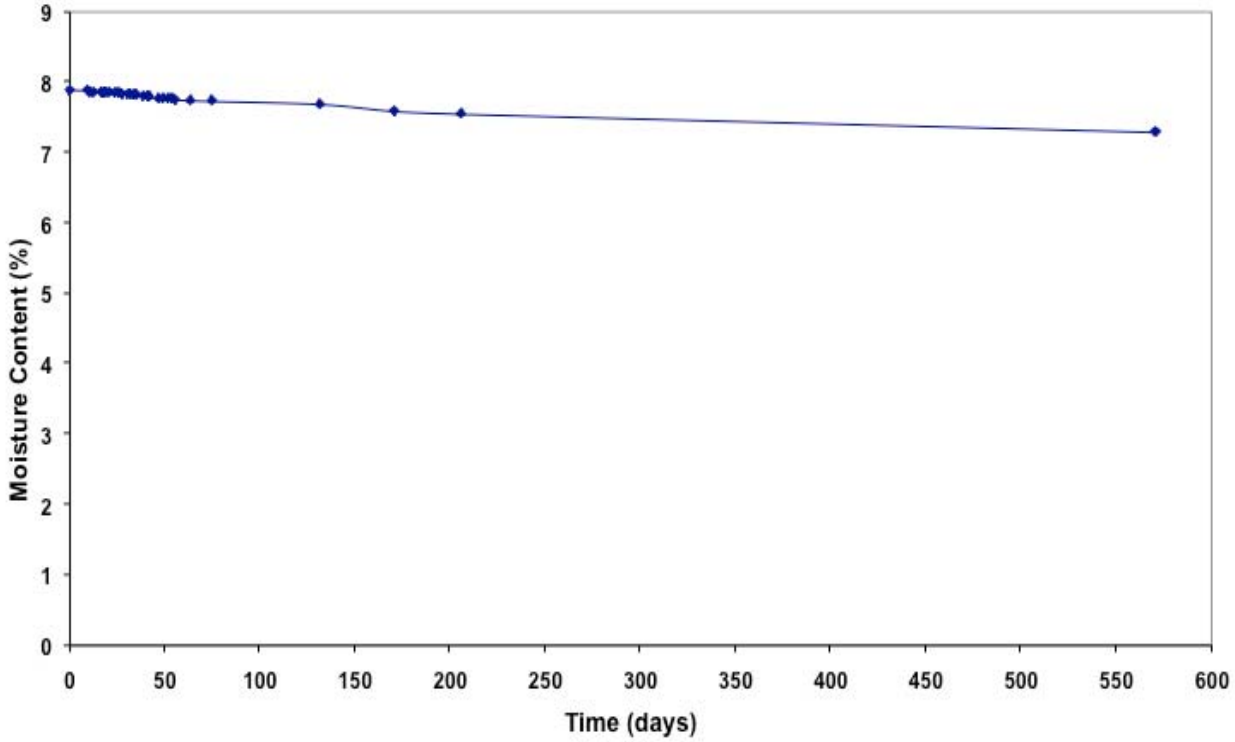

Figure E-14. Variation of moisture content with time, replicate 2, constant moisture.

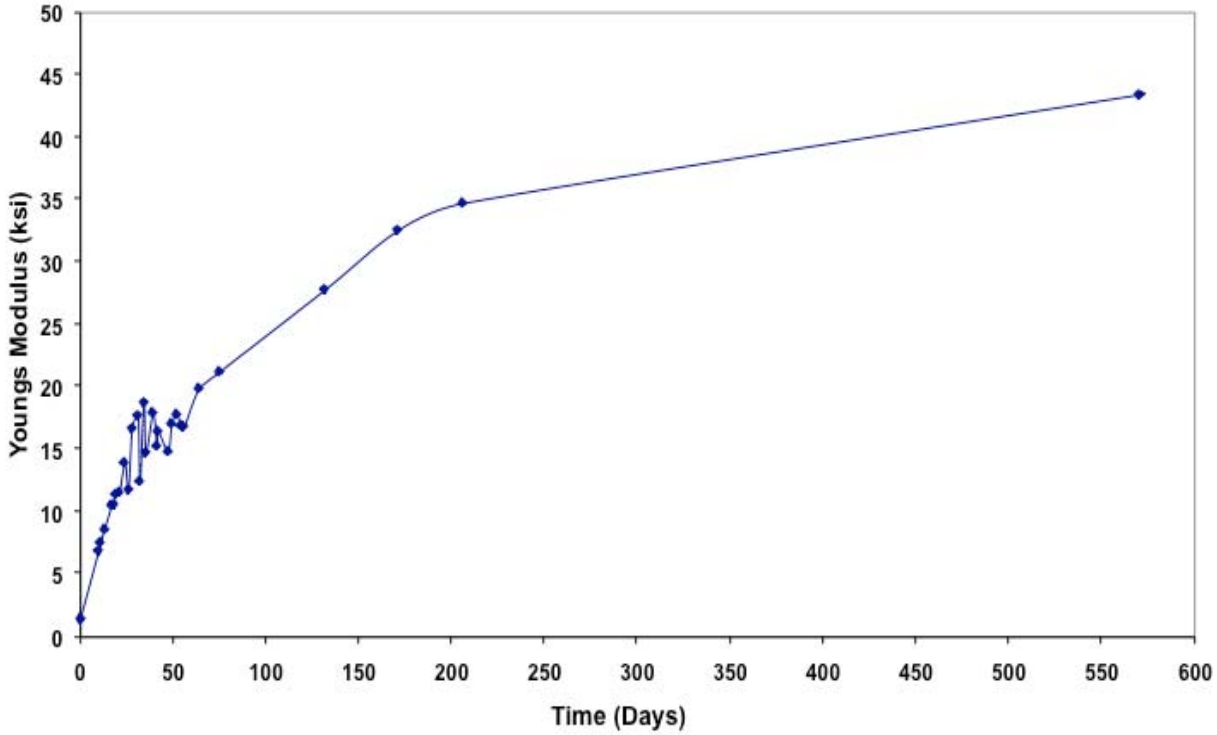

Figure E-15. Variation of Young's modulus with time, replicate 2, constant moisture.

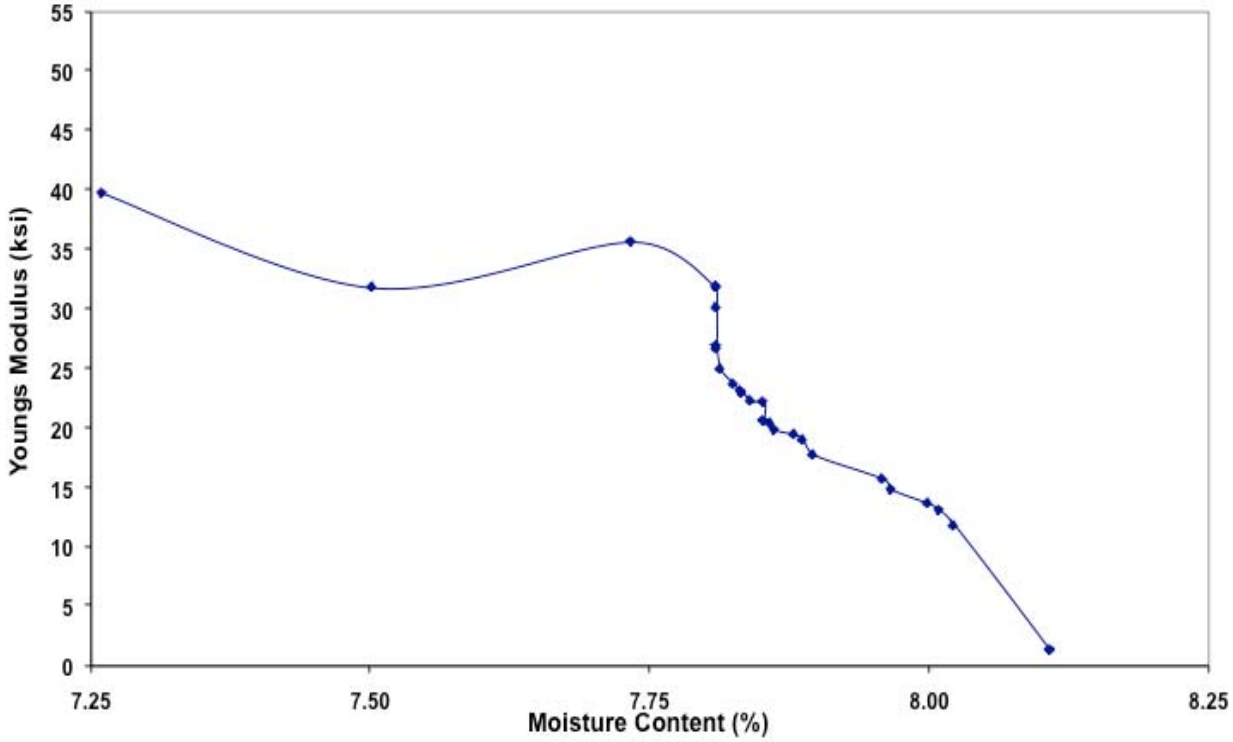

Figure E-16. Variation of Young's with moisture content, replicate 3, constant moisture.

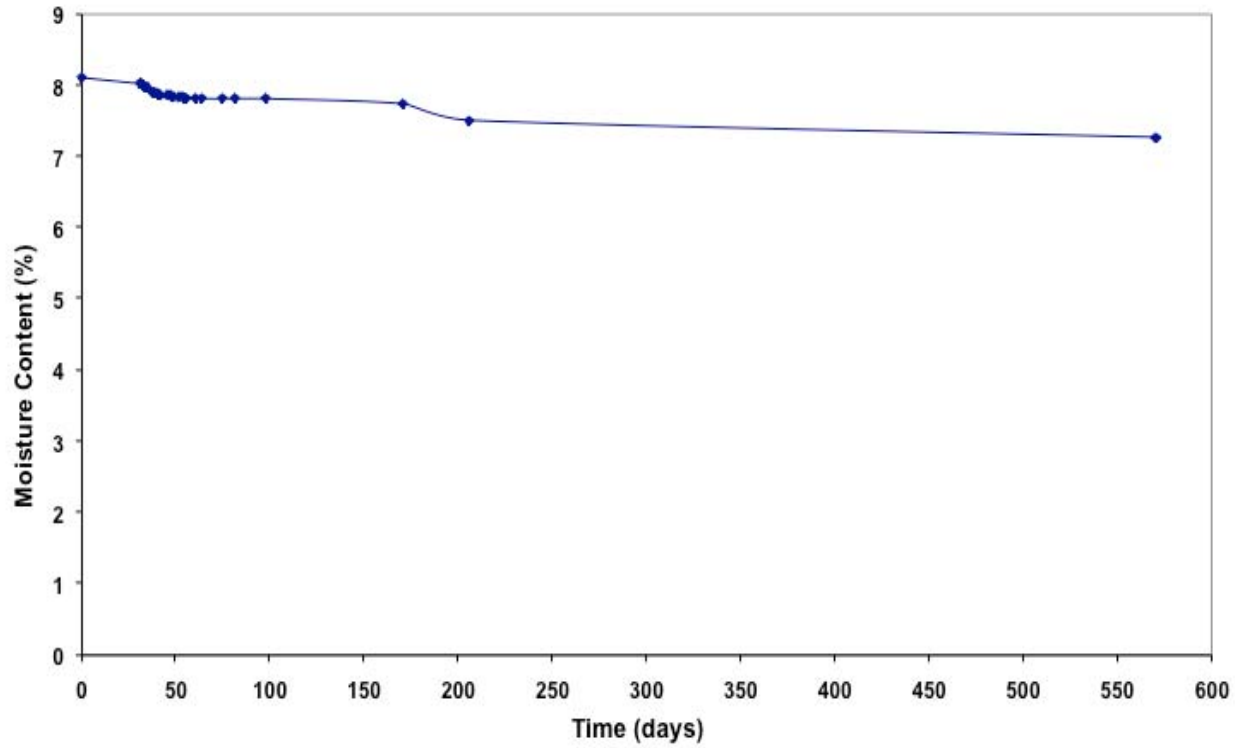

Figure E-17. Variation of moisture content with time, replicate 3, constant moisture.

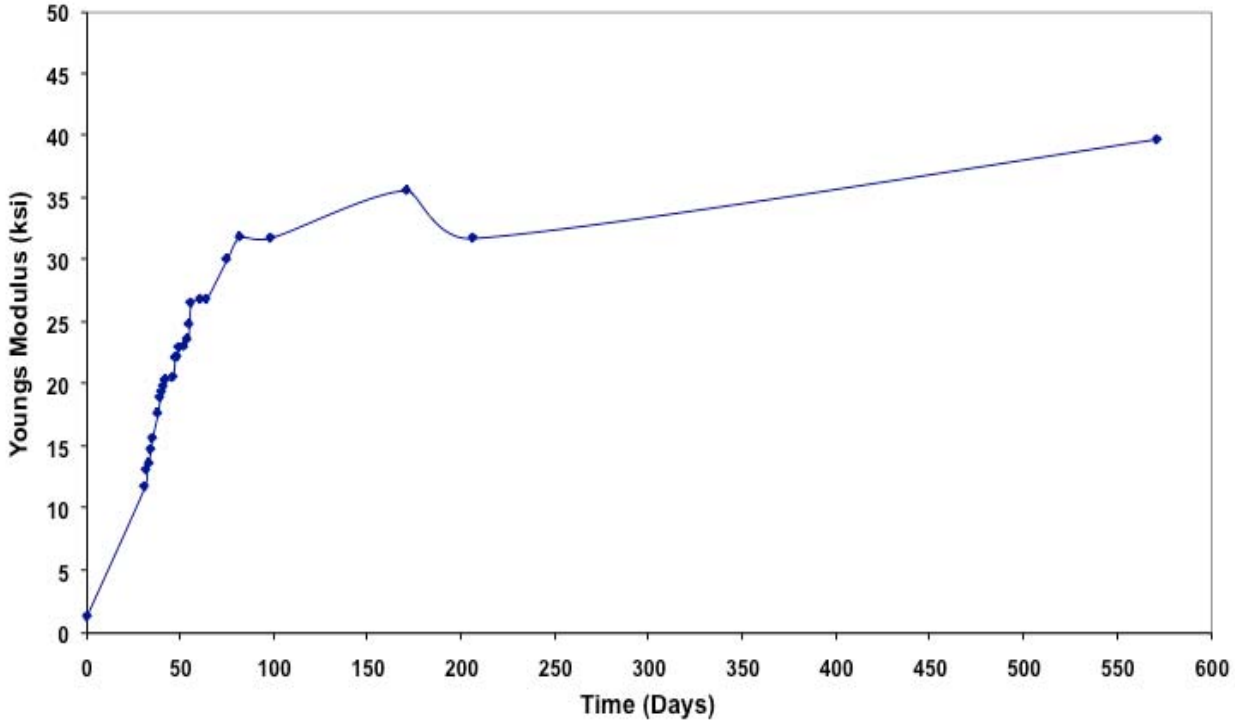

Figure E-18. Variation of Young's modulus with time, replicate 3, constant moisture.

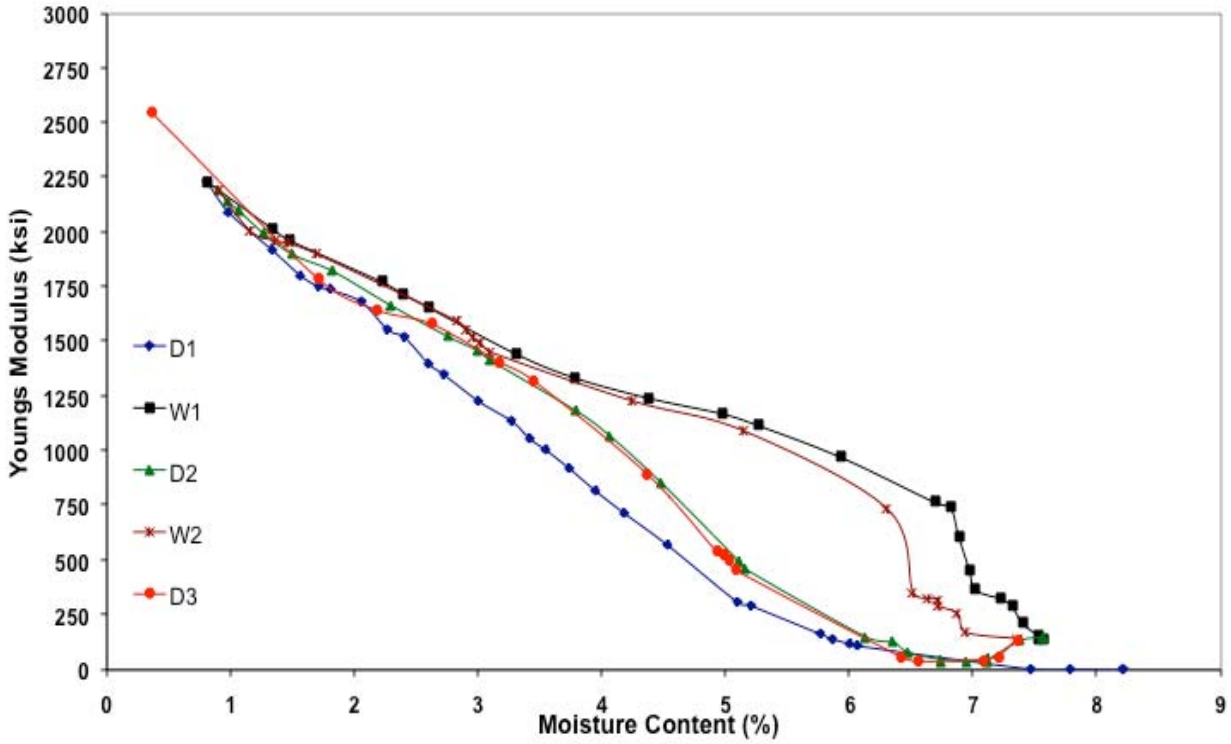

Figure E-19. Variation of Young's modulus with moisture content, replicate 1, wetting and drying.

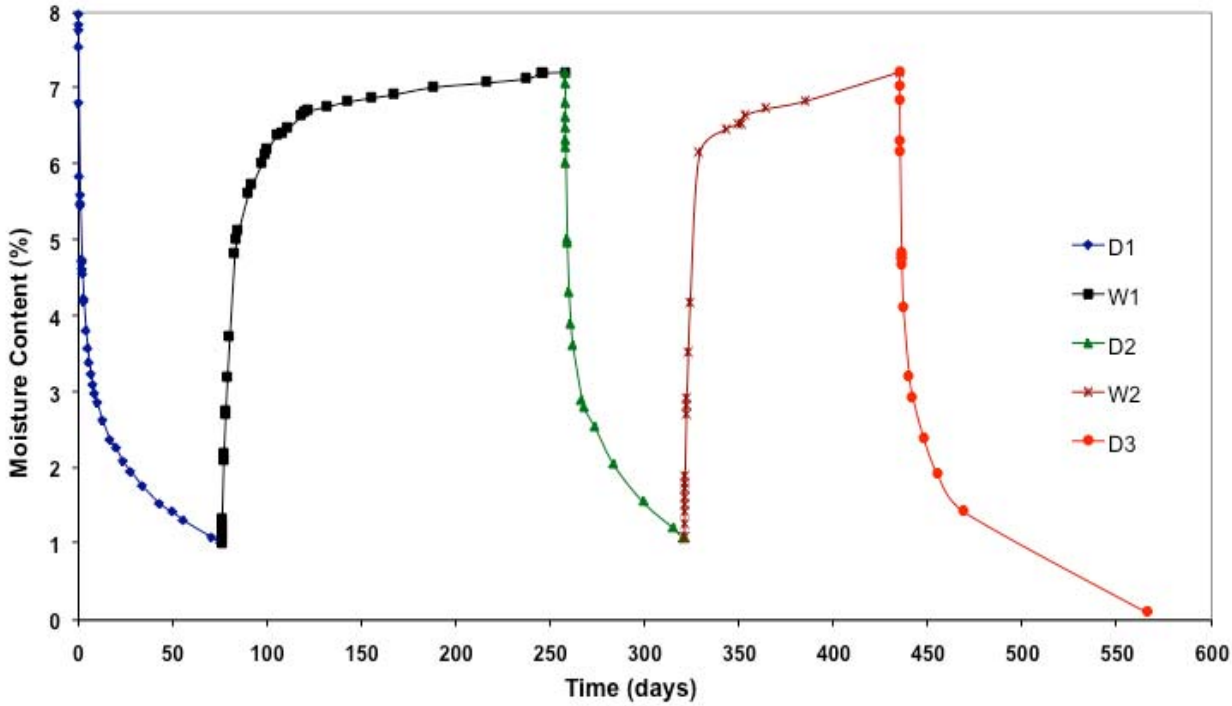

Figure E-20. Variation of moisture content with time, replicate 1, wetting and drying.

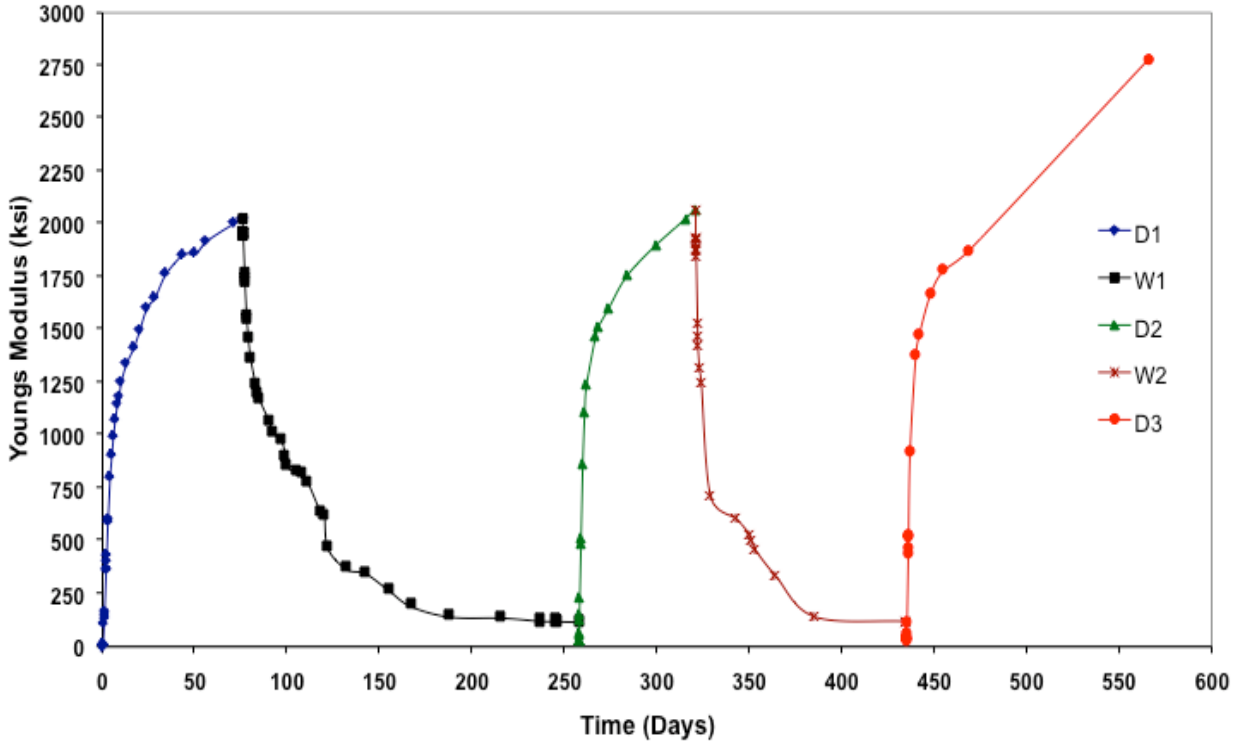

Figure E-21. Variation of Young's modulus with time, replicate 1, wetting and drying.

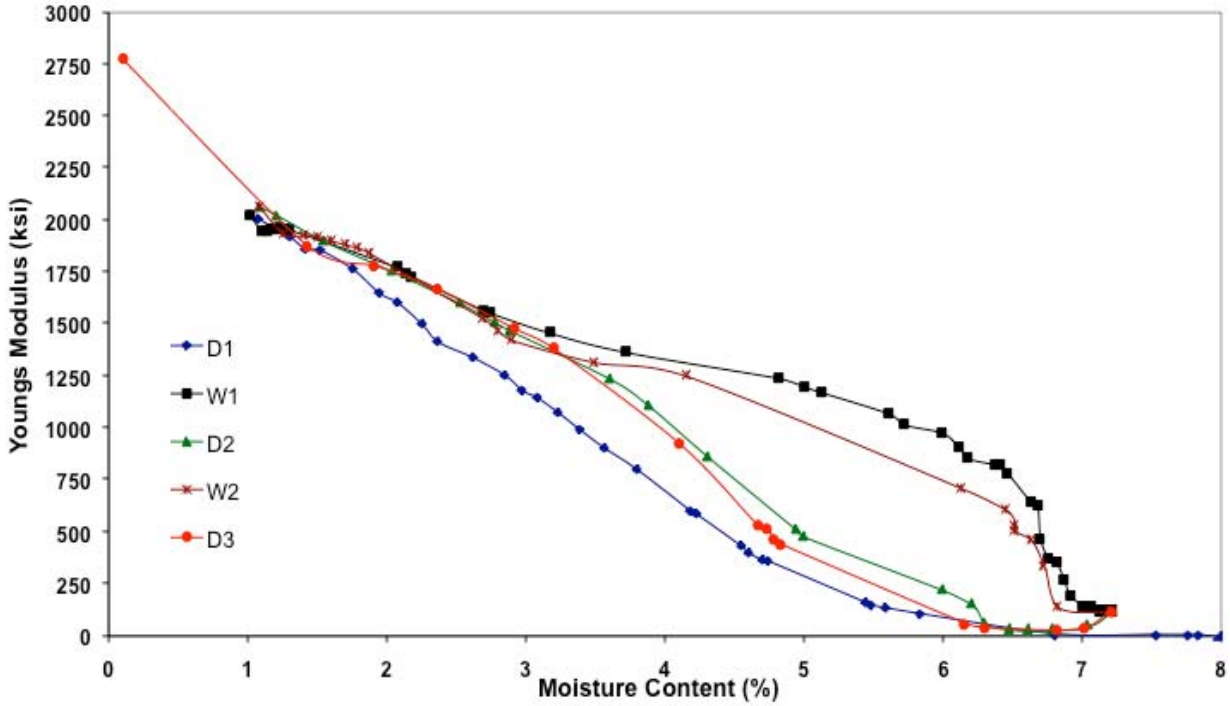

Figure E-22. Variation of Young's modulus with moisture content, replicate 2, wetting and drying.

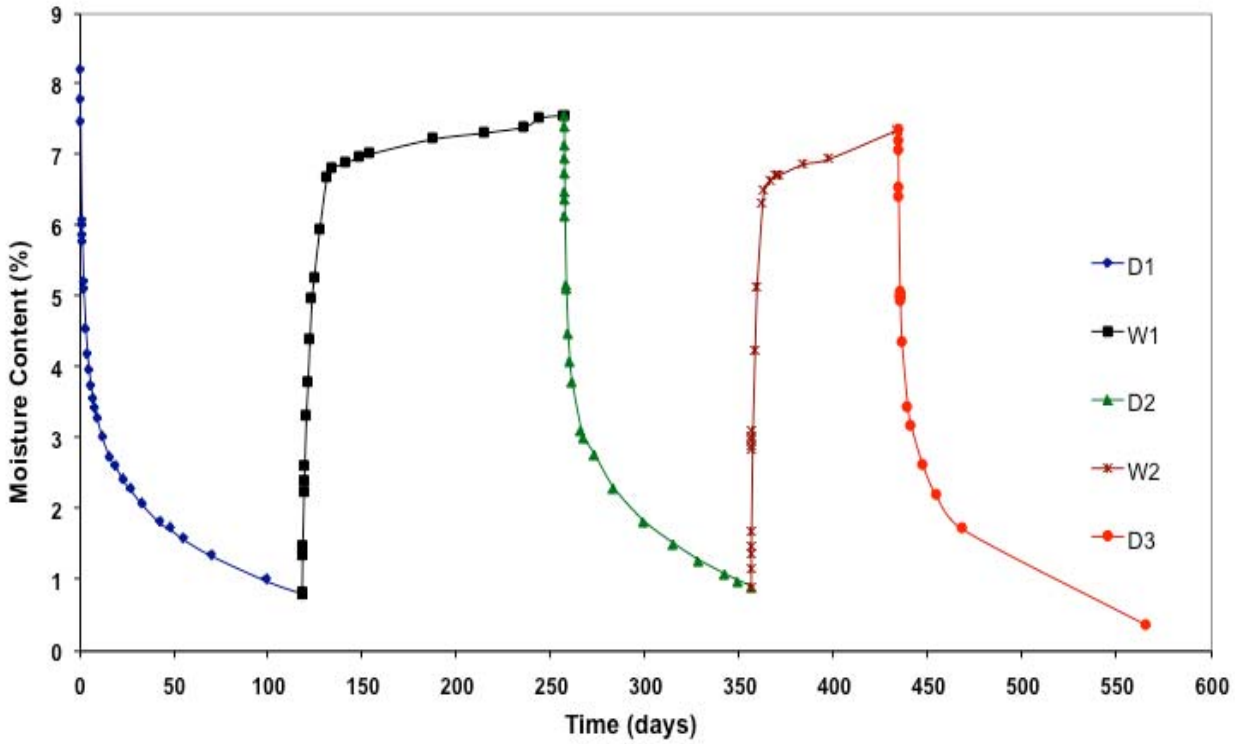

Figure E-23. Variation of moisture content with time, replicate 2, wetting and drying.

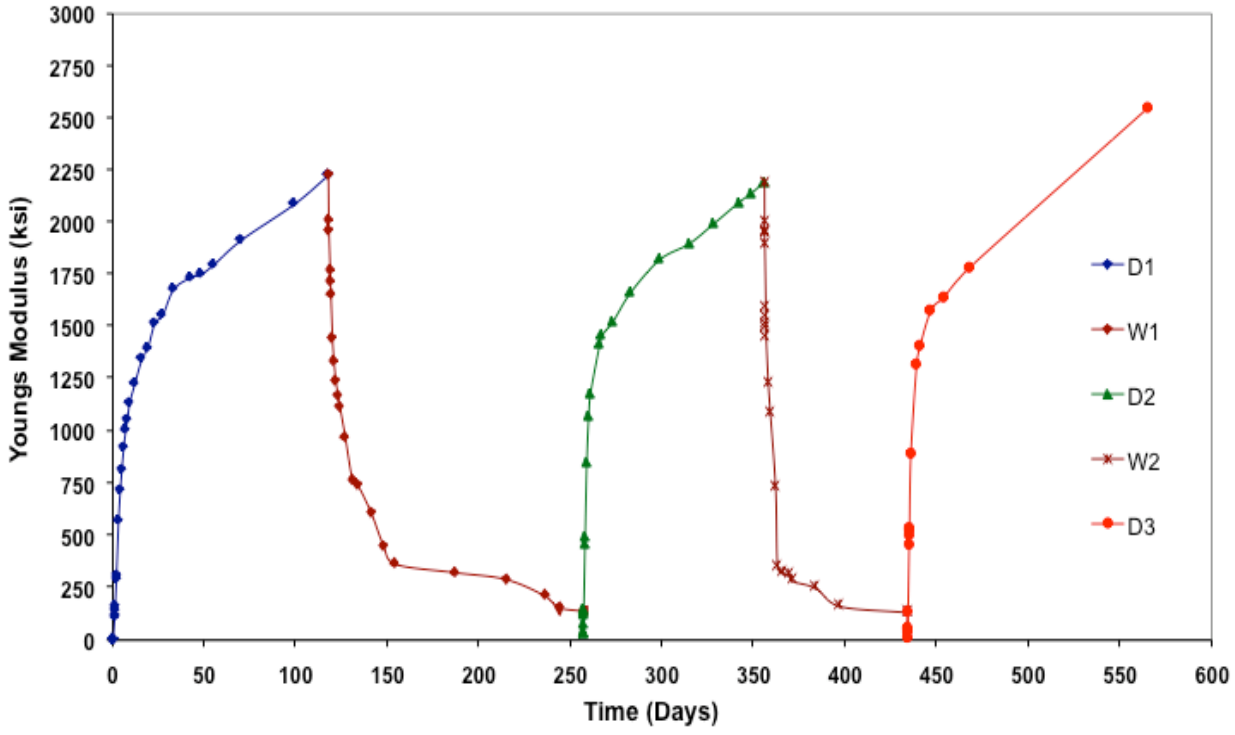

Figure E-24. Variation of Young's modulus with time, replicate 2, wetting and drying.

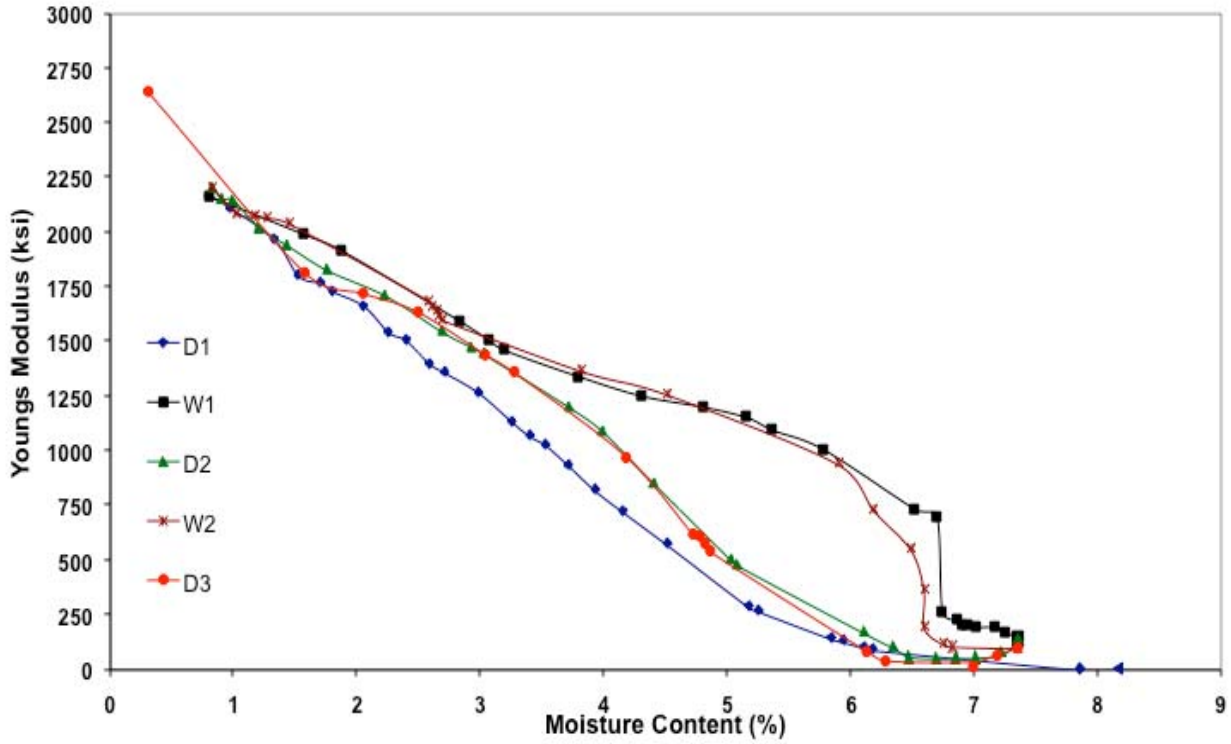

Figure E-25. Variation of Young's modulus with moisture content, replicate 3, wetting and drying.

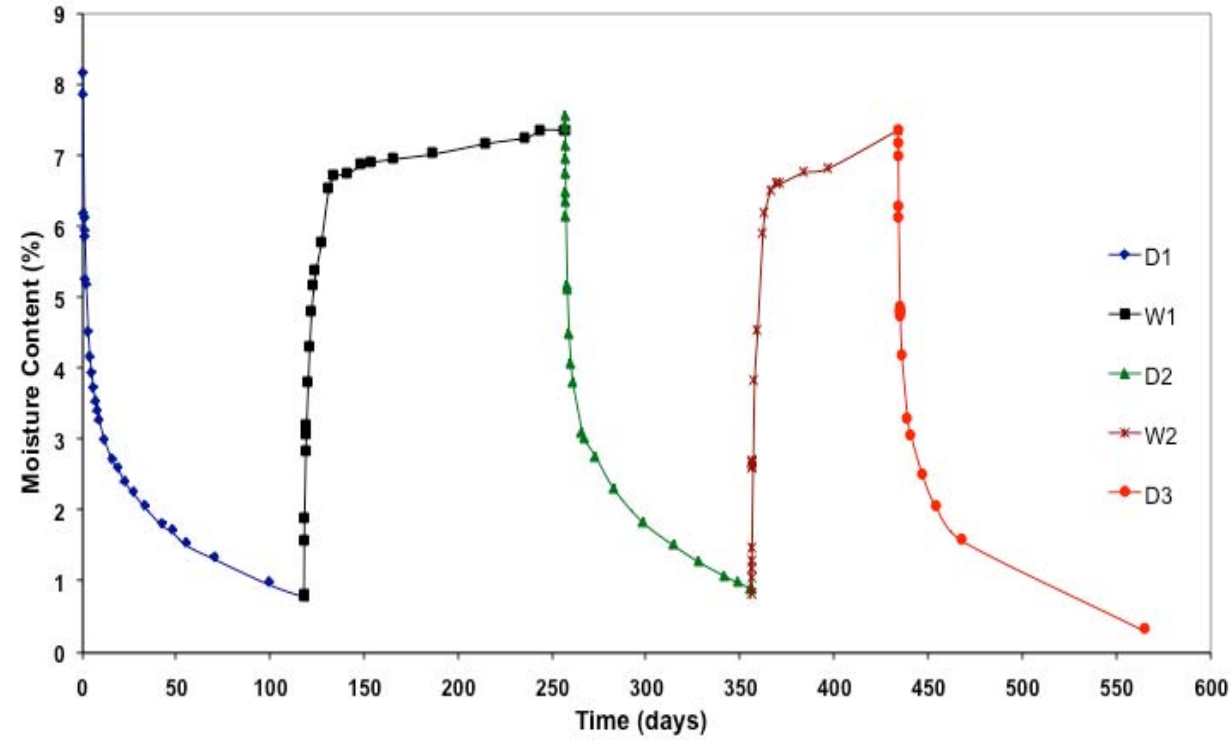

Figure E-26. Variation of moisture content with time, replicate 3, wetting and drying.

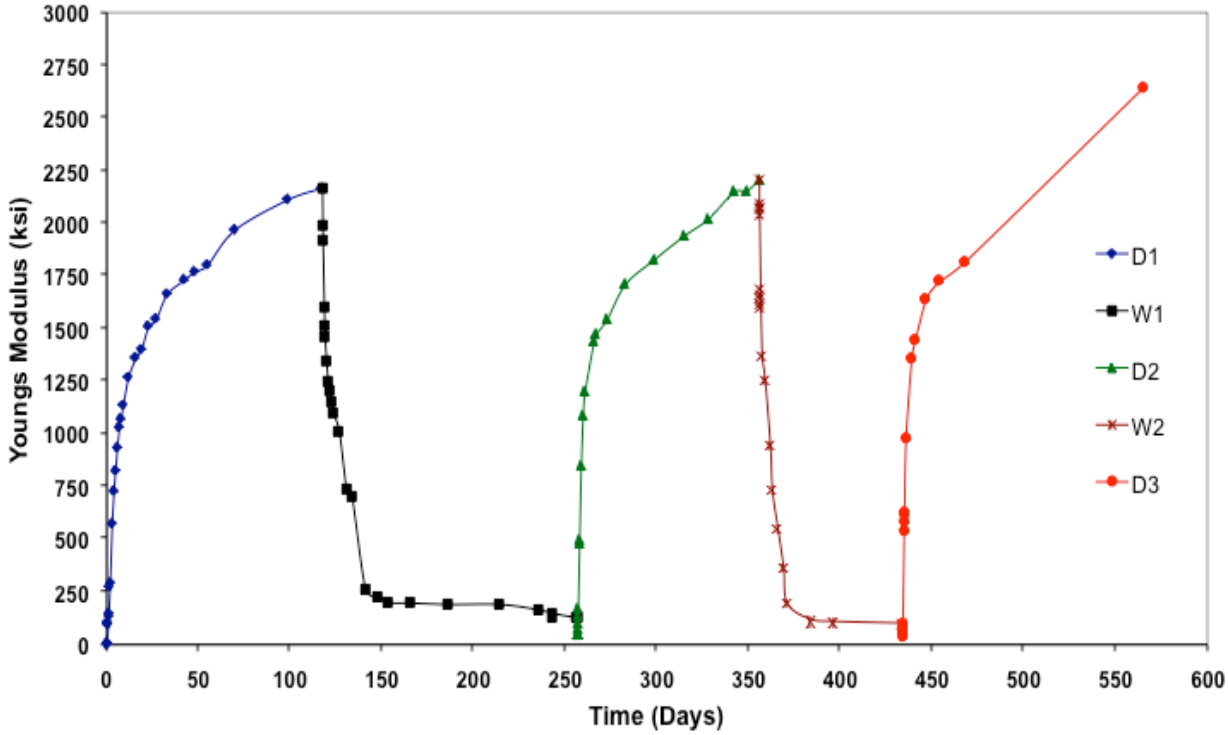

Figure E-27. Variation of Young's modulus with time, replicate 3, wetting and drying.

APPENDIX F
GEORGIA INDIVIDUAL SMALL-STRAIN MODULUS TEST RESULTS

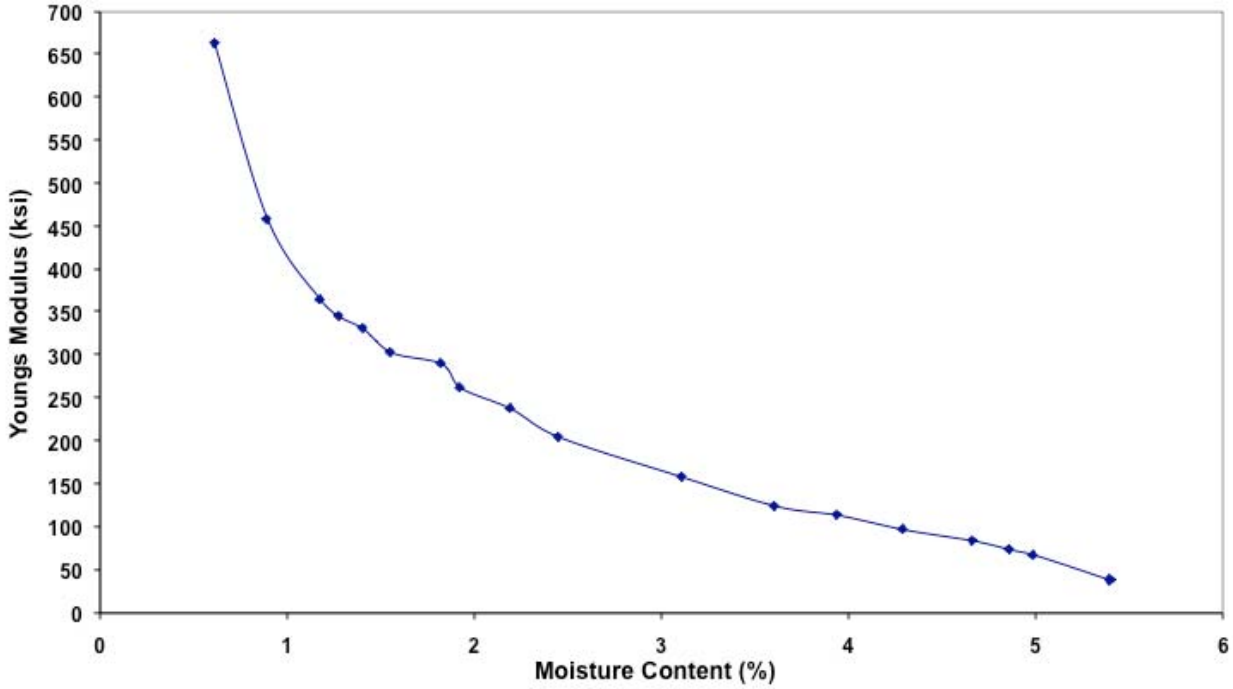

Figure F-1. Variation of Young's modulus with moisture content, replicate 1, laboratory ambient.

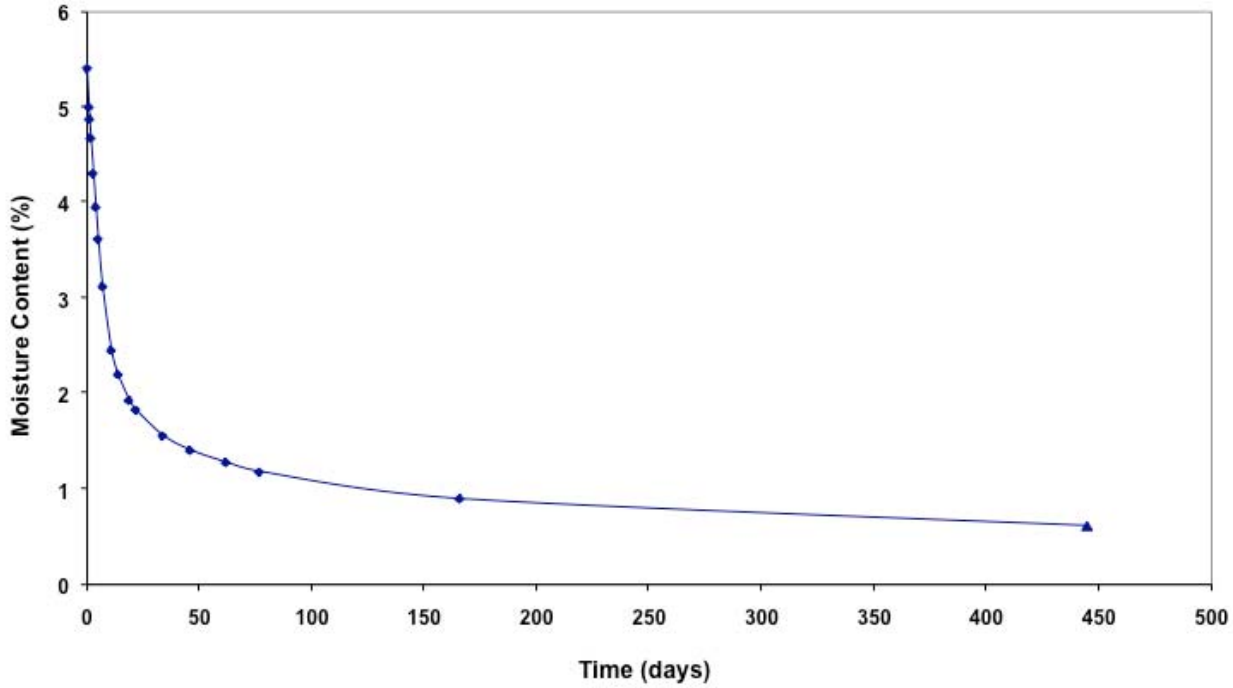

Figure F-2. Variation of moisture content with time, replicate 1, laboratory ambient.

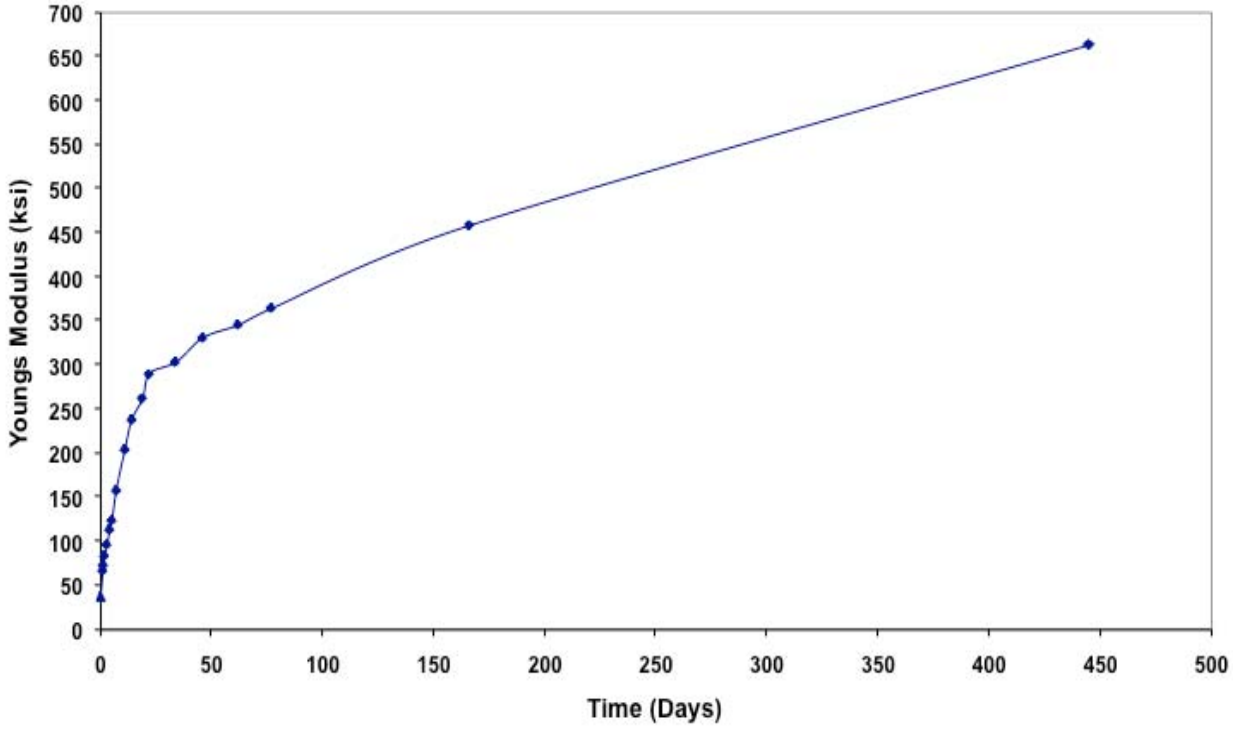

Figure F-3. Variation of Young's modulus with time, replicate 1, laboratory ambient.

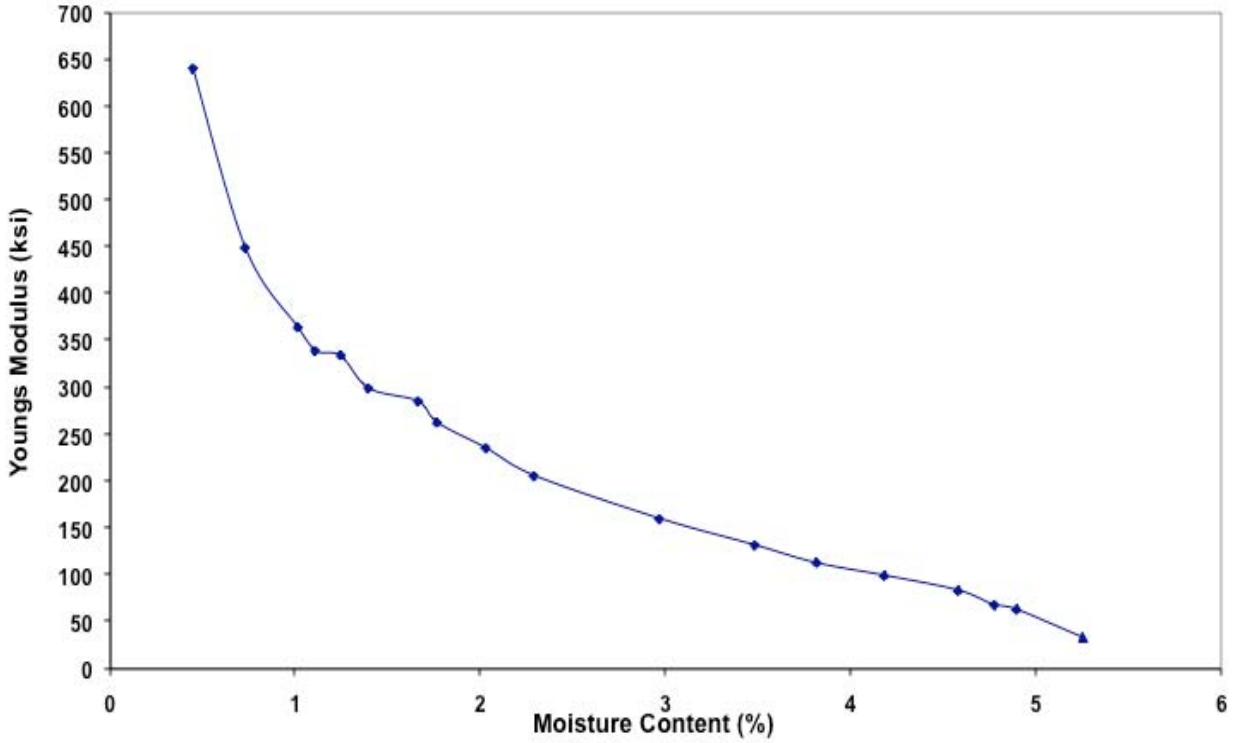

Figure F-4. Variation of Young's modulus with moisture content, replicate 2, laboratory ambient.

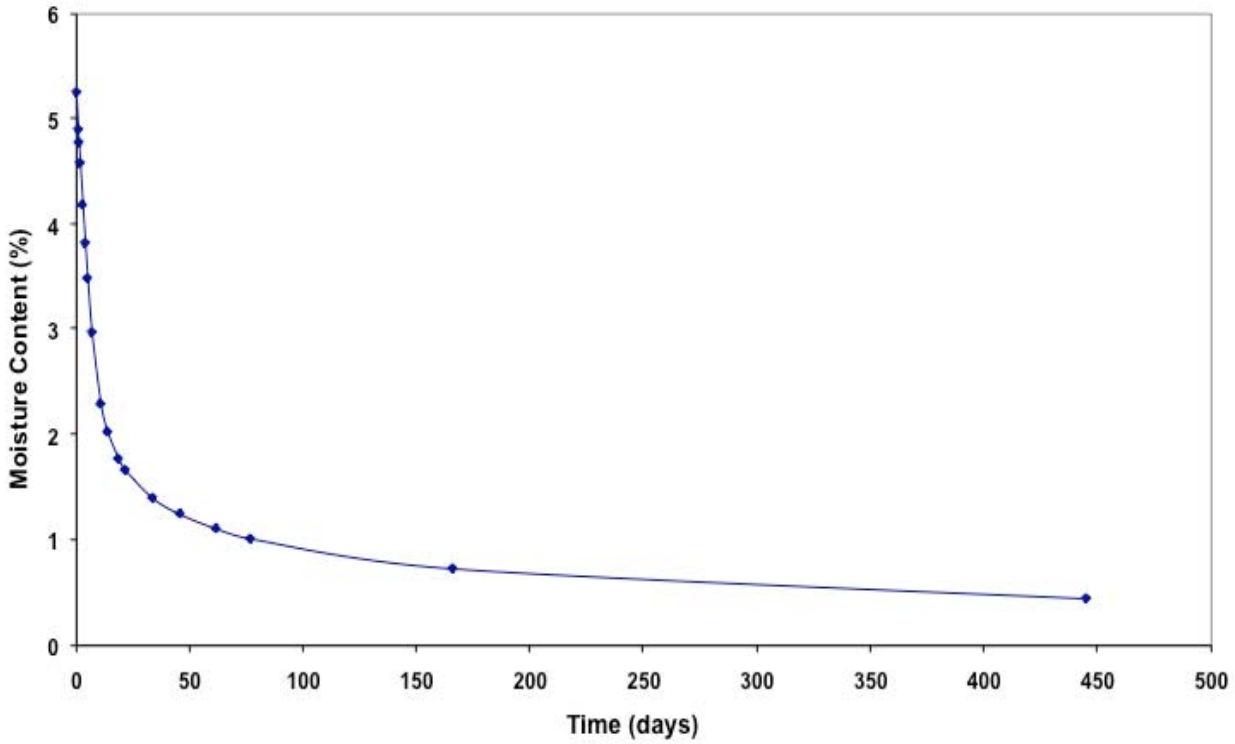

Figure F-5. Variation of moisture content with time, replicate 2, laboratory ambient.

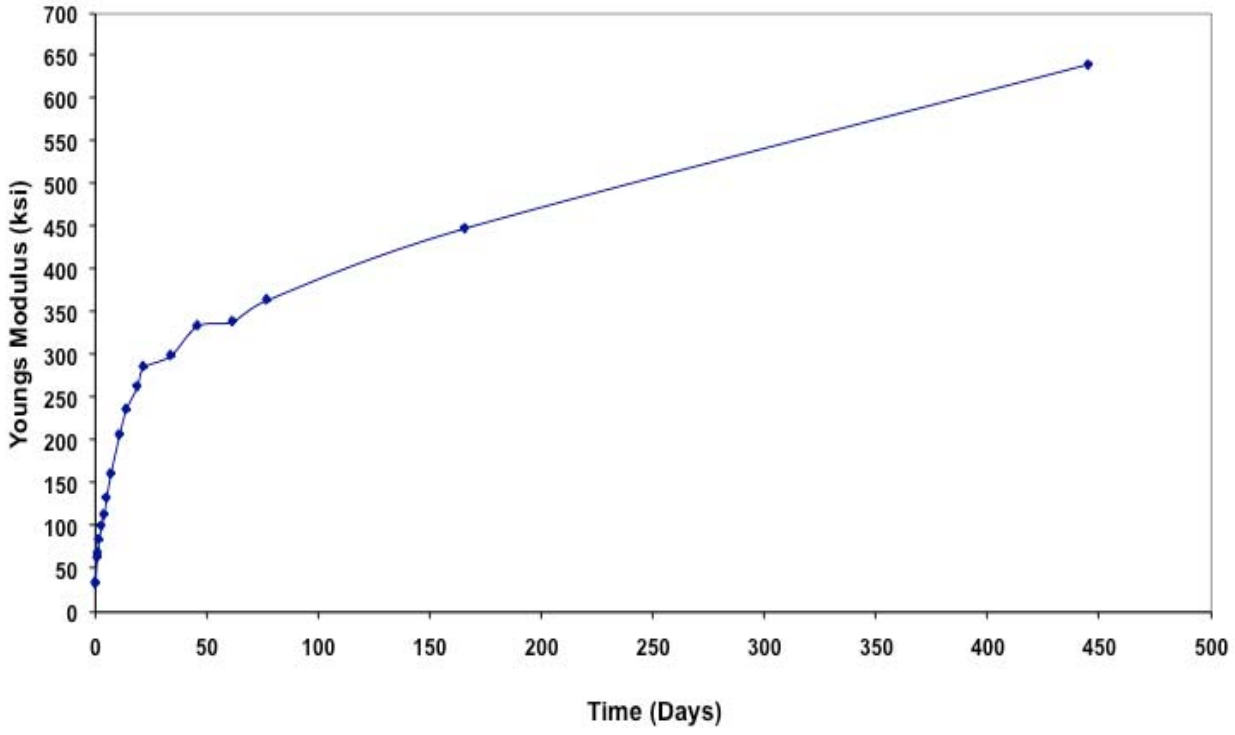

Figure F-6. Variation of Young's modulus with time, replicate 2, laboratory ambient.

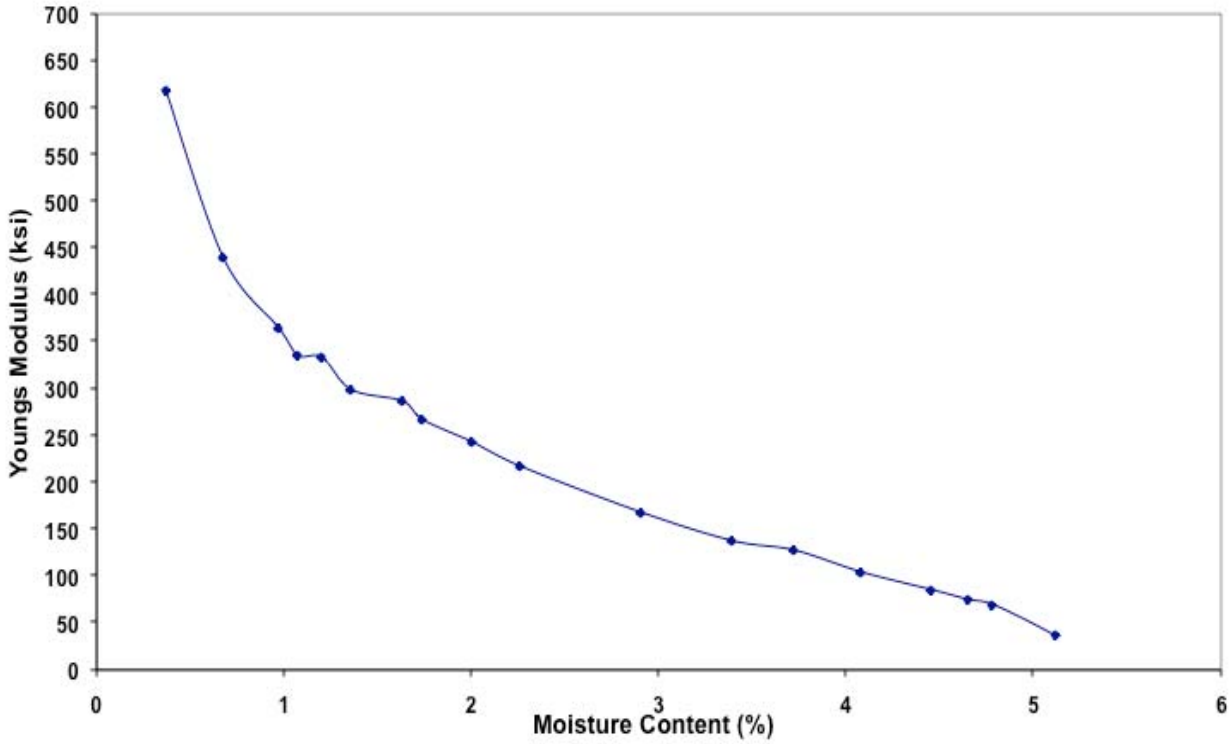

Figure F-7. Variation of Young's modulus with moisture content, replicate 3, laboratory ambient.

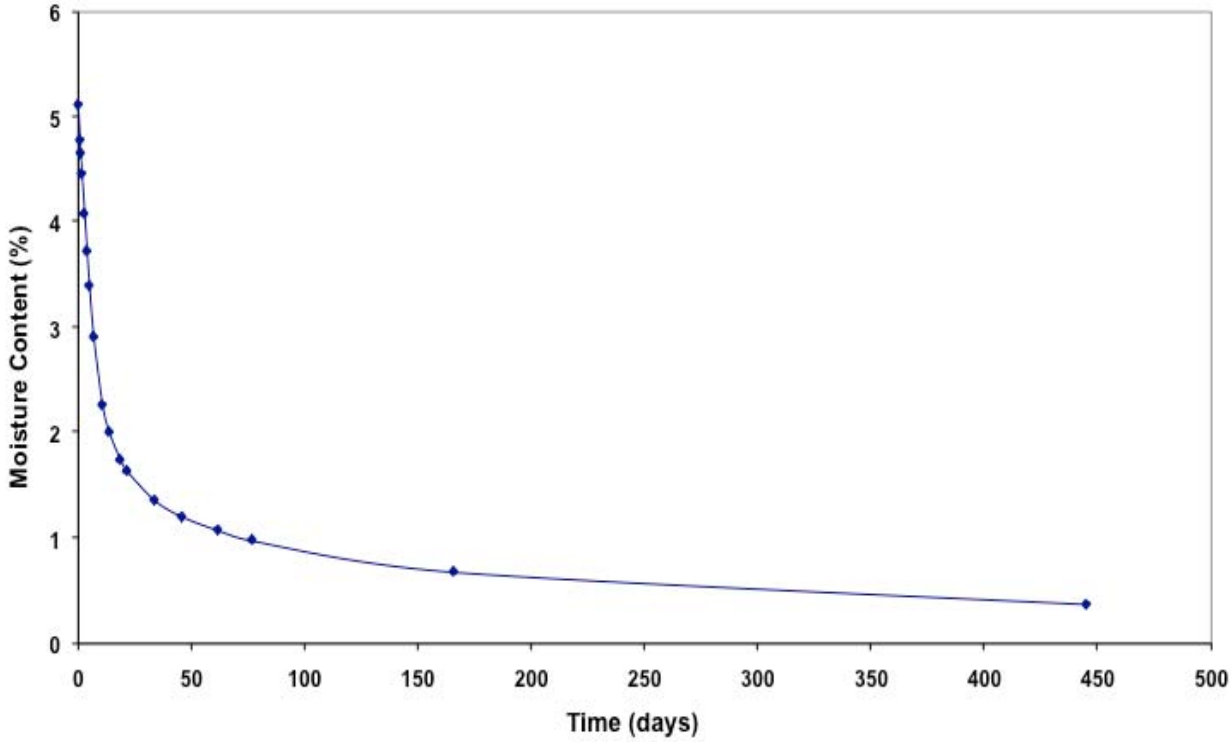

Figure F-8. Variation of moisture content with time, replicate 3, laboratory ambient.

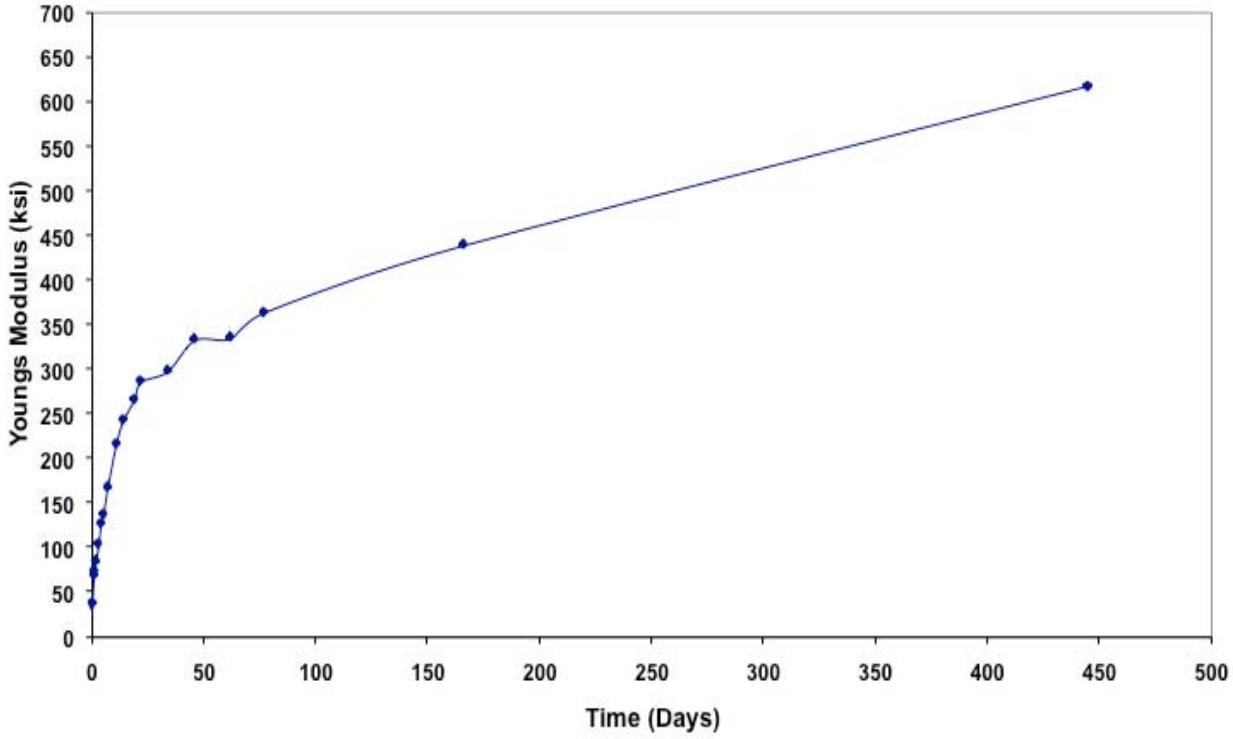

Figure F-9. Variation of Young's modulus with time, replicate 3, laboratory ambient.

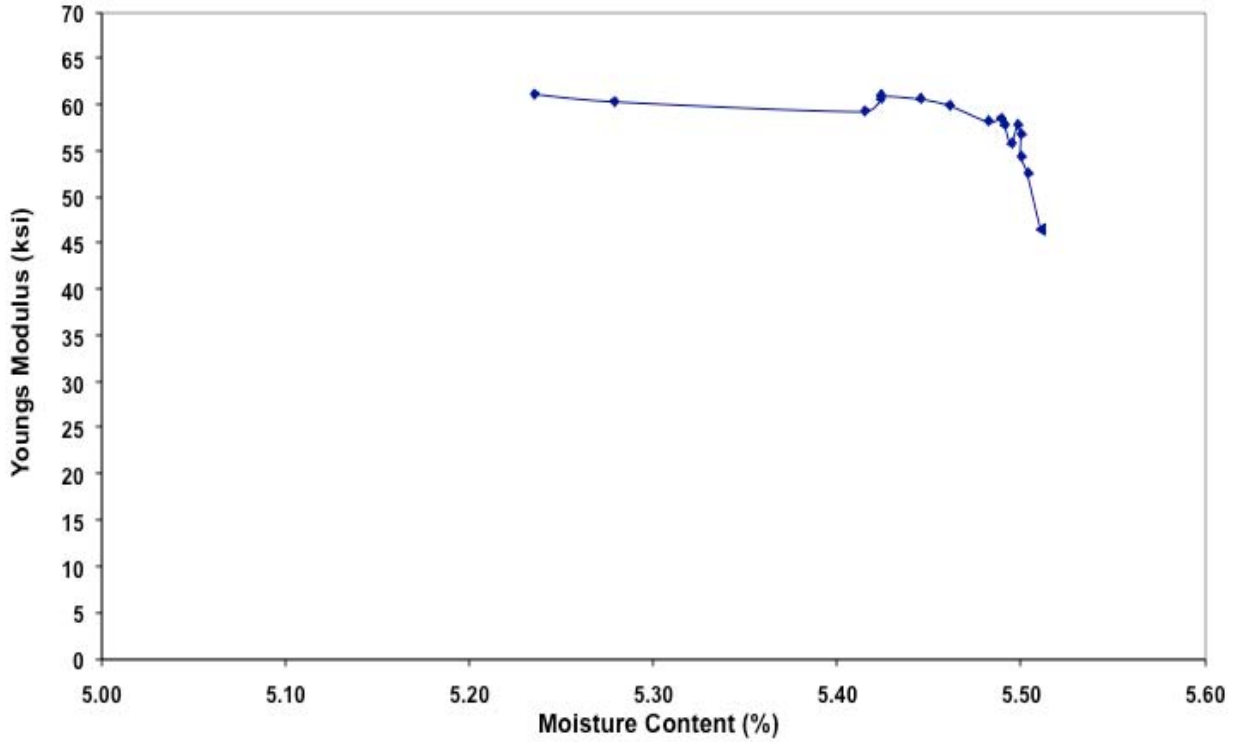

Figure F-10. Variation of Young's modulus with moisture content, replicate 1, constant moisture.

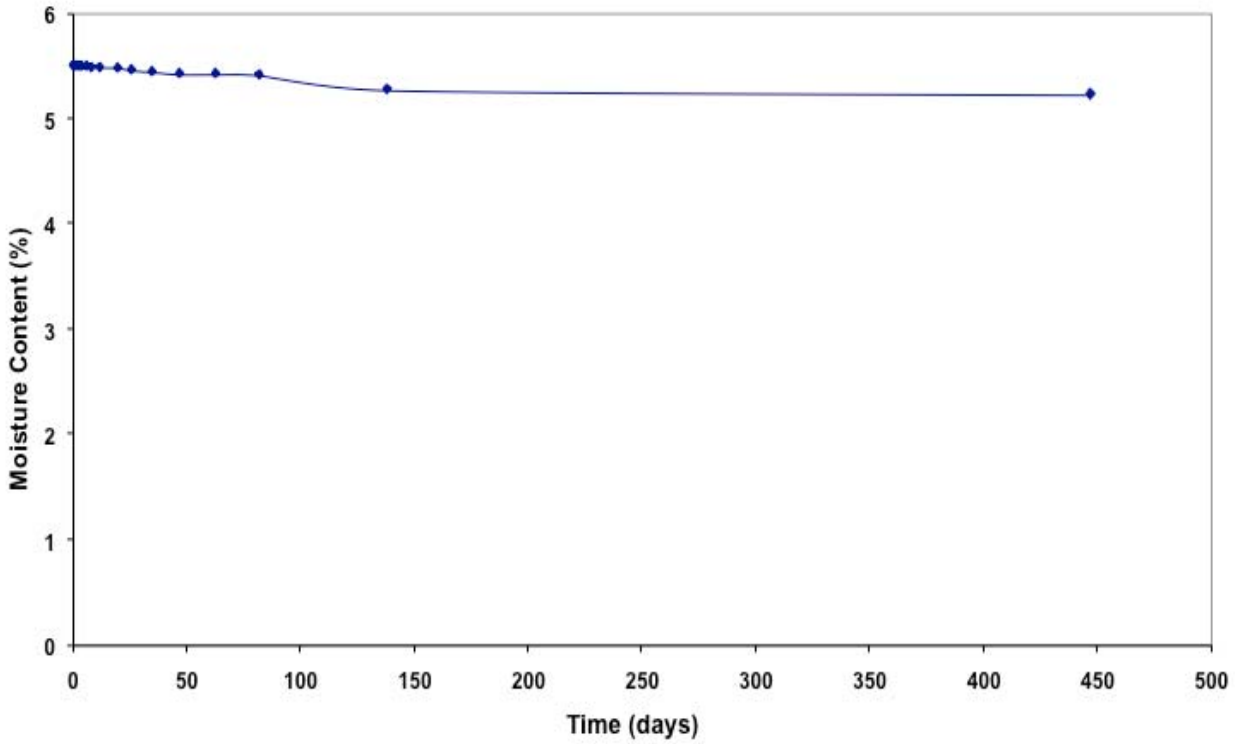

Figure F-11. Variation of moisture content with time, replicate 1, constant moisture.

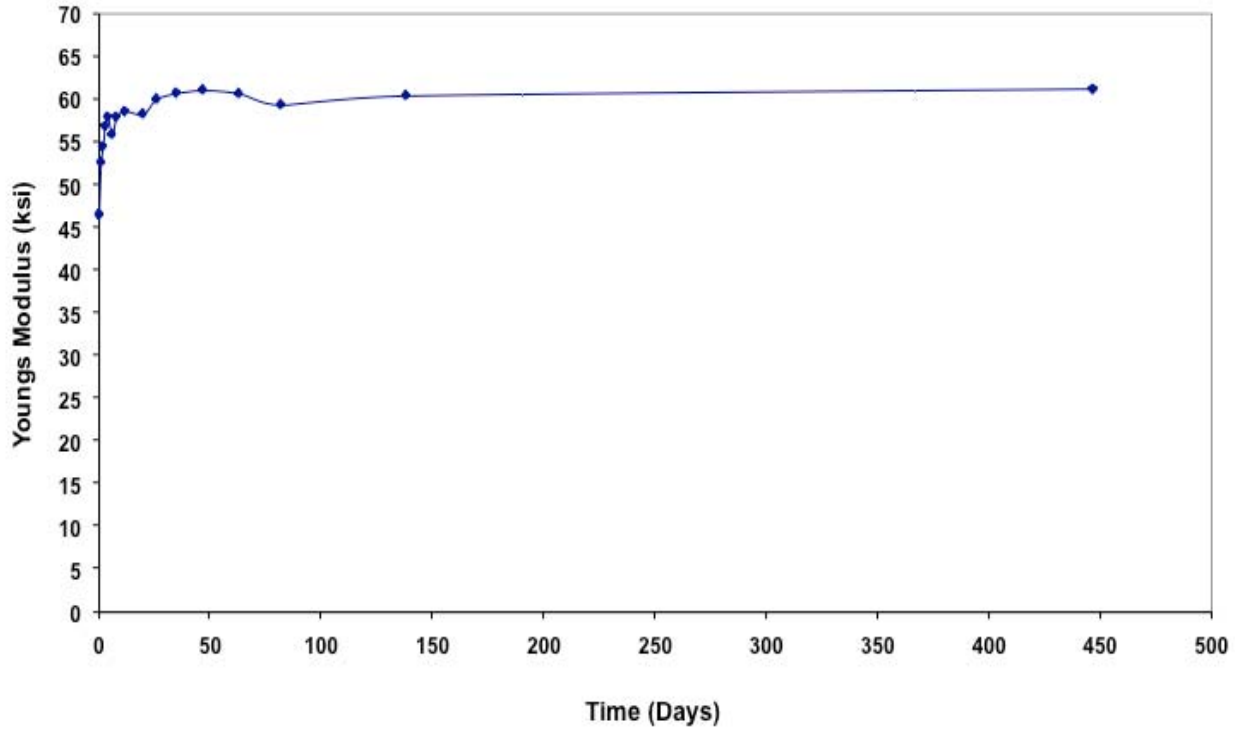

Figure F-12. Variation of Young's modulus with time, replicate 1, constant moisture.

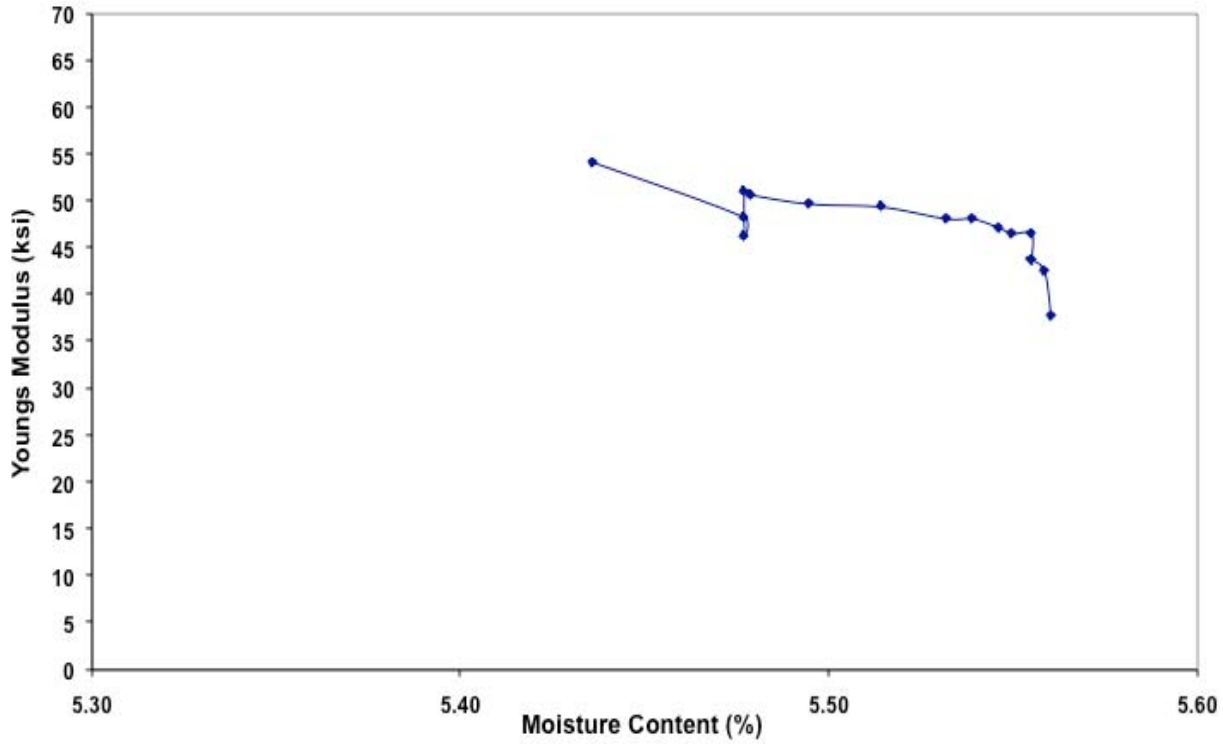

Figure F-13. Variation of Young's modulus with moisture content, replicate 2, constant moisture.

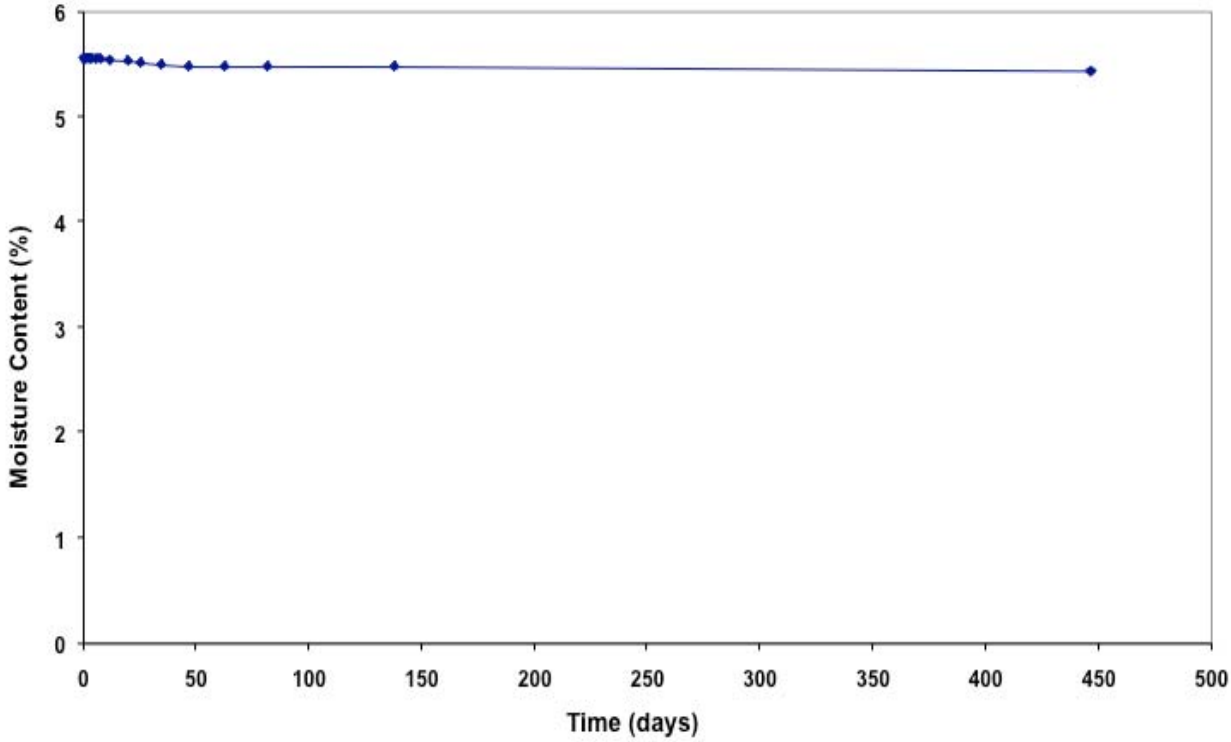

Figure F-14. Variation of moisture content with time, replicate 2, constant moisture.

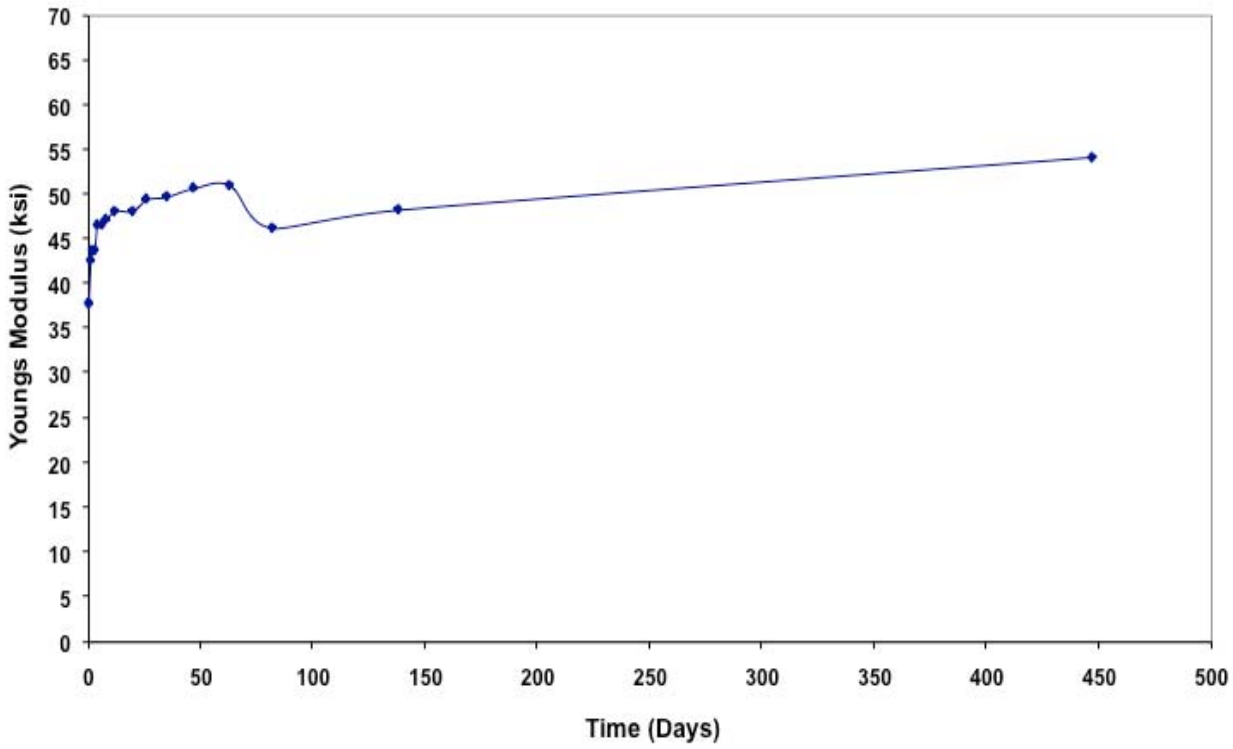

Figure F-15. Variation of Young's modulus with time, replicate 2, constant moisture.

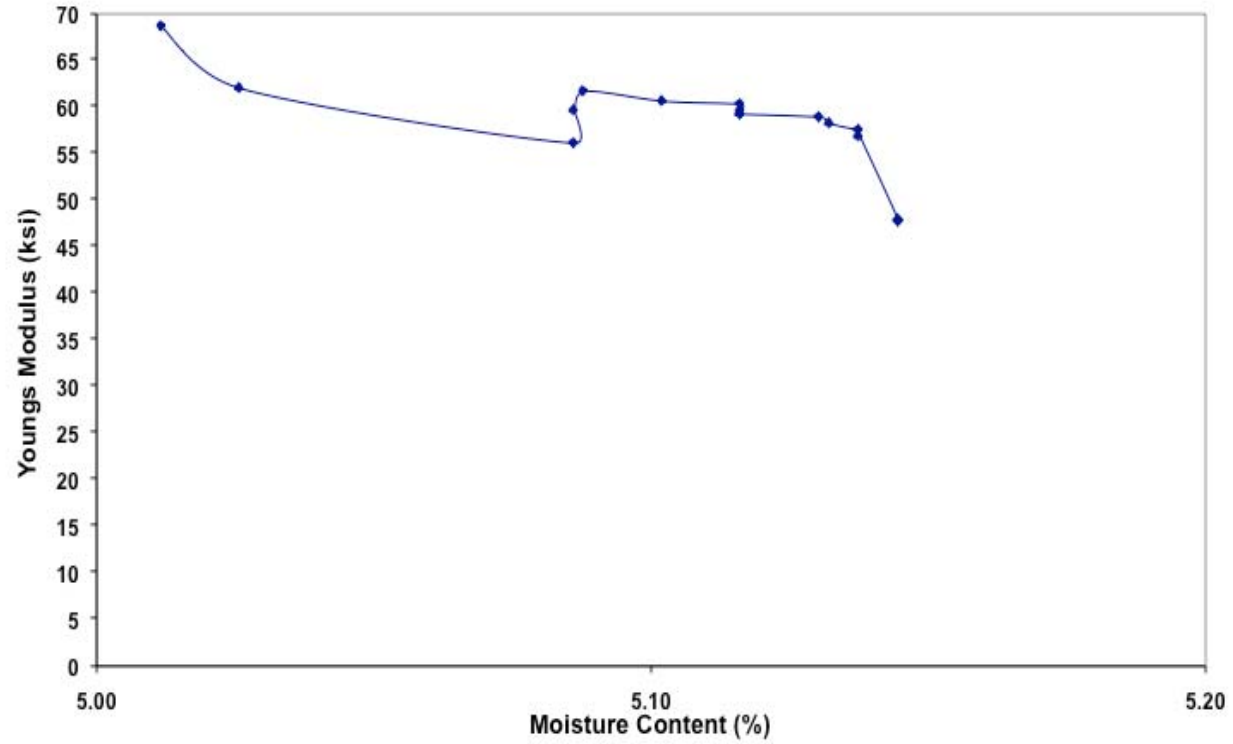

Figure F-16. Variation of Young's with Moisture Content, replicate 3, constant moisture.

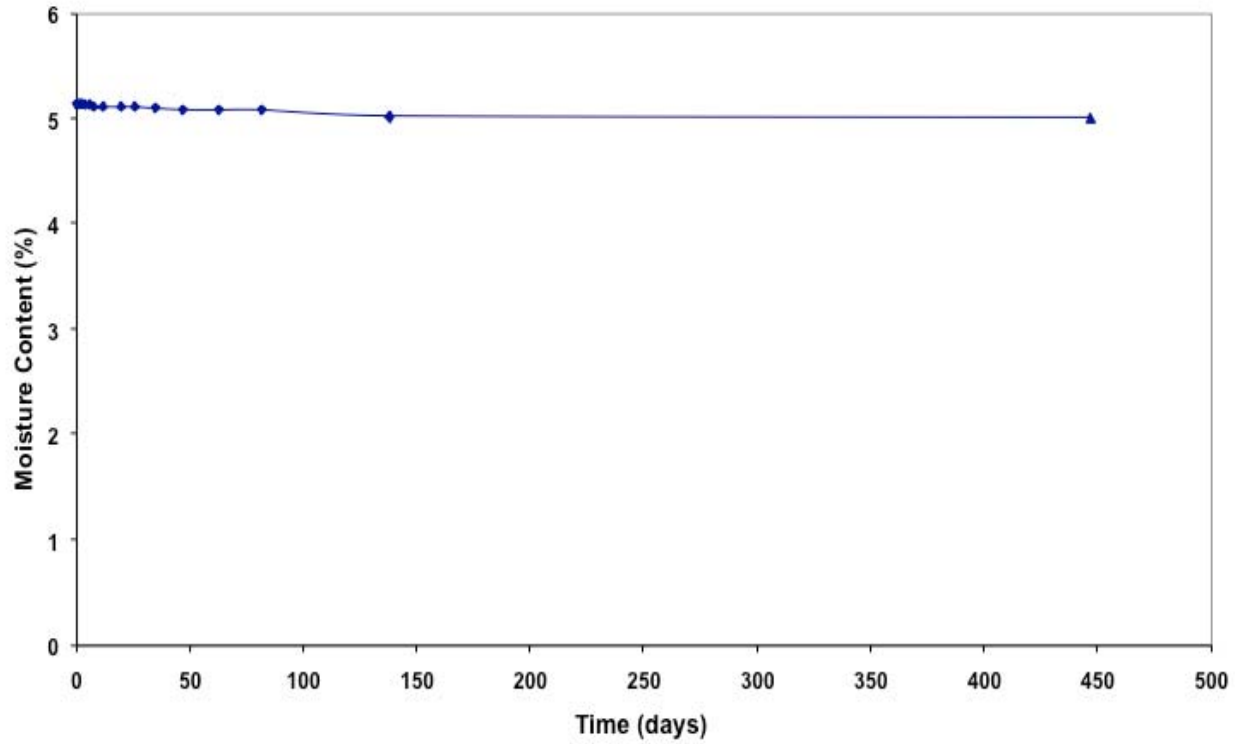

Figure F-17. Variation of moisture content with time, replicate 3, constant moisture.

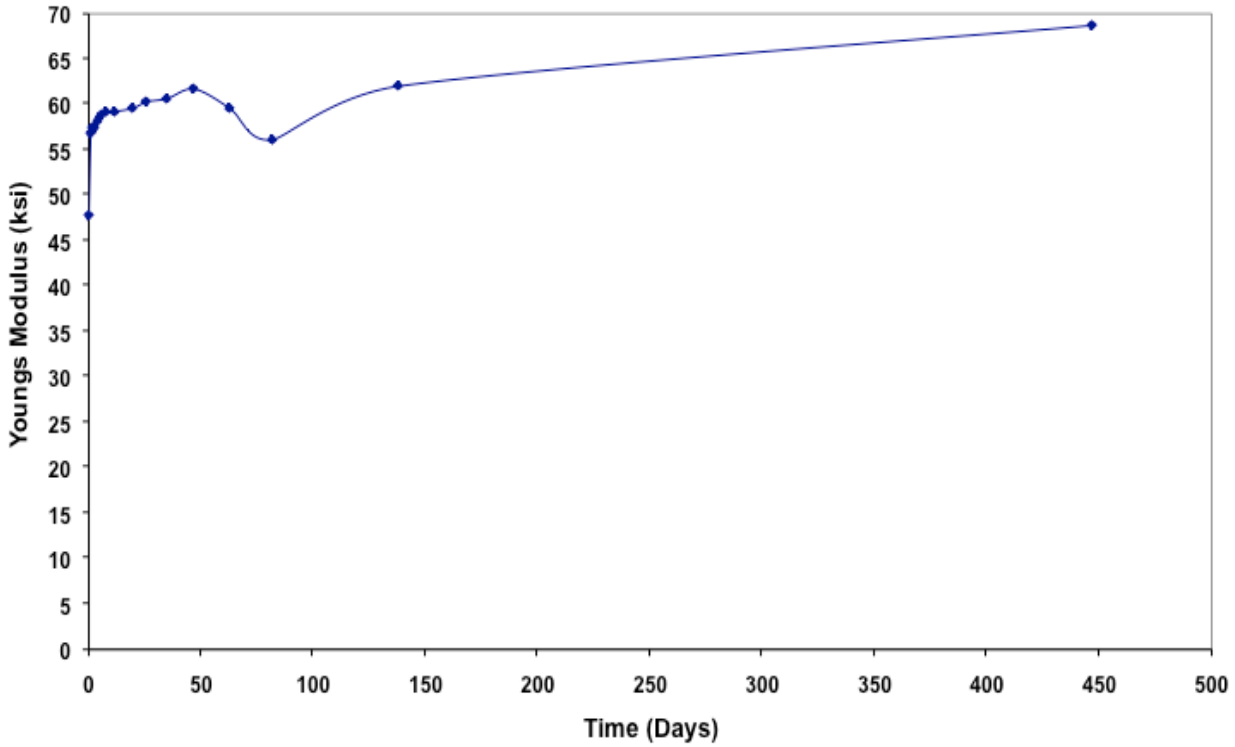

Figure F-18. Variation of Young's modulus with time, replicate 3, constant moisture.

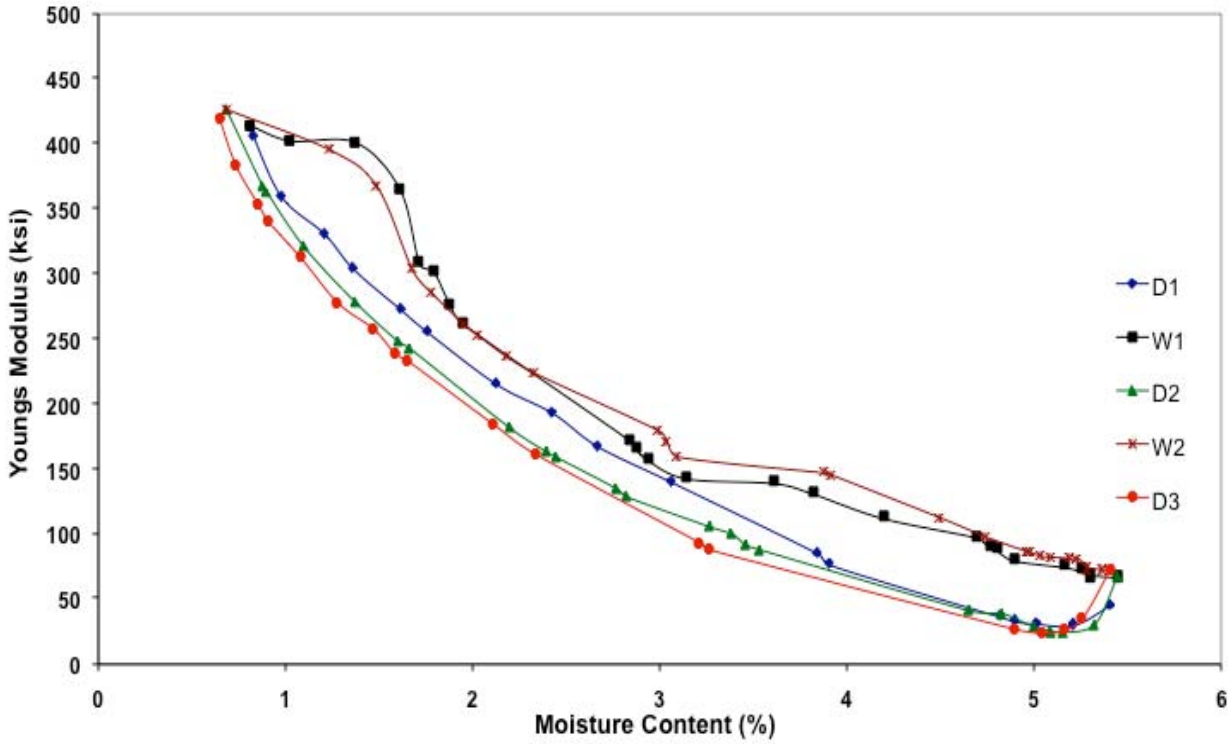

Figure F-19. Variation of Young's modulus with moisture content, replicate 1, wetting and drying.

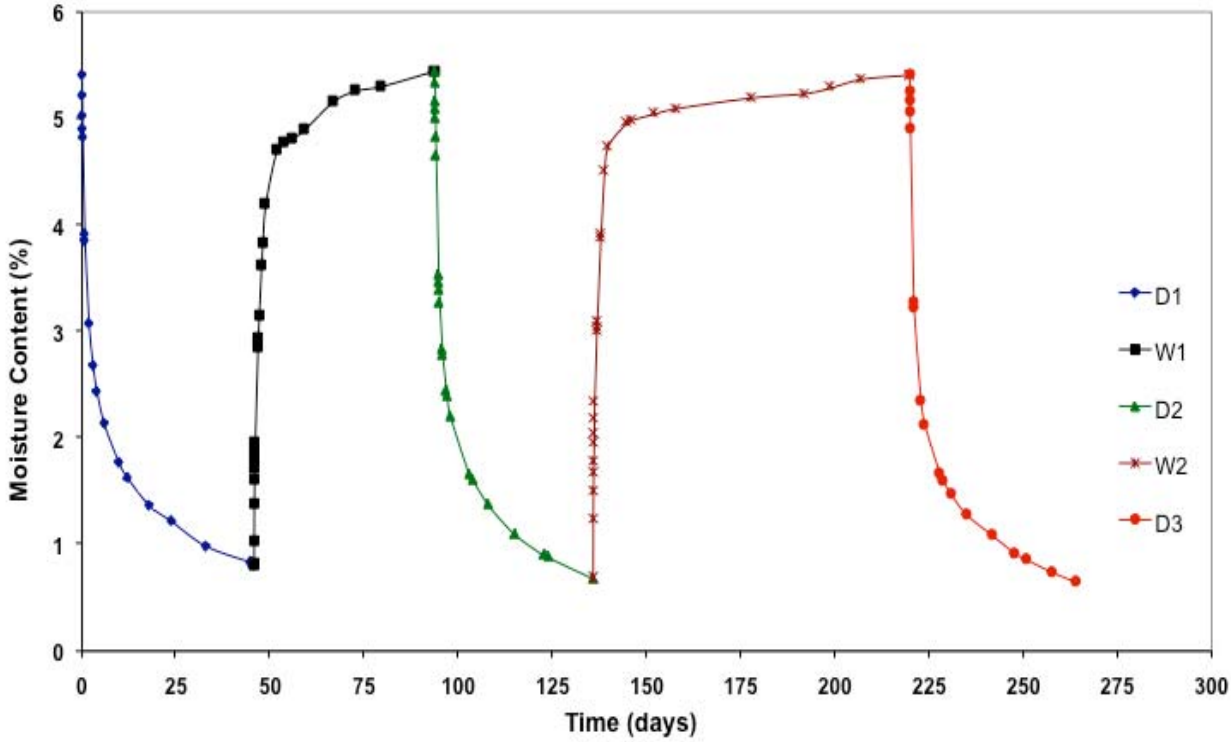

Figure F-20. Variation of moisture content with time, replicate 1, wetting and drying.

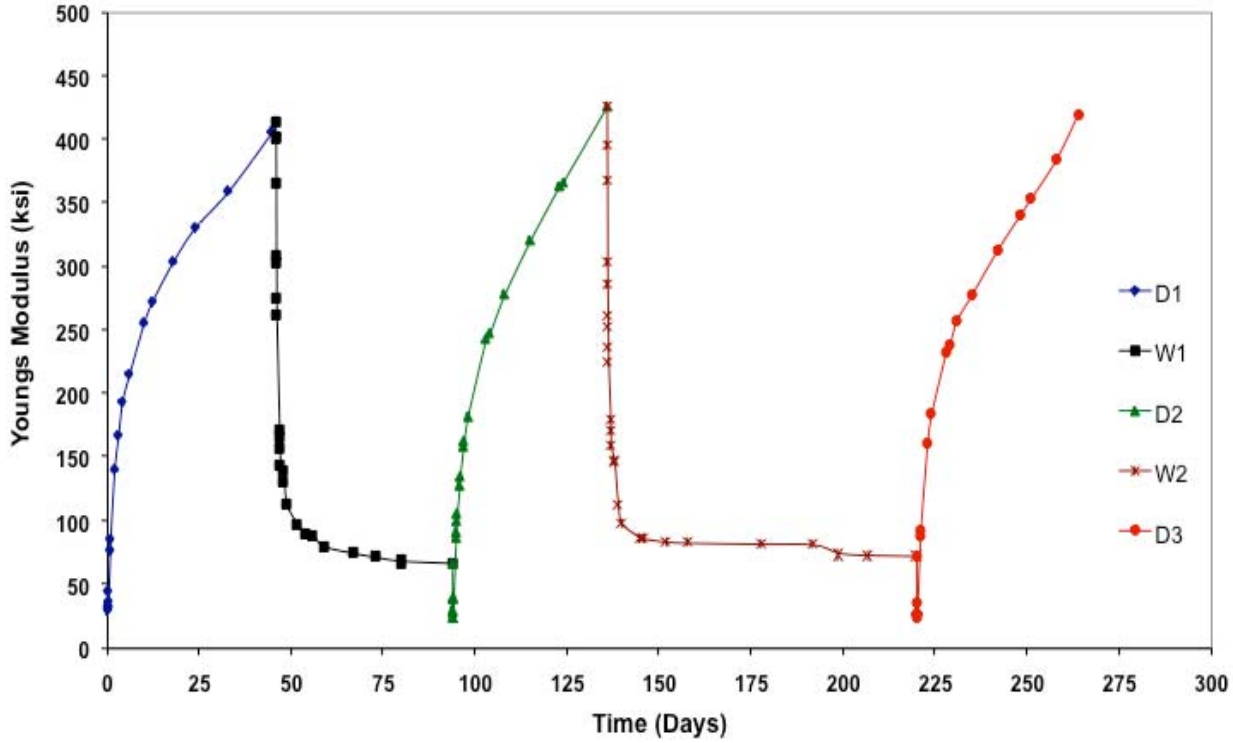

Figure F-21. Variation of Young's modulus with time, replicate 1, wetting and drying.

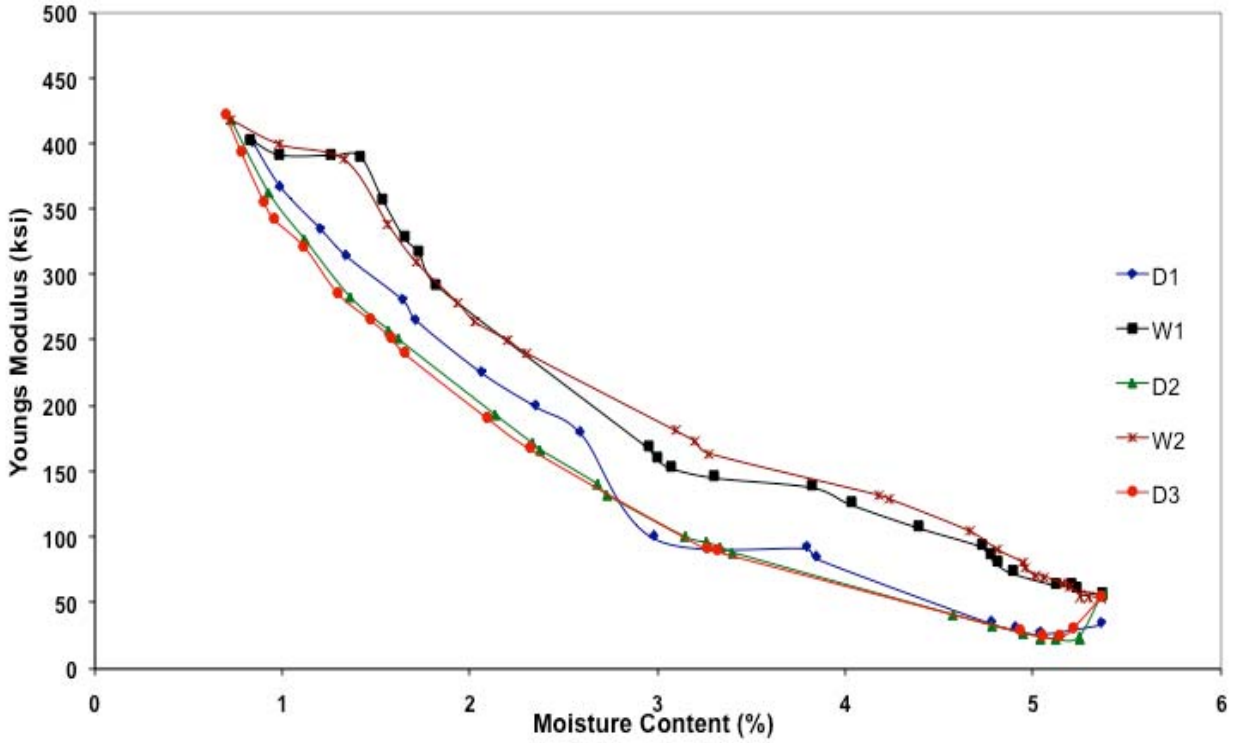

Figure F-22. Variation of Young's modulus with moisture content, replicate 2, wetting and drying.

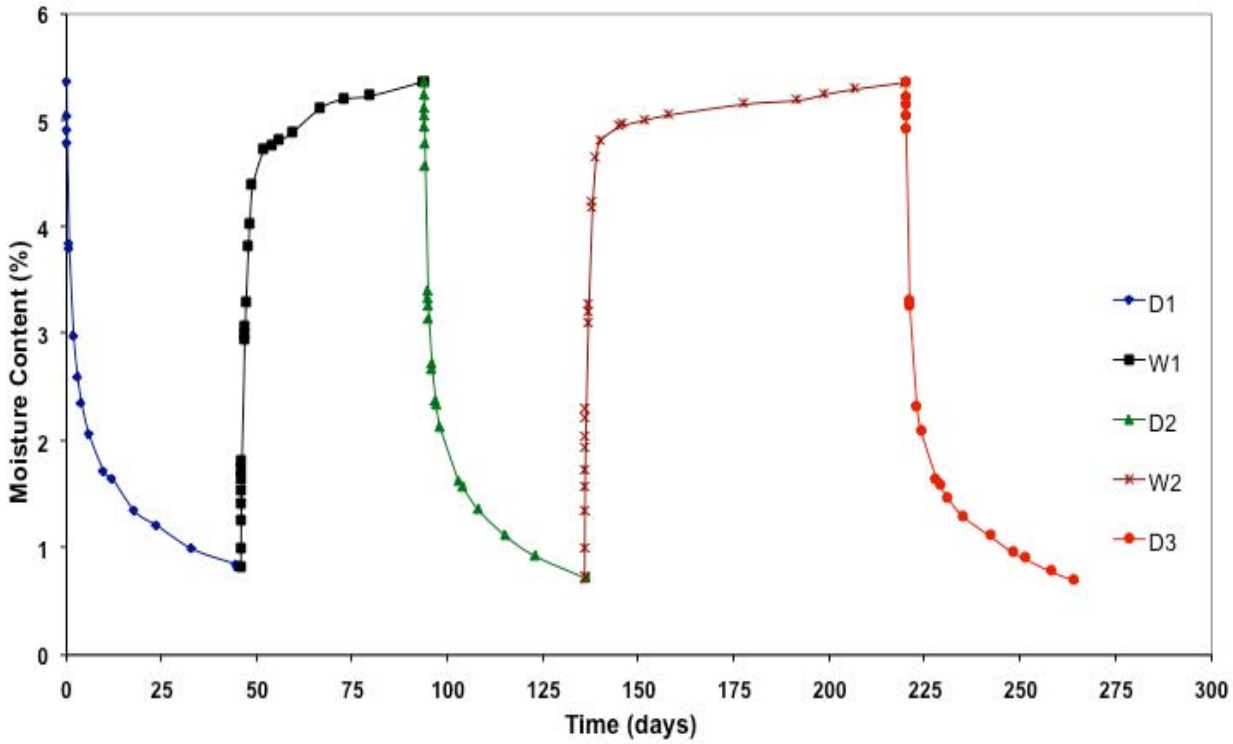

Figure F-23. Variation of moisture content with time, replicate 2, wetting and drying.

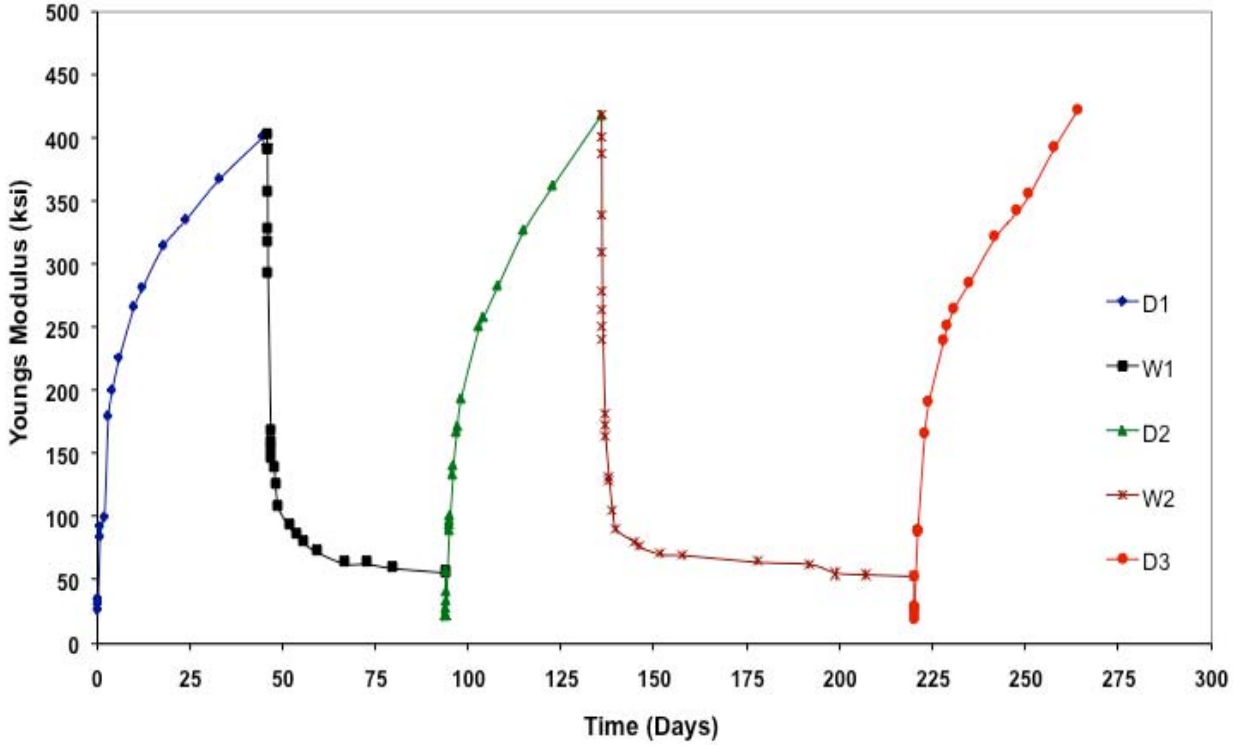

Figure F-24. Variation of Young's modulus with time, replicate 2, wetting and drying.

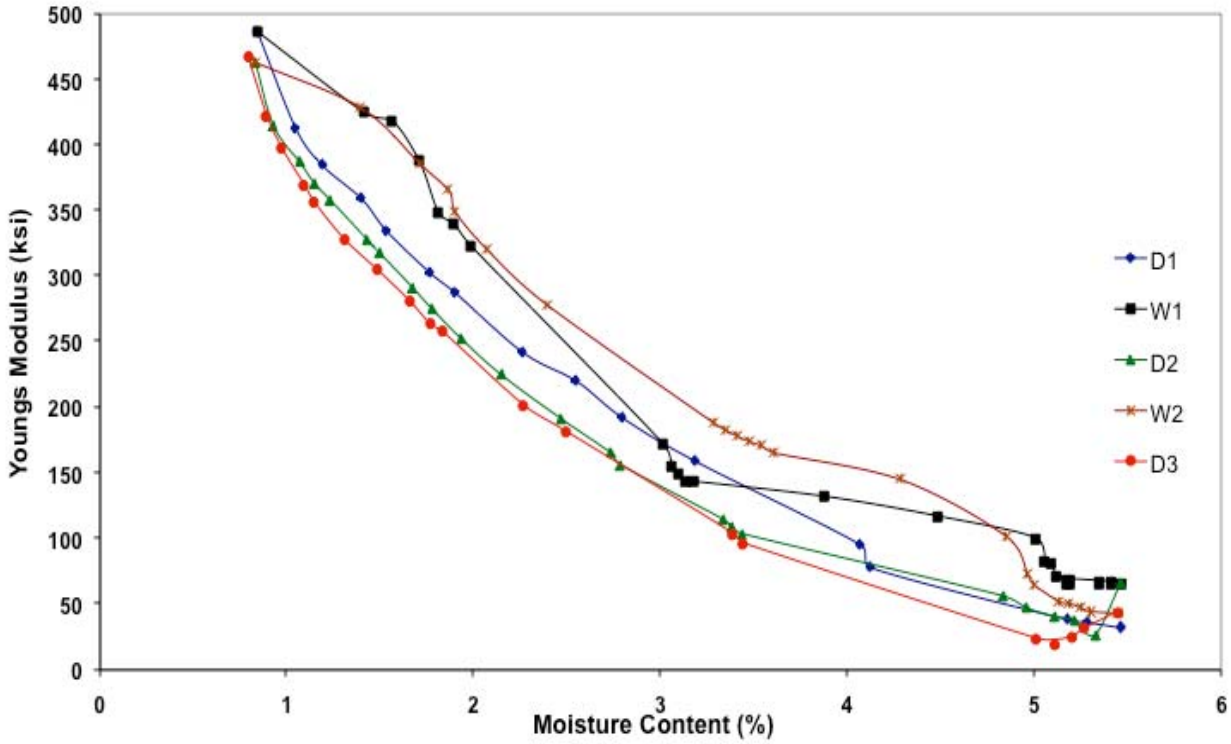

Figure F-25. Variation of Young's modulus with moisture content, replicate 3, wetting and drying.

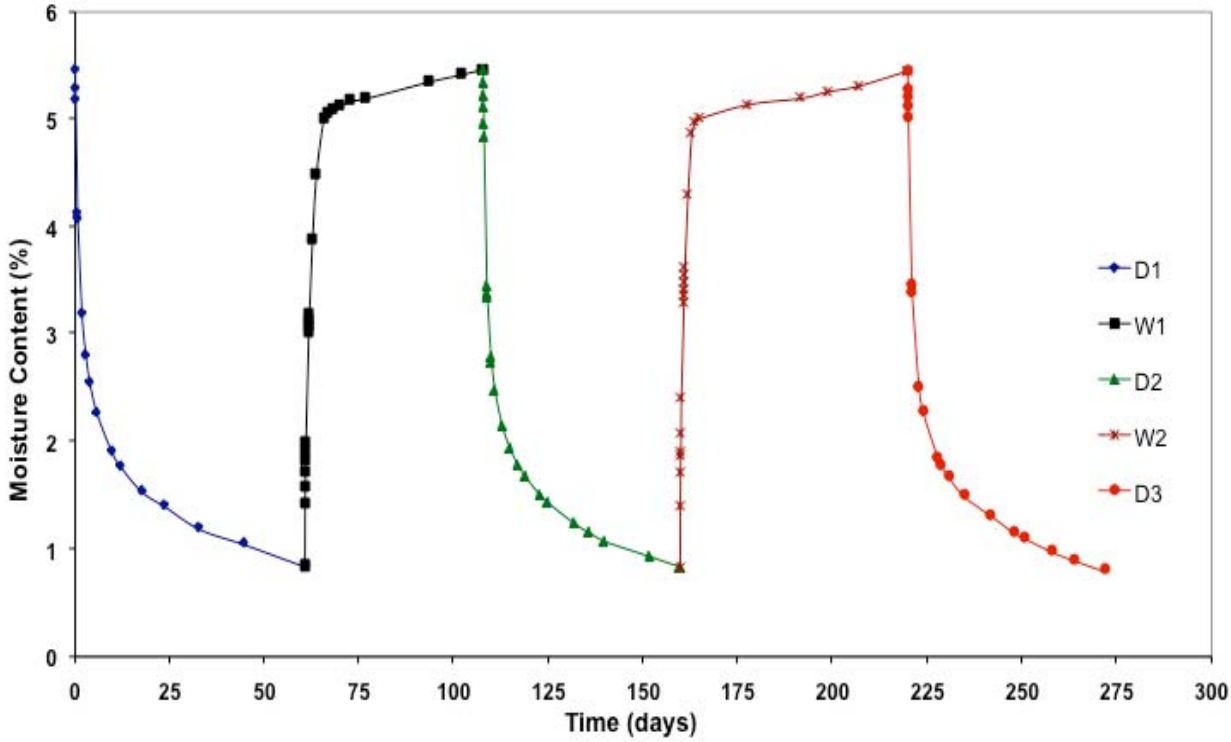

Figure F-26. Variation of moisture content with time, replicate 3, wetting and drying.

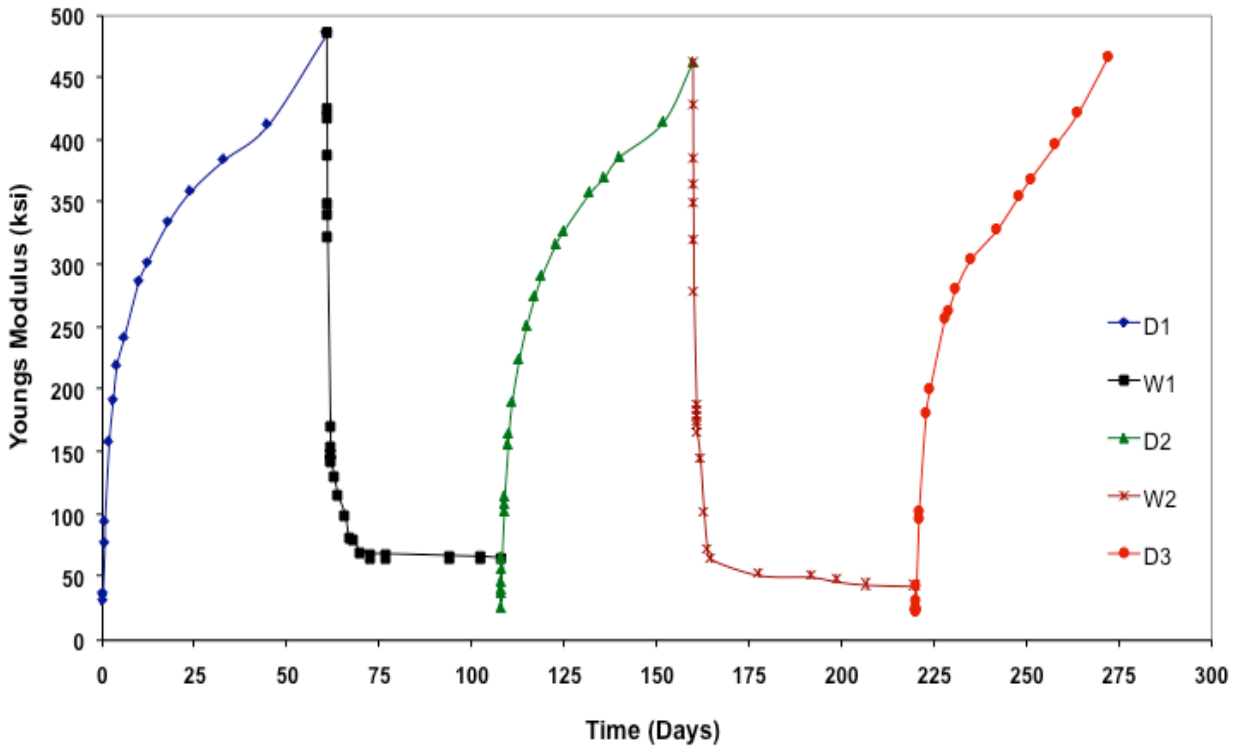

Figure F-27. Variation of Young's modulus with time, replicate 3, wetting and drying.

APPENDIX G
CORE MATERIALS INDIVIDUAL SMALL-STRAIN MODULUS TEST RESULTS

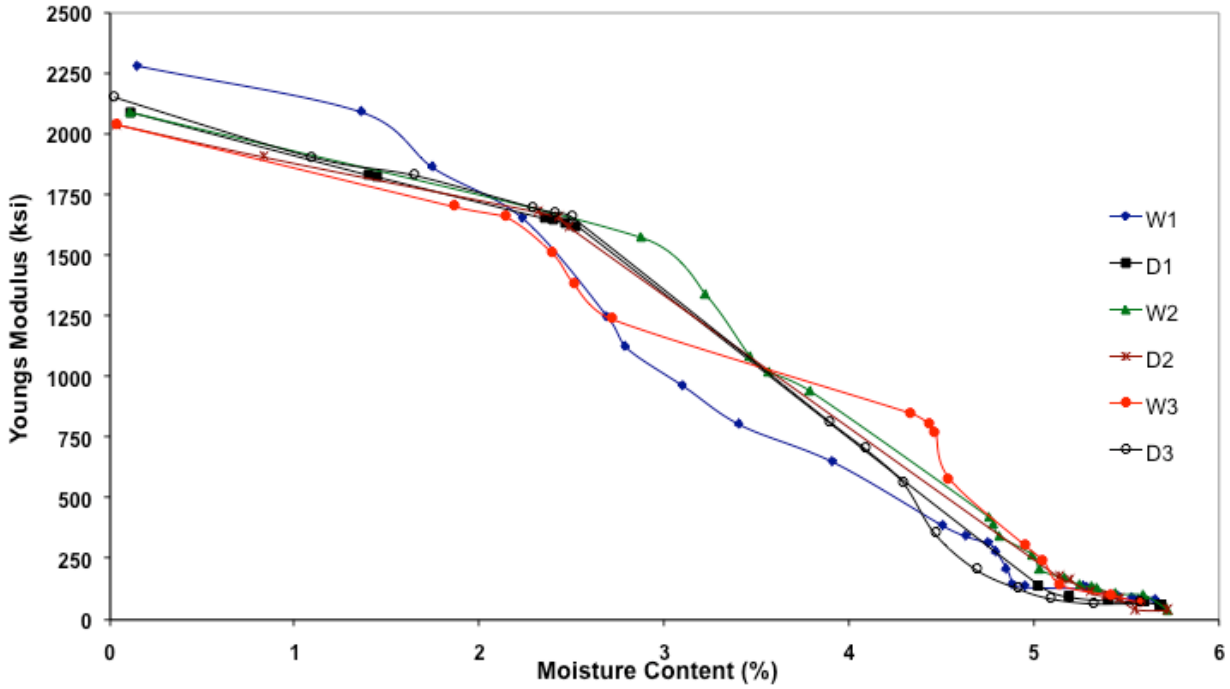

Figure G-1. Variation of Young's modulus with moisture content, field core 1, wetting and drying.

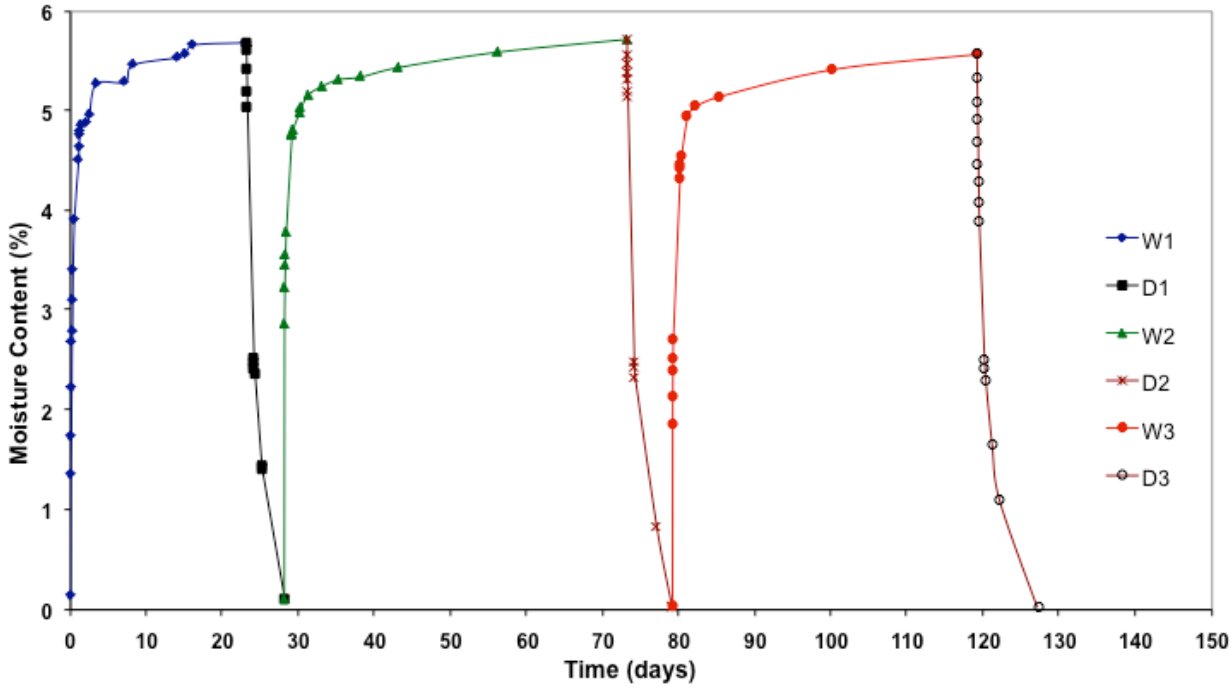

Figure G-2. Variation of moisture content with time, field core 1, wetting and drying.

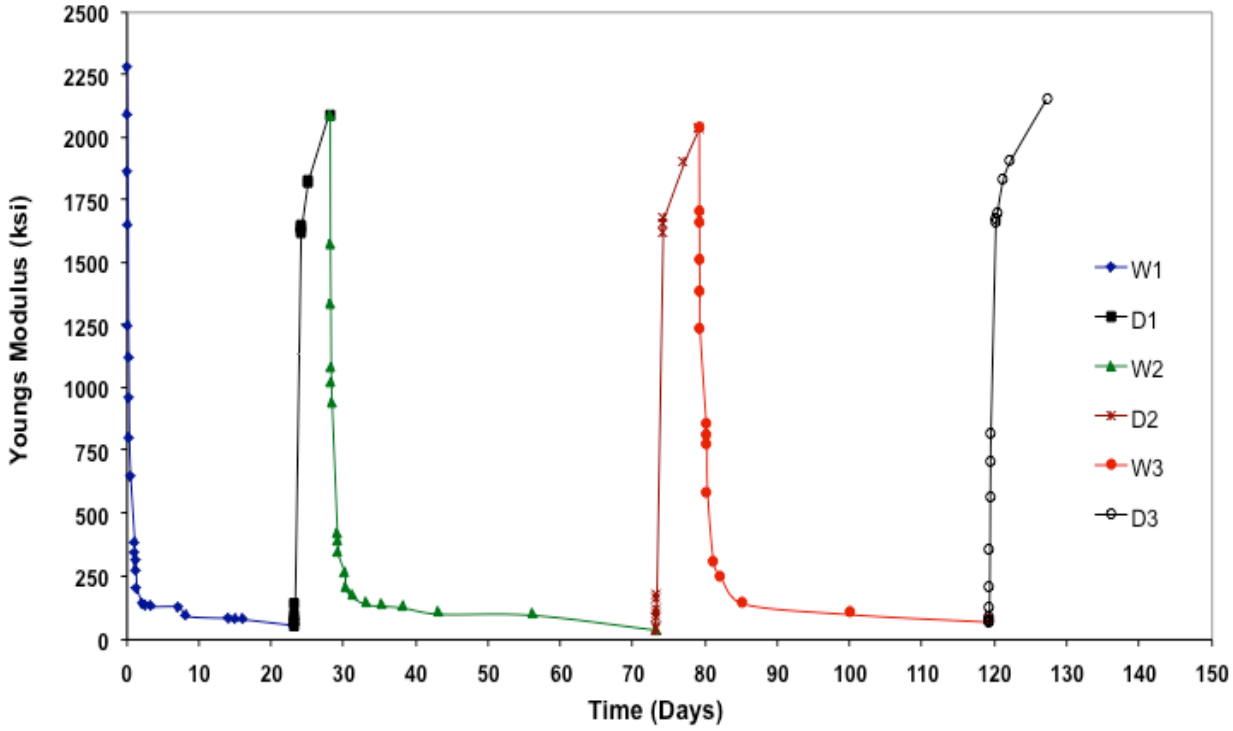

Figure G-3. Variation of Young's modulus with time, field core 1, wetting and drying.

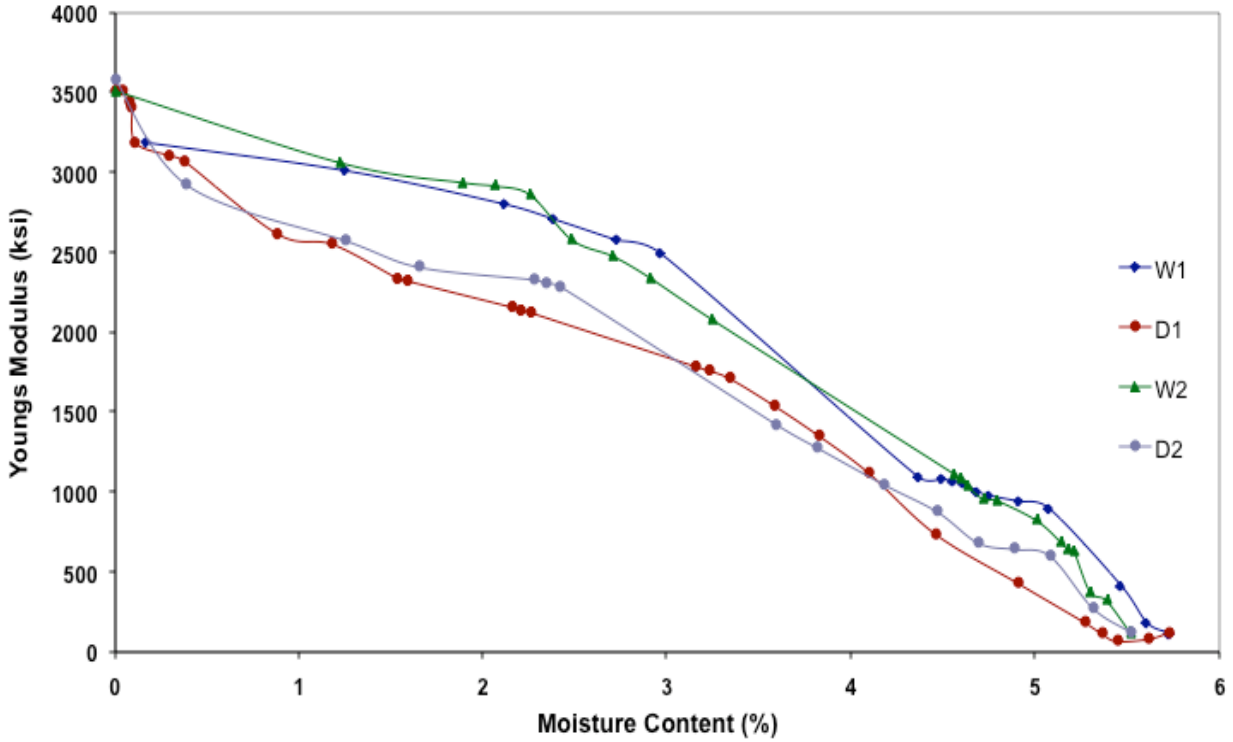

Figure G-4. Variation of Young's modulus with moisture content, field core 2, wetting and drying.

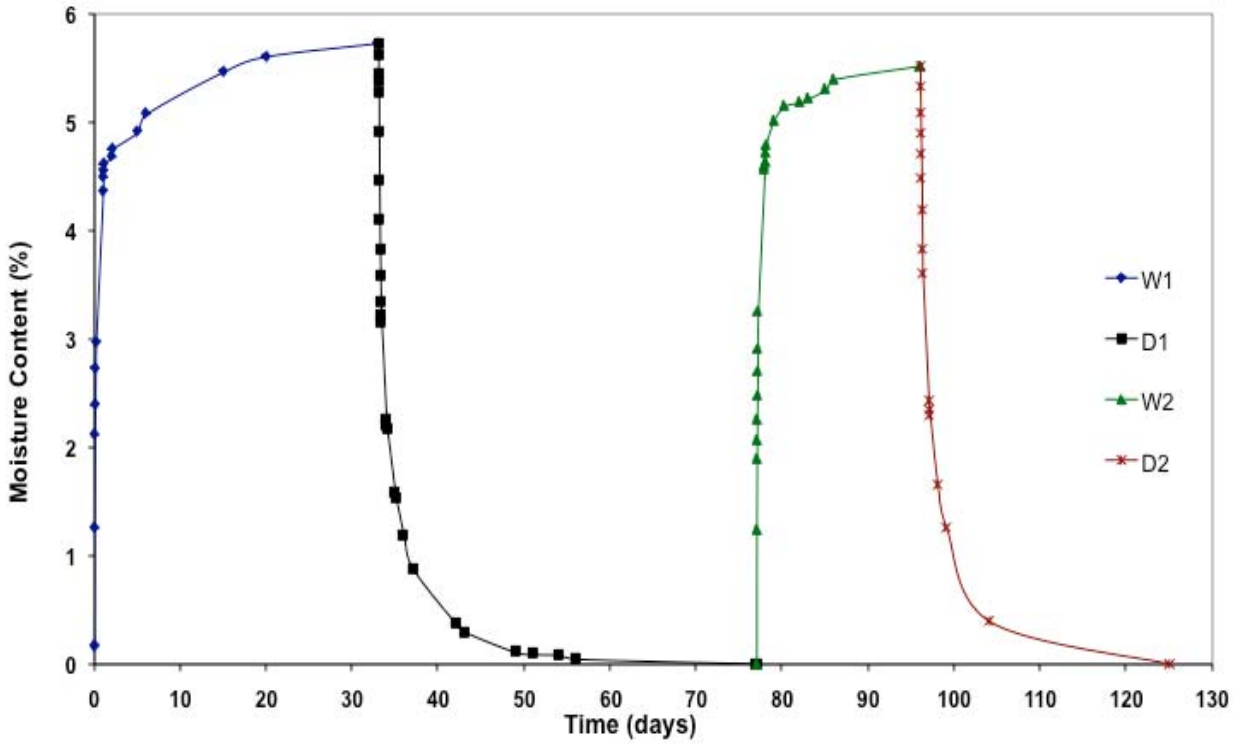

Figure G-5. Variation of moisture content with time, field core 2, wetting and drying.

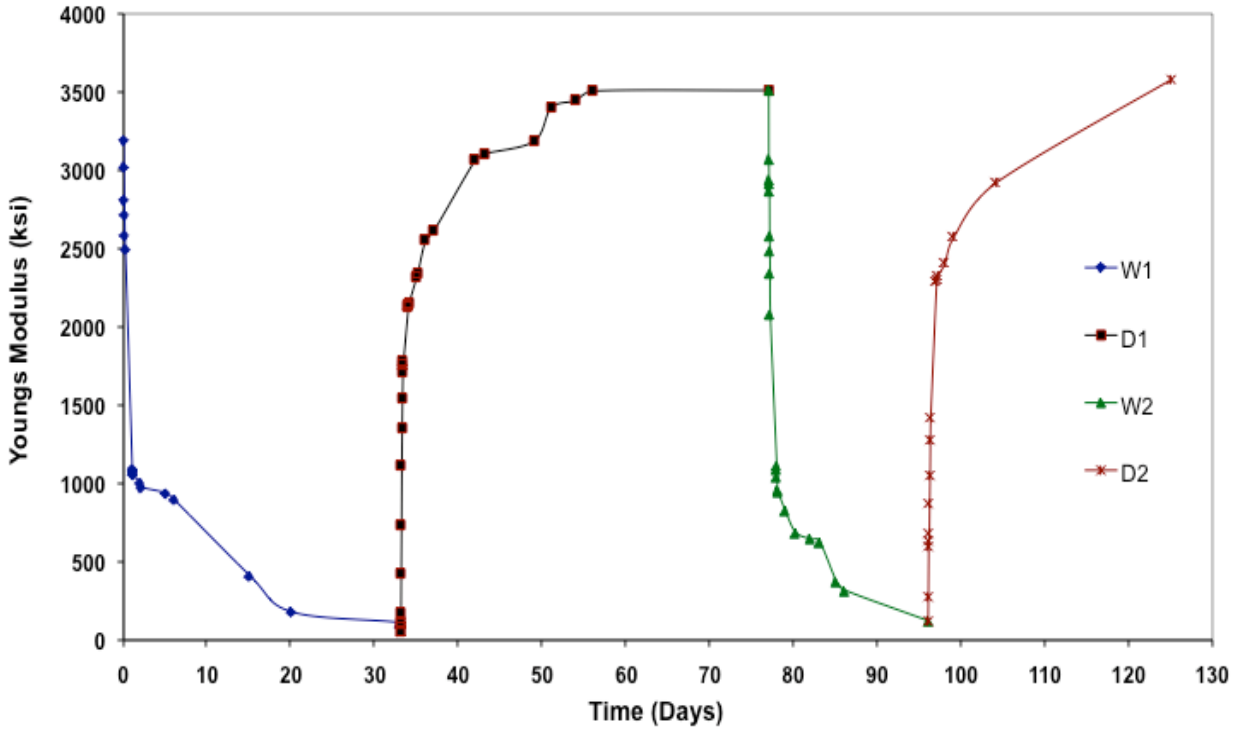

Figure G-6. Variation of Young's modulus with time, field core 2, wetting and drying.

APPENDIX H
COMPARISON OF SMALL-STRAIN MODULUS TEST RESULTS

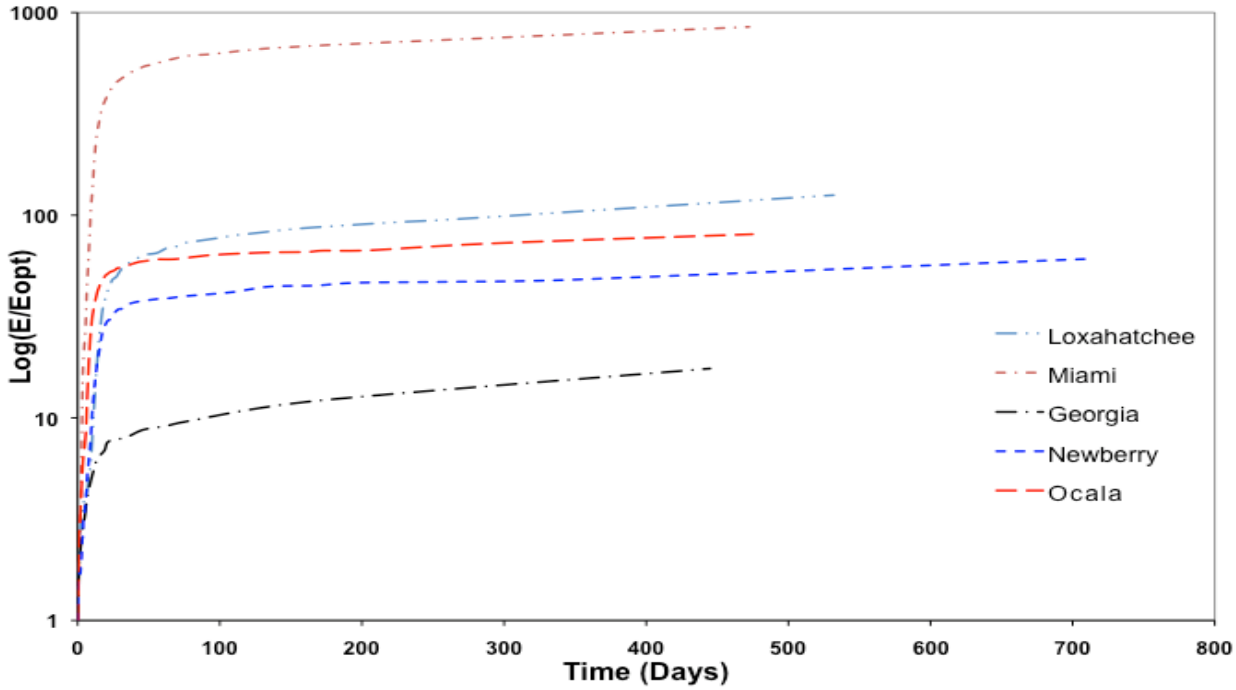

Figure H-1. Variation of rate of change in small-strain modulus with time, replicate 1, laboratory ambient.

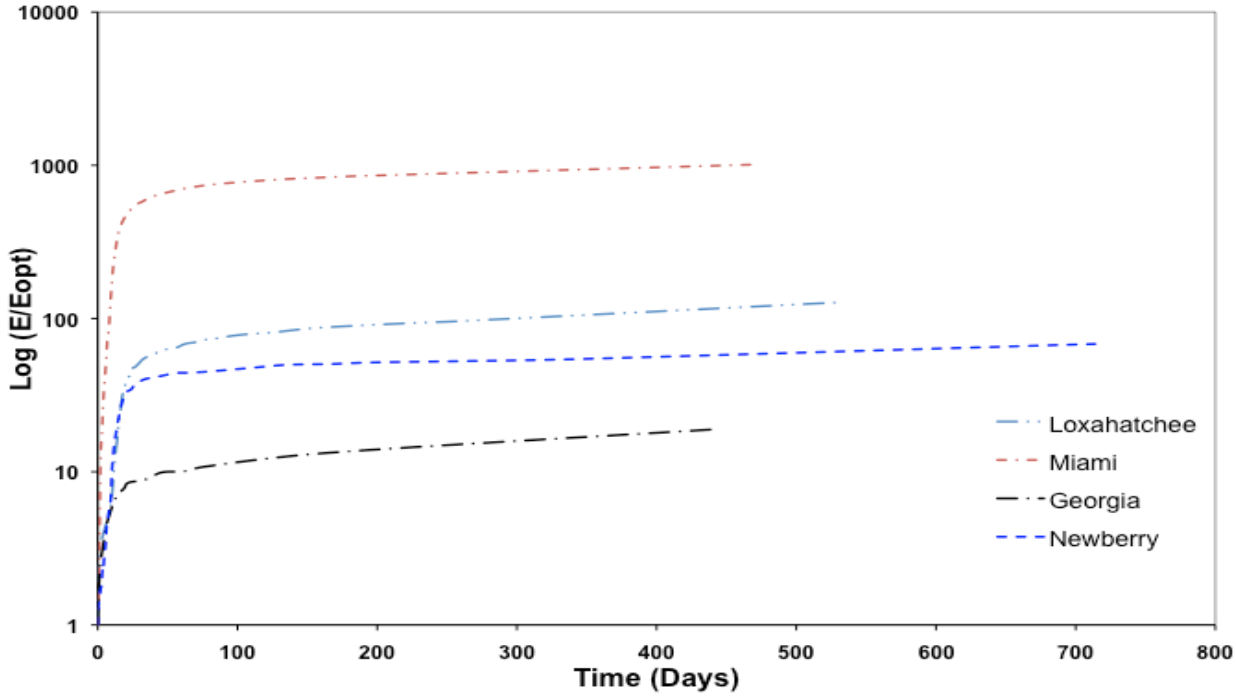

Figure H-2. Variation of rate of change in small-strain modulus with time, replicate 2, laboratory ambient.

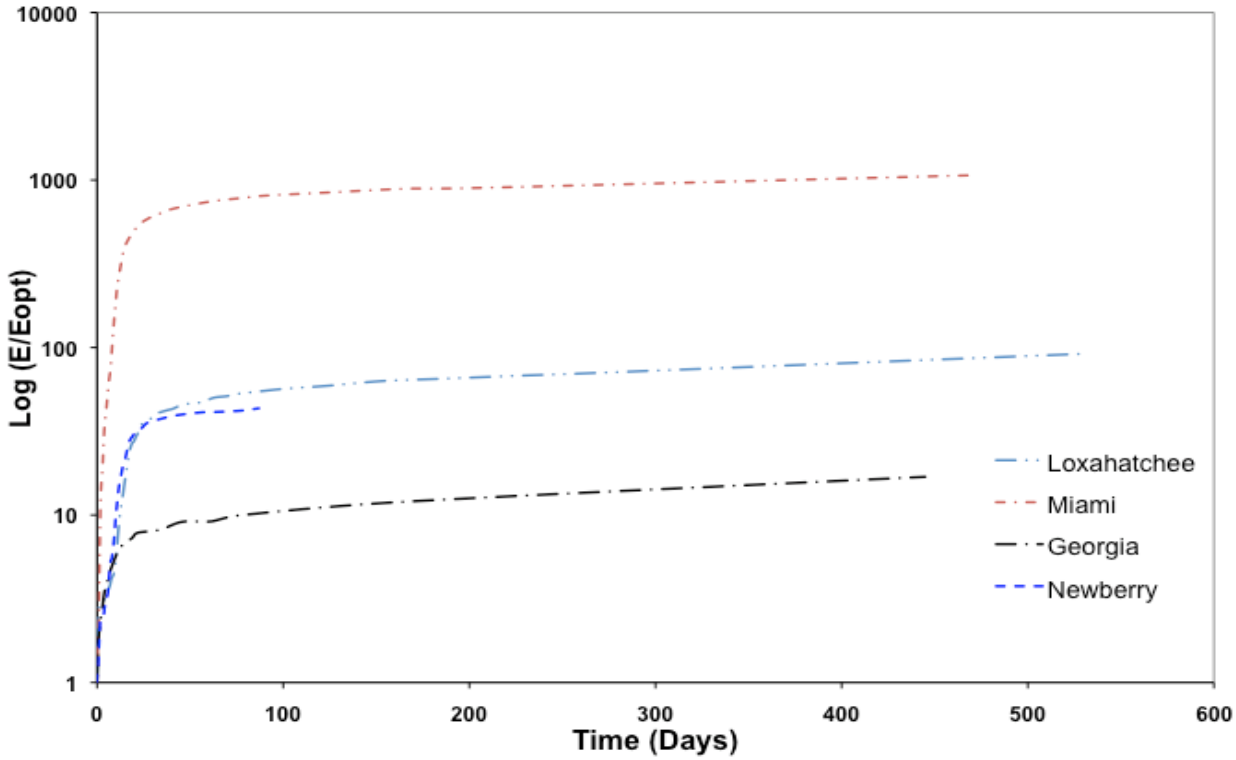

Figure H-3. Variation of rate of change in small-strain modulus with time, replicate 3, laboratory ambient.

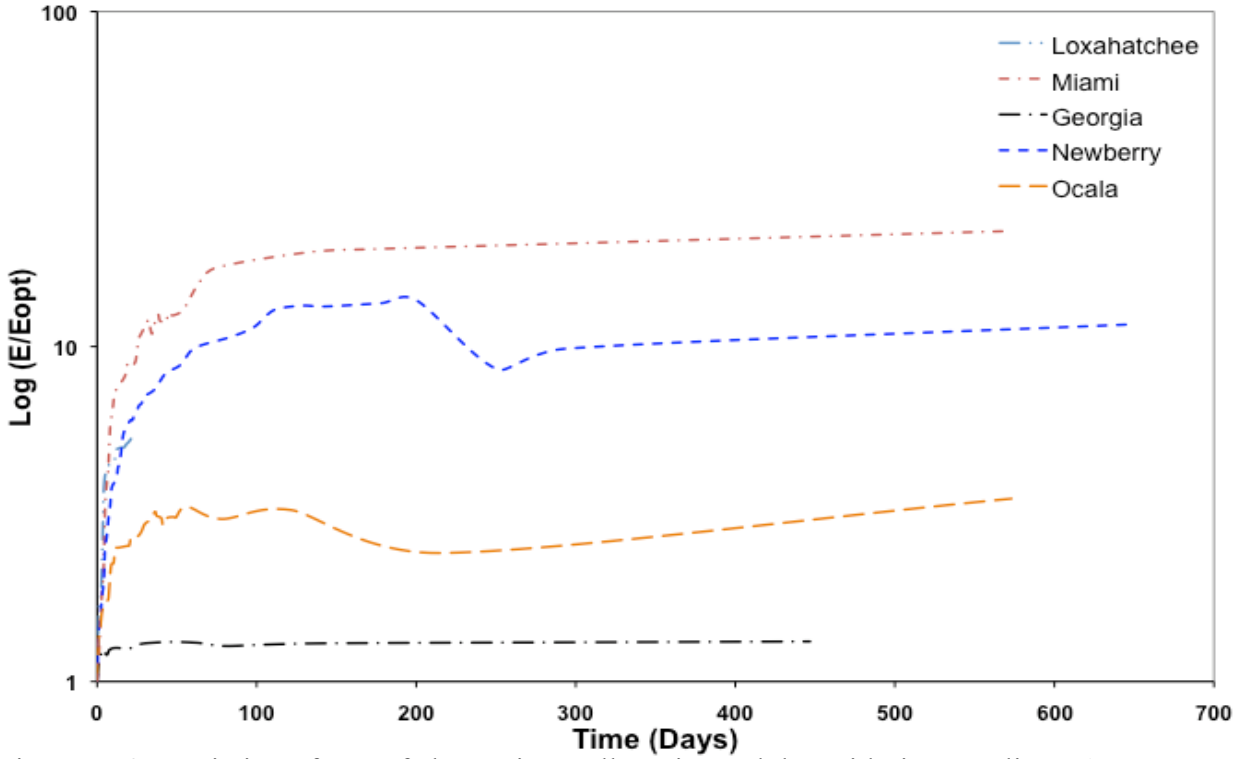

Figure H-4. Variation of rate of change in small-strain modulus with time, replicate 1, constant moisture.

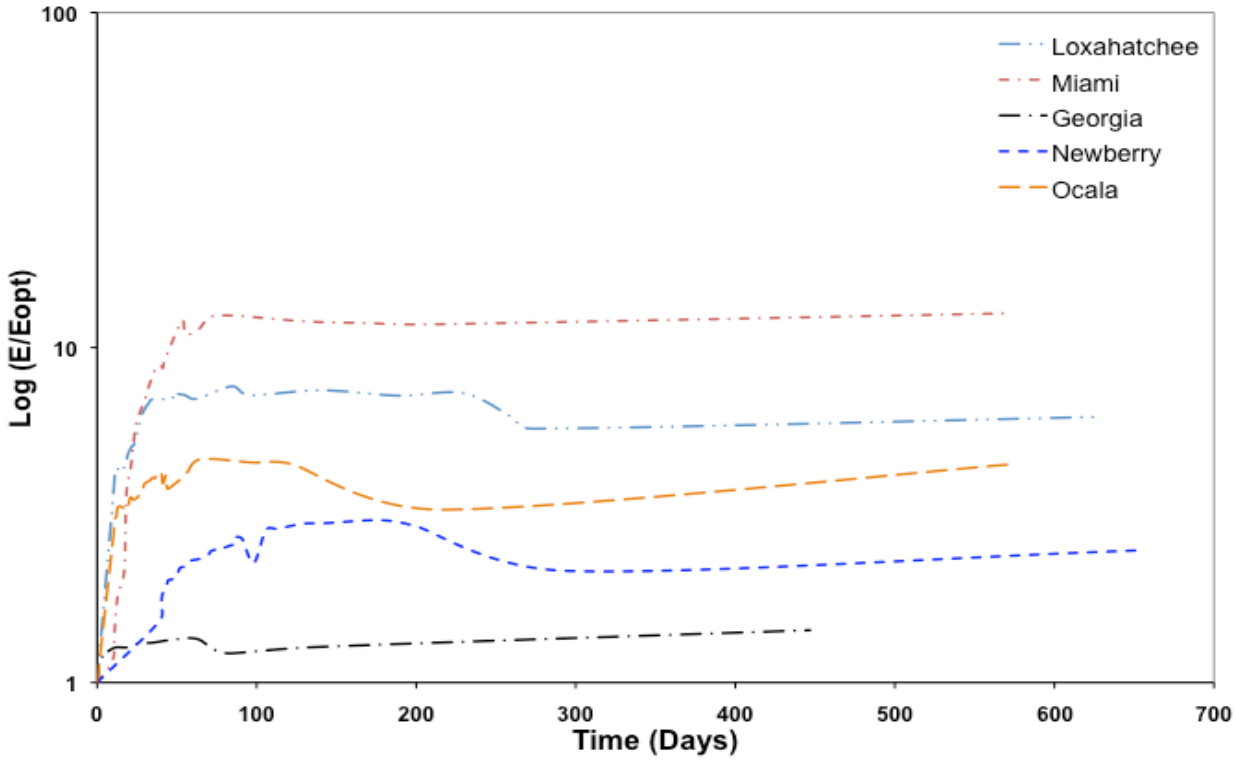

Figure H-5. Variation of rate of change in small-strain modulus with time, replicate 2, constant moisture.

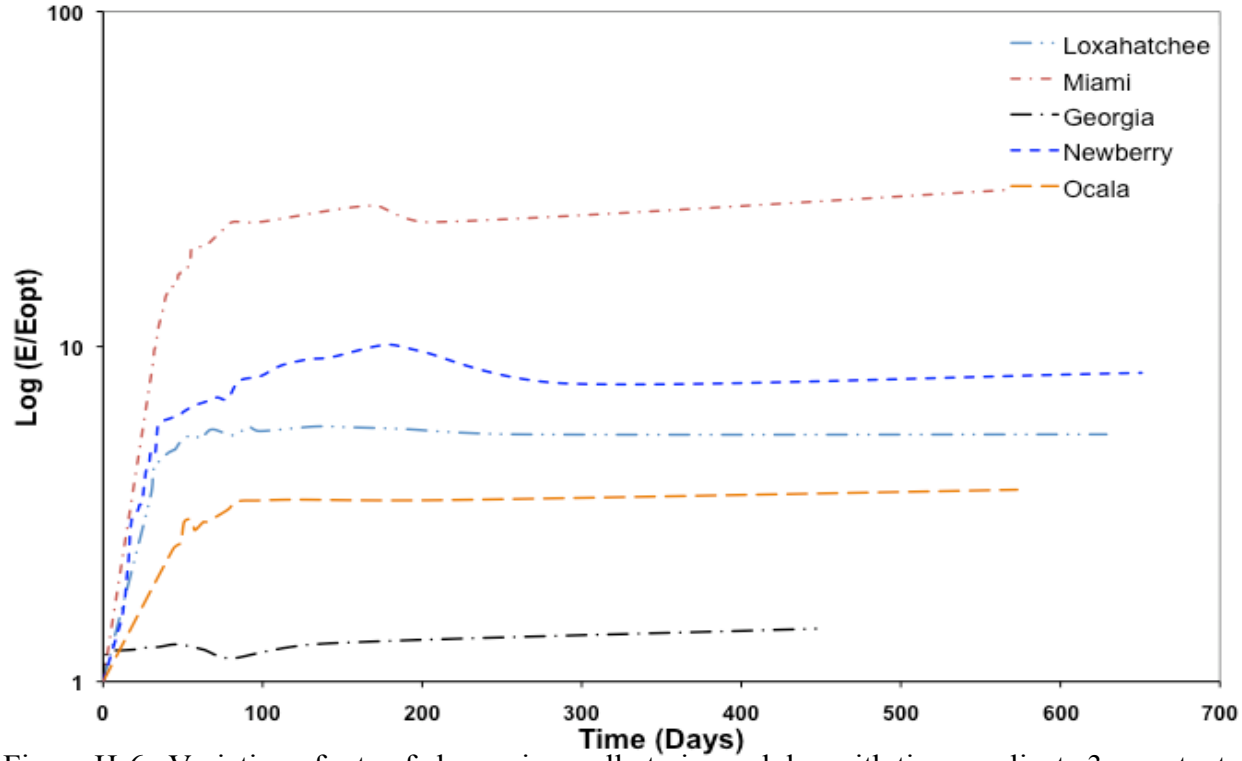

Figure H-6. Variation of rate of change in small-strain modulus with time, replicate 3, constant moisture.

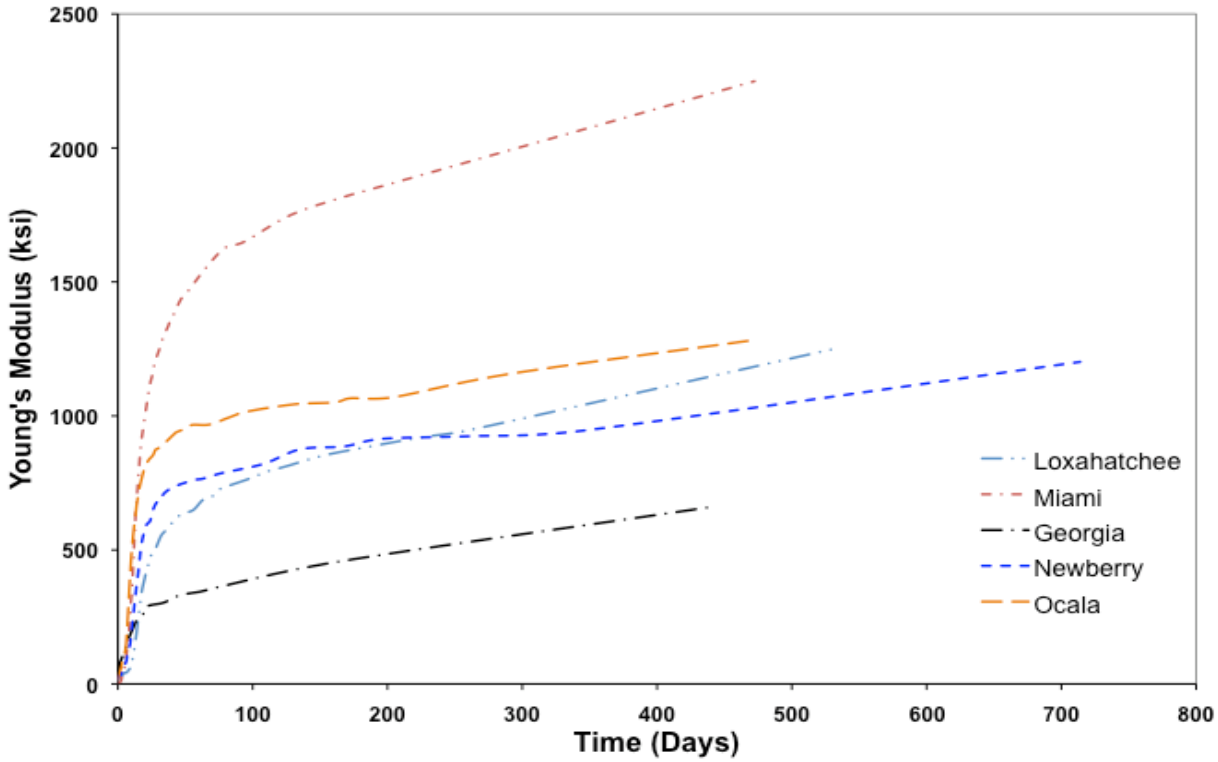

Figure H-7. Variation of Young's modulus with time, replicate 1, laboratory ambient.

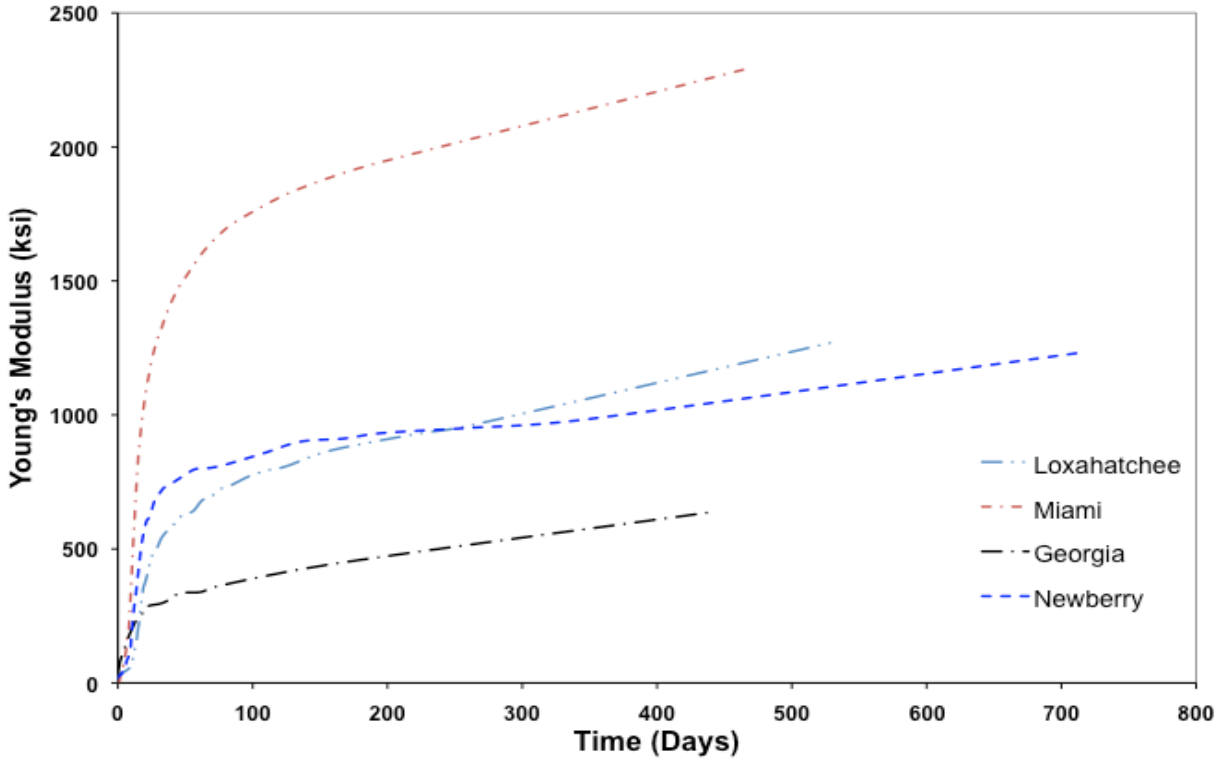

Figure H-8. Variation of Young's modulus with time, replicate 2, laboratory ambient., laboratory ambient.

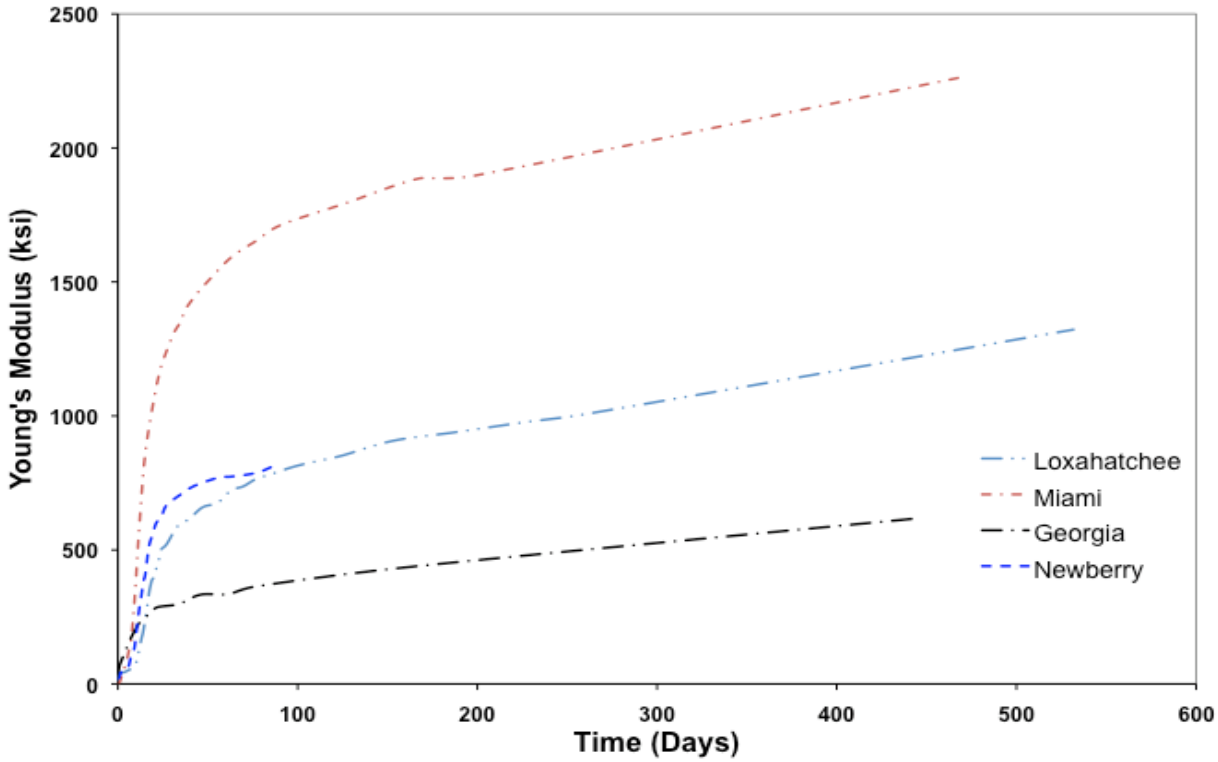

Figure H-9. Variation of Young's modulus with time, replicate 3, laboratory ambient.

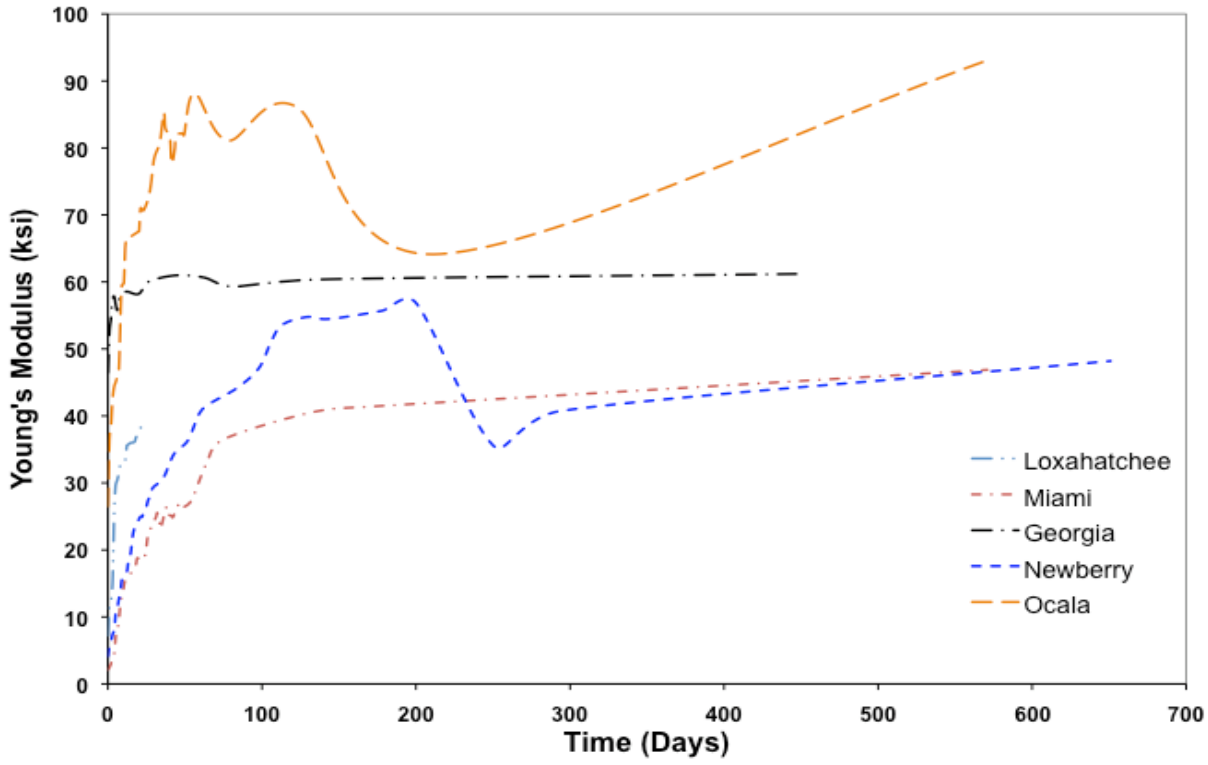

Figure H-10. Variation of Young's modulus with time, replicate 1, constant moisture.

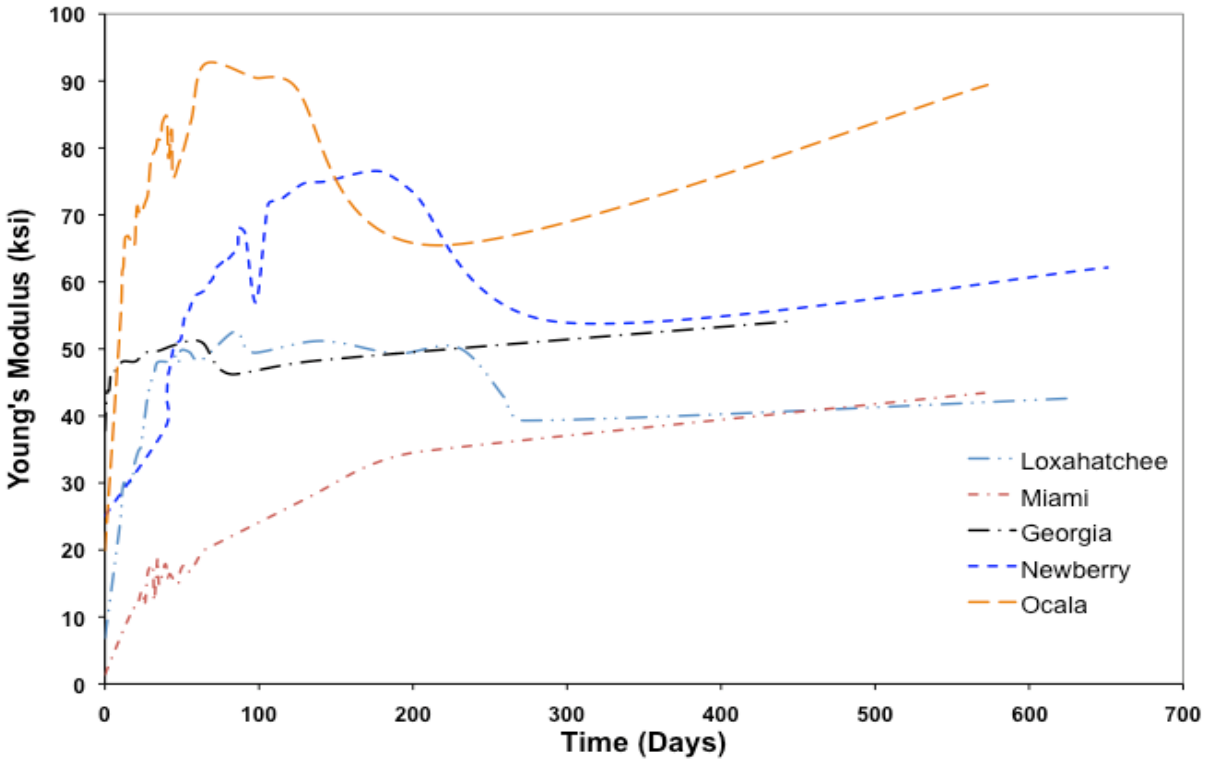

Figure H-11. Variation of Young's modulus with time, replicate 2, constant moisture.

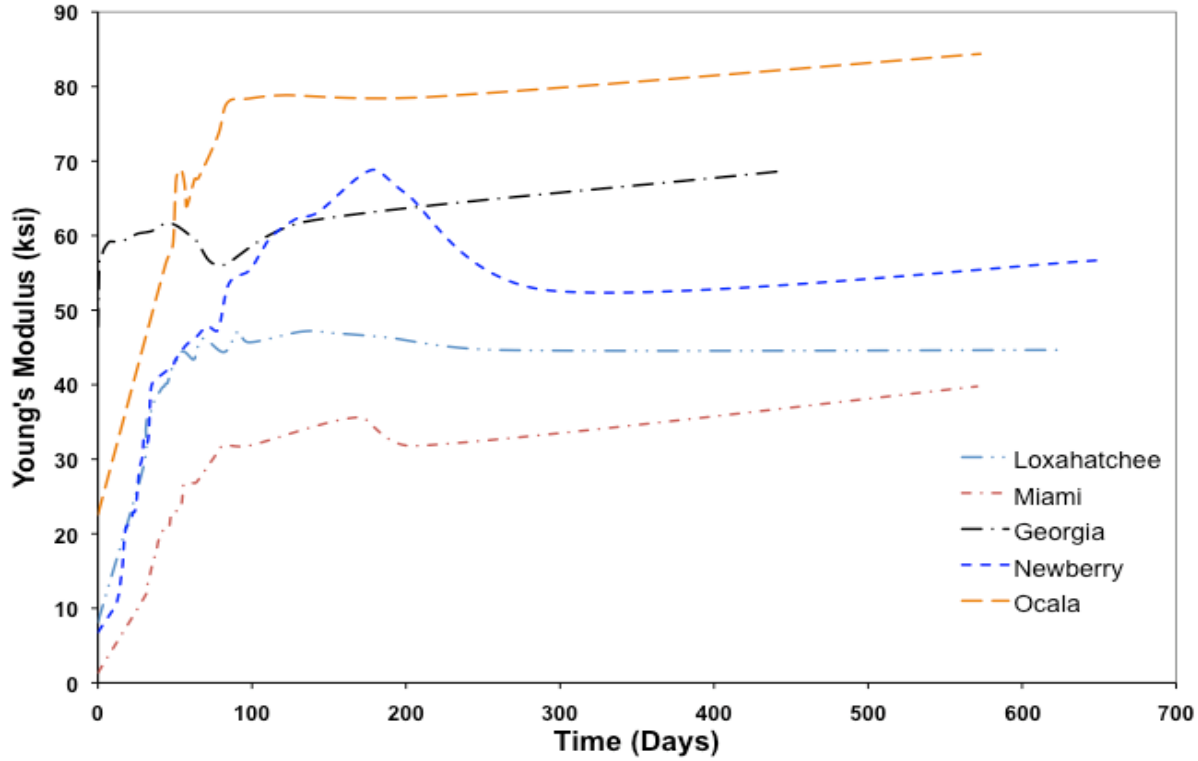

Figure H-12. Variation of Young's modulus with time, replicate 3, constant moisture.

APPENDIX I
INDIVIDUAL LARGE-STRAIN MODULUS TEST RESULTS

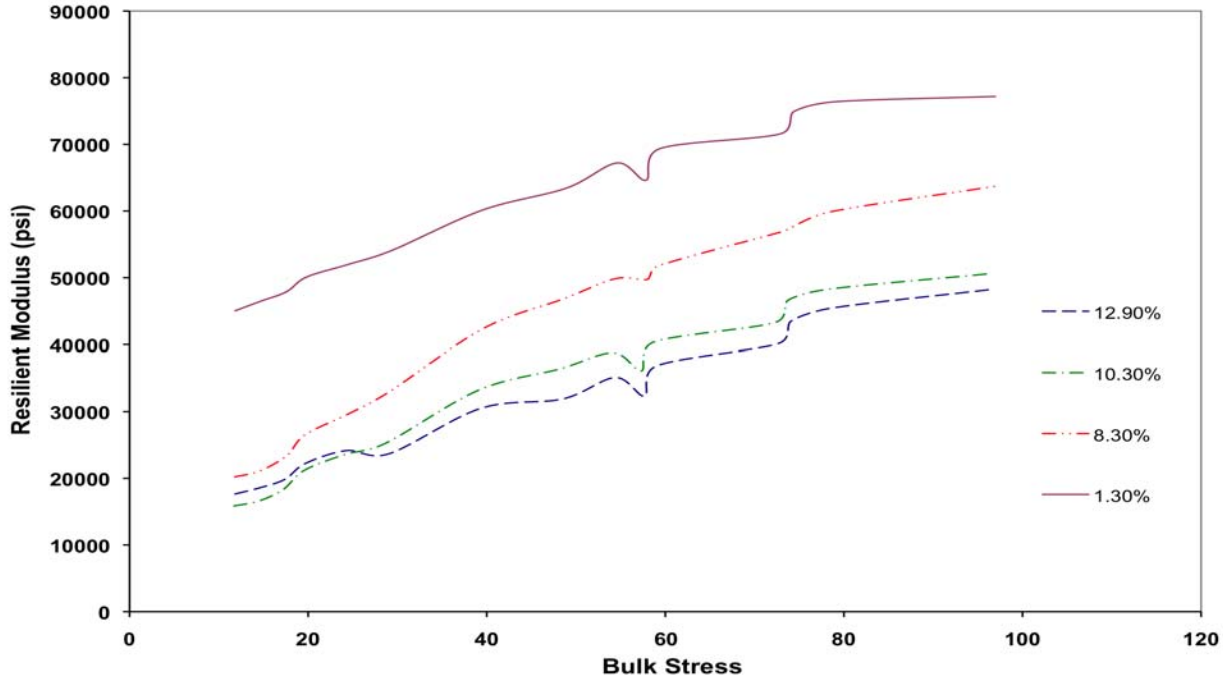

Figure I-1. Variation of resilient modulus with bulk stress, Newberry, replicate 1, outdoor ambient.

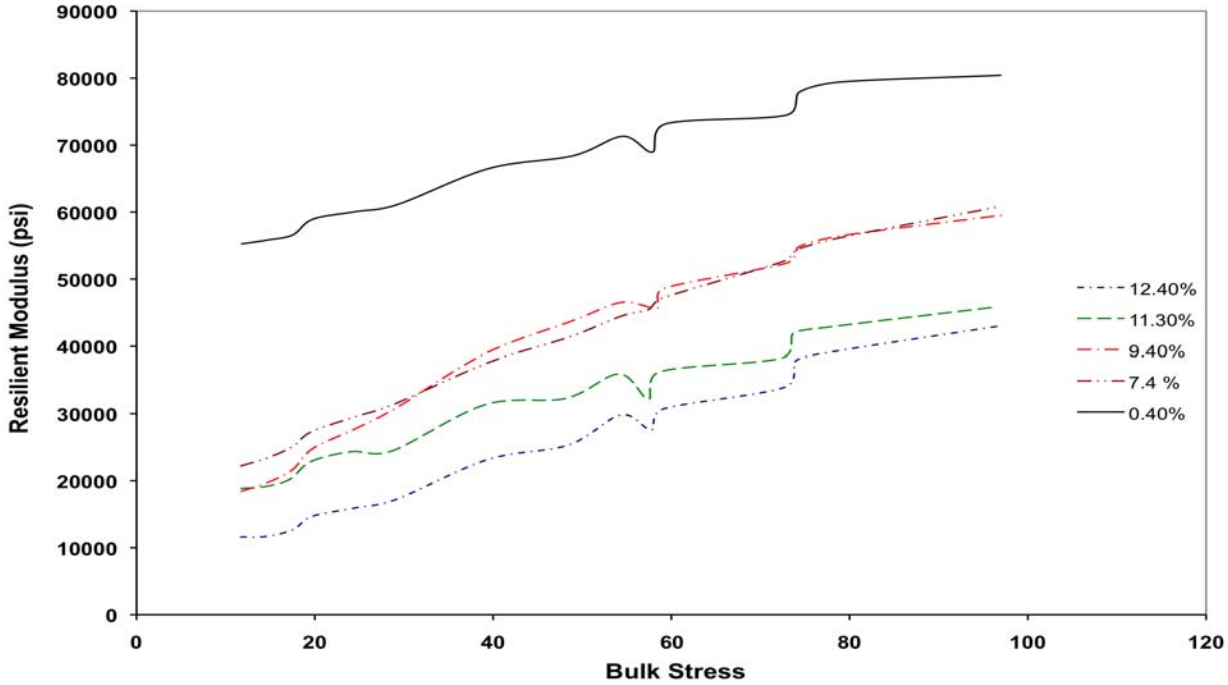

Figure I-2. Variation of resilient modulus with bulk stress, Newberry, replicate 2, outdoor ambient.

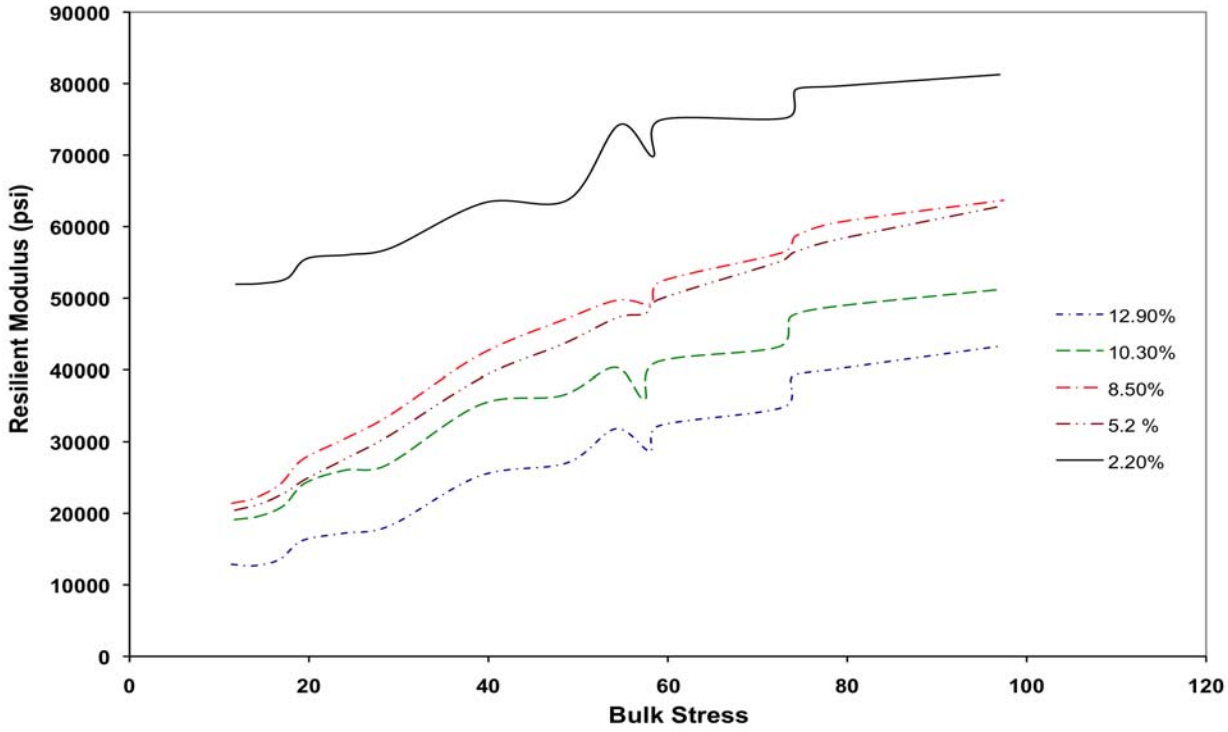

Figure I-3. Variation of resilient modulus with bulk stress, Newberry, replicate 3, outdoor ambient.

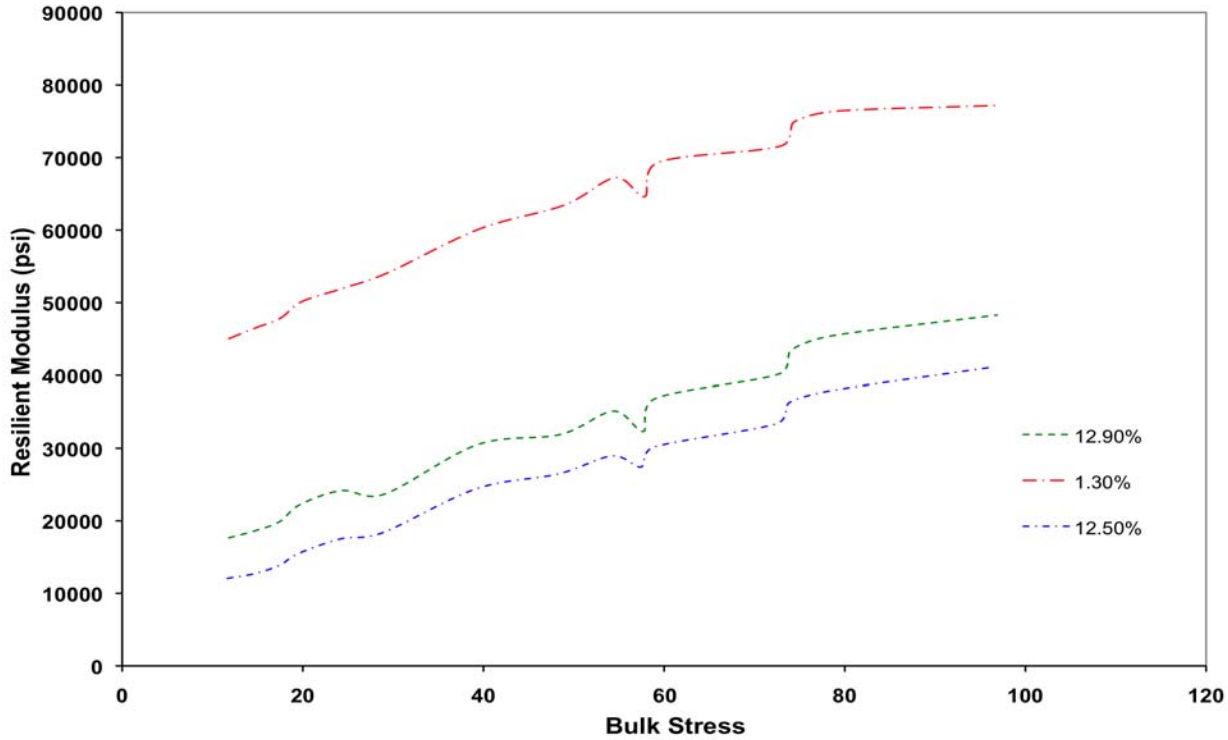

Figure I-4. Variation of resilient modulus with bulk stress, Newberry, replicate 1, wetting and drying.

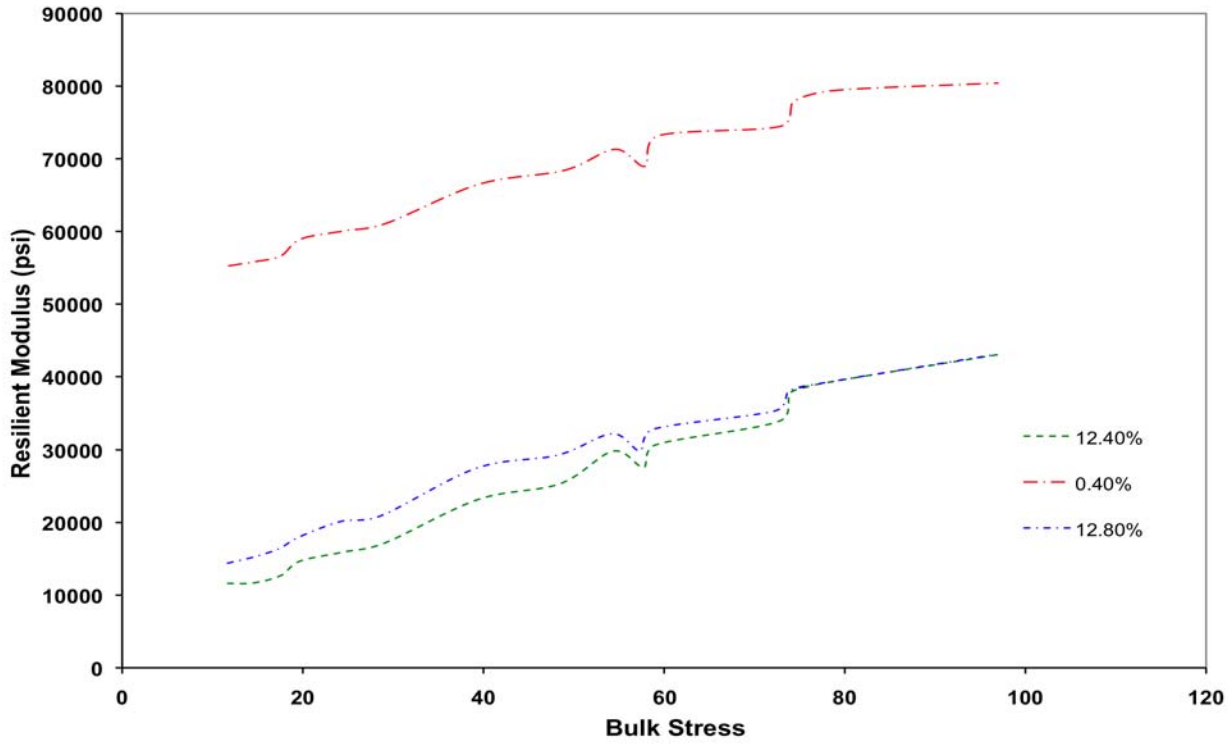

Figure I-5. Variation of resilient modulus with bulk stress, Newberry, replicate 2, wetting and drying.

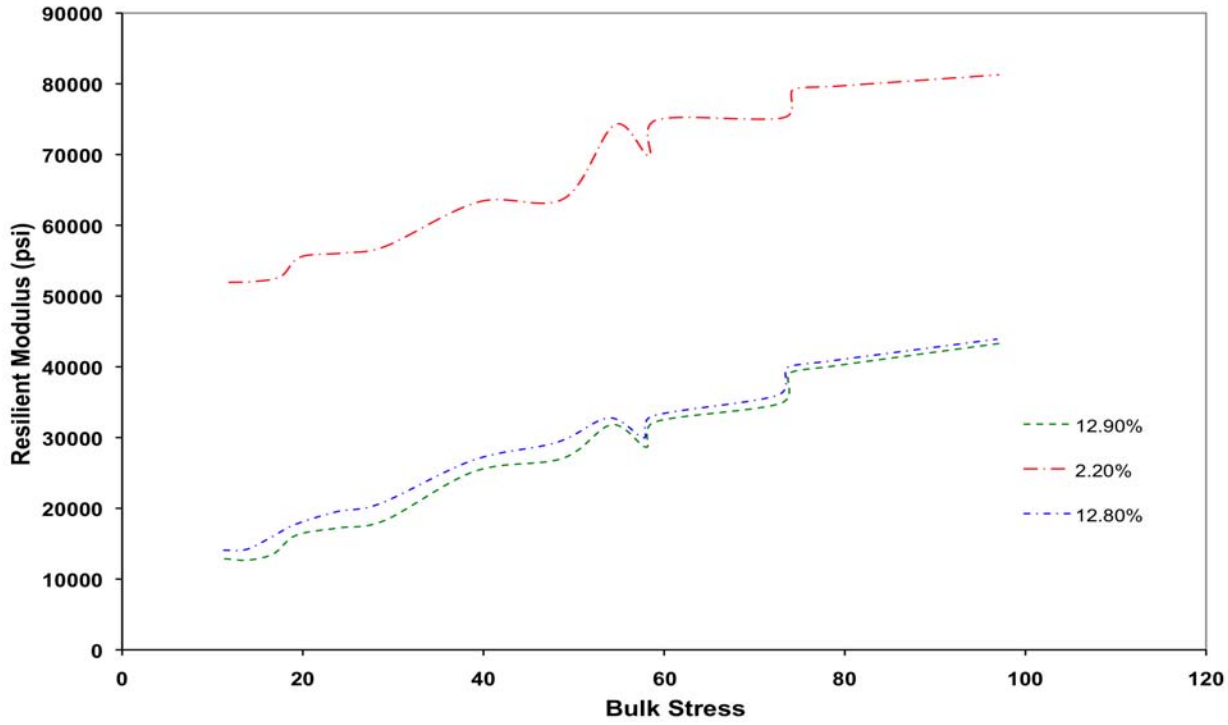

Figure I-6. Variation of resilient modulus with bulk stress, Newberry, replicate 3, wetting and drying.

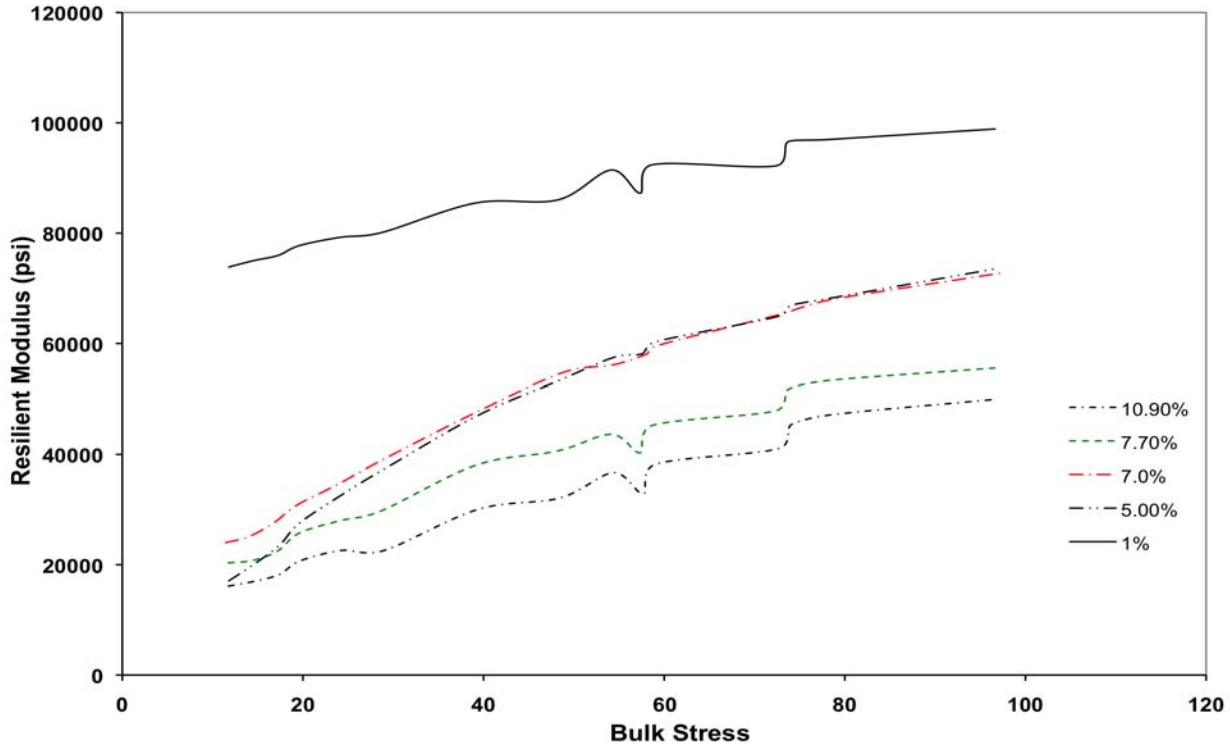

Figure I-7. Variation of resilient modulus with bulk stress, Ocala, replicate 1, outdoor ambient.

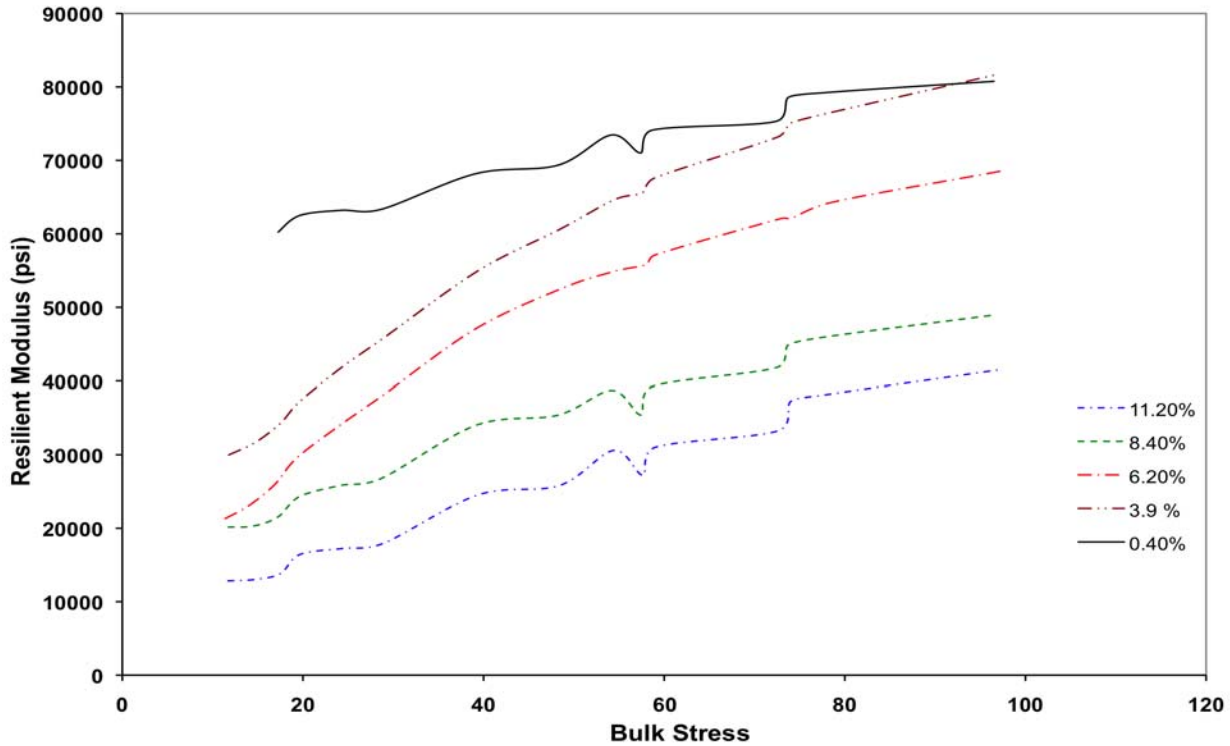

Figure I-8. Variation of resilient modulus with bulk stress, Ocala, replicate 2, outdoor ambient.

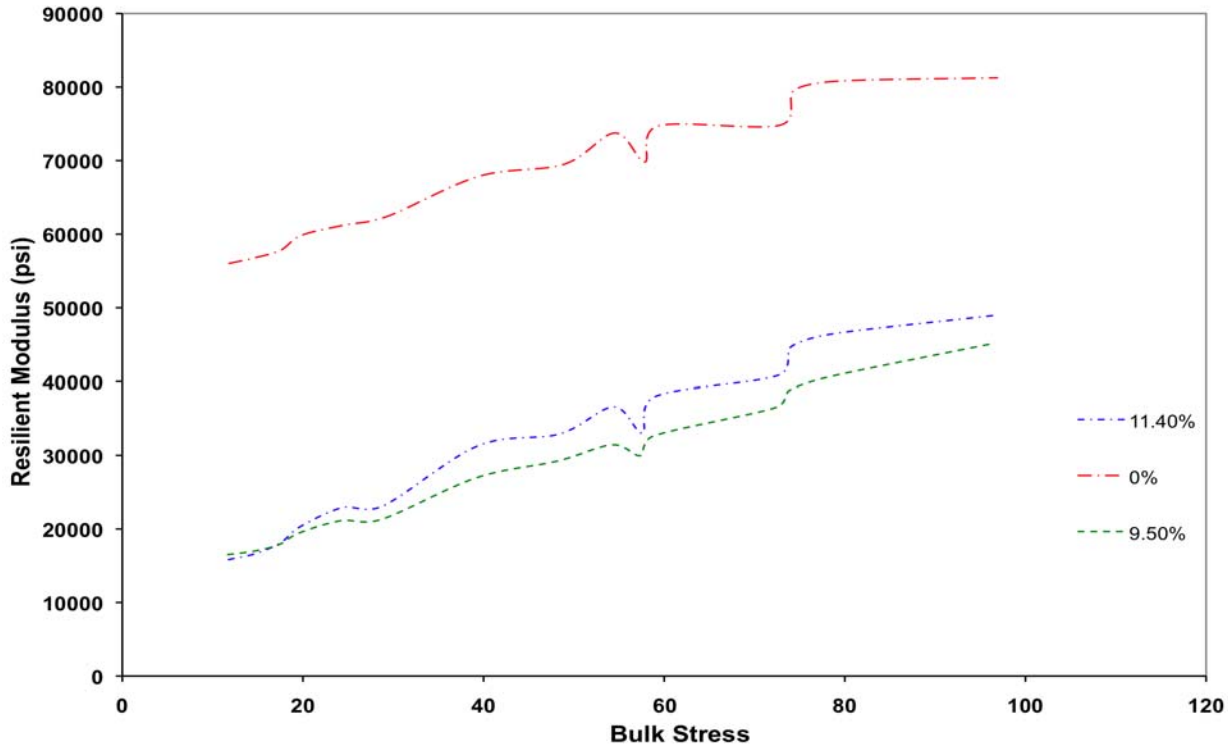

Figure I-9. Variation of resilient modulus with bulk stress, Ocala, replicate 3, outdoor ambient.

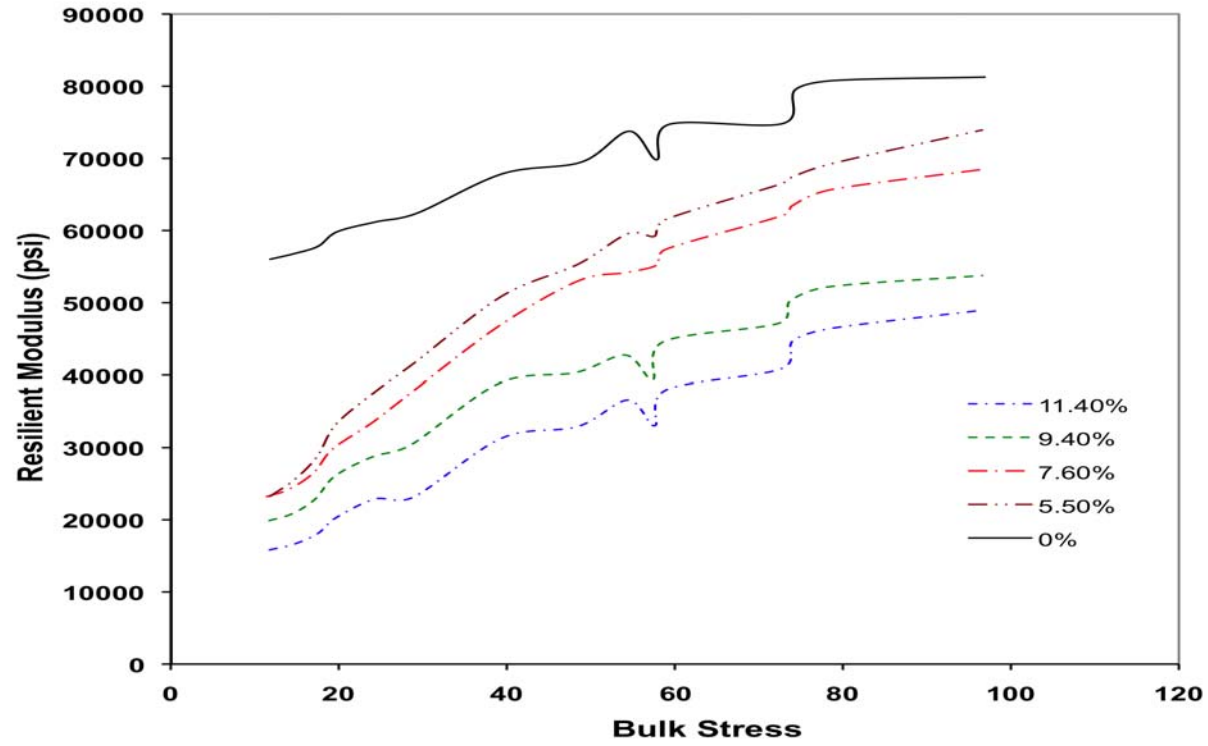

Figure I-10. Variation of resilient modulus with bulk stress, Ocala, replicate 1, wetting and drying.

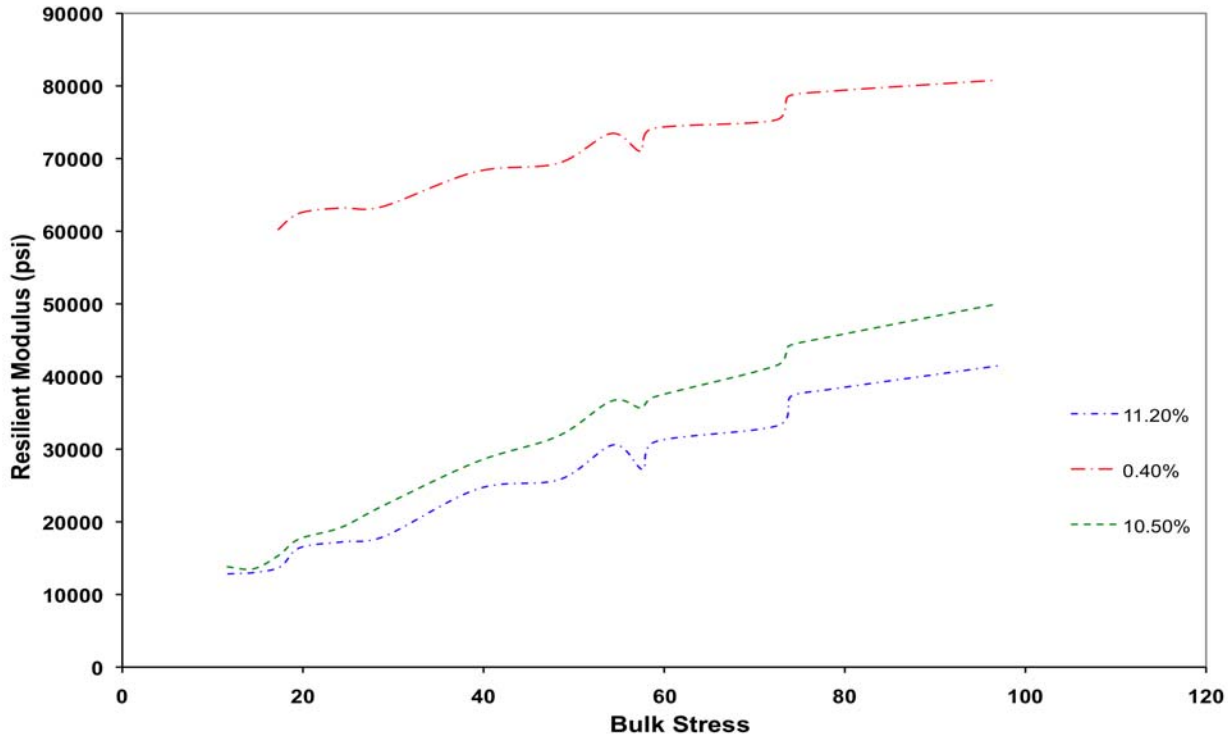

Figure I-11. Variation of resilient modulus with bulk stress, Ocala, replicate 2, wetting and drying.

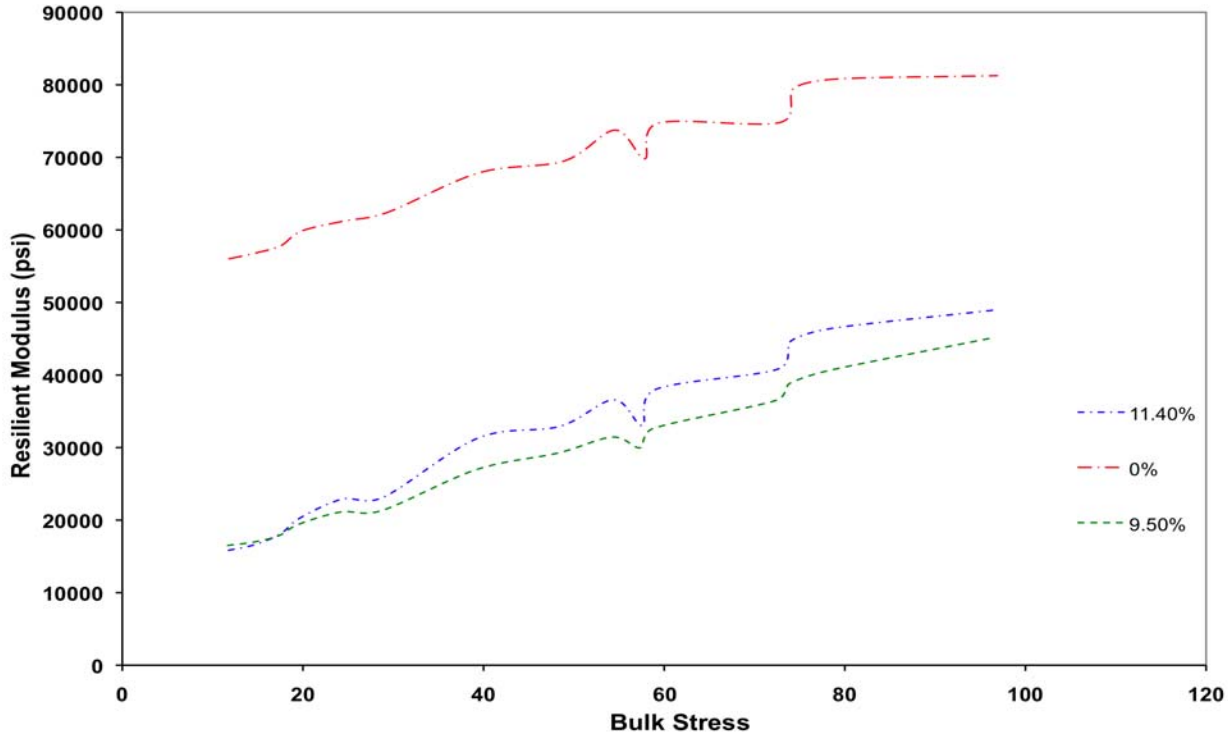

Figure I-12. Variation of resilient modulus with bulk stress, Ocala, replicate 3, wetting and drying.

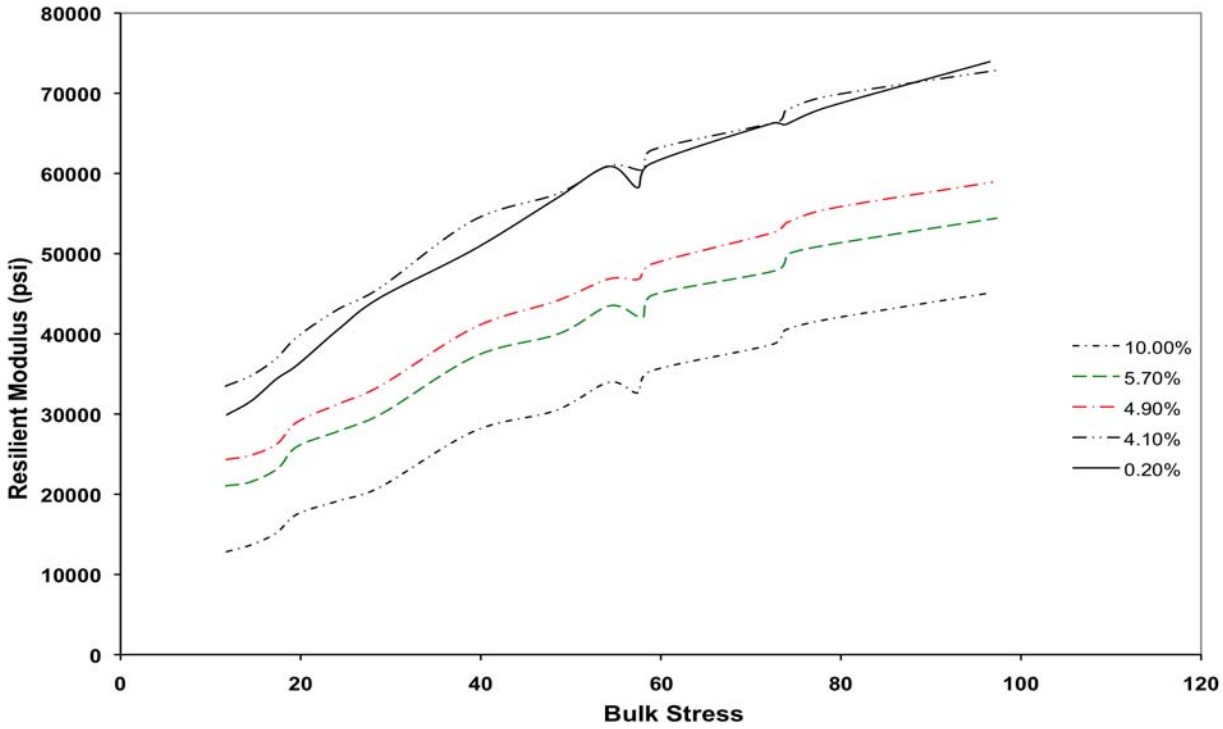

Figure I-13. Variation of resilient modulus with bulk stress, Loxahatchee, replicate 1, outdoor ambient.

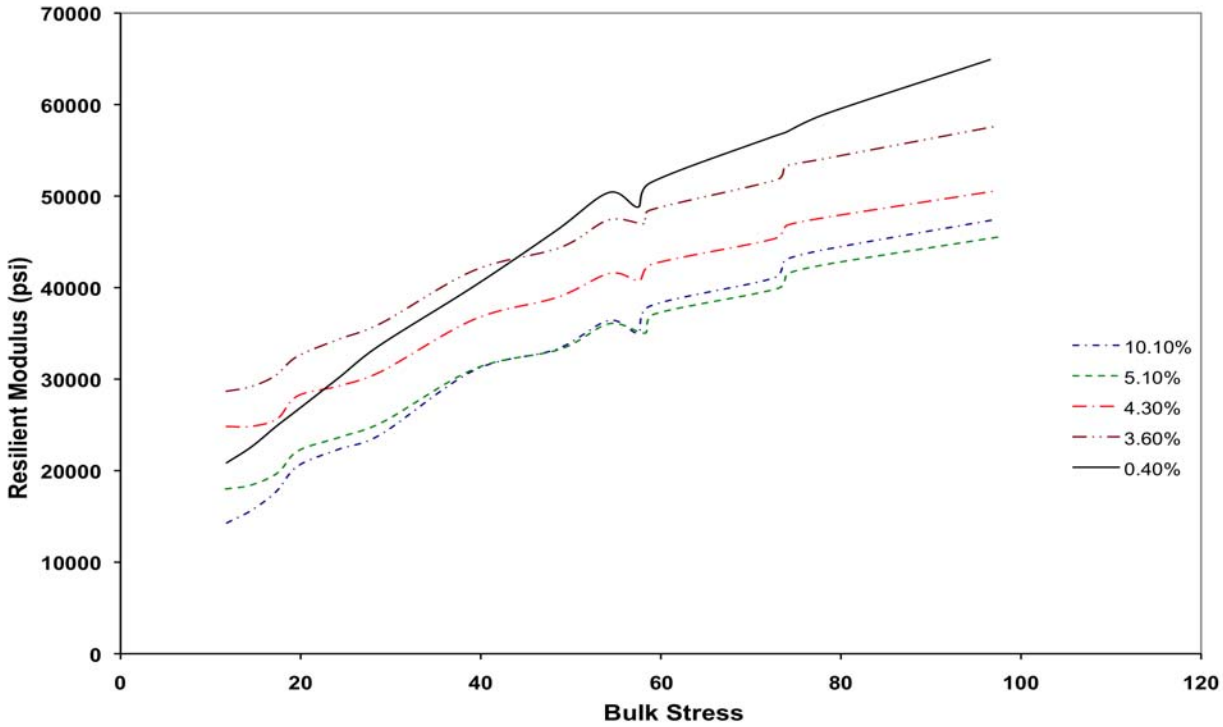

Figure I-14. Variation of resilient modulus with bulk stress, Loxahatchee, replicate 2, outdoor ambient.

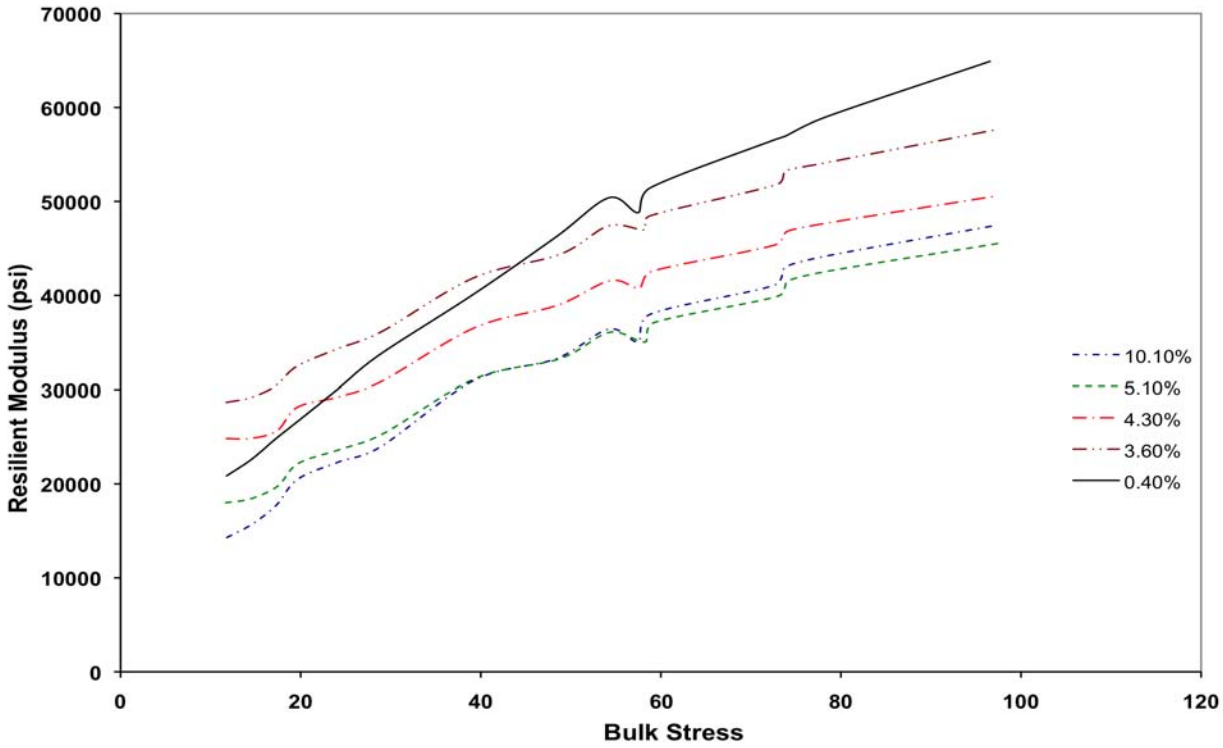

Figure I-15. Variation of resilient modulus with bulk stress, Loxahatchee, replicate 3, outdoor ambient.

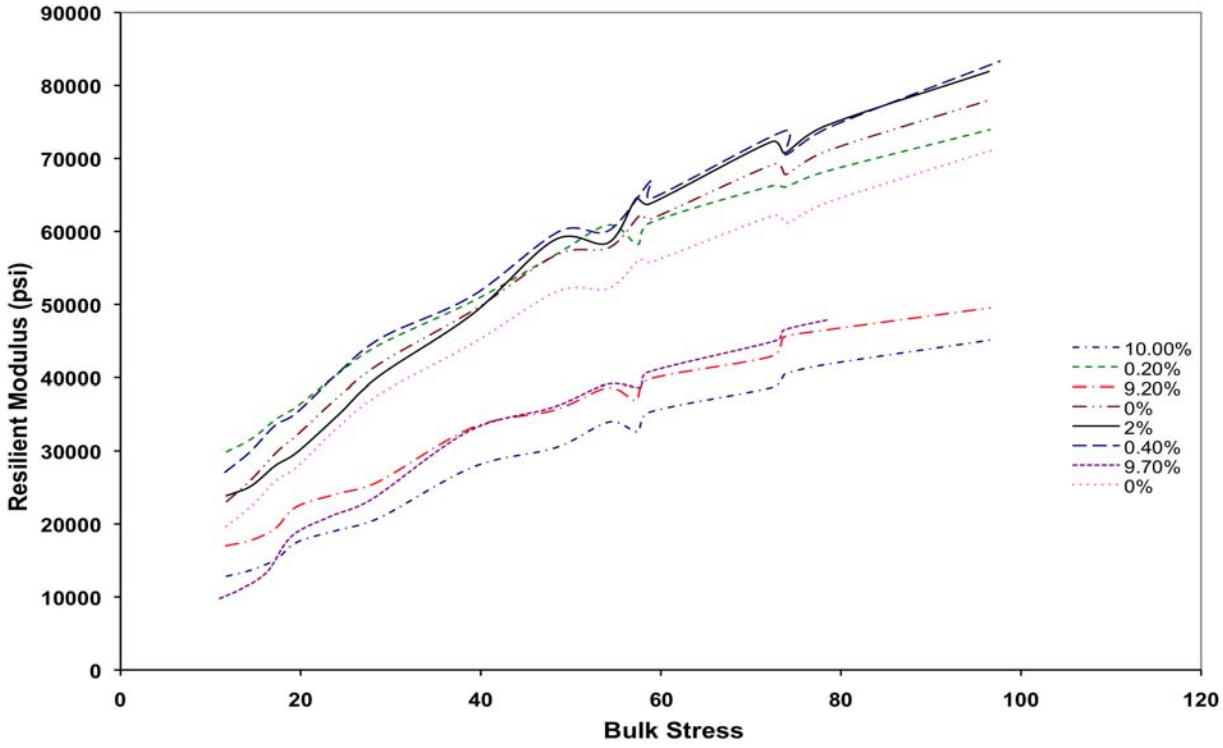

Figure I-16. Variation of resilient modulus with bulk stress, Loxahatchee, replicate 1, wetting and drying.

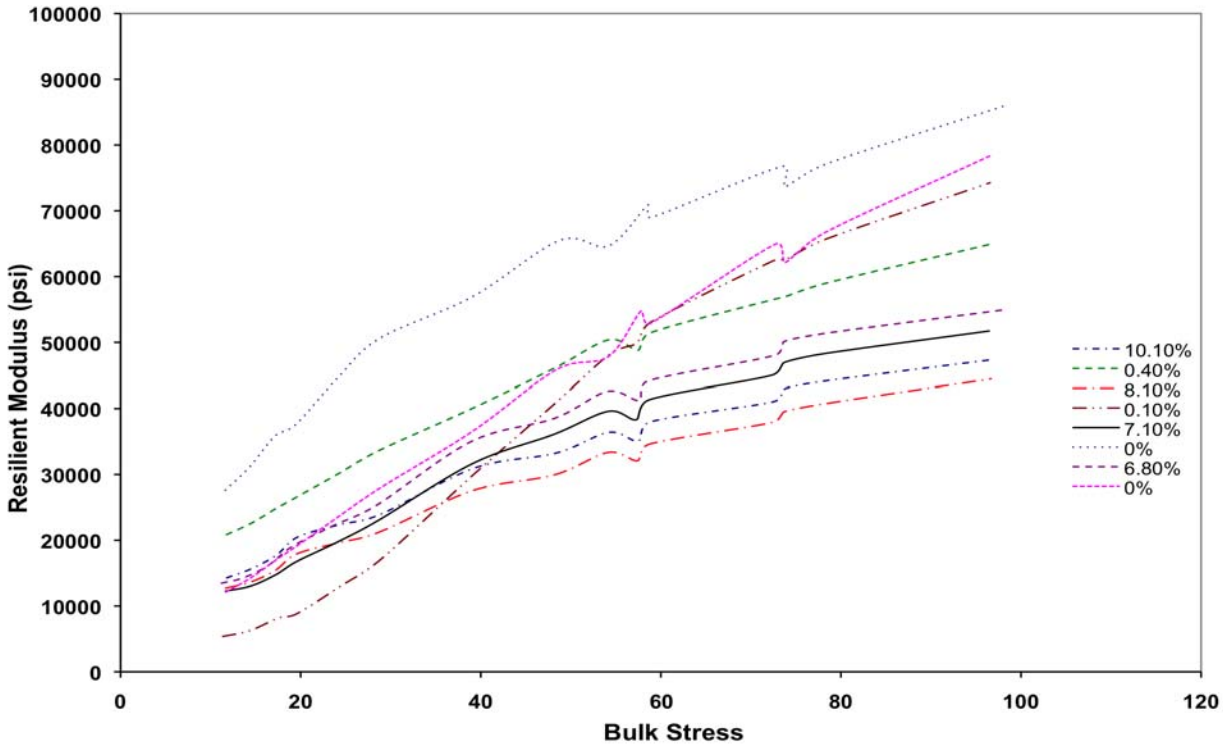

Figure I-17. Variation of resilient modulus with bulk stress, Loxahatchee, replicate 2, wetting and drying.

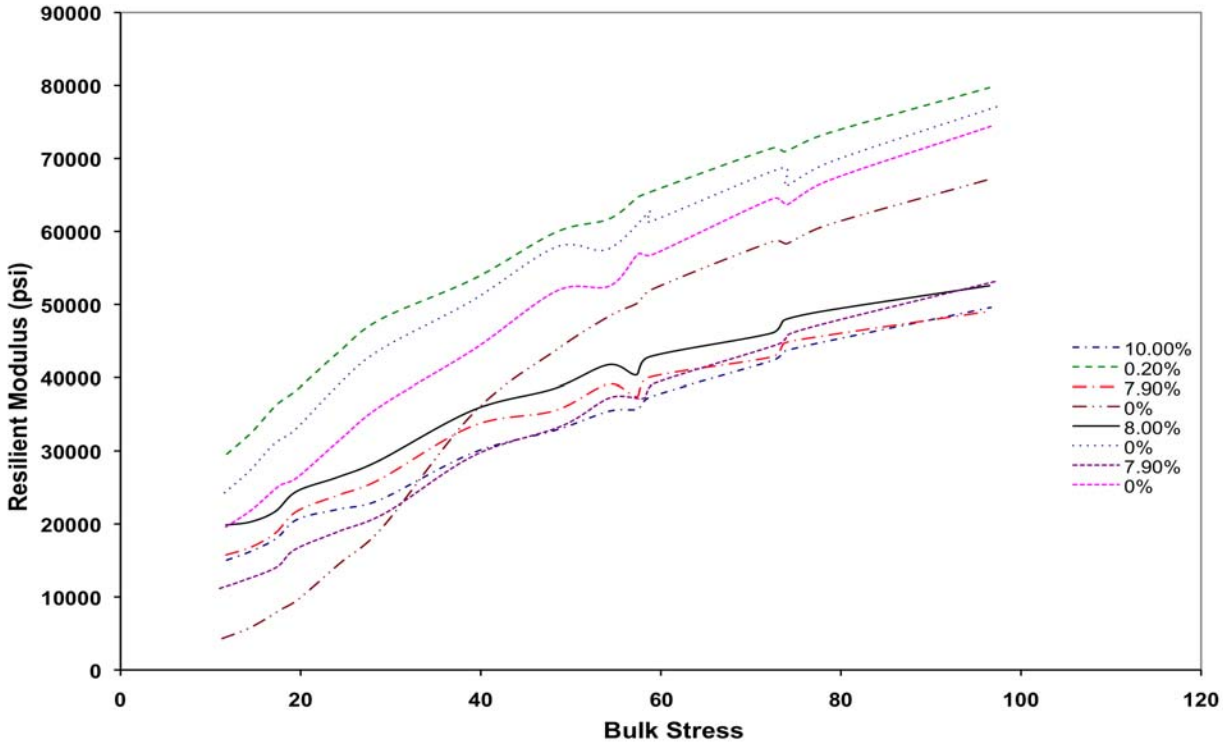

Figure I-18. Variation of resilient modulus with bulk stress, Loxahatchee, replicate 3, wetting and drying.

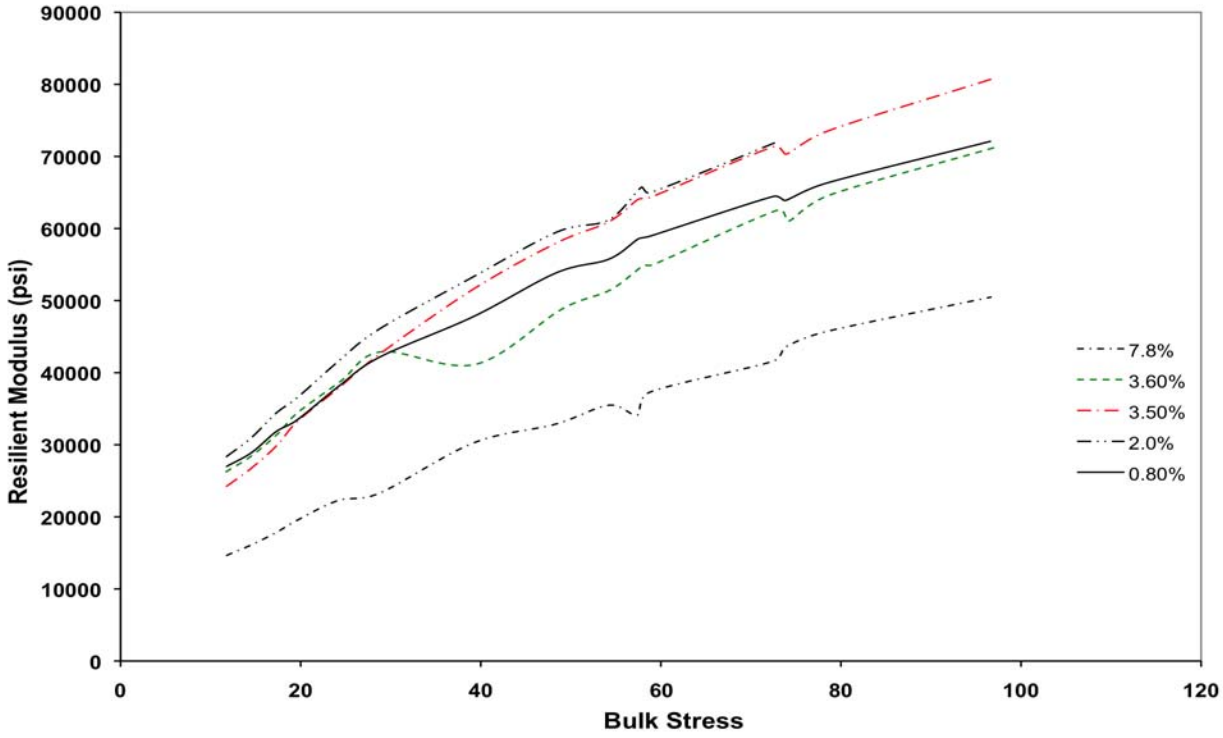

Figure I-19. Variation of resilient modulus with bulk stress, Miami, replicate 1, outdoor ambient.

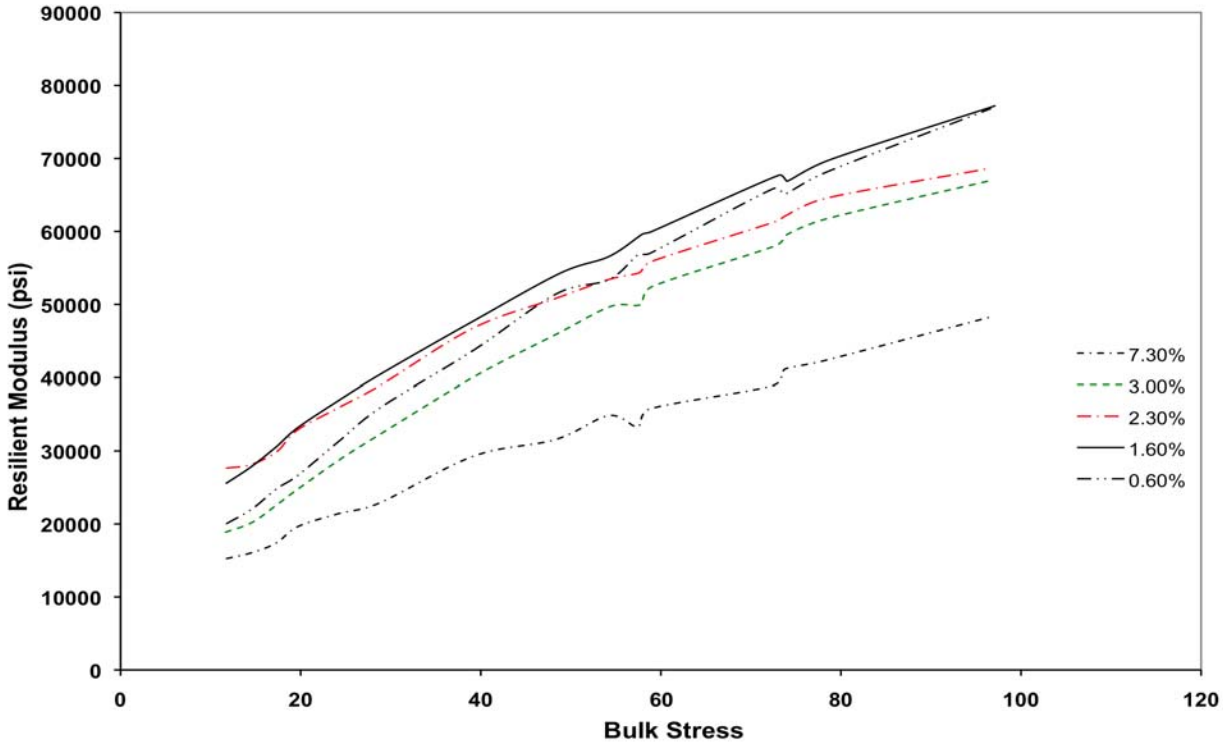

Figure I-20. Variation of resilient modulus with bulk stress, Miami, replicate 2, outdoor ambient.

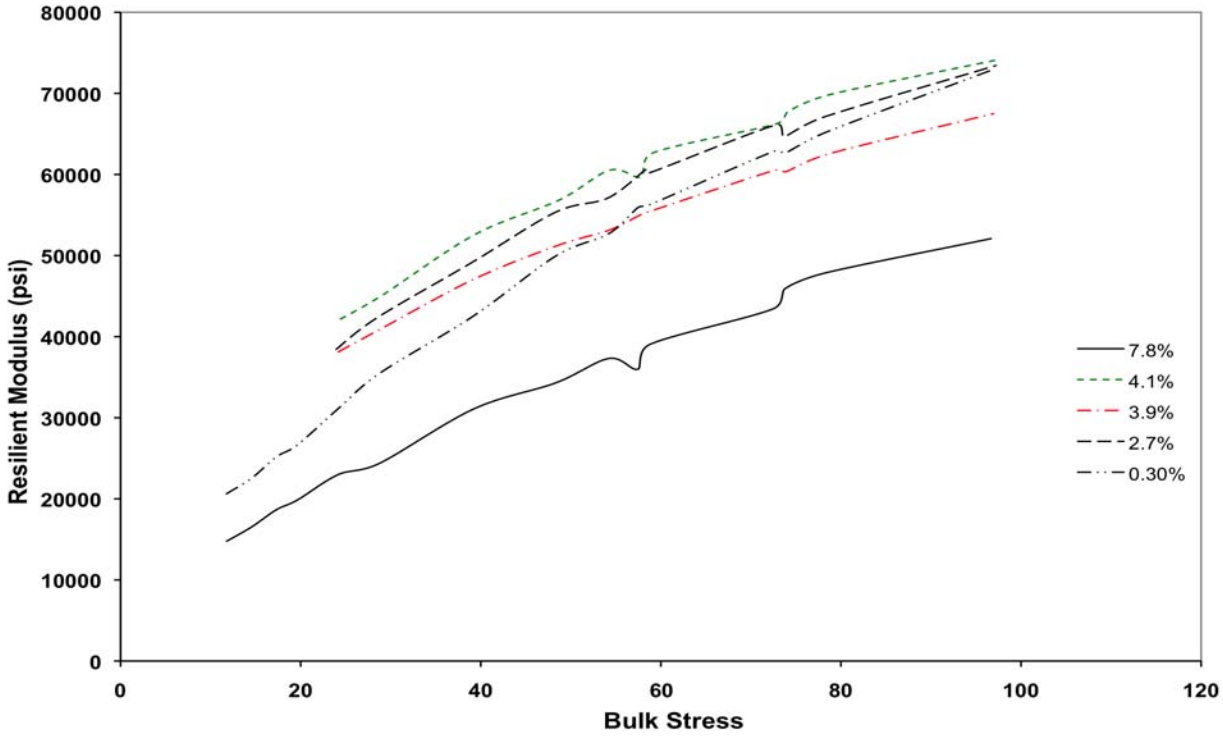

Figure I-21. Variation of resilient modulus with bulk stress, Miami, replicate 3, outdoor ambient.

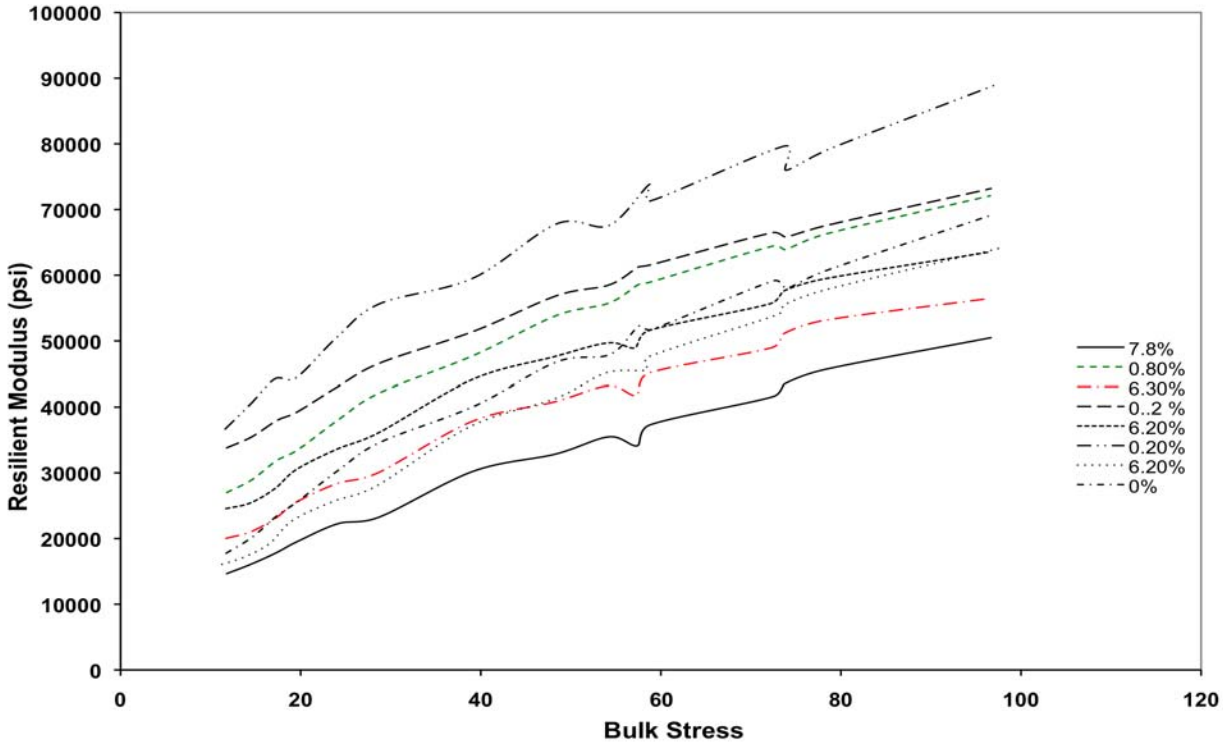

Figure I-22. Variation of resilient modulus with bulk stress, Miami, replicate 1, wetting and drying.

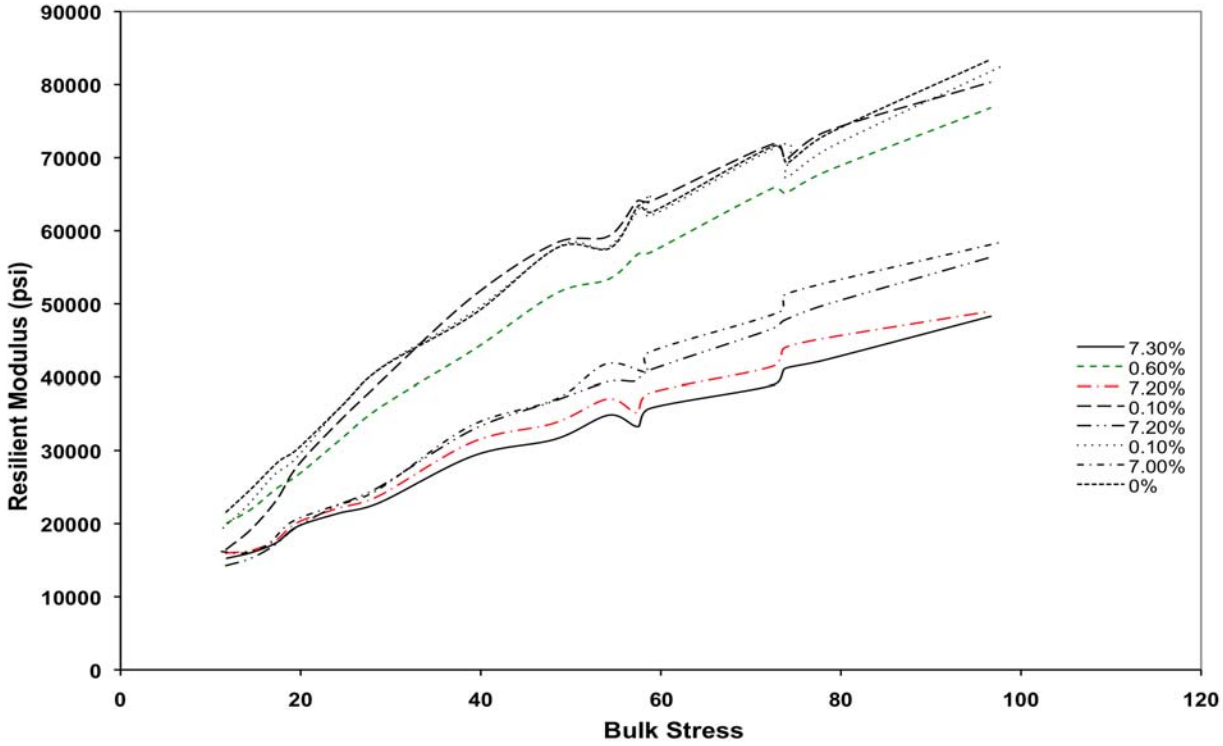

Figure I-23. Variation of resilient modulus with bulk stress, Miami, replicate 2, wetting and drying.

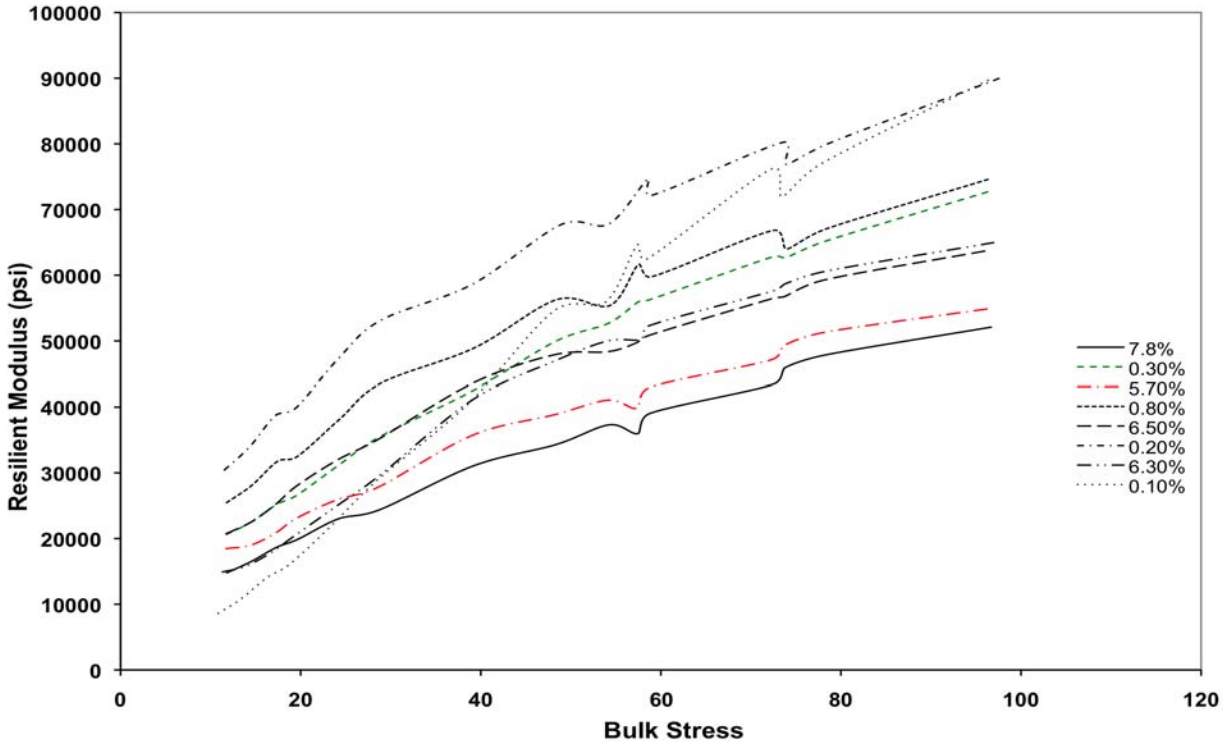

Figure I-24. Variation of resilient modulus with bulk stress, Miami, replicate 3, wetting and drying.

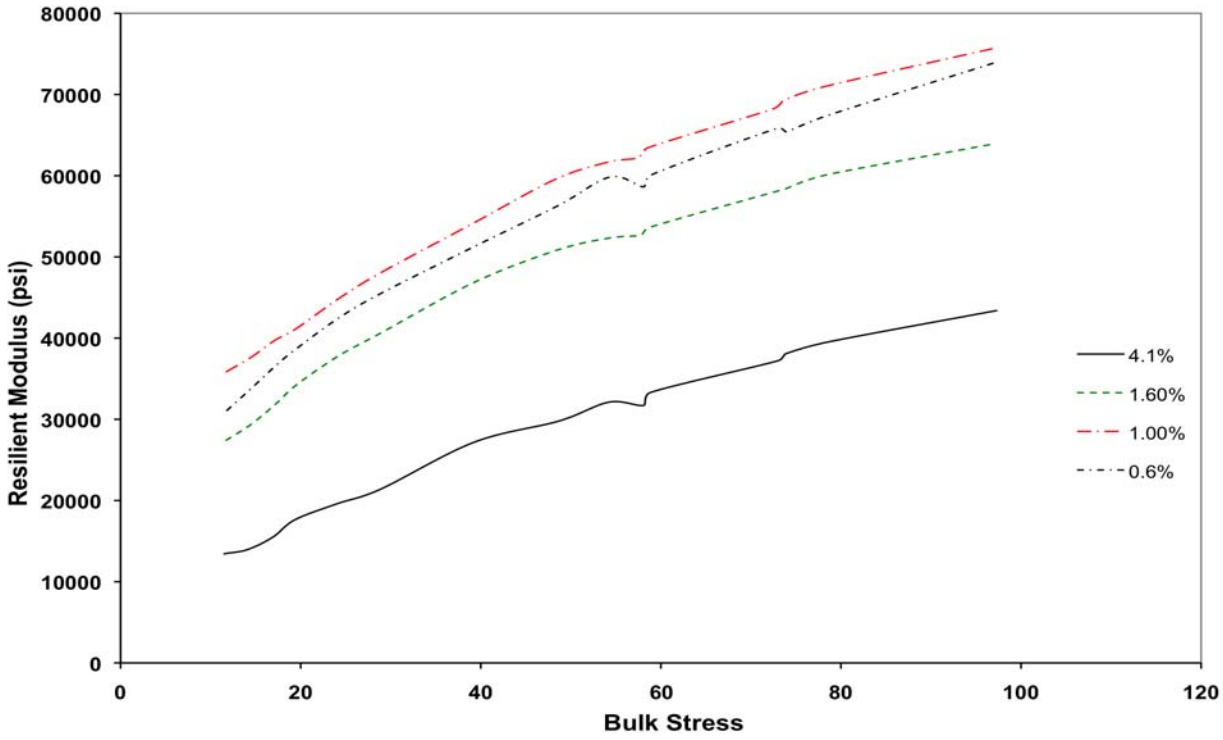

Figure I-25. Variation of resilient modulus with bulk stress, Georgia, replicate 1, outdoor ambient.

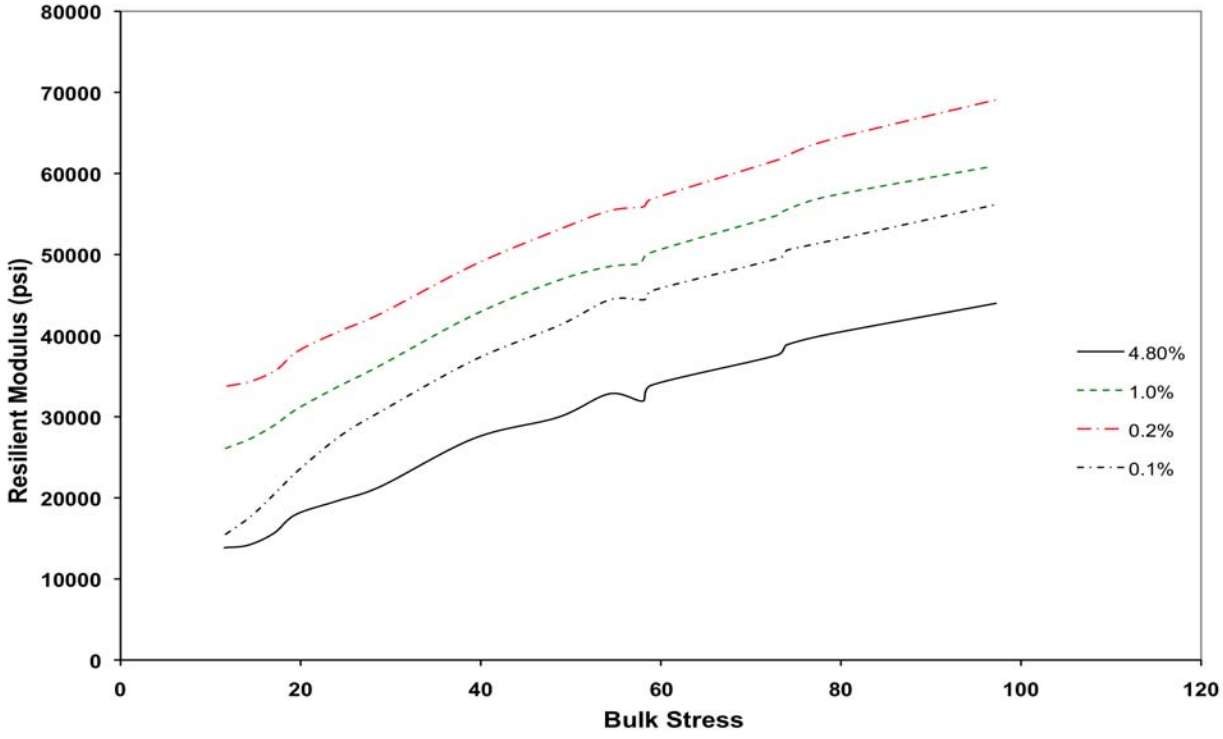

Figure I-26. Variation of resilient modulus with bulk stress, Georgia, replicate 1, wetting and drying.

LIST OF REFERENCES

Afifi, S.S. and Woods, R.D. (1971), "Long-Term Pressure Effects on Shear Modulus of Soils," *Journal of the Soil Mechanics and Foundations Division*, ASCE, Vol. 97, No. 10, October, pp. 1445-1460.

Campos, L.A. (2007), "Investigation of Stiffness Gain Mechanism in Florida Limestone Base Coarse Material," *M.E. Thesis*, University of Florida, May, 67 pp.

Cho, G.C. and Santamarina J. C. (2001), "Unsaturated Particulate Material- Particle Level Study," *Journal of Geotechnical and Geoenvironmental Engineering*, ASCE, Vol. 127, No. 1, January, pp. 84-96.

Fernandez, A. L. (2000), "Tomographic Imaging the State of Stress," *Ph.D. Dissertation*, Georgia Institute of Technology, 298 pp.

Florida Department of Environmental Protection Homepage, Florida Geological Survey, Geology Topics, Ocala Limestone, *http://www.dep.state.fl.us/geology/geologictopics/rocks/ocala_limestone.htm.* Accessed November 2, 2007.

Florida Department of Environmental Protection Homepage, Florida Geological Survey, Geology Topics, Miami Limestone, *http://www.dep.state.fl.us/geology/geologictopics/rocks/miami_limestone.htm.* Accessed November 2, 2007.

Florida Department of Environmental Protection Homepage, Florida Geological Survey, Geology Topics, Anastasia Formation Coquina, *http://www.dep.state.fl.us/geology/geologictopics/rocks/anastasia.htm.* Accessed November 2, 2007.

Florida Department of Transportation Homepage, State Materials Office, Geotechnical Materials System, Aggregate Acceptance, Source Maps, *http://www.dot.state.fl.us/statematerialsoffice/laboratory/geotechnical/aggregates/maps/index.htm.* Accessed November 1, 2007.

Gartland, J.D. and Eades J.L. (1979), "Laboratory Investigation of Natural Cementation Phenomena in Florida Limestone Base Course Materials," *Florida Limerock Cementation Investigation, S-18-77 Sponsored by the FDOT*, Department of Geology, University of Florida, June 30.

Hardin, B. O. and Richart, F. E., Jr. (1963), "Elastic Wave Velocities in Granular Soils," *Journal of the Soil Mechanics and Foundations Division*, ASCE, Vol. 89, No. SM1, February, pp. 33-65.

Kalinski, M. E. and Thummaluru, M. S. R. (2005), "A New Free-Free Resonant Column Device for Measurement of Gmax and Dmin at Higher Confining Stresses," *Geotechnical Testing Journal*, ASTM, Vol. 28, No. 2, pp. 1-8.

Keyser J.H., Eades J.L., Ruth B.E., Zimpfer W.H., Smith L.L. (1984), "Marginal Aggregates for Highway Pavements," *Bulletin of the International Association of Engineering Geology*, No. 30, Paris, pp. 425-429.

Kim, D. S., Kweon, G. C., and Lee, K. H. (1997), "Alternative Method of Determining Resilient Modulus of Compacted Subgrade Soils Using Free-Free Resonant Column Test," *Transportation Research Record 1577*, TRB, Washington, D. C., pp. 62-69.

Kim, D. S. and Stokoe, K. H., II (1992), "Characterization of Resilient Modulus of Compacted Subgrade Soils Using Resonant Column and Torsional Shear Tests," *Transportation Research Record 1369*, TRB, Washington, D. C., pp. 83-91.

Lu, N. and Likos, W. J. (2005), *Unsaturated Soil Mechanics,* John Wiley & Sons Inc, New York, 556 pp.

McClellan, G.H., Ruth, B.E., Eades, J.L., Fountain, K.B., and Blitch, G. (2001), "Evaluation of Aggregates for Base Course Construction," *Final Report for FDOT, State Contract No. B-9886*, WPI 0510753, September.

Menq, F. Y. (2003). "Dynamic Properties of Sandy and Gravelly Soils," *Ph.D. Dissertation*, The University of Texas at Austin, May, 363 pp.

Mitchell, J. K. and Soga, K. (2005), *Fundamentals of Soil Behavior*, 3rd Edition, John Wiley & Sons, Inc., Hoboken, New Jersey, 577 pp.

Nazarian, S., Yuan, D., and Arellano, M. (2002), "Quality Management of Base and Subgrade Materials with Seismic Methods," *81st Annual Meeting Compendium of Papers CD-ROM*, Transportation Research Board, Washington, D. C., January.

Nazarian, S., Yuan, D., Tandon, V., and Arellano, M. (2002), "Quality Management of Flexible Pavement Layers with Seismic Methods," *Research Project 0-1735*, *Development of Structural Field Testing of Flexible Pavement Layers Conducted for Texas Department of Transportation*, Research Report 1735-3F, December.

Qian, X., Gray, D.H., and Woods, R.D. (1993), "Voids and Granulometry; Effects on Shear Modulus of Unsaturated Sands," *Journal of Geotechnical Engineering*, ASCE, Vol. 119, No. 2, February, pp. 295-314.

Qian, X., Gray, D.H., and Woods, R.D. (1991), "Resonant Column Tests on Partially Saturated Sands," *Geotechnical Testing Journal*, 14(3), pp. 266-275.

Richart, F. E., Jr., Hall, J. R., Jr., and Woods, R. D. (1970), *Vibrations of Soils and Foundations*, Prentice-Hall, Inc., Englewood Cliffs, New Jersey, 414 pp.

Schmertmann, J. H. (1992), "The Mechanical Aging of Soils," *Journal of Geotechnical Engineering*, ASCE, Vol. 117, No. 9, September, pp. 1288-1330.

Singh, A., Roberson, R., Ranaivoson, A., Siekmeier, J., and Gupta, S. (2006), "Water Retention Characteristics of Aggregate and Granular Materials," *Unsaturated Soils 2006, Geotechnical Special Publication No. 147*, G. A. Miller, C. E. Zapata, S. L. Houston, and D. G. Fredlund, Eds., American Society of Civil Engineers, pp. 1326-1337.

Smith L.L. and Lofroos W.N. (1981), "Pavement Design Coefficients: A Re-evaluation of Florida Base Materials," *State of Florida Department of Transportation, Research Report FL/DOT/OMR-235/81*, February.

Wu, S., Gray, D. H., and Richart, F. E., Jr. (1984), "Capillary Effects on Dynamic Modulus of Sands and Silts," *Journal of Geotechnical Engineering*, ASCE, Vol. 110, No. 9, September, pp. 1188-1203.

Wu, S. M. and Woods, R. D. (1987), "Time Effects on Shear Modulus of Unsaturated Cohesionless Soils," *Soil-Structure Interaction*, A. S. Cakmak, Ed., Elsevier, New York, pp. 243-256.

Zimpfer, W.H. (1979), "Florida Limerock Investigation; Strength Gain Study," *Florida Department of Transportation Interim Report No.2*, State Project Number U-03, December.

Zimpfer, W.H. (1988), "Review of FDOT Flexible Pavement Base Studies," *Final Report for the Florida Department of Transportation,* State Project Number 997000-7350, June.

Zimpfer, W.H., Smith, L.L., Potts, C.F., and Fuller, S.L. (1973), "Structural Layer Coefficients for Flexible Pavement Design," *Final Report Submitted to the Florida Department of Transportation*, Research Report 177, 45 pp.